SELECTIVE C–H AND ALKENE FUNCTIONALIZATION VIA ORGANIC PHOTOREDOX CATALYSIS

Nicholas Paul Ralph Onuska

A dissertation submitted to the faculty at the University of North Carolina at Chapel Hill in partial fulfillment of the requirements for the degree of Doctor of Philosophy in the Department of Chemistry

Chapel Hill
2021

Approved by:

David Nicewicz

Erik Alexanian

Jeffrey Aubé

Alexander Miller

Andrew Moran

ABSTRACT

Nicholas Paul Ralph Onuska: Selective C–H and Alkene Functionalization Via Organic Photoredox Catalysis
(Under the direction of David A. Nicewicz)

Photoinduced electron transfer (PET) can be defined as the promotion of an electron transfer reaction through absorption of a photon by a reactive species in solution. Photoredox catalysis has leveraged previous knowledge of PET processes to enable a wide variety of high value chemical transformations. Most early work in the field of photoredox catalysis centered around the use of visible-light absorbing transition metal catalyst systems based on ruthenium or iridium polypyridyl scaffolds, organic redox chromophores offer a more sustainable, accessible, and versatile alternative to these complexes. Organic photoredox catalysts are often less expensive, easier to prepare, and have expanded redox windows relative to many known transition-metal photoredox catalysts, enabling the generation of a wider variety of single electron reduced/oxidized species. This ultimately translates into the development of previously undiscovered modes of reactivity. Herein is described the development and mechanistic study of a several C–H and alkene functionalization reactions facilitated by visible light-absorbing acridinium salts, as well as the discovery and characterization of a neutral organic radical which possess one of the most negative excited state oxidation potentials observed to date.

Through single electron oxidation of protected secondary amines, the corresponding neutral alpha-carbamyl radical species may be generated and utilized in a formal carbon-carbon bond forming C–H functionalization reaction. Electron rich arenes are amenable to functionalization *via* net oxidative or redox neutral pathways using similar catalytic systems.

Upon generation of an electrophilic arene cation radical through PET, diazoacetate derivatives undergo nucleophilic addition to these intermediates, affording formal C–H functionalization products containing a new sp^3-sp^2 carbon-carbon bond.

Methods for the anti-Markovnikov functionalization of activated olefins are also accessible *via* photoredox catalysis. Acridinium salts are shown to serve as competent catalysts in electrophilic hydroazidation reactions of activated olefins in combination with a sterically hindered thiol hydrogen atom transfer catalyst.

An investigation of the photophysical behavior of a neutral acridine is presented. A combined spectroscopic, computational, and experimental study suggests excitation of this species leads to the population of several extremely reducing doublet excited states. The *in situ* generation and excitation of this species enables a variety of catalytic reductive photoredox transformations.

TABLE OF CONTENTS

LIST OF FIGURES

LIST OF ABBREVIATIONS

AIBN	Azobisisobutyronitrile
Boc	Tert-butoxycarbonyl protecting group
Cbz	n-carboxybenzyl protecting group
CFL	Compact fluorescent lamp
DCA	Dicyanoanthracene
DCE	Dichloroethane
DIPEA	Diisopropylethylamine
DMPU	N, N′-Dimethylpropyleneurea
DMSO	Dimethylsulfoxide
Dtbppy	4,4'-Di-Tert-butyl-2,2'-bipyridine
Equiv.	Molar equivalents
Et	Ethyl group
EWG	General electron withdrawing group
Fc	Ferrocene
Fmoc	Fluorenylmethyloxycarbonyl
GC-MS	Gas chromatography/mass spectrometry
HCl	Hydrochloric acid
HMDSO	Heaxmethyldisiloxane
HOMO	Highest occupied molecular orbital
LED	Light emitting diode
LUMO	Lowest occupied molecular orbital
Me	Methyl group
MVK	Methyl vinyl ketone
Nuc	General nucleophile

OAc	Acetate
OMe	Methyloxy
PET	Photoinduced electron transfer
Ph	Phenyl group
$PhCF_3$	Trifluorotoluene
PhMe	Toluene
ppy	2-phenylpyridine
SCE	Saturated calomel electrode
sec-BuLi	Secondary butyllithium
TFA	Trifluoroacetate
TFE	Trifluoroethanol
TICT	Twisted intramolecular charge transfer
TMS	Trimethylsilyl
$TMSN_3$	Trimethylsilyl azide
TRIP-SH	Triisopropylthiophenol
Ts	4-Methylbenzenesulfonate

Chapter 1 : ORGANIC PHOTOREDOX CATALYSIS

1.1: Introduction

For the past several decades, modern organic chemistry has largely been dominated by synthetic methods which proceed *via* the chemistry of positively and negatively charged closed-shell organic species, such as carbocations, carbanions, enolates, and alkoxides. While crucial to the science of organic chemistry, the reactivity of these high-energy species lead to relatively low chemoselectivity in complex molecular environments. For example, the high basicity and nucleophilicity of lithium stabilized carbonanions results in the observed low regioselectivity in reactions with substrates containing multiple electrophilic or basic functionalities. This concept can be thought of as a manifestation of the classic "reactivity/selectivity principle" familiar to many students of chemistry. To address this fundamental limitation, there has been increased focus on the development of new synthetic methodologies which are highly chemo- and/or site-selective in nature. These reactions can be applied to biologically and medicinally relevant organic molecules which are densely populated with sensitive functional groups, offering an avenue to the late-stage modification of complex drug targets or natural products. To this end, research in organic free radical chemistry has experienced a marked resurgence in recent years as a framework for the development of highly selective and efficient synthetic methods. Relative to closed-shell species, reactions utilizing open-shell, odd-electron species (such as cation/anion radicals/neutral radicals) benefit from reduced sensitivity to steric effects, increased chemoselectivity, and enhanced stereocontrol in many cases.

The numerous examples of complex and highly selective radical reactions serving as key steps in the synthesis of natural products provide evidence of the unique and synthetically versatile characteristics of organic radical intermediates.[1–3]

One differentiating factor among various free-radical based methods is the manner of generating the radical species. Classical reaction conditions consist of a radical initiator, such as AIBN or benzoyl peroxide, and a stochiometric chain carrying radical species, most often tributyltin hydride. While an efficient and synthetically useful process, the use of stoichiometric organotin reagents is a significant safety concern. Premature reduction of radical intermediates *via* hydrogen atom transfer is also potentially problematic in the presence of a stochiometric hydrogen atom source. Furthermore, radical generation is limited to substrates which can undergo radical atom transfer processes with the chain carrying tributylstannyl radical, such as alkyl halides and activated C–H bonds. To circumnavigate these issues, a large body of modern free radical literature in the past decade has been focused on radical generation *via* a process which has come to be known as "photoredox catalysis". Photoredox catalysis relies on the use of photoinduced electron transfer (PET) reactions of excited state, light-absorbing catalysts for the generation of reactive radical species.

1.2: Photoinduced Electron Transfer

Following the absorption of a photon of suitable energy, an electron within the highest occupied molecular orbital (HOMO) of a molecule is promoted to the lowest occupied molecular orbital (LUMO), generating a singlet excited state ($\mathbf{S_0}$) (assuming singlet ground state spin configuration). This $\mathbf{S_0}$ state may then undergo decay to the starting ground state electron configuration *via* one of several pathways: (a) fluorescence emission; (b) thermal/vibrational relaxation/energy transfer; (c) intersystem crossing *via* spin flipping to form a corresponding

triplet excited state (**T_0**). The amount of time that is required for the excited state molecule to decay *via* photon emission is quantified as the fluorescence lifetime (**τ_f**). In a similar matter, rate constants for the associated intersystem crossing and phosphorescence (triplet emission) processes can be obtained. These values can describe quantitatively how much time is available for the excited state of the molecule to participate in intermolecular chemistry through PET.

The ability of an excited state molecule to act as either an electron donor *or* electron acceptor is quantified by the corresponding excited state oxidation potential ($\boldsymbol{E^*_{ox}}$) or excited state reduction potential ($\boldsymbol{E^*_{red}}$), respectively. This value is given in volt units and is estimated according to the general equation below ($\boldsymbol{E^*_{red}}$ given as example), where $\boldsymbol{E_{red}(cat^*/cat^{\bullet -})}$ is the ground state reduction potential of the molecule and $E_{0,0}$ is the excited state energy of the corresponding excited state.

$$\boldsymbol{E^*_{red}(cat^*/cat^{\bullet -}) = E_{red}(cat^*/cat^{\bullet -}) + E_{0,0}}$$

$E_{0,0}$ refers to an approximation of the energy difference between the lowest energy vibrational state of a given excited state, **S_1**, and the lowest energy vibrational state of the ground state (**S_0**) molecule. One method for the approximation of this value (**$E_{0,0}$**) involves determining the energy at which the intersection of normalized symmetrical absorbance and emission spectra of the molecule occurs. **$E_{red}(cat/cat^{\bullet -})$**, the ground state reduction potential, can be obtained using cyclic voltammetry and is a measure of the ability of the molecule to act as an electron transfer agent in the ground state.

The driving force for a given photoinduced electron transfer reaction (**ΔG_{PET}**) can be calculated using both the *excited state* reduction/oxidation potential of a photoredox catalyst (**$E^*_{red}(cat/cat^{\bullet -})$** or **$E^*_{ox}(cat^{+\bullet}/cat)$**) and the *ground state* reduction/oxidation potential of a

potential electron transfer substrate (**(E^*_{red}(sub/sub$^{\bullet-}$)** or **E_{ox}(sub$^{+\bullet}$/sub)**) according to the equation below (example given for an excited state reductant):

$$\Delta G_{PET} = -\mathcal{F}(E^*_{ox}(cat^*/cat^{+\bullet}) - E_{red}(sub/sub^{\bullet-})$$

where $\mathcal{F}$ is the Faraday constant (23.061 kcal V^{-1} mol^{-1}). This approximation derived from the classical Nerst equation assumes contributions from solvent-dependent energy differences are insignificant, and as such an electrostatic work term is not included. The thermodynamic driving force for PET processes can be predicted based on the *ground state* oxidation or reduction potential of a substrate and the corresponding *excited state* reduction or oxidation potential of the light absorbing species. In even more general terms, an electron transfer between an excited state *oxidant* (**A**) and ground state *reductant* (**B**) is predicted to be thermodynamically favorable (i.e. $\Delta G_{PET} < 0$) when the excited state reduction potential of **A** is greater than the ground state oxidation potential of **B**. In this manner, a range of substrates which may be compatible with a given PET catalyst can be predicted based on electrochemical data alone.

1.3: Organic Photoredox Catalysts

Since the inception of modern photoredox catalysis in the late 2000s, beginning with seminal work of Nicewicz and MacMillan, polypyridyl complexes of iridium and ruthenium have been shown to serve as effective catalysts in an incredibly wide range of chemical transformations relying on the generation of odd-electron intermediates.[4,5] While versatile and efficient, the widespread applicability of these catalysts systems in industry is hampered by the high cost of relevant transition-metal precursors. In contrast, organic photoredox catalysts are lower in cost and, in many cases, can affect many of the same transformations as transition metal-based catalysts. Additionally, organic photoredox catalysts serve as more potent excited

state oxidants and reductants than many transition metal complexes, enabling the generation of otherwise inaccessible odd-electron intermediates (**Figure 1.1**).

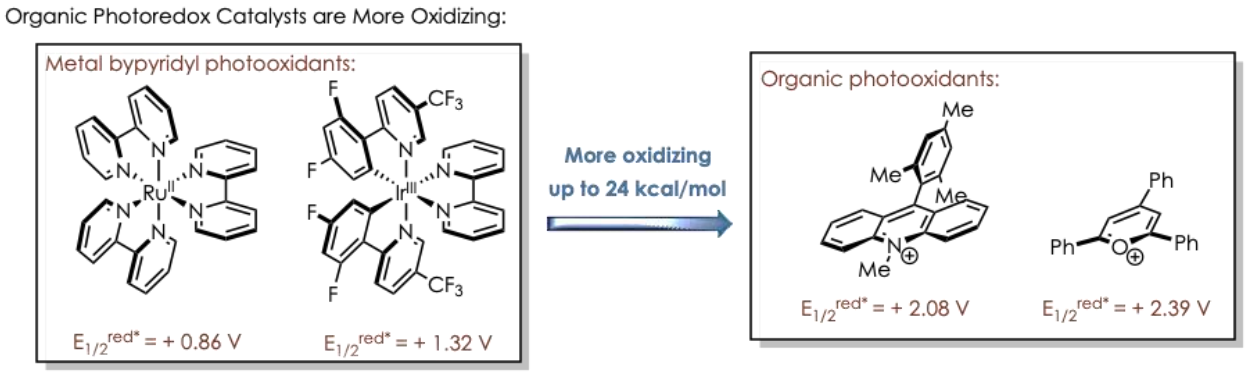

Figure 1.1: Comparison of excited state reduction potentials of organic and inorganic photoredox catalysts (potentials given vs. SCE)

Chapter 2 : GENERATION AND TRAPPING OF α-CARBAMYL RADICALS *VIA* ORGANIC PHOTOREDOX CATALYSIS

2.1: Introduction

Nitrogen-containing compounds are ubiquitous in modern organic chemistry. As of 2012, over 70% of FDA approved drugs contain at least one nitrogen atom.[6] Furthermore, the basicity and redox-active nature of nitrogen-containing compounds make them important scaffolds in agrochemical and materials sciences as well as in the synthesis of biologically active natural products. Some representative structures of molecules of these classes are given below (**Figure 2.1**). There are currently >3700 simple amine building blocks available from Sigma-Aldrich, making methodologies which harness simple amine reactants inherently broad in scope due to the wide commercial availability of requisite starting materials.

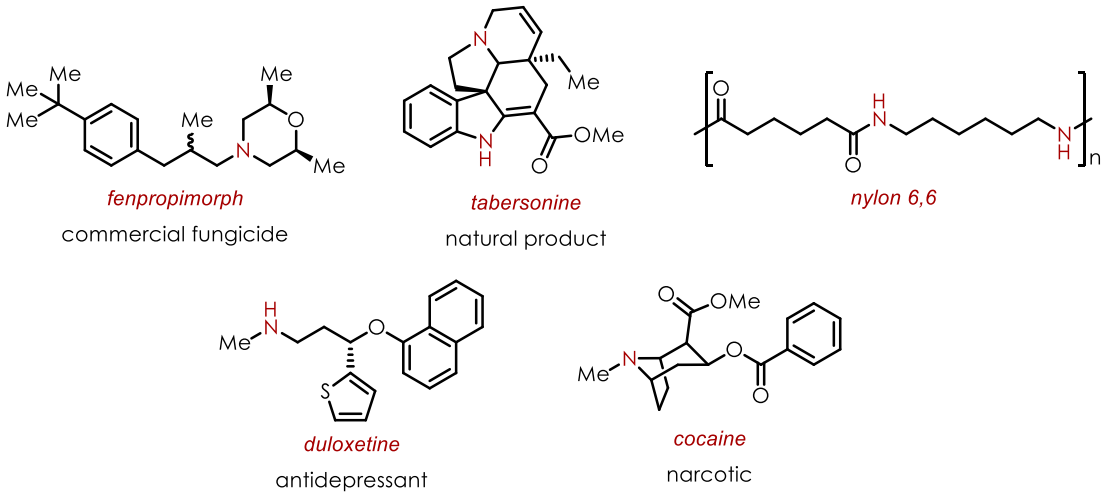

Figure 2.1: Important nitrogen containing compounds

Substituted saturated nitrogen heterocycle scaffolds are typically prepared *via* a *de novo* synthesis of the primary ring system of the heterocycle with a ring-forming step utilized as a final synthetic manipulation (**Figure 2.2**). Unfortunately, application of this method for the construction of more structurally elaborate heterocycles often requires lengthy synthetic manipulations to prepare the required acyclic starting materials. Previous methods have utilized double S_N2 displacement reactions, electrophilic cyclizations, and Wacker-type oxidative cyclizations to form these products from corresponding linear precursors.[7–9]

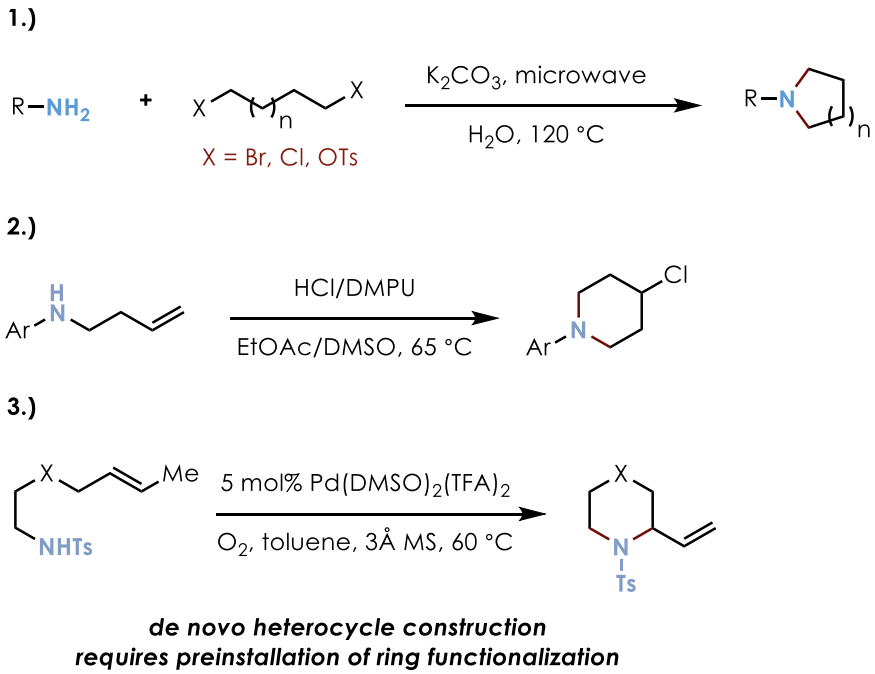

Figure 2.2: Ring closing methods for the synthesis of saturated nitrogenous heterocycles

Difficulties associated with the synthesis of complex cyclization precursors can be circumnavigated using methods which allow for the direct functionalization of the heterocyclic scaffold. Typical functionalization strategies which utilize cyclic amines include directed lithiation, transition-metal-catalyzed cross couplings, and electrochemical iminium generation. Following treatment with *sec*-BuLi/(–)-sparteine, Boc-protected amines are efficiently lithiated

in an enantioselective fashion, yielding products with modest levels of enantioselectivity following trapping with an appropriate electrophile (**Figure 2.3**).[10]

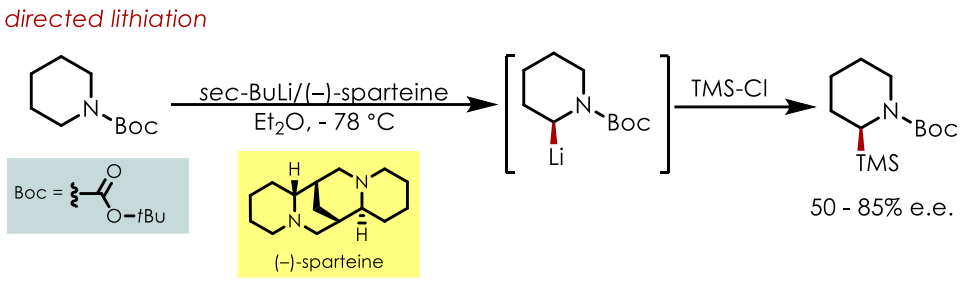

Figure 2.3: Enantioselective directed metalation of Boc-protected amines using *sec*-butyllithium and sparteine

While directed metalation methods are typically wide in the scope with respect to electrophilic partners, the use of harsh organolithium reagents makes the late-stage synthetic implementation of such a strategy intolerant towards more complex amine substrate containing base- or nucleophile-sensitive functional groups. Additionally, the manipulation of organometallic reagents requires the strict exclusion of both oxygen and water from the reaction mixture. As such, methods which enable amine functionalization under mild conditions offer more tolerant, alternative pathways to synthetically similar disconnections.

Aside from direct trapping with electrophiles, lithiated amines generated *via* directed metalation may serve as precursors to nucleophilic cross-coupling partners, such as organozinc reagents.[11] In the example below, enantioselective lithiation of Boc-pyrrolidines allowed access to the corresponding enantioenriched organozinc species upon exposure to zinc chloride. This intermediate can then be coupled with aryl bromides in good yields and enantioselectivities under Negishi-type conditions (**Figure 2.4**). Interestingly, potentially basic/electrophilic ketone substituents are well tolerated under the reaction conditions, indicating that the *in situ* generated

organozinc species is not sufficiently nucleophilic or basic to cause functional group incompatibilities in this case.

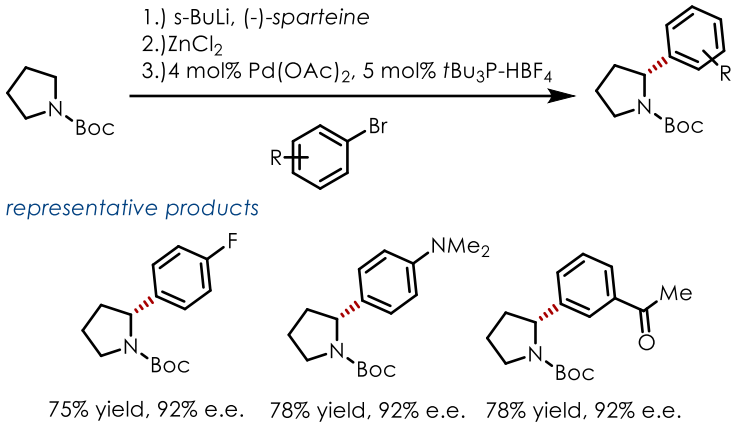

Figure 2.4: Tandem ortho-metallation/cross-coupling strategy for the synthesis of 2-substituted Boc-amines

There are many known electrochemical methods which exploit the oxidative generation and trapping of iminium ions from amines, ultimately leading to electrophilic behavior at the carbon atoms adjacent to the redox active nitrogen atom.[12–16] Alternatively, deprotonation of the presumptive intermediary amine cation radical leads to the generation of an α-amino radical, which are known to react in a nucleophilic fashion with electron deficient alkenes. Following a secondary reduction or hydrogen atom transfer step, α-alkylated products are accessible. Such strategies are generalized in the figure below (**Figure 2.5**).

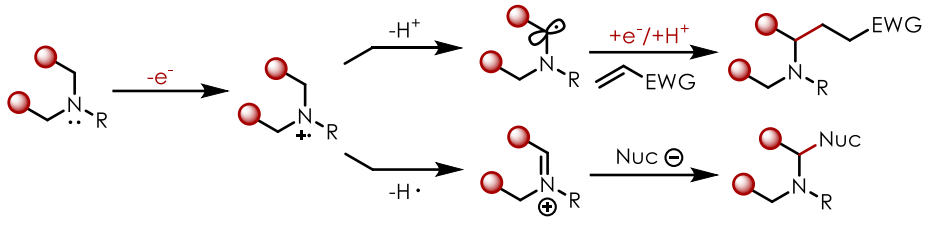

Figure 2.5: Single electron approaches to amine functionalization

While electrochemical methods remain useful for the generation of these families of reactive intermediates, recent research has shown photoredox catalysis can serve as a manifold through which analogous transformations are possible. In 2010, Stephenson and co-workers developed a formal Aza-Henry reaction of tetrahydroisoquinoline derived substrates catalyzed by $Ir(ppy)_2(dtbbpy)PF_6$ in the presence of irradiation from common household compact fluorescent lamps (**Figure 2.6**).[17]

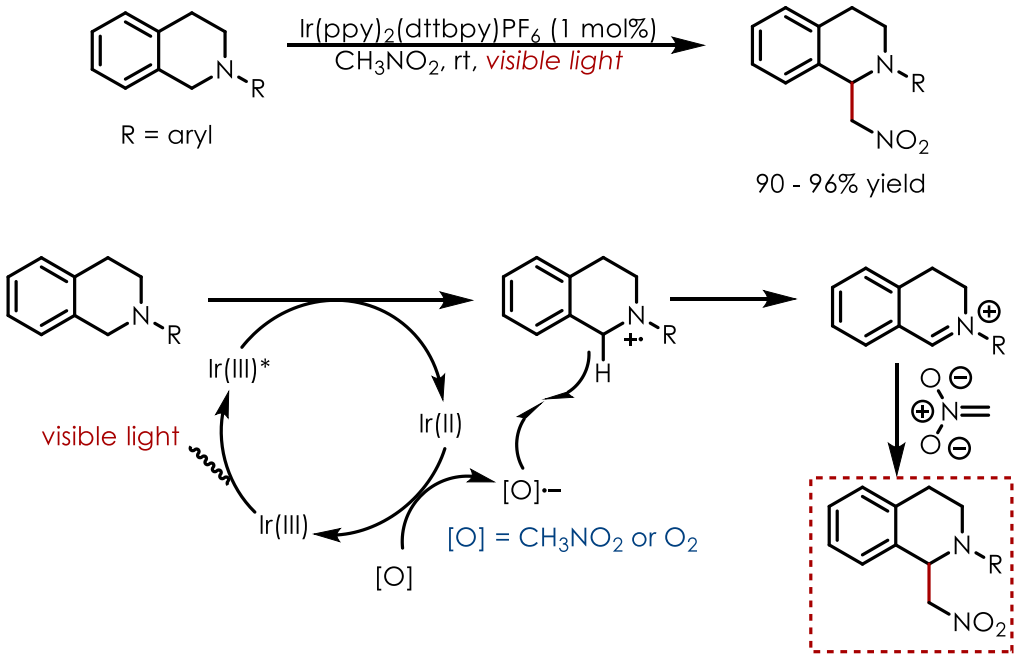

Figure 2.6: Photoredox Aza-Henry reaction developed by Stephenson and coworkers

Following excitation with visible light, the oxidizing excited state of the iridium catalyst undergoes a reductive quenching event with the tetrahydroisoquinoline starting material, leading

to the generation of a highly reducing Ir(II) species.[18] Either nitromethane or molecular oxygen may be reduced by the Ir(II) complex, regenerating the ground state photooxidant as well as a species (denoted as $[O]^{\bullet -}$ in the above scheme) which can abstract a hydrogen atom from the amine cation radical, generating the required iminium species. This iminium ion is then intercepted by nitromethane anion present in solution to yield the observed α-functionalized amine products.

Amino radicals may be generated by photoredox decarboxylation of α-carboxy amines, desilylation of α-trimethylsilyl amine cation radicals or direct deprotonation of amine cation radicals, among other methods which activate amines *via* direct hydrogen atom abstraction using organocatalysts. Photoredox catalysis has emerged as an efficient and mild method for the requisite single electron oxidation steps in these neutral radical generation processes.[19–25] Studies by Yoon, Mariano, and Rueping have demonstrated the generation of nucleophilic α-amino radicals from simple dialkylanilines utilizing iridium and ruthenium polypyridyl photoredox catalysts (**Figure 2.7A**). Similarly, the MacMillan group has reported the decarboxylative alkylation of alpha-carboxy amines facilitated by an iridium photoredox catalyst (**Figure 2.7B**).

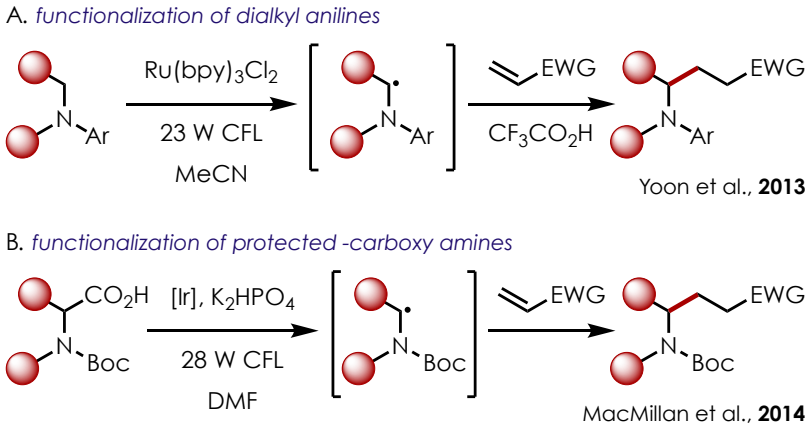

Figure 2.7: Previous methods for the generation of alpha-amino radicals using photoredox catalysis

However, the oxidation of the amine nitrogen by the excited state of these catalysts is only exergonic for amines containing n-aryl linkages, which typically have oxidation potentials between +0.5 and +1.0 V (vs. SCE).[26] This electrochemical requirement precludes the generation of α-carbamyl radicals from simple Boc-protected secondary amines using Ru- and Ir- containing catalysts due to the endothermicity of the requisite electron transfer steps, as the oxidation potentials of most Boc-protected secondary amines are >1.8 V vs. SCE. Additionally, while these previous methods provide straightforward routes to α-functionalized amines, the requirement of the n-aryl functionality may limit the downstream utility of these products. Our group has developed a wide range of both alkene hydrofunctionalization and arene C−H functionalization reactions utilizing acridinium-based organic photoredox catalysts. These transformations are enabled by the extremely potent photooxidant behavior of these types of catalysts. Depending on the substituents present on the acridinium core, acridinium-based photocatalysts possess singlet excited state reduction potentials ranging from +1.62 to +2.15 V vs SCE.[27] Additionally, the use of simple organic dyes as photoredox catalysts benefits from reduced cost, toxicity, and overall environmental impact compared to traditional transition metal-based photooxidants. We envisioned that oxidation of *N*-Boc-protected secondary amines, and subsequent generation and trapping of corresponding α-carbamyl radicals could be enabled by a strongly oxidizing photocatalyst of this type. Indeed, electron transfer between the excited state of acridinium **Mes-Acr-BF$_4$** and Boc-piperidine is predicted to be exergonic based on their corresponding redox potentials, while analogous electron transfer processes utilizing common iridium or ruthenium photoredox catalysts are predicted to be thermodynamically unfavorable (**Figure 2.8**).

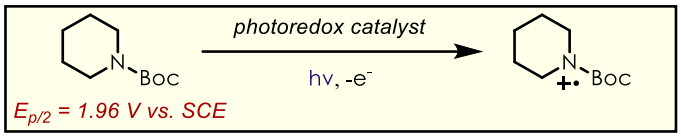

catalyst	E^*_{red}	ΔG_{ET}
$Ru(bpy)_3^{2+}$	+0.77 V	+ 27.4 kcal/mol
$Ir[dF(CF_3)ppy]_2(dtbpy)^+$	+1.21 V	+ 17.3 kcal/mol
Mes-Acr-BF_4	+2.15 V	- 4.4 kcal/mol

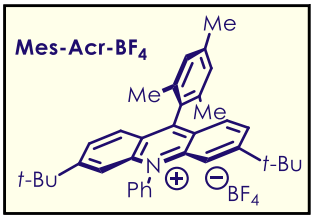

Figure 2.8: Calculated thermodynamics of electron transfer between Boc-piperidine and acridinium salt Mes-Acr-BF_4

2.1: Reaction Discovery and Optimization

Based on this information and previous work from our laboratory utilizing acridinium salt photoredox catalysts, we set out to develop a redox neutral C–H functionalization reaction of protected secondary amines facilitated by the catalytic generation of α-carbamyl radicals.

Reaction development began with the investigation of the reaction between an equimolar ratio of methyl vinyl ketone (**B**) and Boc-piperidine (**A**) in the presence of 5 mol% of an acridinium photooxidant under 450 nm LED irradiation in dichloroethane (DCE) under nitrogen. We anticipated that avoiding secondary alkylation of the amine substrate would be one of the main challenges associated with this process. While both the undecorated and 2,7-dimethyl-9-mesityl-*N*-phenyl acridinium tetrafluoroborate catalysts (Figure 2.9, **Catalyst A** and **Catalyst B**, respectively) gave < 5% yield of the desired monoalkylated product, use of the 3,6-di-*tert*-butyl-9-mesityl-*N*-phenyl acridinium tetrafluoroborate (Catalyst C/**Mes-Acr-BF_4**) afforded the desired product in 33% yield, as determined by GC-MS analysis, after a 20 hour reaction time **(Figure 2.9)**. This is in accordance with previous work from our group which identified this catalyst as a more robust variant of acridinium salt catalysts due to the increased steric bulk around the electrophilic acridinium ring system, blocking nucleophilic deactivation of the catalyst.

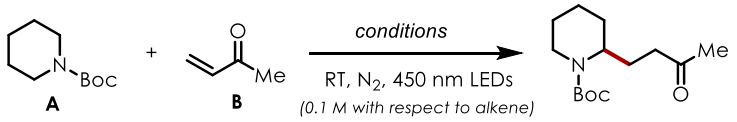

catalyst	solvent	time	yield	[A]/[B]
A	DCE	20 h	< 5 %	1:1
B	DCE	20 h	< 5 %	1:1
C	DCE	20 h	33 %	1:1
C	DCM	20 h	51 %	1:3
C	PhMe	20 h	12 %	1:3
C	$MeNO_2$	20 h	13 %	1:3
C	$PhCF_3$	20 h	5 %	1:3
C	$CHCl_3$	20 h	28 %	1:3
C	MeCN	20 h	29 %	1:3
C	DCM	20 h	57%	2:1
C	DCM	20 h	68 %	3:1
C	DCM	20 h	65 %	4:1
C	DCM	1 h	31 %	3:1
C	DCM	3 h	58%	3:1
C	DCM	6 h	79%	3:1
C	DCM	9 h	63%	3:1
C	DCM	12 h	71%	3:1

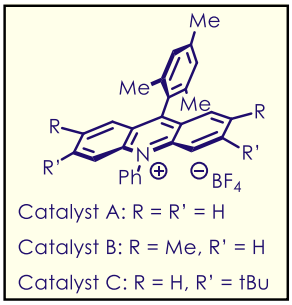

Figure 2.9: Initial reaction optimization and solvent screening

A small screen of solvents indicated that the use of dichloromethane (DCM) in the place of DCE gave a marginal increase in yield. Other solvents, such as trifluorotoluene ($PhCF_3$), nitromethane ($MeNO_2$), chloroform, toluene (PhMe), acetonitrile (MeCN), and CCl_4 led to diminished yields of product, even when increasing equivalents of methyl vinyl ketone, This type of strong solvent dependence has been observed for other transformations developed by our group that rely on acridinium catalyst systems.

Along with the desired monoalkylated piperidine product, a second GC-MS peak, corresponding to a mass matching that of the *bis*-alkylated product was observed for reactions that gave >20% yield. It was postulated that by increasing the equivalents of Boc-amine relative to methyl vinyl ketone or lowering the concentration, this secondary alkylation step may be outcompeted. Lowering the concentration (with respect to alkene reactant) in several increments ranging from 0.1 M to 0.025 M was found to have a negligible effect on product yields. However, inverting the stoichiometry from a 1:3 to a 3:1 ratio of amine to methyl vinyl ketone

gave a significant increase in yield of the desired monoalkylated product. Lastly, after monitoring product yield across a 24 hour period by GC-MS sampling, 6 hours was found to be the optimal reaction time, affording the desired product in 79% yield. Past this 6 hour point, higher order alkylation products become more prevalent, decreasing the overall yield of the desired product. To confirm that a form of product inhibition was responsible for these observations, several experiments were performed and are summarized in **Figure 2.10**.

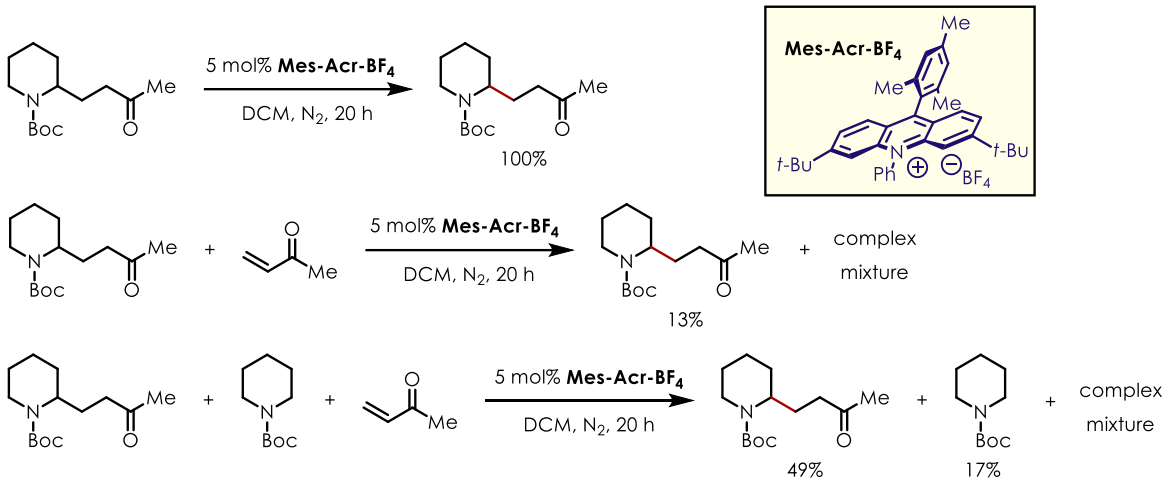

Figure 2.10: Product inhibition experiments

Subjection of the reaction product to the reaction conditions with no methyl vinyl ketone present lead to quantitative recovery of starting material, indicating that the product does not likely undergo any type of oxidative degradation. In the presence of 1 equivalent of methyl vinyl ketone, 87% of the desired product reacted further to afford a mixture of multiply alkylated products. Furthermore, the reaction between 1:1 ratio of Boc-piperidine and mono-alkylated product and 1 equivalent of methyl vinyl ketone gave only 49% of the desired product and 17% returned starting material, with multiply alkylated side products comprising the remaining mass balance. Together, these experiments indicate that the products of the reaction are competent substrates for further reaction and, additionally, react at rates similar to the rate of non-alkylated

starting material, giving complex mixture of products when using a 1:1 stoichiometry of amine and Michael acceptor.

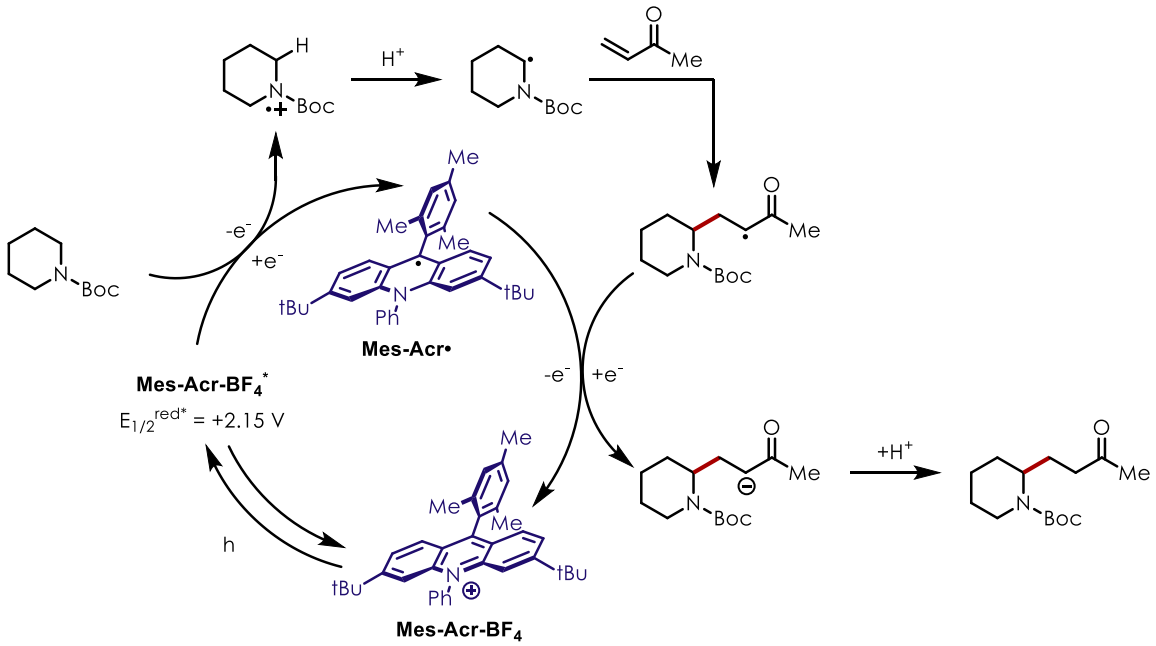

Figure 2.11: Proposed mechanism for the photoredox alkylation of secondary amines catalyzed by Mes-Acr-BF_4

While the mechanism for this process still requires further investigation, the reaction is believed to proceed through a mechanistic pathway analogous to previously reported transformations utilizing α-amino radicals (**Figure 2.11**). Upon excitation with visible light, the ground-state acridinium photooxidant, **Mes-Acr-BF_4**, is promoted to its highly oxidizing singlet excited state, **Mes-Acr-BF_4^***, which undergoes a single electron transfer step with Boc-piperidine**,** giving the corresponding carbamyl cation radical along with the reduced form of the catalyst, **Mes-Acr•**. After deprotonation of the resulting carbamyl cation radical, the generated α-carbamyl radical undergoes radical conjugate addition to the activated alkene to give an α-keto radical (in cases involving unsaturated ketone acceptors). To complete the catalytic cycle, the α-keto radical is then reduced by **Mes-Acr•** to give the corresponding enolate, which upon

protonation gives the desired product and the ground state catalyst, **Mes-Acr-BF$_4$**. Since a deprotonation step is required to generate the requisite α-carbamyl radical, the addition of a Brønsted base may accelerate this process. It also worth noting that, in previous studies of the photoredox-enabled radical additions of α-amino radicals, Brønsted and Lewis acids have been shown greatly accelerate the rate of α-amino radicals to electron poor alkenes in some cases.[19,22]

In contrast to studies by Yoon and coworkers, the addition of various Lewis and Brønsted acids were detrimental to the above reaction, completely shutting down the reaction in many cases.[22] Furthermore, the addition of Brønsted bases also led to diminished yields of the desired product (**Figure 2.12**).

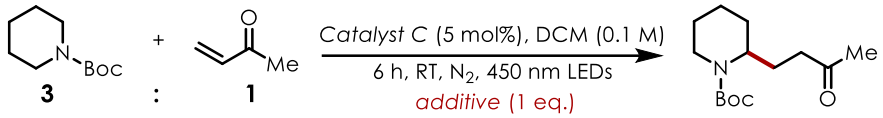

additive	yield
none	79 %
HCO_2H	33 %
$MeCO_2H$	42 %
TsOH	< 5 %
NH_4Cl	43 %
$NaBF_4$	36 %
$LiBF_4$	28 %
$Sc(OTf)_3$	< 5 %
$Zn(OTf)_2$	23 %
$Ce(OTf)_3$	12 %
2,6-lutidine	12 %
K_2CO_3	19 %
pH 9 buffer	21 %

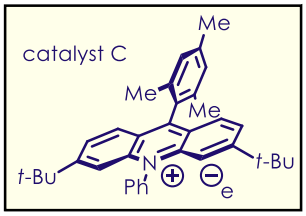

Figure 2.12: Effects of Lewis acids and Brønsted Acids and bases on reaction yield

Since secondary alkylation reactions of the product are kinetically competent with the desired pathway, the addition of these types of additives may accelerate secondary alkylation while simultaneously accelerating the desired reaction, leading to an overall diminished yield of mono-alkylated product.

2.3: Scope of Photoredox C–H Alkylation Reaction

After identifying the optimized reaction conditions, we set to explore the scope of this transformation (**Figure 2.13**).

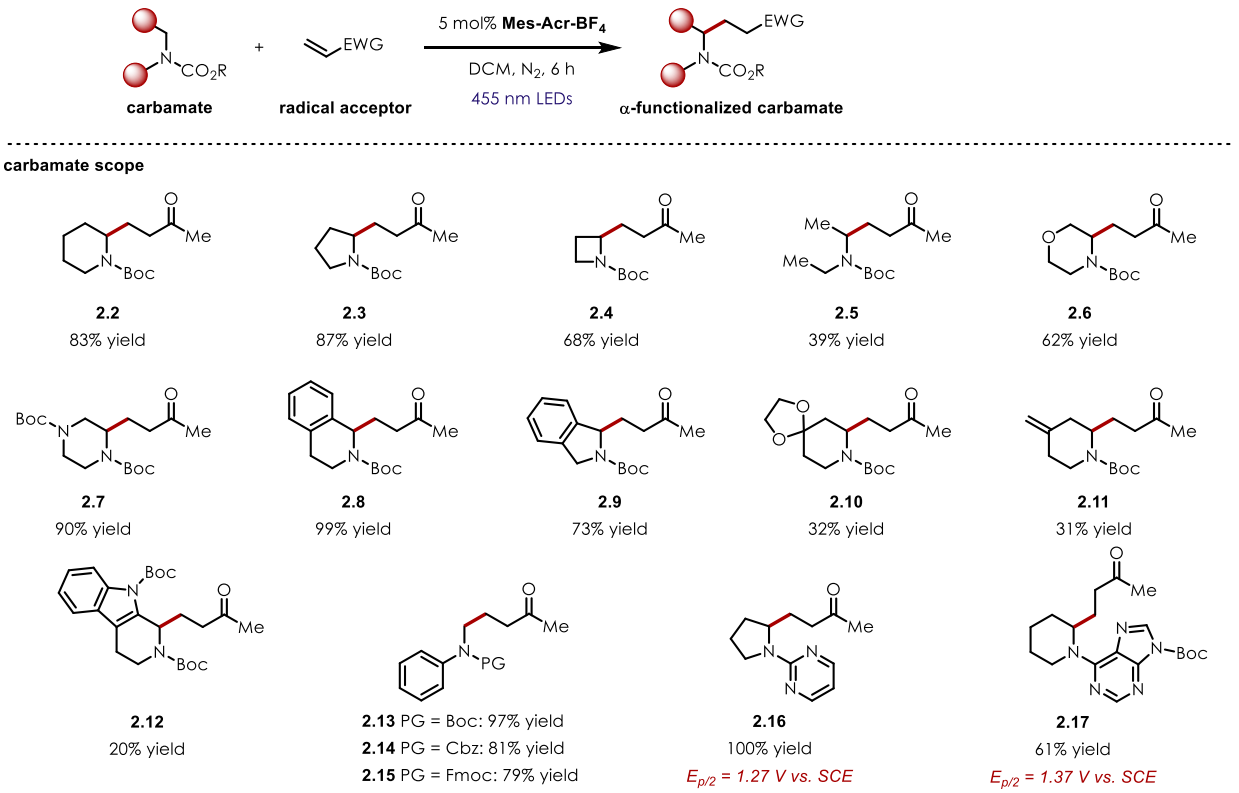

Figure 2.13: Carbamate scope of photoredox C–H alkylation reaction

N-Protected cyclic amines were shown to be compatible under these conditions with piperidine, pyrrolidine, and azetidine-based substrates being converted to the desired C−H functionalized adduct in good yields (**2.2**−**2.4**). The acyclic variant, *N*-Boc-diethyl amine was functionalized to give **2.5**, albeit in slightly diminished yield. Heteroatom-containing substrates, such as protected morpholine and *N*,*N'*-(*bis*)Boc-piperazine, were both converted to a single adduct, giving the desired products (**2.6**, **2.7**). In the case of **2.7**, no functionalization alpha to the oxygen atom was detected due to the ether functionality being well outside the redox window of typical acridinium photocatalysts.[26] Carbamates derived from benzylic secondary amines were

also efficient substrates, with *N*-Boc-isoquinoline giving **2.9** in excellent yield and *N*-Boc-isoindoline giving **2.9** in good yield. Other simple functional groups could be tolerated under these conditions. An acetal-bearing substrate was converted to **2.10** as a single product; similar to 6, no reactivity was detected at the C−H bonds α to the oxygen atoms. Olefins outside the oxidative range of **Mes-Acr-BF$_4$** were also tolerated, with no reactivity occurring at the typically labile allylic C−H bonds (**2.11**). The fused tetrahydropyridoindole was converted to **2.12** as a single regioisomer with functionalization occurring solely at the pseudobenzylic position. In addition to *N*-Boc protecting groups, other common carbamate protecting groups, such as carboxybenzyl (Cbz) and fluorenylmethyloxycarbonyl (Fmoc), were shown to perform similarly, acting as efficient protecting groups for this transformation (**2.13**–**2.15**). Other electron-withdrawing substituents were well tolerated under this manifold. n-Substituted pyrimidine and purine were also functionalized to give the analogous α-amino functionalized adduct in good yields (**2.16**, **2.17**).

At this point, the versatility of the radical acceptor was investigated (**Figure 2.14**).

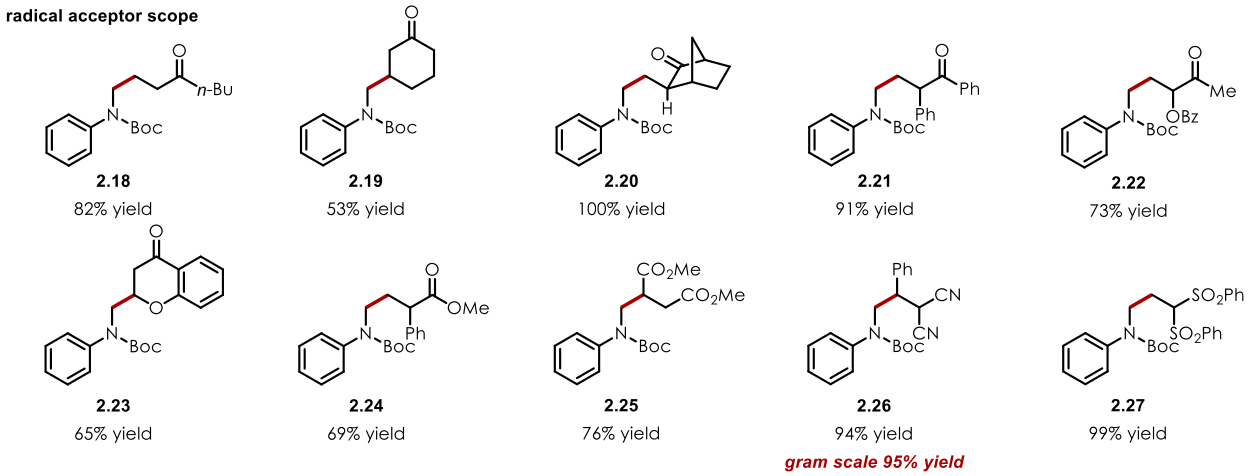

Figure 2.14: Scope of olefin radical acceptors in photoredox C–H alkylation reaction

Due to the efficiency of MVK as an acceptor in this sequence, we initially sought to utilize similar compounds while expanding the scope. Other simple aliphatic radical acceptors (**2.18**−**2.20**) performed well in this manifold, with **2.20** formed as a single diastereomer in quantitative yield. α-Functionality relative to the withdrawing group of the acceptors was well tolerated allowing access to compounds **2.21** and **2.22** in good yields. Similarly, β-substituted acceptors could be used in this reaction, with chromone giving the expected product **2.23** in good yield. The identity of the withdrawing group could also be altered, with methacrylate derivative and dimethyl fumarate giving the desired C−H functionalization adducts in good yield (**2.24**, **2.25**). Nitrile-bearing acceptors were also tolerated with benzylidenemalononitrile giving adduct **2.26** in excellent yield. Sulfonyl withdrawing groups could also be implemented under these conditions with compound **2.27** being formed in near quantitative yield. Additionally, compound **2.26** was prepared on gram scale using a photochemical flow reactor in 95% isolated yield, indicating that this transformation is amenable to scale-up under flow conditions.

More electron-rich aromatic and heterocyclic Boc-amines were not amenable to the desired transformation, with pyridine and thiophene containing substrates only giving trace amounts of alkylated products when subject to the optimized conditions using methyl vinyl ketone as an electrophile (**Figure 2.15A**). The electron-rich nature of these substrates may lead to a spin density that is localized in the aromatic pi-system, rather than the amine, disfavoring the formation of the requisite α-carbamyl radical. Furthermore, all attempts to affect an intramolecular alkylation using a tethered acrylate or enone (**Figure 2.15B)** failed, even in the presence of exogenous bases or acids.

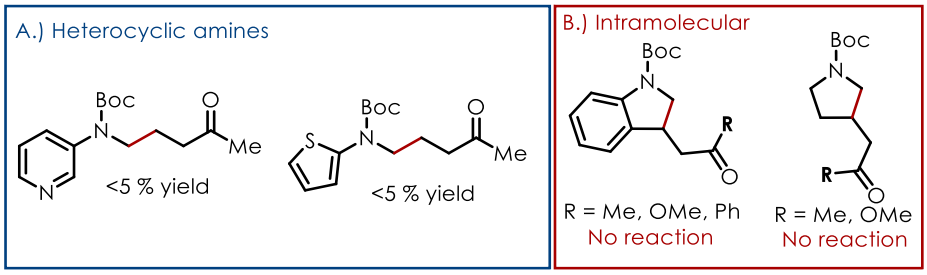

Figure 2.15: Problematic substrates and reaction modes

2.4: Mechanistic Studies and Application to Natural Product Synthesis

To determine the ultimate source of protons in this transformation, deuterium labeling studies utilizing *tert*-butyl (methyl-d_3)(phenyl)carbamate as the amine reaction partner were conducted. Following reaction of the deuterated amine with benzylidinemalononitrile under the optimized reaction conditions, 76% deuterium incorporation was observed at the presumptive site of protonation (**Figure 2.16C**).

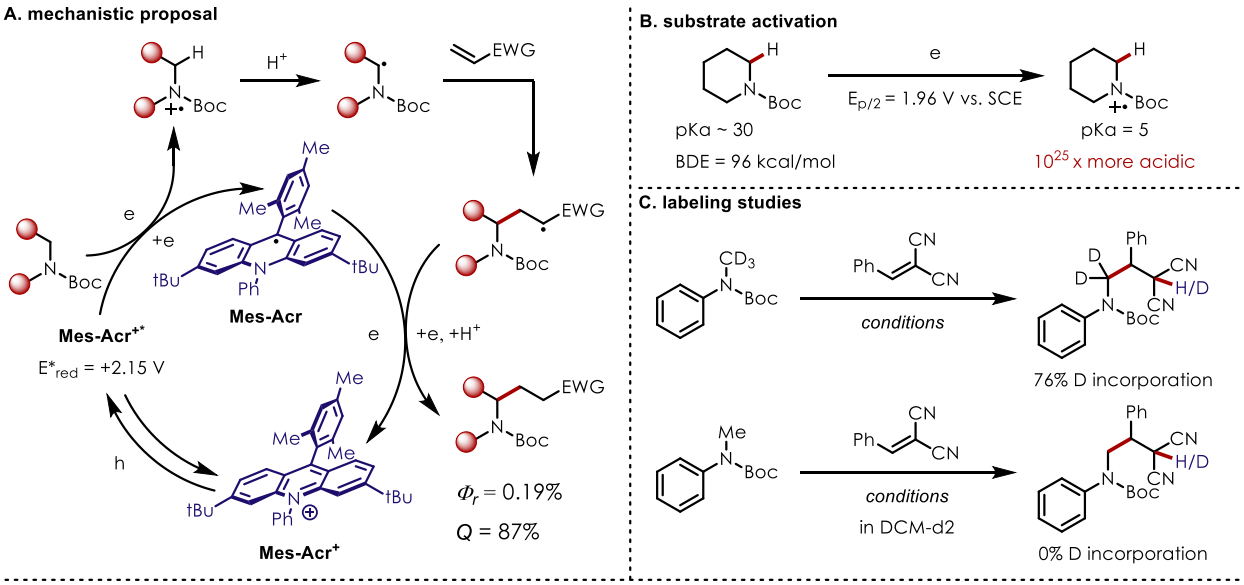

Figure 2.16: Proposed mechanism, mode of substrate activation, and deuterium labeling experiments

The small degree of hydrogen incorporation in the product is attributed to protonation from adventitious water during isolation. This result indicates that the carbamyl cation radical may ultimately serve as the source of protons in this system. This observation is in accordance with the greatly increased acidity of carbamyl cation radicals relative to the neutral parent amine (**Figure 2.16B**). A calculated bond dissociation energy of the α-carbamyl C−H bond in *N*-Boc piperidine, along with the experimentally determined redox potential were used to estimate the pKa of the amine cation radical, giving an estimated pKa of 5 (see appendix A for details of calculations).[28]

Furthermore, reaction of the analogous proteo-substrate in deuterated DCM resulted in 0% incorporation of deuterium, indicating that the solvent is not able to serve as a source of protons under the optimized reaction conditions. Stern−Volmer quenching studies of this system show the carbamate efficiently quenches the excited state of the acridinium photocatalyst (**Figure 2.17**).

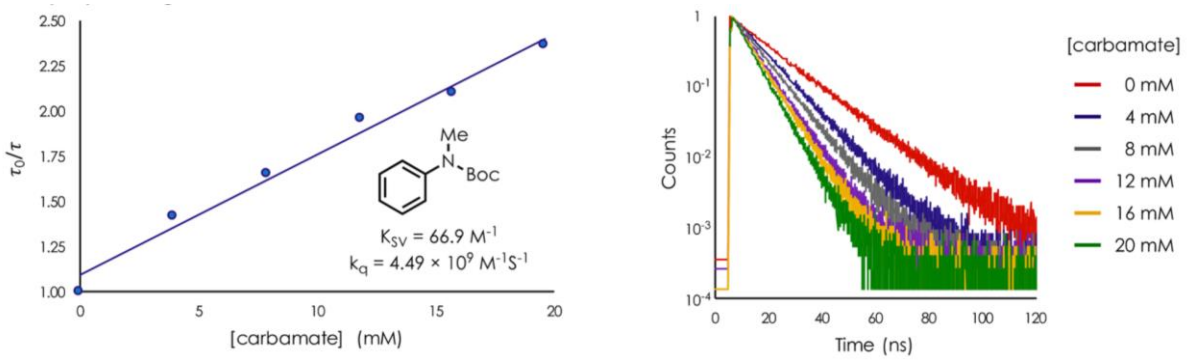

Figure 2.17: Stern-Volmer quenching experiments utilizing Mes-Acr-BF_4 and Boc-piperidine

In the absence of carbamate, the excited state lifetime of **Mes-Acr-BF$_4$** was measured to be 14.9 ns. Incrementally increasing the carbamate concentration to 20 mM gave a steady decrease in excited state lifetime to 6.3 ns (see appendix A for details). This result shows that the excited state of the acridinium catalyst is efficiently quenched by the carbamate substrate. The photochemical quantum yield (Φr) of the reaction between *N*-Boc-piperidine and methyl vinyl ketone to form compound 2 was determined to be 0.19 ± 0.03% (N = 2) with a quenching fraction (Q) of 0.87.[29] The low quantum yield and efficient quenching indicate that back electron transfer between the generated cation radical and the reduced form of the catalyst is a very prevalent process which is in competition with formation of the desired product. Though these values support the proposed mechanism, a slow, yet productive, chain mechanism cannot be completely ruled out. Lastly, we sought to probe the stereoselectivity of this reaction through the introduction of substituents on the piperidine core (**Figure 2.18A**).

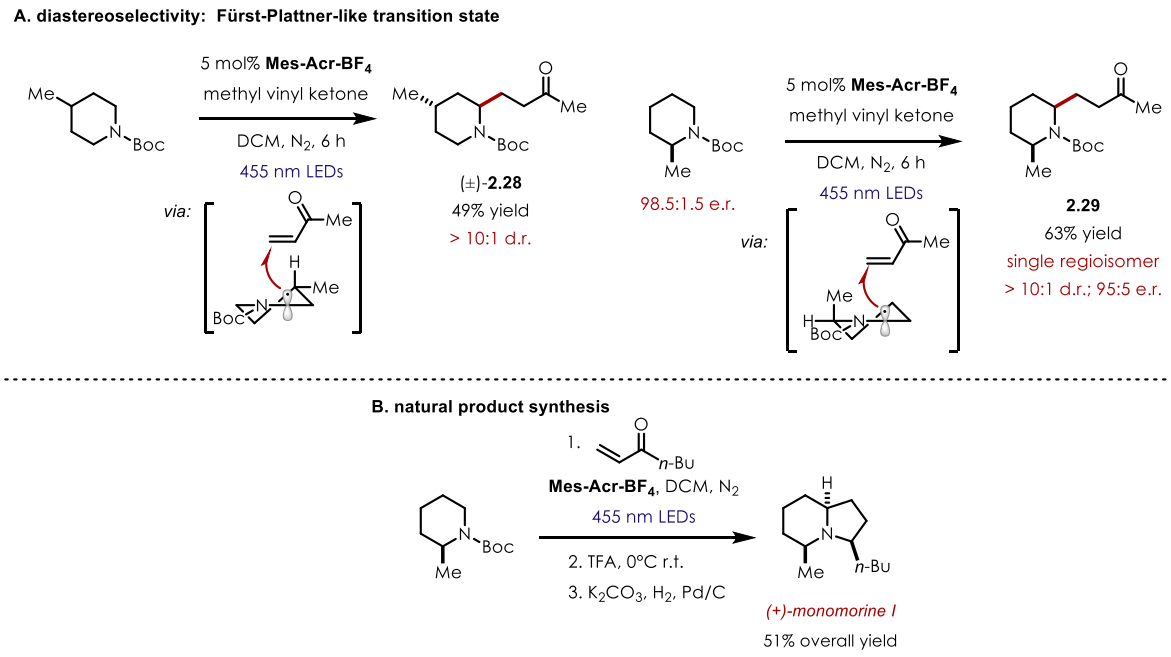

Figure 2.18: Diastereoselectivity in C–H alkylation reaction and application to natural product synthesis

Using 4-methyl *N*-Boc piperidine as the substrate afforded adduct **2.28** in high diasteroselectivity (>10:1). The stereochemical outcome of the reaction can be rationalized as proceeding through a pseudo-half-chair conformation of the radical intermediate akin to a Fürst-Plattner-type transition state model used for the rationalization of stereocontrol in cyclohexene-type systems.[30] Diastereoselectivity is ultimately controlled *via* a chair-like transition state (product development control). When enantioenriched 2-methyl-Boc-piperidine is reacted with methyl vinyl ketone, **2.29** is formed as a single regioisomer in high diastereoselectivity (>10:1) with minimal erosion of the C5-methyl stereocenter (see appendix A for experiments probing enantioerosion). A similar model also predicts the stereochemical outcome of this transformation. The 2-methyl group occupies the pseudo-axial position to minimize $A^{1,3}$ interactions with the equatorial carbamate group.[31,32] The diasteroselectivity of these transformations parallels the selectivity observed in nucleophilic addition to cyclic iminium species, which may be predicted using a similar stereochemical model.[33–36]

Additionally, the formation of **2.29** with syn-diastereocontrol underscores the complementarity of this methodology to previously reported lithiation/alkylation sequences, which favor formation of the analogous *anti*-diastereomer.[10] This result inspired us to pursue the total synthesis of the trail ant pheromone (+)-monomorine I (**Figure 2.18B**). The three-step synthesis began with the coupling of enantiopure *N*-Boc-2-methylpiperidine and butyl vinyl ketone, followed by a simple deprotection and reductive amination sequence to afford the natural product in 51% overall yield and good d.r. (Scheme 1B). In conclusion, we have developed conditions to selectively alkylate carbamates to afford elaborate secondary amines with easily removable protecting groups in up to quantitative yield. Using a photochemical flow reactor, this transformation is easily scalable with comparable yields to the analogous batch reactions.

Furthermore, the synthetic utility of this transformation is highlighted through an expedient enantioselective synthesis of indolizidine alkaloid monomorine I.

Chapter 3 : ANTI-MARKOVNIKOV HYDROAZIDATION OF ACTIVATED OLEFINS *VIA* ORGANIC PHOTOREDOX CATALYSIS

Reproduced in part with permission from Onuska, N. P. R.; Schutzbach-Horton, M. E.; Rosario Collazo, J. L.; Nicewicz, D. A. *Synlett.*, **2020**, *31* (1), 55 – 59. Copyright 2020 Thieme.

3.1: Markovnikov and Anti-Markovnikov Alkene Functionalization

One of the first reactions of alkenes encountered by students of organic chemistry is classical electrophilic activation, typically using diatomic halogens such as bromine. In this instance, the alkene initially reacts with the electrophile to form an intermediate bromonium ion. Addition of bromide as a nucleophile affords the difunctionalized product wherein a pi-bond has been broken and two new sigma bonds have been formed. The regioselectivity for this process is ultimately controlled by the relative positive charge density at each carbon atom in the bromonium ion. Due to hyperconjugative effects, ring opening of the bromonium occurs *via* nucleophile addition to the more substituted carbon center. When applied to the classical reaction of mineral acids with alkenes, the regioselectivity observed is known as “Markovnikov” selectivity (**Figure 3.1**). As such, reactions which formally result in the delivery of a nucleophile to the less stabilized position of an olefin are said to proceed with “anti-Markovnikov” selectivity.

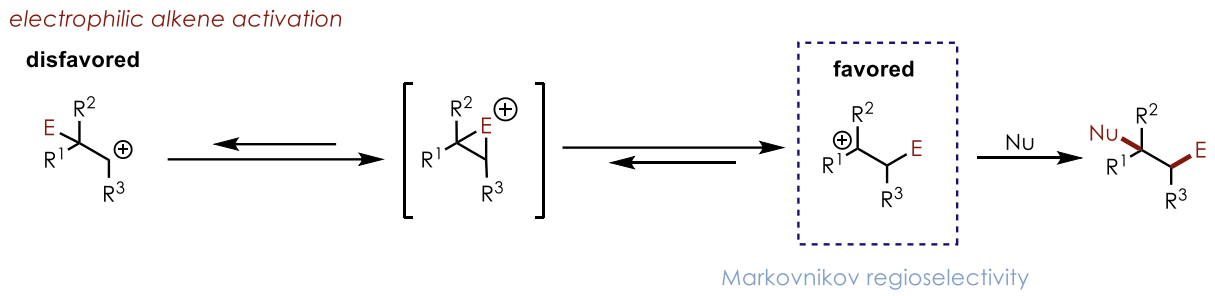

Figure 3.1: Electrophilic alkene activation with Markovnikov selectivity

Alkene cation radicals, intermediates formed *via* the one electron oxidation of a neutral alkene, possess dramatically increased electrophilicity relative to neutral alkenes.[37–41] As such, they are susceptible to nucleophilic trapping to generate a neutral radical species (in the case of an anionic nucleophile). The regioselectivity of this process is controlled by the stability of radical species which forms following nucleophilic addition. In most cases, this leads to the functionalization of alkenes in an *anti-Markovnikov* fashion (**Figure 3.2**).

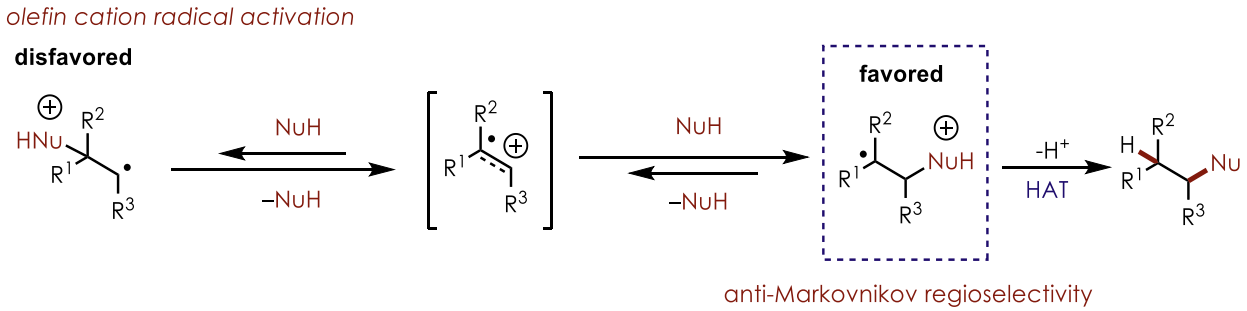

Figure 3.2: Nucleophilic addition to alkene cation radicals with anti-Markovnikov selectivity

Previous work from the Nicewicz group has leveraged the unique reactivity of alkene cation radicals to develop a wide variety of anti-Markovnikov alkene functionalization reactions based on the use of acridinium salts as catalytic, light-activated oxidants in combination with a hydrogen atom donor co-catalyst. This co-catalyst additionally functions as a catalytic oxidant

for the regeneration of the ground state catalyst species. Typical hydrogen atom donors include aryl and alkyl thiols and malononitrile derivatives. Through this general manifold, the group has published methods for the intra- and intermolecular hydroamination and hydrocarboxylation, hydroetherification, and anti-Markovnikov addition of mineral acids across oxidizable alkenes (**Figure 3.3**).[42–44]

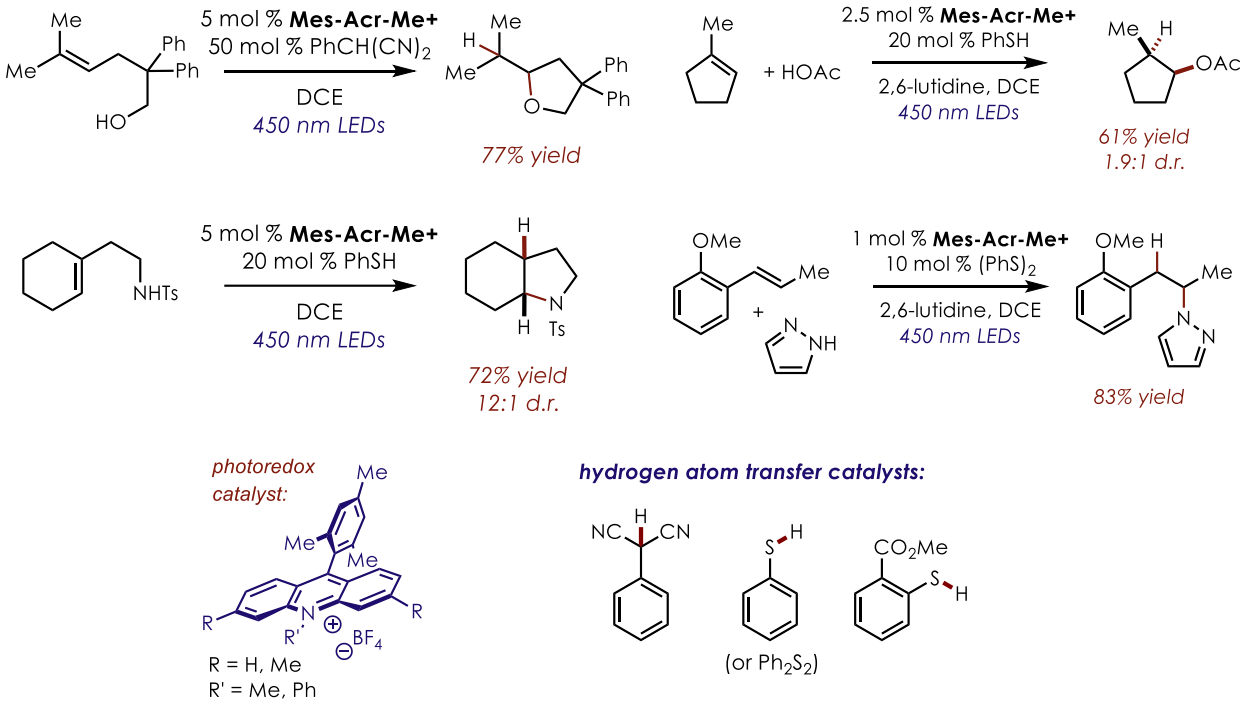

Figure 3.3: Anti-Markovnikov hydrofunctionalization reactions developed by the Nicewicz group utilizing acridinium photoredox catalysts

Based on this work and the known nucleophilicity of the azide anion, we believed that we may be able to achieve the formal anti-Markovnikov hydroazidation of alkenes under photoredox conditions in a similar fashion to these previously published methods.

3.2: Introduction to Organic Azides

The ubiquity of nitrogenous functional groups in industrially and medicinally important organic molecules cannot be overstated. Due to their known importance, the development of reactions which can introduce nitrogen-based functionality to a molecular scaffold has been a well-traversed area of research. Organic azides serve as versatile precursors to primary amines following a simple hydrogenation or Staudinger reduction. Outside of their utility as amine surrogates, the biological stability and diverse reactivity of azides has lead to the development of a variety of bioconjugation methods which hinge on so-called azide "click chemistry" – typically in the form of copper-catalyzed [3+2] Huisgen-type cycloadditions or Staudinger ligation processes (**Figure 3.4**).[45–49]

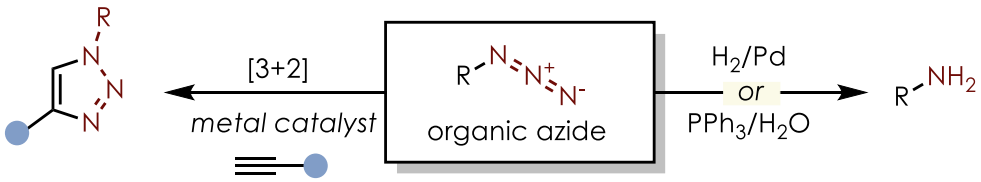

Figure 3.4: Utility of organic azides

Organic azides are typically prepared *via* S_N2–type substitution reactions, utilizing an inorganic azide source (often sodium azide) and a primary or secondary alkyl halide or by using Mitsunobu type conditions. However, this limits the scope of possible azide products to those that can be tracked to commercially available or synthetically viable alkyl halide/alcohol precursors. The direct reaction of hydrazoic acid (HN_3) with olefins is known, but often limited to substrates which produce stabilized carbocations following protonation and requires the use of excess HN_3.[50] Compounded with the well-documented hazards associated with the use of HN_3, including explosivity and toxicity, the direct reaction of alkenes with hydrazoic acid is a less practical solution to the preparation of organic azides in a small-scale laboratory setting.

Several transition metal-mediated and radical hydroazidation reactions have been reported in recent years. In 2005, Carreira and coworkers reported a hydroazidation reaction of simple unactivated olefins using an *in situ* prepared cobalt Schiff base complex in the presence of a substochiometric quantity of hydroperoxide oxidant, silane, and tosyl azide (**Figure 3.5A**).[51] While this method is mild and tolerant of a variety of functional groups, examples utilizing styrenes or other types of electron-rich olefin substrates are limited. Electrophilic nitrogen-centered azide radicals engage in anti-Markovnikov addition reactions with unactivated olefins (**Figure 3.5B**).[52–55] Azide radicals may be generated using hypervalent azido-iodine compounds in combination with a copper catalyst or photoredox catalyst, affecting the hydroazidation of simple olefins.[56,57]Xu and co-workers reported the generation of azide radicals using a benziodoxole organocatalyst in the presence of water and trimethylsilylazide ($TMSN_3$).[58] This reaction proceeds smoothly with a variety of mono-, di- and tri-substituted olefins bearing a number of potentially sensitive functional groups. However, more electron-rich olefins, including substituted and unsubstituted styrenes, enol ethers and enamines proved unreactive under the optimized conditions.

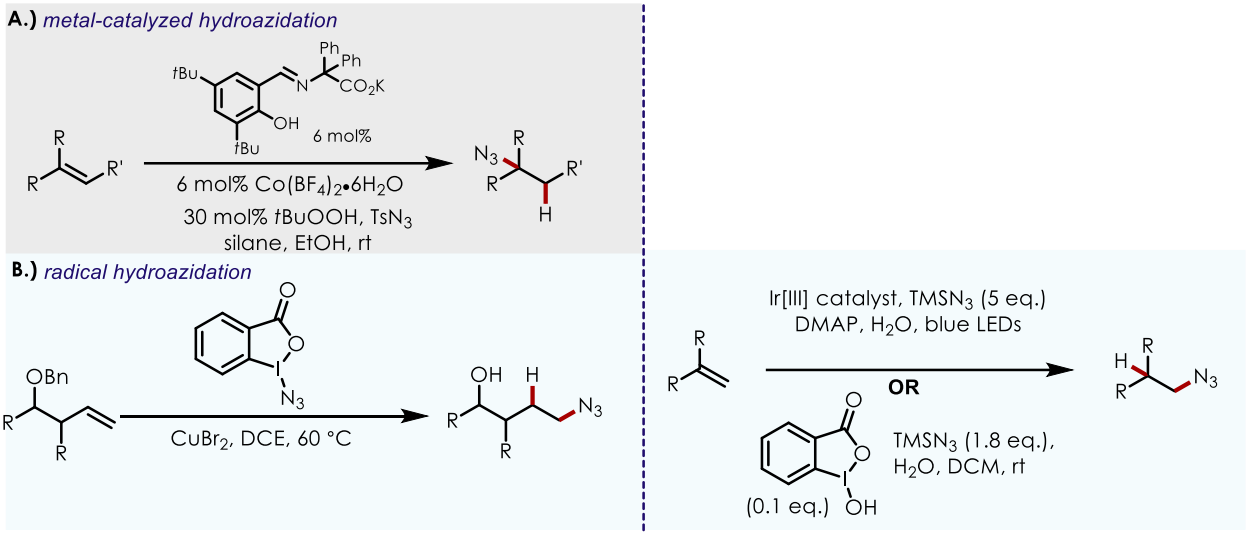

Figure 3.5: Modern methods for alkene hydroazidation

To our knowledge at the time of this work, methods for the direct anti-Marknovnikov hydroazidation of activated alkenes were unknown. As such, we sought to develop a hydroazidation reaction that would operate smoothly on these more electron-rich substrates. A methodology which would enable the hydroazidation of styrenyl substrates is particularly interesting due to the known biological activity of phenylethylamine derivatives.[59]

3.3: Reaction Discovery and Optimization

Based on previous work from our group focused on alkene hydrofunctionalization reactions, we envisioned that photoredox catalysis may be a useful tool to develop a methodology enabling the anti-Markovnikov hydroazidation of this class of substrates. Reaction development began utilizing indene as a substrate in the presence of 5 mol% of acridinium photooxidant **Mes-Acr-BF$_4$**, 20 mol% of diphenyl disulfide, and 2.0 equivalents of sodium azide in trifluoroethanol (TFE, 0.1 M), a solvent commonly employed in past reactions that was also thought to act as a proton source (**Figure 3.6**).

entry	azide source	co-catalyst	solvent	yield
1*	NaN_3 (2.0 eq.)	Ph_2S_2 (20 mol %)	TFE (0.1 M)	30%
2*	NaN_3 (2.0 eq.)	Ph_2S_2 (20 mol %)	MeCN (0.1 M)	N.R.
3	$TMSN_3$ (2.0 eq.)	TRIP-SH (20 mol %)	TFE (0.1 M)	75%
4	$TMSN_3$ (1.25 eq.)	TRIP-SH (20 mol %)	TFE (0.1 M)	**75%**

* = with 1.0 eq. $TBABF_4$, 5 mol% catalyst

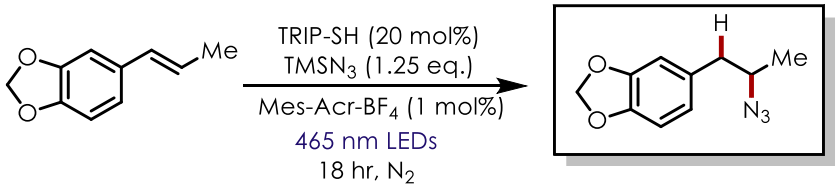

entry	solvent	yield
5	TFE:MeCN (9:1, 0.1 M)	91%
6	TFE:MeCN (7:1, 0.1 M)	79%
7	TFE:MeCN (3:1, 0.1 M)	75%
8	TFE (0.1 M)	**97%**

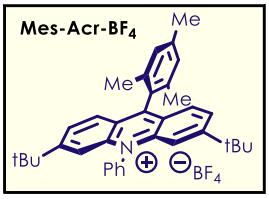

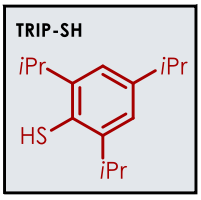

Figure 3.6: Optimization of anti-Markovnikov alkene hydroazidation reaction

Tetrabutylammonium tetrafluoroborate ($TBABF_4$, 2.0 equiv.) was added under the assumption that the tetrabutylammonium cation would serve as a phase transfer agent, helping to solubilize azide ions (**Figure 3.6, entry 1**). Following irradiation for 18 hours, the desired hydroazidation product was formed in 30% yield (by ^1H NMR using HMDSO as an internal standard). Along with the desired product, a nearly equal amount of the corresponding thiol-ene product resulting from addition of a thiyl radical formed *via* homolysis of diphenyl disulfide to the olefin was observed. When acetonitrile (MeCN) was used as the solvent under otherwise identical conditions, only returned alkene starting material was observed following irradiation. By exchanging the hydrogen atom transfer catalyst from diphenyl disulfide to the bulkier 2,4,6–triisopropylthiophenol (TRIP–SH), the desired product was formed in 75% yield with no

formation of thiol-ene byproducts. Further optimization showed that the loadings of acridinium photocatalyst and $TMSN_3$ could be lowered to 1 mol% and 1.25 equivalents, respectively, with no adverse effect on the yield of the hydroazidation product (**Figure 3.6, entry 4**). Interestingly, in a series of experiments utilizing various TFE/MeCN solvent mixtures and isosafrole as the substrate, the yield of the desired hydroazidation product decreased from 91% to 75% as the percentage of acetonitrile in the solvent mixture was increased from 10% to 25% (**Figure 3.6, entry 5-8**).

Previously reported spectroscopic investigations of the reaction between alkene cation radicals and various nucleophiles have demonstrated that hydrogen bonding and solvent polarity have profound effects on the rates of nucleophilic addition to these reactive species.[40,60] More specifically, previous work from the Schepp group has demonstrated that the addition of azide anion to alkene cation radicals is strongly affected by hydrogen bond attenuation of redox potentials. The kinetics of the reaction between styrene cation radicals and azide anion has been previously studied *via* flash photolysis transient absorption spectroscopy. In non-hydrogen bonding solvents, such as acetonitrile, azide ion (N_3^-) is oxidized by the alkene cation radical to yield azide radical ($N_3\cdot$) and the corresponding neutral alkene before productive nucleophilic addition can occur. The azide radical then quickly equilibrates with a second equivalent of azide ion to generate an inactive, non-nucleophilic $N_6^{\cdot-}$ radical anion dimer with an estimated equilibrium constant of ~200 M^{-1} (in MeCN) which is identifiable by an absorption centered at 700 nm.[61] However, when trifluoroethanol is used as the solvent, no absorption attributed to the formation of $N_6^{\cdot-}$ is identifiable. Following flash photolysis of TFE solutions of styrene derivatives in the presence of azide ion, an absorption maxima between 350-380 nm is observed, indicating the formation of a benzylic radical resulting from nucleophilic addition of azide ion to

the alkene cation radical.[41] Furthermore, the peak potential observed *via* cyclic voltammetry for oxidation of azide ion is shifted +0.5 V in TFE versus MeCN, indicating that hydrogen bonding is capable of dramatically attenuating the redox potential of this anionic species (E°_{peak} (MeCN) = 0.275 V vs. Fc, E°_{peak} (TFE) = 0.802 V vs. Fc). When reacted in TFE solution, the alkene cation radical is no longer able to oxidize the azide ion, and productive nucleophilic addition takes place. This previous work is in accordance with our observations during reaction optimization.

3.4: Scope of Photoredox anti-Markovnikov Hydroazidation Reaction

With optimized conditions in hand, the scope of this transformation with respect to alkene partners was explored (**Figure 3.7**). Beta-substituted styrene derivatives were found to be excellent substrates for this transformation, with β–methylstyrene affording the desired hydroazidation product **3.9** in 98% yield (*via* NMR, using HMDSO as an internal standard). Simple alkyl-, aryl-, and chloro- styrene derivatives were all smoothly converted to the corresponding secondary azide products in good yields (**3.11-3.14**). A variety of phenolic substrates were well-tolerated under the optimized reaction conditions, including those bearing benzoyl (**3.22**), benzyl (**3.24**), and silyl (**3.25**) protecting groups. Aromatic ester product **3.27** was isolated in 70% yield with no transesterification observed. A more oxidizable napthalene-derived substrate afforded the hydroazidation product in good yields as well (**3.26**). Substrates containing potentially labile benzylic C–H bonds were converted to the desired products in excellent yield and no functionalization was detected at these reactive C–H sites (**3.10, 3.17, 3.28**). Notably, a substrate containing a terminal alkene was converted to the anti-Markovnikov hydroazidation product **3.30** in 71% isolated yield with no functionalization of the unactivated alkene detected, highlighting the complementarity of this method to other known radical

hydroazidation reactions. Heterocyclic quinoline and thiophene substrates were functionalized to give the corresponding azide products **3.31** and **3.32** in 55% and 65% yield, respectively. Terminal styrene derivatives underwent the desired transformation in poor to moderate yields. Notably, diphenyl disulfide was identified as a more efficient hydrogen atom transfer catalyst than TRIP–SH for these substrates. Due to the lack of substituents in the *beta*-position, these styrenes are prone to oligomerization *via* radical mechanisms. To combat this, a less sterically hindered HAT catalyst must be employed to accelerate the rate of HAT versus oligomerization. Oxidizable vinyl ethers were also competent reactants, with products **3.6** and **3.7** isolated in 58% and 78% yield. Product **3.7** is formed following elimination of the tertiary alcohol in hydroazidation product of substrate **3.8** during chromatography.

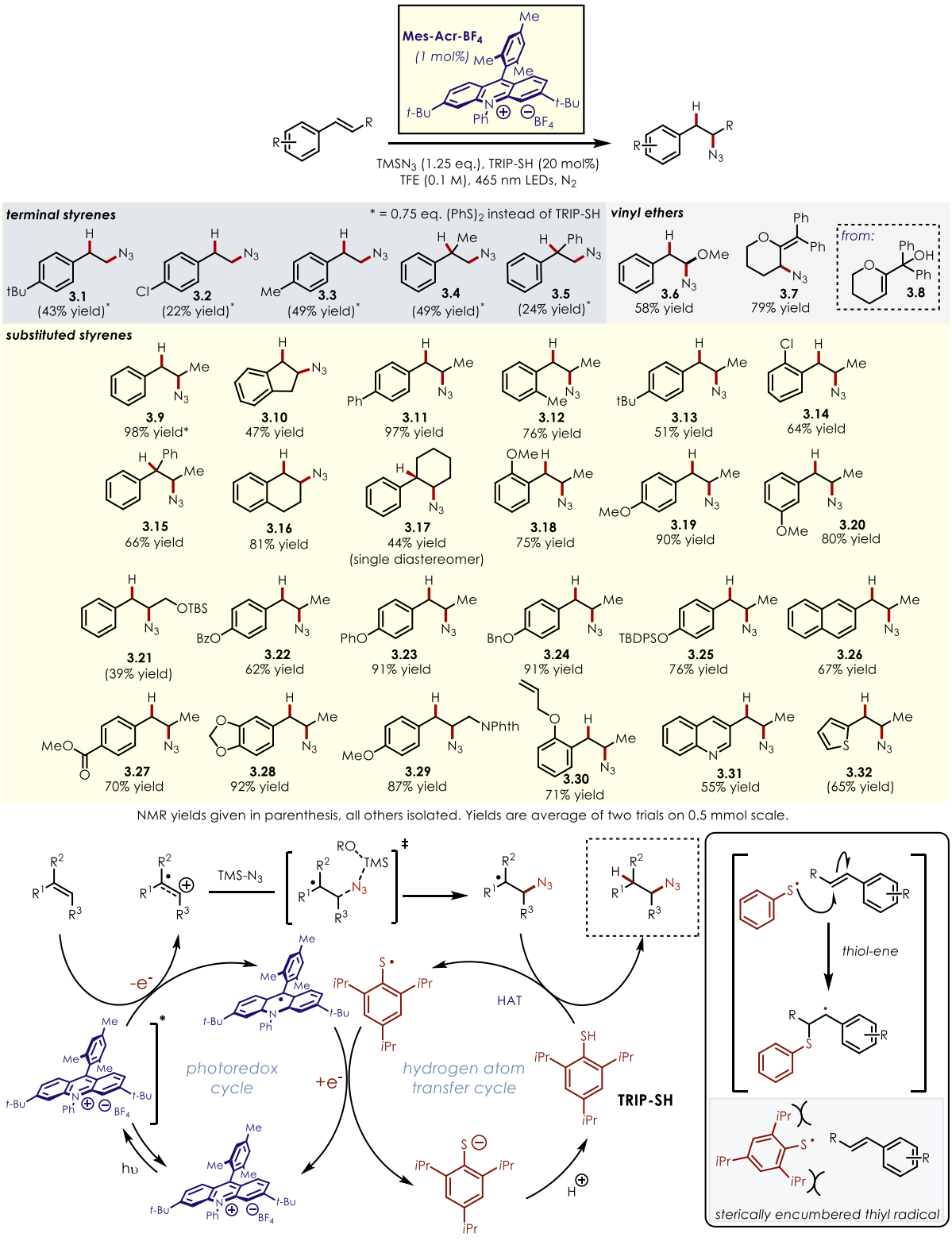

Figure 3.7: Scope of photoredox anti-Markovnikov hydroazidation reaction and proposed mechanism

3.5: Results and Discussion

Based on previous mechanistic investigations, the following mechanism is proposed: Following excitation by 465 nm light, the excited state of the acridinium catalyst engages in photoinduced electron transfer with the alkene substrate, yielding the corresponding alkene cation radical and the reduced form of the catalyst. Nucleophilic addition of azide ion to the alkene cation radical generates a neutral radical species. Based on our observations, it is not clear whether free azide ion is generated prior to addition to the alkene cation radical. It is possible that a termolecular transition state involving a solvent molecule-assisted desilylation/nucleophilic addition is operative or that an azide silicate species could be the nucleophile. However, it is likely that some free azide ion is in solution due to hydrolysis of $TMSN_3$ by advantageous water in the reaction mixture, as strict exclusion of water was not maintained. The benzylic radical engages in hydrogen atom transfer with TRIP–SH, generating the desired anti-Markovnikov hydroazidation product and a thiyl radical. This thiyl radical then oxidizes the reduced form of the catalyst, regenerating the ground state **Mes-Acr-BF_4** as well as a thiolate anion. This anion is then protonated by solvent to yield the starting cocatalyst and close the catalytic cycle.

In conclusion, we have developed an organic photoredox anti-Markovnikov hydroazidation reaction of electron-rich olefin substrates. By utilizing electrophilic cation radical intermediates, previously problematic hydroazidation reactions involving activated olefins now proceed efficiently and in high yields with low loadings of both photocatalyst and $TMSN_3$. Furthermore, the transformation proceeds in the absence of any transition metals using TMS–N_3 as the only stochiometric reagent.[26] This method fills a significant gap in the literature regarding alkene hydroazidation chemistry.

Chapter 4 : REGIOSELECTIVE ARENE C–H ALKYLATION *VIA* ORGANIC PHOTOREDOX CATALYSIS

4.1: Introduction to Arene C–H Functionalization

Aromatic rings are without doubt the most ubiquitous and fundamental building block in modern medicinal chemistry. A recent survey of drug molecules from large pharmaceutical companies determined that upwards of 99% of compounds examined contained at least one aromatic ring, underscoring the pervasiveness of this structural moiety in molecules of medicinal interest.[62,63] Of course, molecules which ultimately become targets of drug design campaigns are limited to structures accessible through chemical synthesis. A large portion of research conducted in organic chemistry in the past century has focused on the development of various reactions of aromatic rings. One of the most frequently cited examples of high impact research in this area is the development of aryl-aryl couplings based on palladium catalysis. The seminal work in this field was the subject of the 2010 Nobel Prize in Chemistry, which was awarded jointly to Richard F. Heck, Ei-ichi Negishi, and Akira Suzuki for their discoveries of a variety of palladium-catalyzed carbon-carbon bond forming reactions. In addition to aryl carbon-carbon bonds, a variety of carbon-heteroatom linkages are common in biologically active molecules, including C-N, C-O, and C-S bonds. To this end, the development of synthetic methods for the formation of these structures has been an active area of research, particularly in the fields of transition metal catalysis and organocatalysis. Classically, palladium catalyzed cross-couplings

function to couple an electrophile (often an aryl halide or pseudohalide, such as a sulfonate ester) and a nucleophile (often a boronic acid or organometallic species) in a catalytic manner. Following oxidative addition of an aryl halide/pseudohalide to a palladium(0) species, transmetallation of the nucleophilic partner furnishes a Pd(II)-*bis*-aryl complex, which undergoes reductive elimination to form the desired bond and close the catalytic cycle. While there are many commercially available aryl halide coupling partners, the prerequisite of these functional handles often limits the application of this method to molecules which can be purchased affordably or synthesized quickly. This detracts from the ability of these methods to modify late-stage pharmaceutical structures as the relevant cross-coupling handles must be installed and manipulated throughout the synthetic sequence towards the target. In contrast to this, work in recent years has focused on the development of reactions which result in the formal exchange of an aryl C–H bond for an aryl C-C or C–Heteroatom linkage – colloquially known as "C–H functionalization reactions". There have been several conceptual approaches to this idea utilizing a wide variety of chemistry, including transition-metal mediated reactions, radical reactions, and photoredox catalysis.

Transition metal-based approaches to aromatic C–H functionalization typically revolve around either the use of a directing auxiliary or substrate electronics and/or sterics as the controlling factor for reaction regioselectivity. Several examples which highlight this are given below **(Figure 4.1**).[64–66] Formal C–H insertions into aromatic C–H bonds are possible in the presence of a directing group, such as an amide (**Figure 4.1A**). In this case, an *in situ* generated aryl-Ni(II) species is able to undergo a directed metalation event to generate the Ni(II)-*bi*aryl species required for productive elimination. This process hinges on the ability of the carefully designed amide quinoline auxiliary, which directs the Ni(II) center to the nearby C–H bond and

lowers the energy for the metalation event required in the mechanism. In some cases, substrate sterics or electronics are sufficient to direct the relevant metalation steps with acceptable regioselectivity (**Figure 4.1B-C)**. Unfortunately, many modern synthetic methods for transition metal catalysed undirected aromatic C–H functionalization require the use of aromatic substrate in excess – a feature not desirable for application to the late-stage modification of high value molecules, such as drug intermediates.

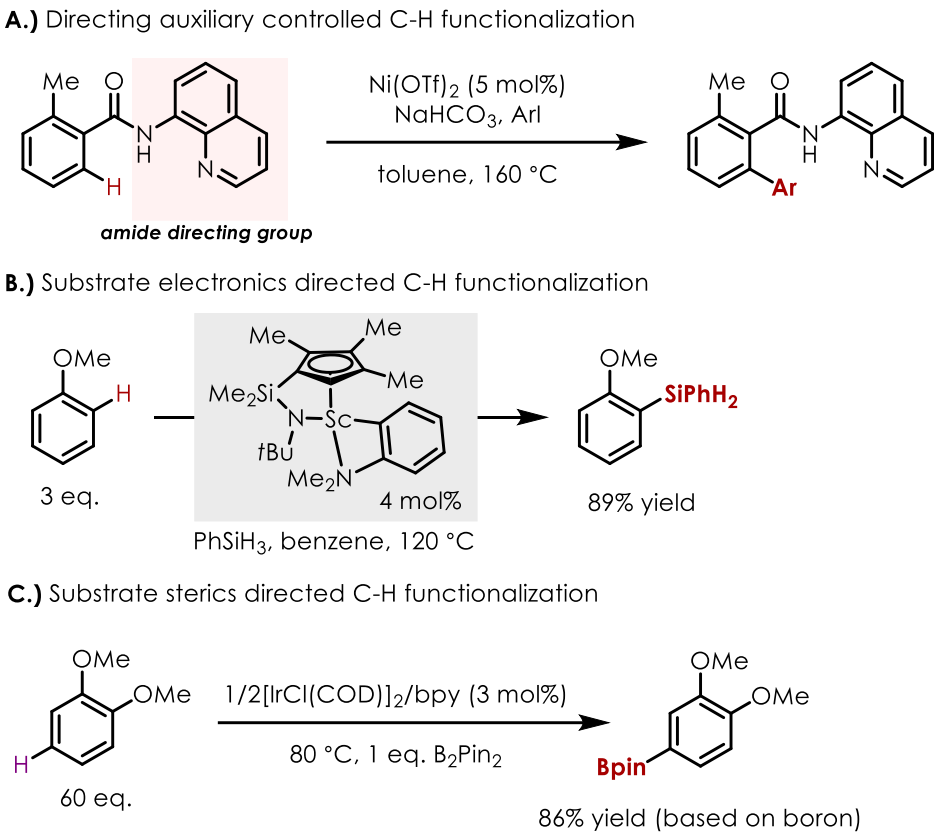

Figure 4.1: Approaches for aromatic C–H functionalization using transition metal catalysis

Compared to so-called "2-electron chemistry", radical reactions are typically tolerant of a wide variety of potentially sensitive functional groups and are thought of as less sensitive to steric hinderance due to the early transition states associated with radical reactions. Due to this, radical chemistry has been utilized in a wide variety of C–H functionalization reactions of

aromatics. One classical example of radical mediated radical aromatic C–H functionalization is the Minisci reaction, a process which results in the formal C–H alkylation of a aza-heteroaromatic substrate *via* radical addition to the aromatic pi-system.[67] In 2010, Baran and coworkers reported a persulfate/nitrate oxidant system which affects the formal C–H functionalization of heteroaromatics using boronic acids as radical precursors (**Figure 4.2**: Radical methods for aromatic C–H functionalization.[68] While this system benefits from the relatively mild reaction conditions, mixtures of regioisomeric products are obtained in many cases. Nagib and coworkers recently reported a stochiometric C–H functionalization of aromatics utilizing iodane oxidants in combination with strong acids.[69] Depending on the substrate utilized, the iodane oxidant can promote either the generation of electrophilic cation radicals, which are then trapped by nucleophiles, or the generation of highly electrophilic iodonium intermediates which affect formal C–H functionalization reactions of unactivated aromatics through an electrophilic aromatic substitution-type pathway.

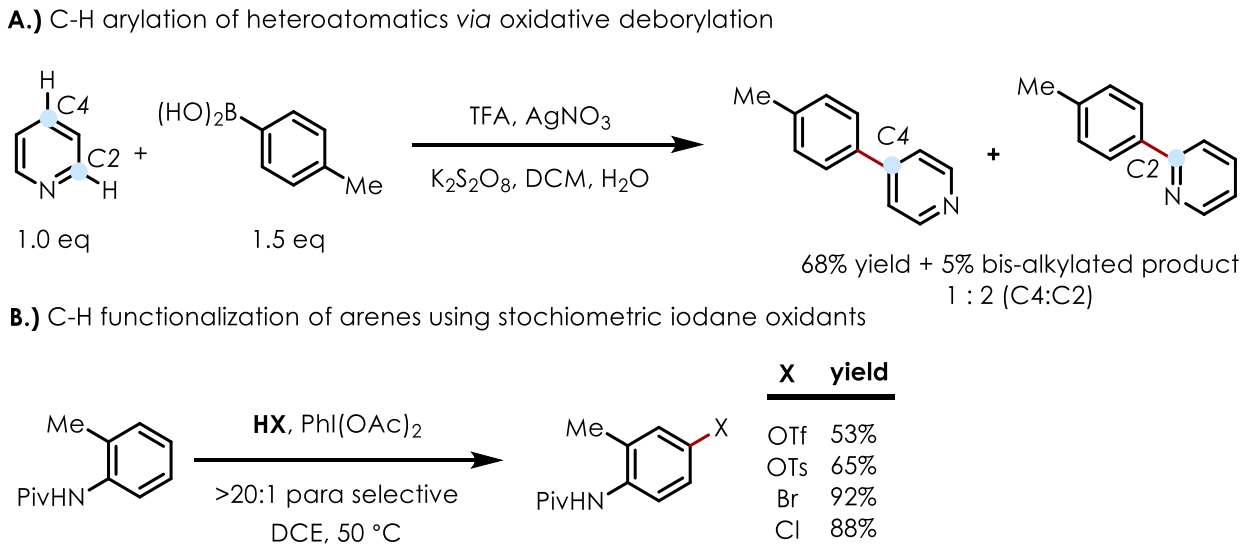

Figure 4.2: Radical methods for aromatic C–H functionalization

Although these methods are undoubtedly important, the use of stochiometric oxidant is often undesirable and can be problematic when scaling potentially exothermic reactions. Furthermore, reactions which utilize strong acids limit the applicability of these methods to more complex settings. As such, methods which can affect these transformations in a catalytic manifold and/or under more mild conditions may be desirable.

In recent years, photoredox catalysis has served as a valuable technology for the slow generation of highly reactive radical species. Through judicious selection of additives, radical traps, and reaction conditions, a wide variety of highly selective and efficient C–H functionalization reactions are now accessible utilizing photoredox catalysis.

One popular strategy has been the use of "redox-active" esters, which serve as neutral radical precursors following single electron transfer from an excited state photoredox catalyst. Stephenson and coworkers have developed methods for the C–H trifluoromethylation of unactivated aromatics *via* the single electron decarboxylation of pyridine n-oxide trifluoroacetate esters (**Figure 4.3**: Catalytic photoredox aromatic C–H trifluoromethylation). The resulting trifluoromethyl radicals undergo addition to the aromatic substrate, which upon single electron oxidation by the ground state of the catalyst and deprotonation affords the desired trifluoromethylated product. This method was also applicable to a wide variety of potentially sensitive pharmaceutical scaffolds, including those bearing base-, acid- and reductively labile groups.[70]

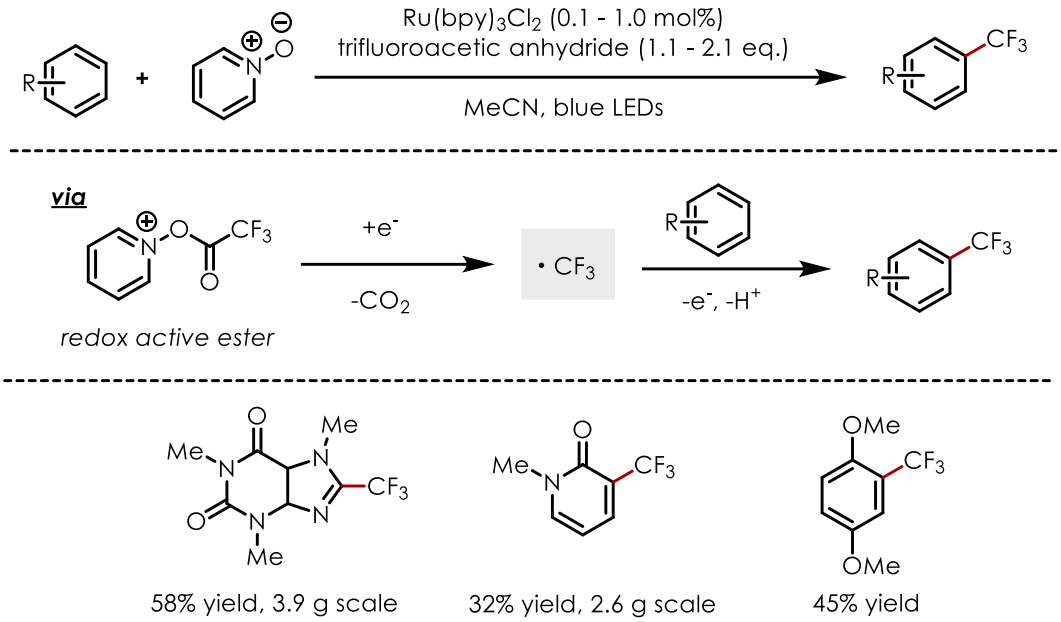

Figure 4.3: Catalytic photoredox aromatic C–H trifluoromethylation

Recently, Ritter and coworkers reported the regioselective synthesis of a variety of aryl sulfonium salts under electrophilic conditions. The corresponding sulfonium salts are able to serve as redox active precursors to carbon centered radicals, allowing for the formation of aryl radicals in this case.[71,72] In combination with an iridium photoredox catalyst and a stoichiometric amount of copper oxidant, these aryl sulfonium salts undergo fluorination in the presence of CsF to afford formal C–H fluorination products across this two-step sequence, highlighting the ability of photoredox catalysis to enable high-value transformations *via* the

formation of reactive intermediate radical species (**Figure 4.4**: Two-step formal aromatic C–H fluorination enabled by photoredox catalysis.

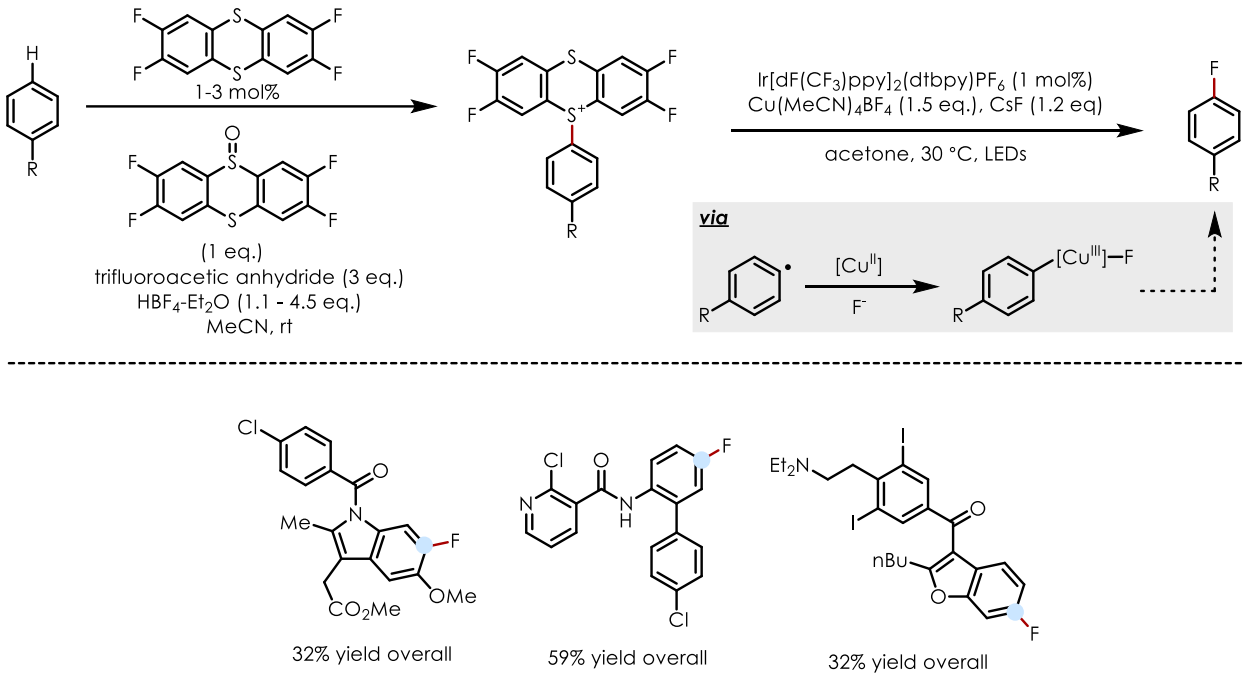

Figure 4.4: Two-step formal aromatic C–H fluorination enabled by photoredox catalysis

Photoredox catalysis has also successfully been applied in combination with a wide variety of transition metal catalysts to achieve tandem radical/organometallic reactions.[73] One well-studied manifold for C–H activation using palladium catalysis is the mechanism of concerted metalation-deprotonation (CMD). During this fundamental organometallic step a metal center, base, and a C–H bond engage in a 4-membered transition state involving C–H cleavage and C-metal bond formation to afford a new organometallic species without a change in metal oxidation state.[74,75] By designing reactions which are able to utilize both CMD and photoredox mechanistic aspects, advantages of both of these fields can be parleyed to achieve impressive reactivity. Sanford and coworkers utilized a combination of palladium acetate and common photoredox catalyst $Ru(bpy)_3Cl_2$ to affect the formation C–H arylation of directing group-equip aromatics.[76] Following a metalation event to form an aryl palladium (II) species, enabled by

coordination of a directing group to the palladium (II) center, an aryl radical, generated *via* photoinduced electron transfer between the excited state ruthenium catalyst and the aryl diazoacetate present in solution, is thought to add to the metal center, generating a new palladium (III) species. A thermodynamically favorable ground state electron transfer between the oxidized ruthenium (II) complex and the palladium (III) biaryl complex affords a palladium (IV) species which is primed to undergo reductive elimination to afford the desired product and reform both starting catalytic species (**Figure 4.5**).

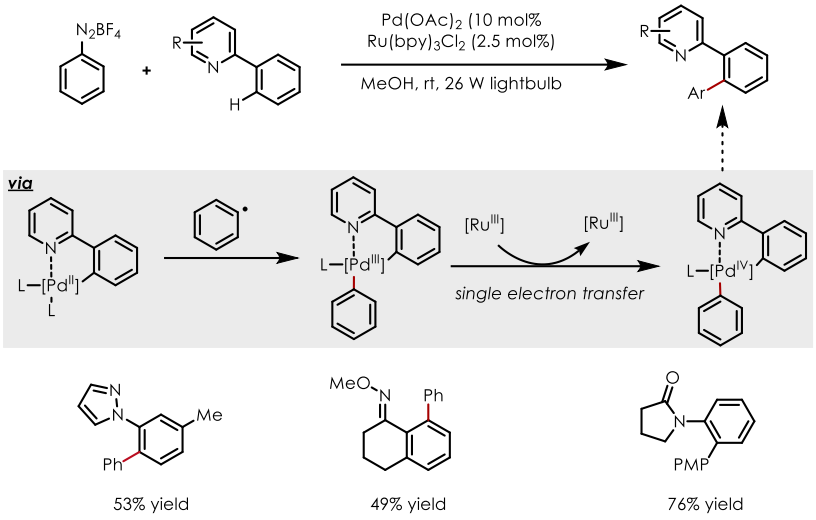

Figure 4.5: Cooperative palladium/ruthenium catalyzed aromatic C–H arylation

Taken together, these examples highlight the wide variety of methods available for the C–H functionalization of aromatic substrates. Although an abundance of new methods have been reported in recent years, many are still hindered by the use of high catalyst loadings, use of excess substrate or coupling partner, and the requirement for directing groups or harsh reaction conditions.

4.2: Introduction to C–H Alkylation Reactions Involving Diazoacetate and Diazoacetate Derived Intermediates

Metallocarbenes are reactive organometallic species which may be generated using a transition metal precursor and diazoacetate derivatives.[77–79] The resulting metallocarbene intermediate may then undergo C–H insertion with reactive C–H bonds (often aryl or alkyl), affording the corresponding alkylated adducts. However, due to the high reactivity of metallocarbenes, aromatic substrates are often required to be present in excess for efficient reactivity. Furthermore, products consisting difficult to separate mixtures of C–H insertion of Buchner ring expansion products are common in these systems (**Figure 4.6**).[78,80]

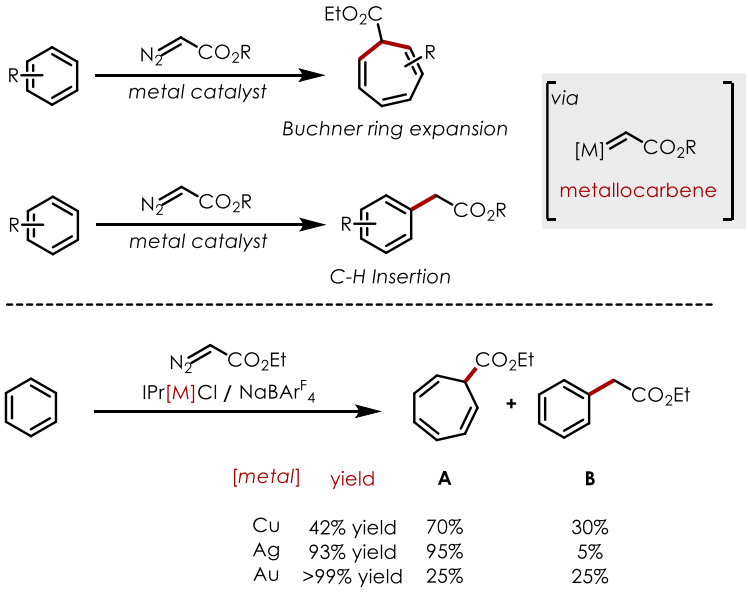

Figure 4.6: Buchner ring expansion and C–H insertion products resulting from metallocarbene reacting with aromatic substrate

Among methodologies based on metallocarbene C–H insertion that do not use several-fold excess of arene, directing groups are often required. Fox[81] and Wang[82] have reported ortho-selective C–H functionalization of heterocycles using diazoacetates. In addition, other directing groups such as purines,[83] azacycles,[84] disubstituted anilines,[85] and phenols,[86] have been utilized in metallocarbene C–H alkylation reactions. Collectively, these directing groups

limit the synthetic applicability of metallocarbene C–H alkylation reactions as they require the pre-installation of functional groups which must later be excised from the target molecule, provided they are not part of the desired final structure.

4.3: Photoredox Catalysis and Diazoalkanes

Recently, Suero and coworkers reported the synthesis of aryl diazoacetate derivatives under photoredox conditions.[87] During the course of this work, it was noted that photolysis of aryldiazoacetates with blue LEDs yields free carbene species that undergo cyclopropanation reactions in the presence of styrene. Subsequently, Davies and coworkers investigated the reactivity of similar photogenerated free carbenes in combination with electron-rich aromatic substrates and alkenes.[88] In these cases, either cyclopropanation or formal C–H insertion was observed. However, the scope of this transformation is specific to aryl diazoacetates and a small number of arene coupling partners (which must be present in excess). This is largely due to the highly reactive nature of free carbenes, which readily undergo C–H insertion reactions with acidic C–H, O-H, and n-H bonds. The products of reaction with solvent are also typically observed in these cases. Due to these factors, C–H functionalization methodologies that rely on the intermediacy of carbenes can be incompatible with certain functional groups and low levels of regiocontrol are often observed.

In recent years, photoredox catalysis has served as the conceptual basis for a number of powerful aromatic C–H functionalization reactions.[89–91] Our group has previously reported arene C–H amination and cyanation methodologies which utilize acridinium salts as organic photoredox catalysts.[92,93] These methods rely on the catalytic generation of aromatic cation radicals via photoinduced electron transfer (PET) between the aromatic substrate and the excited acridinium catalyst. We sought to probe the reactivity of nucleophilic diazoacetates in combination with

electrophilic aromatic cation radicals, as reactions of this type have not been investigated to date. Such transformations would be reminiscent of known metallocarbenoid insertion reactions, while taking place in the absence of metals or superstoichiometric quantities of substrate. Furthermore, previous work from our group has shown moderate to excellent regioselectivity in nucleophilic additions to aromatic cation radicals. The observation of comparable levels of regioselectivity in the addition of diazoacetate derivatives would represent a major improvement over current aromatic C–H functionalization methodologies utilizing metallocarbene/carbene intermediates (**Figure 4.7**: Generalized scheme of proposed photoredox reaction and comparison to prior art). Such a reaction would also be mechanistically distinct from recent work published by Gryko which relies on the generation and alkylation of alpha-keto radicals from diazoacetate derivatives using photoredox catalysis.[94]

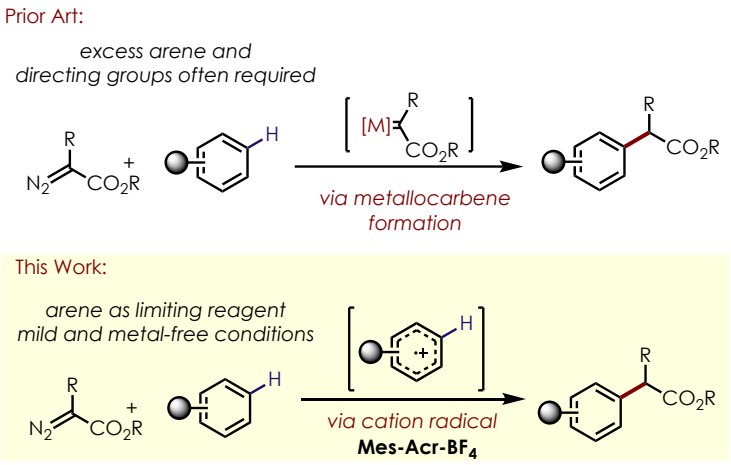

Figure 4.7: Generalized scheme of proposed photoredox reaction and comparison to prior art

Here we report a method for C–H functionalization reactions of arene cation radicals with diazoacetate derivatives generated via organic photoredox catalysis. Computational and

experimental studies support a unique mechanism involving cation radical-meditated aromatic cyclopropanation followed by oxidative ring opening. These results demonstrate the utility of arene cation radicals as versatile intermediates for the construction of carbon-carbon bonds *via* organic photoredox catalysis.

4.4: Reaction Discovery and Optimization

Reaction development began using mesitylene as a substrate and ethyl diazoacetate as a nucleophile in the presence of 5 mol% **Mes-Acr-BF$_4$** under irradiation from 465 nm LEDs. Following a screen of common solvents, a 1:1 mixture of trifluoroethanol (TFE) and acetonitrile was identified as a suitable medium for the reaction. With one equivalent of ethyl diazoacetate in a 1:1 TFE/acetonitrile solvent mixture, the desired C–H functionalized product **4.1a** was isolated in 76% yield (**Figure 4.8**). In some cases, secondary alkylation of the desired product was observed as a minor byproduct at increased ethyl diazoacetate loadings (>2.0 equiv.). Increasing diazoacetate loadings between 1.0 - 2.0 equiv. did not result in a significant increase in yield, presumably due to competitive oxidation of the product of the reaction.

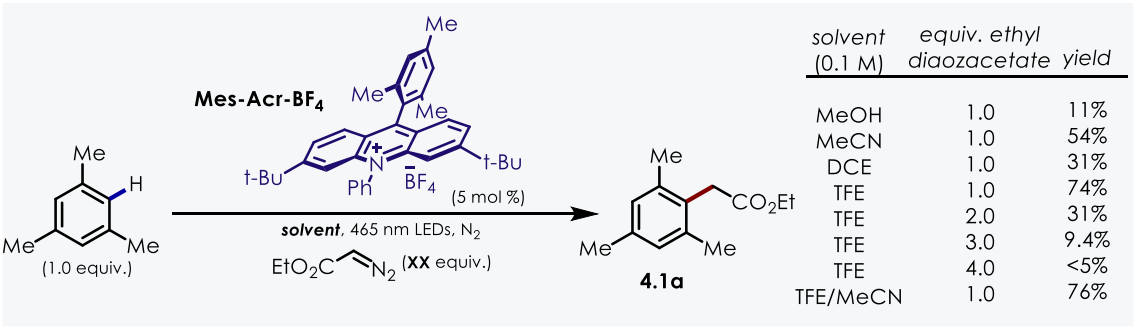

solvent (0.1 M)	equiv. ethyl diaozacetate	yield
MeOH	1.0	11%
MeCN	1.0	54%
DCE	1.0	31%
TFE	1.0	74%
TFE	2.0	31%
TFE	3.0	9.4%
TFE	4.0	<5%
TFE/MeCN	1.0	76%

Figure 4.8: Initial optimization of photoredox C–H alkylation reaction

Control experiments indicated both irradiation and **Mes-Acr-BF$_4$** are required to observe the desired reactivity. Additionally, the addition of various known metallocarbene precursor complexes of rhodium and copper failed to accelerate the reaction or enable the reaction under

irradiation, indicating that trace metals are not responsible for the observed reactivity. Ethyl diazoacetate additionally showed little to no decomposition under the reaction conditions, indicating that direct formation of carbene from ethyl diazoacetate is unlikely. With optimized conditions in hand, the scope of the transformation with respect to both the arene and diazoacetate partners was explored (**Figure 4.9**).

4.5: Scope of Photoredox C–H Alkylation Reaction

Simple alkyl aromatic substrates and electron-rich anisole derived substrates smoothly undergo the desired transformation in poor to good yields, tolerating synthetically useful cross-coupling functional handles such as aryl chlorides (**4.6a**, **4.8a**), bromides (**4.7a**), and tosylates (**4.14a**). Pharmacologically-relevant heterocycles were competent substrates for the reaction, with 2,6-dimethoxypyridine and n-methylindazole furnishing the desired adducts, **4.16a** and **4.17a** with high regioselectivity, albeit in reduced yield. Tyrosine derivatives containing protected amines, acidic C–H bonds and benzylic hydrogens underwent the desired transformation selectively, yielding derivatives **4.19a** and **4.21a** in poor to moderate yield. This method was also applicable to the selective functionalization of drug-like motifs. Under the optimized conditions, flurbiprofen methyl ester and fenoprofen methyl ester furnished the desired products, **4.20a** and **4.22a** respectively with moderate to good regioselectivity, despite relatively low chemical yield. Functionalization ortho- to electron donating groups is observed in most cases, with para- selectivity favored in the presence of increased steric hinderance (**4.8a-4.14a**). In biaryl systems, functionalization is favored on the more electron-rich ring system (**4.4a, 4.8a**). The mass balance for these reactions typically consists exclusively of returned starting material and C–H functionalized product. Following C–H alkylation, the resulting ester products can be converted into formal C–H methylation adducts *via* a simple

hydrolysis/decarboxylation sequence, utilizing a photoredox hydrodecarboxylation method previously developed by our group.[95]

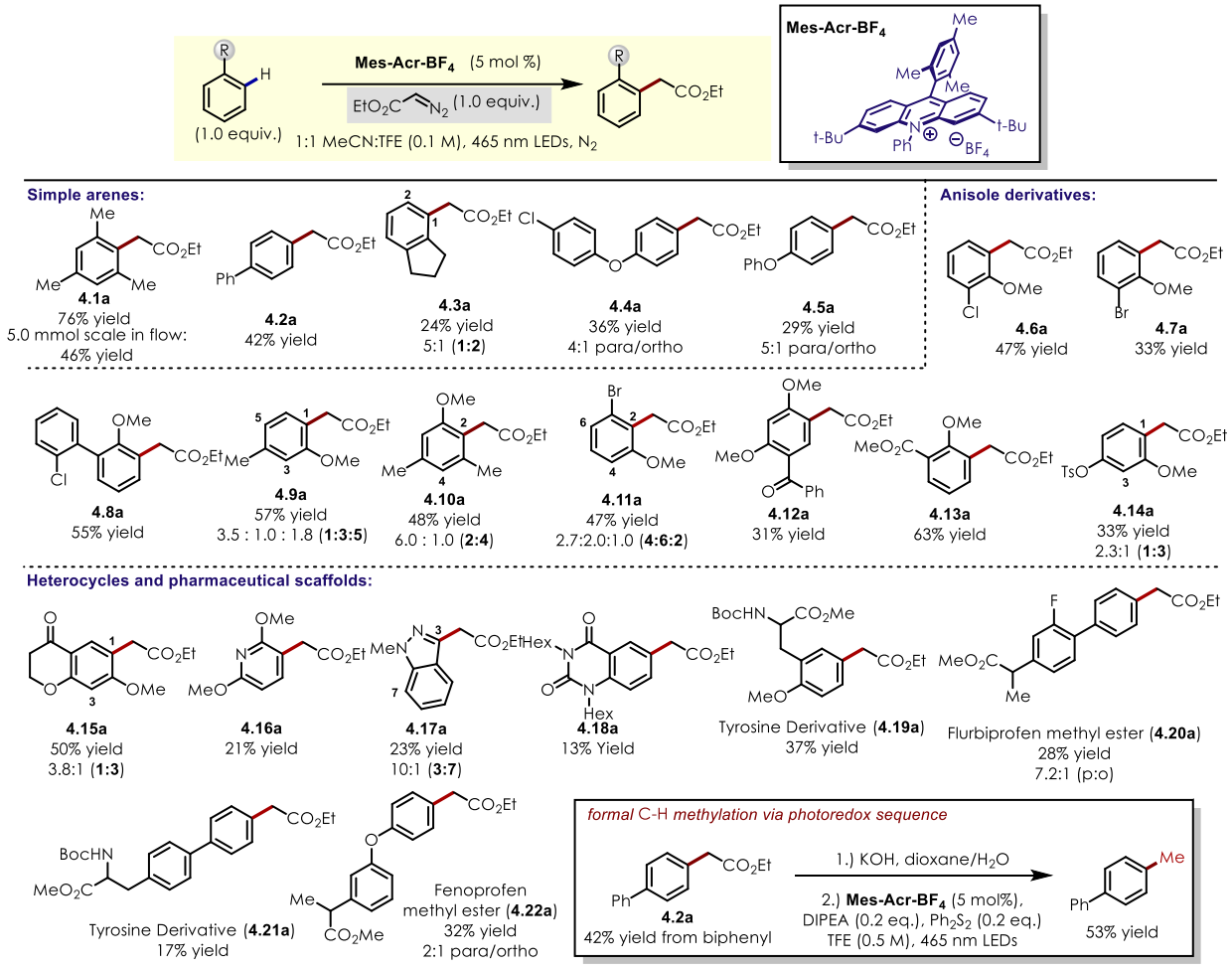

Figure 4.9: Arene scope of photoredox aromatic C–H alkylation reaction

Next, the scope of this transformation with respect to the diazo- compound coupling partner was explored. This reaction proceeded efficiently with simple diazoesters possessing *tert*-butyl, benzyl and cyclopentyl diazoacetates, affording the desired adducts **4.1e**, **4.1c**, and **4.1d** in good to moderate yields. Cyclic diazodihydrofuranone furnished product **4.1b** in 61% yield. Less nucleophilic methyl diazomalonate formed product **4.1f**, albeit with reduced yield.

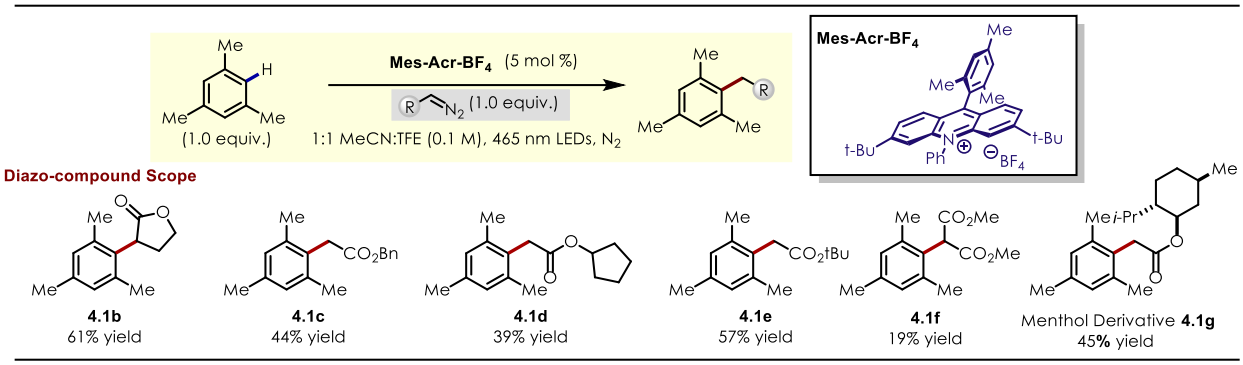

Figure 4.10: Diazo-compound scope of photoredox aromatic C–H alkylation reaction

The installation of *tert*-butyl, benzyl-, and malonate esters are also valuable due to the number of possible further transformations, which can be used to elaborate these products. For example, benzyl esters can be cleaved to the corresponding acid[96], *tert*-butyl esters can be converted to an acid chloride[97] and malonate derivatives can be used in the malonic ester synthesis to give substituted phenyl acetic acids.[98]

4.5: Mechanistic and Computational Studies

To probe the mechanism of this transformation, we conducted a series of experimental and computational investigations. Based on previous studies on the reaction of diazoacetate derivatives with alkene cation radicals, we initially hypothesized that following nucleophilic addition to the aromatic cation radical, electron transfer from the reduced form of the catalyst to the generated cyclohexadienyl radical could trigger a 1,2-hydride shift and expulsion of N_2, leading to the formation of the observed C–H functionalization product (**IV**, **Figure 4.11**). Such a mechanism would be reminiscent of that proposed for the cyclopropanation of alkene cation radicals by Ferreira and coworkers.[99]

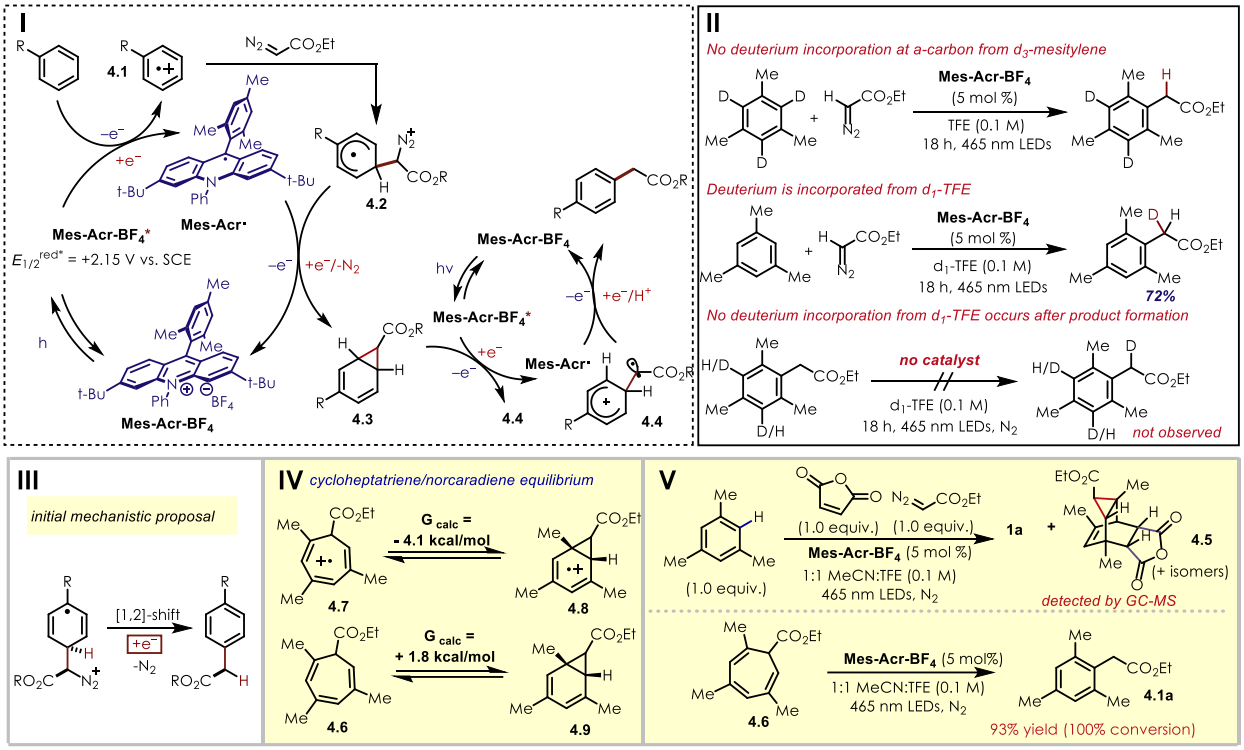

Figure 4.11: Investigation of the mechanism of organic photoredox C–H alkylation. I: Current mechanistic proposal. II: Deuterium labeling studies with d3-mesitylene and d1-TFE. III: Initial mechanistic proposal involving a 1,2-hydride shift. IV: Thermodynamics of the norcaradiene and cycloheptatriene equilibrium. V: Evidence for a norcaradiene intermediate.

When utilizing d_3–Mesitylene as a substrate, no deuterium incorporation was observed in the C–H alkylation product, suggesting that a 1,2-hydride shift is an unlikely step in the mechanism (**II**, **Figure 4.11**). When d_1-TFE is used as the reaction solvent, a mixture of non-deuterated, mono-deuterated and di-deuterated products is observed with the mono-deuterated formed as the major product in 72% yield. The presence of non-deuterated and di-deuterated products in the presence of the singly labeled product was rationalized as the result of enolate equilibration. Treatment of the proteo-product with d_1-TFE did not lead to any observable

deuterium incorporation. This is consistent with a mechanism invoking the protonation of an enolate by the solvent as part of the mechanism.

Based on this evidence, we propose an alternative mechanism as follows **(I, Figure 4.11)**: following excitation by blue light, **Mes-Acr-BF$_4$*** engages in photoinduced electron transfer (PET) with an arene, producing cation radical **4.1** and the reduced form of the catalyst (**Mes-Acr·**). Polar nucleophilic addition of ethyl diazoacetate forms distonic cation radical **4.2**, which is reduced by acridine radical (**Mes-Acr·)** to form the intermediate norcaradiene **4.3** and regenerate ground state **Mes-Acr-BF$_4$**. Following a second PET event, intermediate **3** undergoes ring-opening to form distonic benzylic cation radical **4.4**. Reduction of this intermediate by **Mes-Acr·**, deprotonation (presumably by conjugate base of the solvent) to rearomatize the product, and protonation of the resulting enolate by the solvent closes the second catalytic cycle.

Norcaradienes are known to exist as equilibrium mixtures with the corresponding cycloheptatrienes.[100,101] To further explore the impact of this equilibrium in our system, the free energy change for the interconversion of these species was modeled for intermediates **4.6** and **4.7** (**IV**, **Figure 4.11**). In the neutral species, the cycloheptatriene form (**4.6**) is favored by 1.8 kcal/mol. However, upon oxidation of this species, the equilibrium was calculated to favor norcaradiene cation radical **4.8** by 4.1 kcal/mol. This suggests that, under the reaction conditions, the equilibrium between norcaradiene and cycloheptriene may be driven towards products *via* electron transfer.

To support this proposal, we subjected cycloheptatriene **4.6** to our optimized conditions (**V**, **Figure 4.11**). Following irradiation for 18 h, full conversion of **4.6** to the desired product **4.1a** was observed. Control experiments indicated that the presence of **Mes-Acr-BF$_4$** is required for conversion. A mass corresponding to the desired [4+2] adduct (**4.5**) was observed by GC-MS

upon the inclusion of maleic anhydride (1 equiv.) as a Diels-Alder trap under otherwise optimized conditions, supporting the formation of norcaradiene **4.9** during the reaction.

Diazoacetates bearing aryl substituents, which are known to form free carbenes upon irradiation with blue light, gave solely the product resulting from O-H insertion of trifluoroethanol into the corresponding carbene. Ethyl diazoacetate, which absorbs at 371 nm with no overlap at 465 nm, shows no formation of these O-H insertion byproducts. This suggests that under these reaction conditions a free carbene is not formed and instead ethyl diazoacetate behaves as a polar nucleophile. Control experiments also indicated that the blue LEDs used for this reaction are unable to trigger photolysis of ethyl diazoacetate in a similar manner to aryl diazoacetates. This is in accordance with other experimental and computational data in support of the proposed mechanism given above.

To investigate the energetic feasibility of the proposed mechanism, the reaction between mesitylene and ethyl diazoacetate was modeled using DFT (B3LYP, 6-31+g(d)) calculations (**Figure 4.12**, see appendix for complete computational details). Following oxidation of mesitylene, ethyl diazoacetate undergoes nucleophilic addition to the arene cation radical with a transition state energy of +11.7 kcal/mol and an overall free energy change of +5.9 kcal/mol. The calculated endergonicity of this process is in agreement with the known equilibrium between arene cation radical/nucleophile pairs and the corresponding σ-adducts. [102,103]

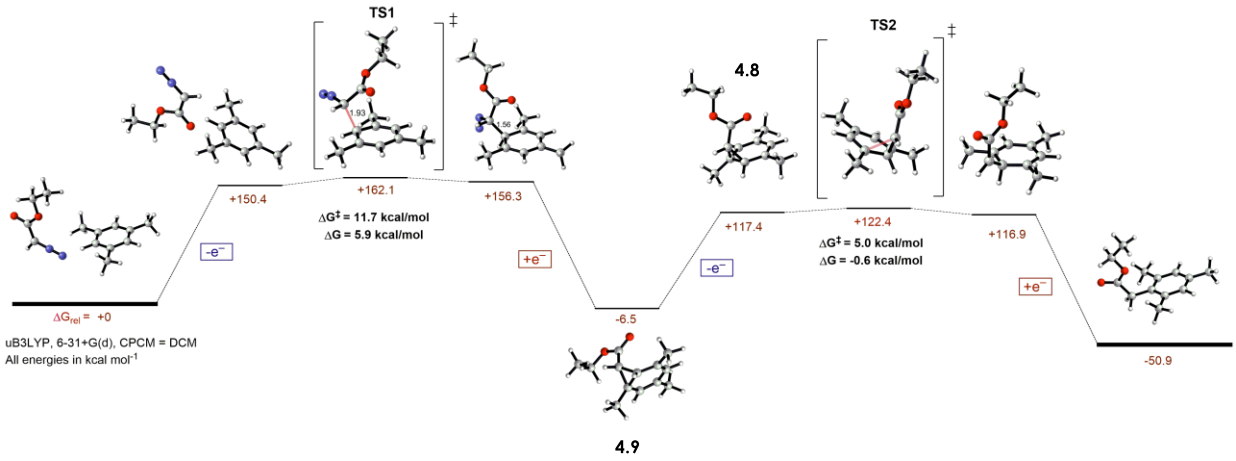

Figure 4.12: Computed reaction coordinate diagram for photoredox catalyzed C–H alkylation reaction

Following single electron transfer from the reduced form of the catalyst to the σ-adduct, a barrierless loss of N_2 and cyclization forms norcaradiene **4.9** with an overall free energy change of -6.5 kcal/mol relative to the starting materials. A second single electron transfer event generates cation radical intermediate **4.8** which then undergoes ring opening to form a distonic cation radical. This process has a calculated transition state energy of +5.0 kcal/mol and an overall free energy change of -0.6 kcal/mol. Following electron transfer from the reduced catalyst and proton transfer, the desired C–H alkylation product is formed. The free energy change for this overall process was calculated to be -50.9 kcal/mol.

In conclusion, we have developed an operationally simple, metal-free site-selective aromatic C–H alkylation which utilizes equimolar quantities of coupling partners, unlike known metallocarbene chemistry which requires excess arene substrate to achieve efficient reactivity. This transformation is compatible with a range of aromatic substrates, including those containing known pharmaceutical motifs and cross-coupling handles. Experimental and computational studies suggest a unique mechanism involving cyclopropanation of arene cation radicals and

subsequent oxidative ring opening. This work represents both a fundamental insight into the reactivity of aromatic cation radicals and a valuable approach for the formation of sp^3–sp^2 bonds through a C–H functionalization manifold in the absence of transition metal catalysts.

Chapter 5 : DISCOVERY AND CHARACTERIZATION OF ACRIDINE RADICAL PHOTOREDUCTANTS

5.1: Introduction

Photoinduced electron transfer (PET) is a phenomenon wherein the absorption of light by a chemical species provides an energetic driving force for an electron transfer reaction.[104–107] This mechanism is relevant in many areas of chemistry, including the study of natural and artificial photosynthesis, photovoltaics, and photosensitive materials. In recent years, research in photoredox catalysis has leveraged PET for the catalytic generation of both neutral and charged organic free radical species. These technologies have enabled a wide range of previously inaccessible chemical transformations and have seen widespread utilization in both academic and industrial settings. These reactions are often catalyzed by visible-light absorbing organic molecules or transition-metal complexes of ruthenium, iridium, chromium, or copper.[73,108] While a wide variety of closed shell organic molecules have been shown to behave as competent electron transfer catalysts in photoredox reactions, there are only limited reports of PET reactions involving *neutral organic radicals* as an excited state donor or acceptor. This is perhaps somewhat unsurprising in light of previously reported doublet excited state lifetimes for neutral organic radicals, which are typically several orders of magnitude shorter than singlet lifetimes for known transition metal photoredox catalysts.[109–113] Herein we document the discovery, characterization, and reactivity of a neutral acridine radical with a maximum excited state

oxidation potential of -3.36 V vs. SCE: significantly more reducing than elemental lithium and marking it as one of the most potent chemical reductants reported.[114]

5.2: Approaches Towards Net Reductive Photoredox Catalysis

In recent years, several highly reducing photoredox systems have been developed and utilized in reactions centered around the generation of high energy, single electron reduced intermediates. In 2014, König and coworkers reported a series of two-photon driven reductive dehalogenation reactions of electron-deficient arenes catalyzed by a perylene diimide catalyst (**PDI**).[115] Following excitation by visible light, the excited state **PDI** catalyst engages in PET with triethylamine present in the reaction mixture, yielding the metastable PDI radical anion and the corresponding amine cation radical (**Figure 5.1**). Spectroscopic studies indicated that direct excitation of the radical anion species gives rise to a reducing excited state which can transfer an electron to the halogenated substrate, forming the corresponding aryl radical anion. This radical anion then quickly fragments to yield an aryl radical and a halide anion. This aryl radical may then be intercepted by a radical trap – *N*-methylpyrrole in this case. Experiments with internal radical traps supported the formation of aryl radicals during the course of this reaction. Although limited in scope due to the moderate reducing power of the excited state PDI radical anion, this work laid the conceptual groundwork for several methodologies relying on overall two-photon mechanisms.

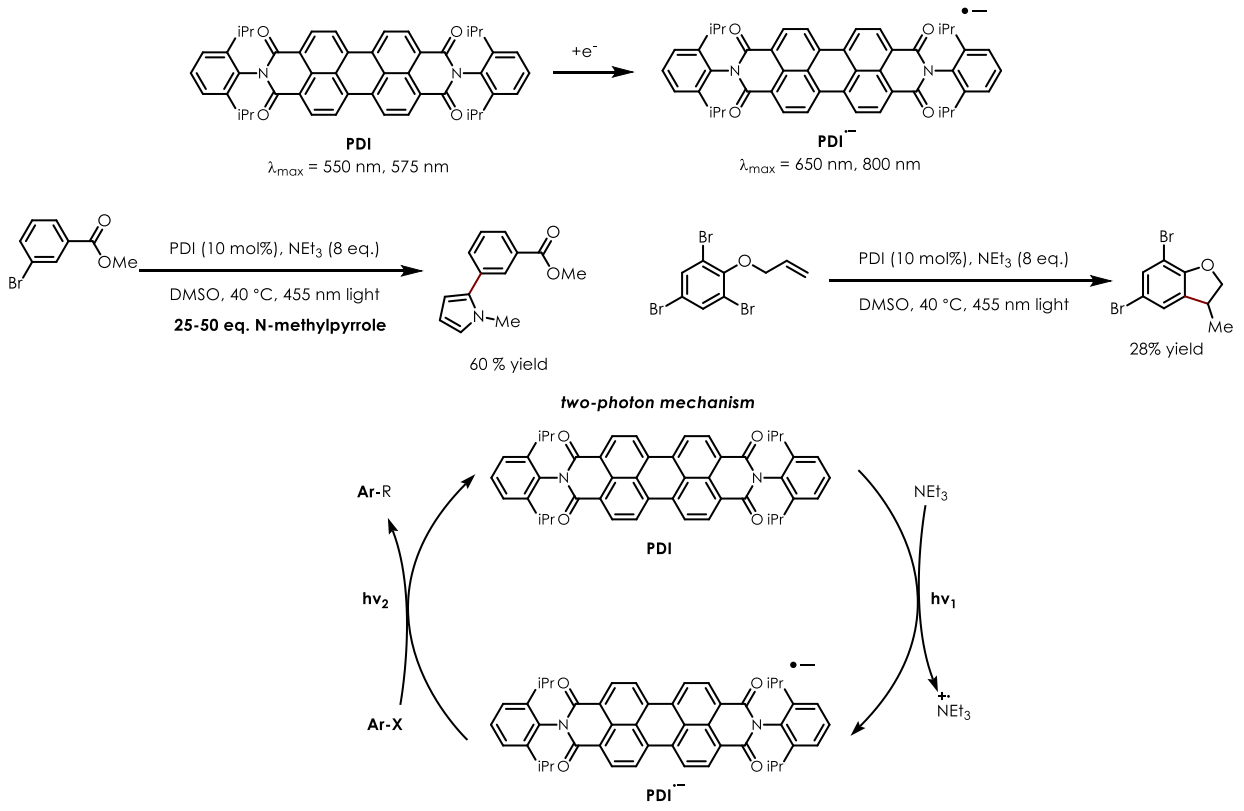

Figure 5.1: Reductive arylation of halogenated arenes catalyzed by PDI

Several years later, 9,10-dicyanoanthracene (DCA) was reported to function as a catalytically competent precursor for the generation of the corresponding excited state radical anion.[116] The excited DCA radical anion has a maximum excited state oxidation potential of -2.5 V vs. SCE and is capable of reducing aryl bromides and electron-poor aryl chlorides. However, more electron-rich aryl chlorides proceed in very poor yields due to the reducing limits of the excited state radical anion (**Figure 5.2**).

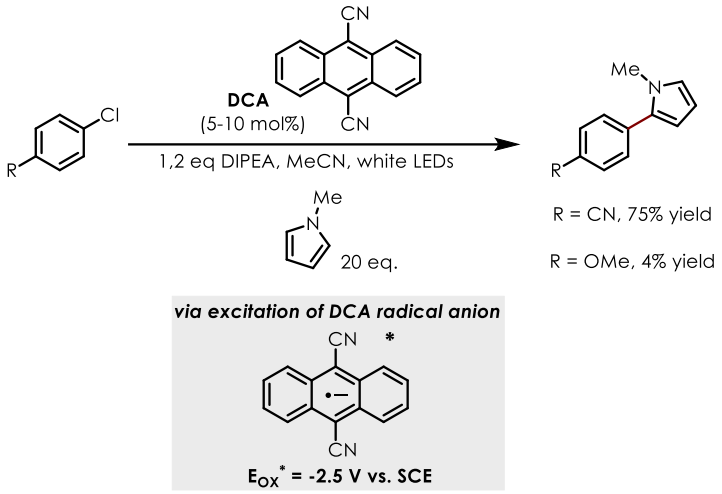

Figure 5.2: Reductive arylation catalyzed by DCA

Both methods rely on the generation of the active reducing species *via* an initial photoinduced electron transfer step. Although effective, the introduction of two single electron transfer steps into a single catalytic cycle often leads to reduced reaction efficiency versus reactions involving only a single PET step. One approach to this is the use of an electrode as the source of source of electrons, forming the desired radical anion species *via* cathodic reduction. Compared to methods which utilize chemical reductants to affect the generation of the active catalytic species, electrochemical activation benefits from the lack of byproducts associated with oxidative degradation of chemical reductants or side reactions of these intermediates (for example, back electron transfer between the reduced substrate and ground state catalyst).

Recently, Lambert, Lin, and coworkers reported the electrochemical generation of DCA radical anion and utilization of this species in a PET mechanism in a process they refer to as "electrophotocatalysis" (despite the fact that this process is not catalytic in "electrons" or "photons").[117] Following electrochemical generation of the radical anion and excitation by visible light, the radical anion of the catalyst engages in PET with the aryl halide substrate,

yielding an aryl radical and a halide anion following fragmentation. This aryl radical is then trapped in a second step by *bis*(pinocolato)diboron to afforded borylated products (**Figure 5.3**).

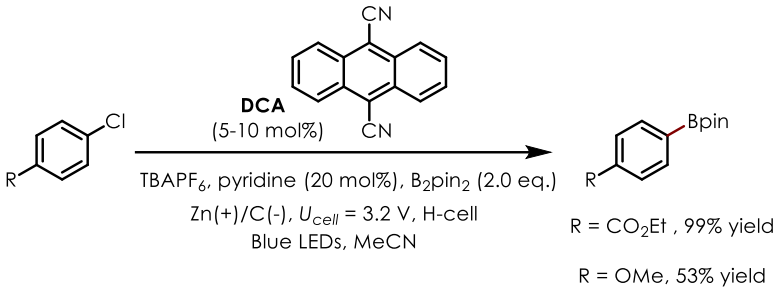

Figure 5.3: Conditions for "electrophotocatalytic" borylation

These radicals may also be trapped with n-methylpyrrole or bis(trimethylstannane) to afford alkylated or stannylated products in good yields. Interestingly, compared to previously work utilizing DCA radical anion as the active excited state reductant, a much wider electrochemical window of substrates are accessible, including electron-rich aryl chlorides with reduction potentials as high as -2.9 V vs. SCE.

In a closely related electrochemical/photochemical system, Wickens and coworkers identified imide **NpMI** as a suitable catalyst for the reductive phosphorylation and alkylation of electron-rich aryl halides under irradiation and constant current electrolysis.[118] This system is even more strongly reducing than that described by Lambert et. al., and can affect the reductive phosphorylation of substrates with reduction potentials as negative as -3.4 V vs. SCE (**Figure 5.4**).

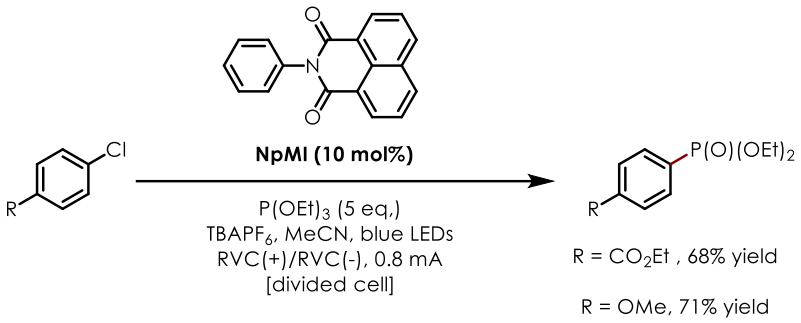

Figure 5.4: Conditions for reductive phosphorylation catalyzed by an imide radical anion

5.3: Neutral Organic Radicals as Excited State Reducing Agents

While several radical anions and cations have been utilized as excited state electron transfer catalysts, photoinduced electron transfer reactions of neutral organic radicals are far sparser in the literature. It is known that diphenylmethyl radicals generated *via* flash photolysis of the corresponding diazo- compound or tetraphenylacetone are capable of undergoing PET in the presence of a quenching species. Early studies focused on PET reactions of this radical with electron acceptors, such as alkyl halides.[111] Diphenyl methyl radical possesses an absorbance maximum in the 332-334 nm range, with a corresponding excited state energy of 2.38 eV. In combination with the known ground state oxidation potential of this species, the excited state oxidation potential of the radical may be estimated to be -1.9 V vs. SCE. Indeed, quenching is observed (k_q = (1.3 ± 0.1) x 10^8 M^{-1} s^{-1} in methanol) in the presence of carbon tetrachloride, affording products corresponding to the recombination of the benzylic cation and chloride ion generated following PET (**Figure 5.5**). This work establishes a strong precedent for reductive PET from neutral radical species.

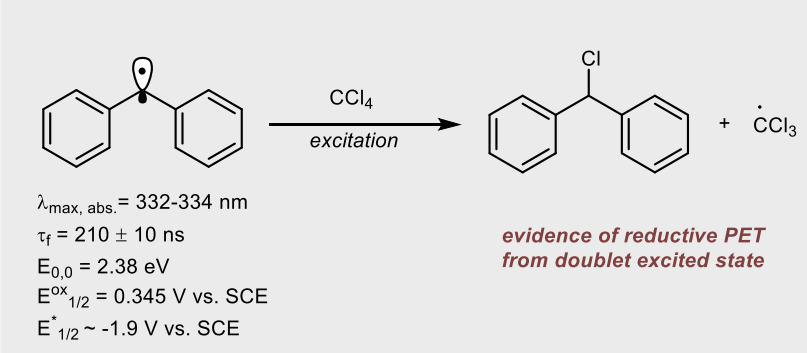

Figure 5.5: Photoinduced electron transfer reaction of diphenylmethyl radical

Our lab, as well as others, have published numerous examples highlighting the diverse reactivity of acridinium salts, such as **Mes-Acr-BF$_4$**, as photooxidation catalysts in the excited state (**Figure 5.6**).[44]

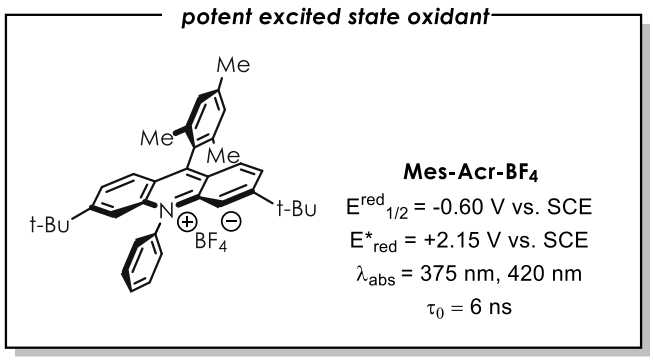

Figure 5.6: Photophysical properties of Mes-Acr-BF$_4$

Upon absorption of visible light, the corresponding excited state of the acridinium salt is populated and may be quenched *via* electron transfer from an electrochemically-matched substrate, resulting in the formation of an acridine radical, **Mes-Acr•** (**Figure 5.7**).

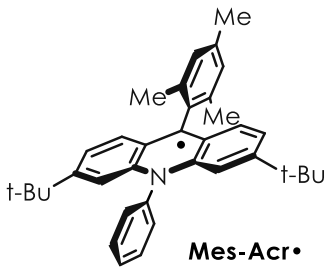

Figure 5.7: Structure of stable radical Mes-Acr•

In past work utilizing acridinium photoredox catalysts, this radical is typically oxidized to regenerate the parent acridinium and close a catalytic cycle. During previous mechanistic studies conducted by our laboratory, it was noted that solutions of **Mes-Acr•** generated *via* reduction of **Mes-Acr-BF$_4$** with cobaltocene were indefinitely stable under oxygen-free conditions and possessed two major absorption features (350-400 nm and 450-550 nm; **Figure 5.8**).[119]

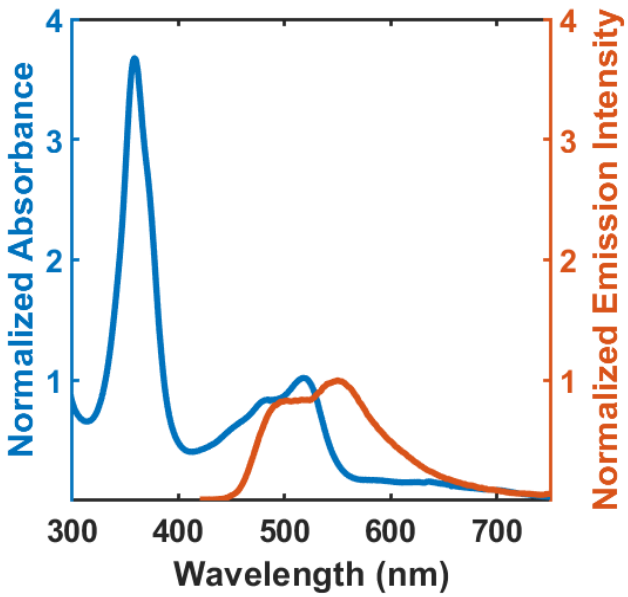

Figure 5.8: Absorption and emission spectra of Mes-Acr•, collected in MeCN

5.4: Acridine Radicals as Potent Excited State Reducing Agents

These observations led us to explore the photophysical behavior of this radical, with a focus on identifying potential PET behavior. Previous studies have detailed the *in situ* generation and excitation of stable cation radical and anion radical species and their use in catalytic reactions,[115,120–123] indicating the potential feasibility of this strategy and prompting our studies of the photophysical behavior of **Mes-Acr•**.

Curiously, initial absorbance and emission measurements indicated that emission is occurring from a higher energy state than the lowest energy absorption band. This is referred to as *anti-Kasha* fluorescence, as emission appears to be occurring from a state higher in energy than the lowest energy absorbance feature.[124,125] Although relatively uncommon due to the relative rates of intersystem crossing and vibrational relaxation, this photophysical behavior has been previously observed in organic molecules - particularly those which have restricted excited state vibrational modes.[126,127] The restriction of vibrational modes slows relaxation from a higher order excited state to the lowest energy excited state, leading to emission/reaction directly from this higher energy excited state without relaxation. Such behavior has been previously ascribed to the formation of twisted intramolecular charge transfer (TICT) states. In a TICT state, vibrational relaxation is slowed through adoption of a twisted metastable geometry in the corresponding excited state. Upon investigation of the excited state dynamics of **Mes-Acr•**, two primary excited states were identified as being responsible for the observed spectral features, tentatively assigned as a lower energy doublet (**D_1**) and higher energy twisted intramolecular charge transfer state (**TICT**). Twisted intramolecular charge transfer states have been previously observed in analogous acridinium systems containing hindered rotational modes, leading us to suspect similar photophysical features in the corresponding radical.[128,129] The excited state energy for the doublet

excited state of **Mes-Acr•** is estimated by averaging the energies of the lowest energy absorption maximum and the highest energy emission observed upon 484 nm excitation. The energy of the proposed higher order excited state is estimated by averaging the energies of the emission maximum near 490 nm and the maximum of the corresponding excitation spectrum monitored at this wavelength (see appendix for full details of excited state energy calculations). Estimation of excited state energies in this fashion gives values of 2.31 eV for the energy of the proposed D_1 excited state and 2.76 eV for the corresponding higher energy TICT excited state. Using the known electrochemical potential of **Mes-Acr•**[92] the excited state oxidation potentials of these states were estimated to be -2.91 V vs. SCE and -3.36 V vs. SCE, respectively. To our knowledge, these values represent some of the most negative excited state oxidation potentials reported for an organic molecule.

5.5: Computational Investigation of Mes-Acr• Photophysics

Before we proceed to discuss the calculated excited state energies, we consider the key orbitals involved in the low-lying excited states. To evaluate possible charge transfer pathways in this system, molecular orbital visualizations were performed following DFT geometry optimizations for **Mes-Acr•**. The singly occupied molecular orbital (SOMO) density, or donor density, is localized on acridine core and the lowest unoccupied MO (LUMO+1), or acceptor density, is localized on the *N*-phenyl ring of **Mes-Acr•** (**Figure 5.9**).

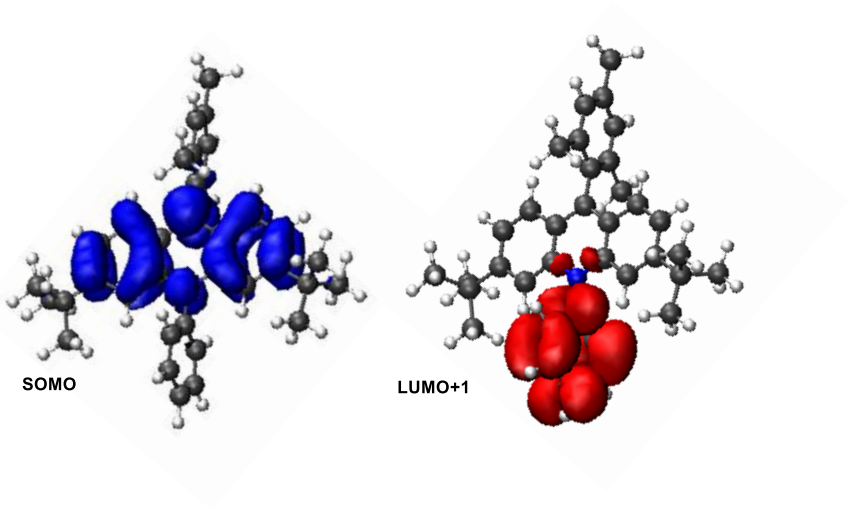

Figure 5.9: DFT-generated molecular orbital plots of Mes-Acr•

Based on this observation of small spatial overlap between these two orbitals, it seems possible that a relatively low-lying excitation of an intramolecular CT (charge transfer) state involving the polarization of electron density from the acridine core to the *N*-phenyl ring will be involved in the excited dynamics of this species. To better understand the effect of rotation of the *N*-phenyl ring on the excited state energetics of the acridine radical, we employ the recently reported polarization consistent TD-DFT based framework for obtaining excited state energies of solvated molecular systems. The approach addresses dielectric polarization consistently by invoking the same dielectric constant in the screened range separated hybrid (SRSH) functional parameters and in the polarizable continuum mode (PCM). SRSH-PCM was benchmarked well in calculating CT state energies of solvated donor-acceptor complex and in analyzing the spectral trends of several pigments with increased accuracy where conventional TD-DFT calculations fail to reproduce the observed trends (see appendix for full computational details).[130–133]

The calculated doublet excited state energies for **Mes-Acr•** agree very well (within 0.1 eV) with values estimated *via* spectroscopic measurements for both the absorption and emission

spectra (**Figure 5.10**). The lowest energy calculated D_1 state, possessing an excited state energy of 2.29 eV, agrees with the experimentally determined D_1 value of 2.31 eV. Additionally, two excited states possessing significant charge transfer character were identified and the corresponding energies were calculated to be 2.75 and 2.78 eV, matching closely with estimated spectroscopic values for the proposed TICT state energy of 2.76 eV. As such, the identified D_1 (2.29 eV) state is assigned as an untwisted exitonic state, while the calculated 2.78 eV state is assigned as a TICT state. These excited state energy values also correspond well with previously reported excited state energies for neutral radical species.[111] Additionally, visualizations of the geometries of the corresponding TICT state indicate significant rotation of the *N*-phenyl ring (36 degrees) relative to the more planarized geometry of the D_1 state, providing further evidence of the profound effects of *N*-phenyl rotation on excited state energy.

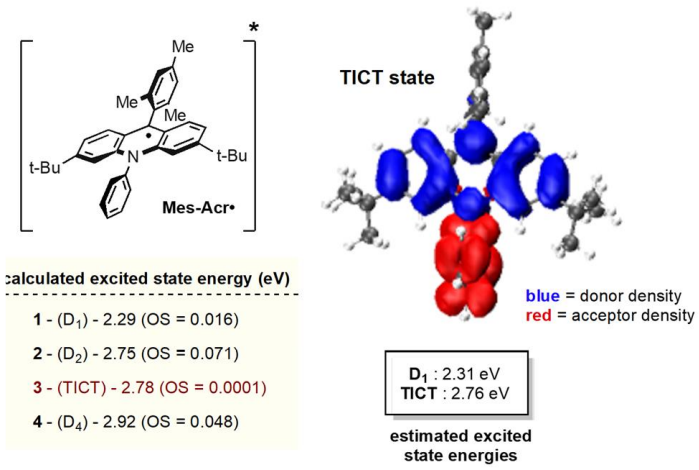

Figure 5.10: Calculated excited state energies for Mes-Acr• and orbital density map for TICT state

5.6: Transient Absorption Study of Mes-Acr• Photophysics

To further probe the excited state behavior of **Mes-Acr•**, transient absorption experiments were performed (**Figure 1D**).

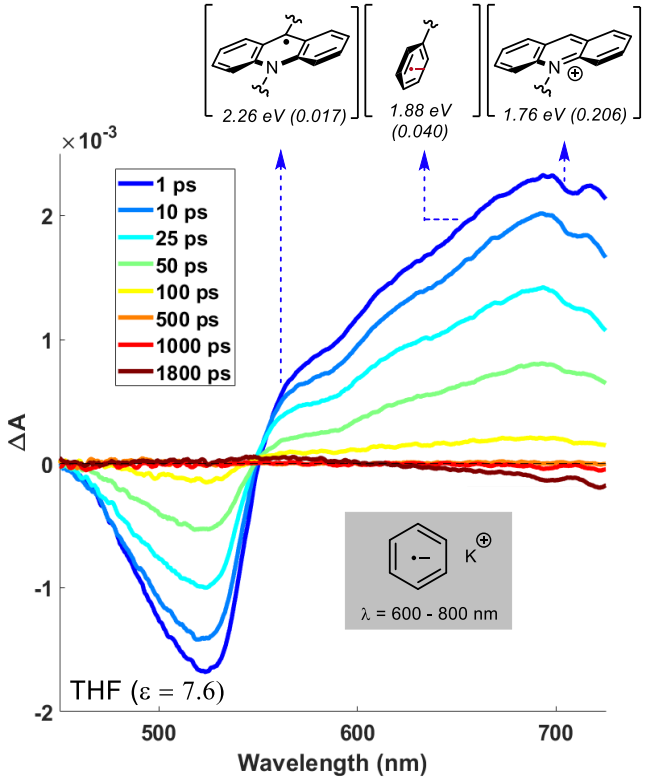

Figure 5.11: Transient absorption spectra for Mes-Acr• in THF following 400 nm pulse and calculated excited state absorbances (calculated oscillator strengths given in parenthesis)

At early pump-probe delay times in THF, the ground state of **Mes-Acr•** is bleached ($\Delta A < 0$) and excited state absorbance resonances ($\Delta A > 0$) with maxima at 550 nm and ~650 nm are observed (**Figure 5.11**). Aromatic radical anions are known to exhibit broad absorbances in the 600-800 nm range as are aqueous solvated electrons.[134–136] The observed excited state absorbance signal at ~550 nm also matches the absorbance profile expected for a general acridine exitonic structure. Simple first-order decay to the ground state occurs after ~100 ps,

matching well with previously reported values for excited state lifetimes of organic radicals. TD-DFT calculations indicate that other red-shifted absorptions present are well matched with energies calculated for a general acridinium structure. These spectral features support the formation of a charge transfer state possessing both aromatic radical anion and acridinium features, as expected for the proposed TICT state.

In acetonitrile, following the initial 400 nm pulse excited state absorbance features resembling those observed in THF develop quickly (**Figure 5.12**). After approximately 50 ps, these absorbances begin to decay and new excited state absorbances located near 450 nm and 550 nm, expected for lower energy locally excited (LE) states develop. While the effects of solvent polarity on the excited state dynamics of **Mes-Acr•** still the subject of future studies, these initial results seem to indicate a long-lived TICT state which is formed in THF, while the formation of LE states is favored in acetonitrile. Initial calculations of excited state geometries indicate that the *N*-phenyl ring is twisted by ~30 degrees in the locally excited state of **Mes-Acr•**, relative to the corresponding TICT state. As such, the implication of changing solvent polarity on ring rotation may lead to the observed changes in excited state dynamics. Future computational studies will be targeted towards expanding our understanding of the excited state dynamics of this species, particularly with respect to the effects of n-aryl rotation on excited state energies and electronic distributions of excited states.

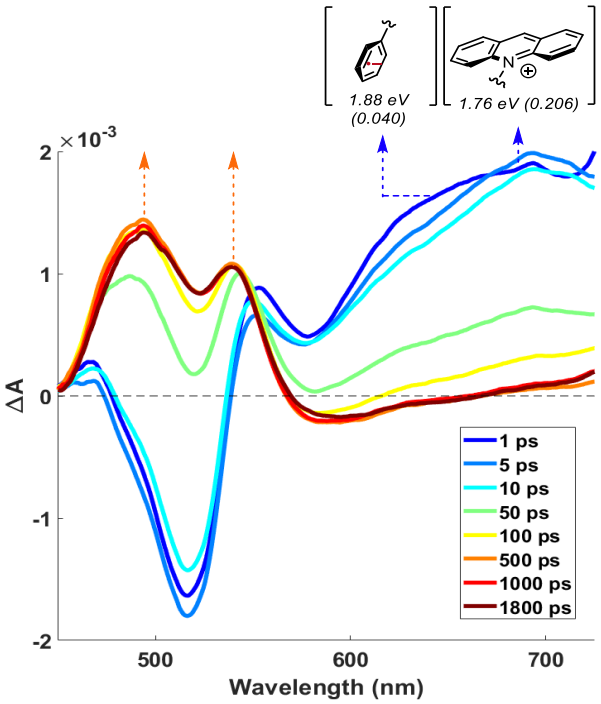

Figure 5.12: Transient absorption spectra for Mes-Acr• in MeCN following 400 nm pulse and calculated excited state absorbances (calculated oscillator strengths given in parenthesis)

5.6: Development of Reductive Transformations Facilitated by Mes-Acr•

With an initial understanding of the excited state behavior of **Mes-Acr•** developed, we sought to utilize this species as a catalytic reductant in a photoredox manifold. Previous work in reductive photoredox catalysis has established the reduction of aryl halides as a common benchmark reaction for these types of transformations.[137–140] Furthermore, the extremely potent reducing behavior of the acridine radical should enable the reduction of a wide range of electronically diverse substrates.

Diisopropylamine (DIPEA) was identified as a suitable single electron reductant for the generation of **Mes-Acr•** from **Mes-Acr-BF$_4$** *in situ*. Following excitation, **Mes-Acr-BF$_4$** undergoes single electron reduction *via* electron transfer from DIPEA, generating the desired

radical **Mes-Acr•.** Control experiments indicated that after ~60 s of irradiation at 390 nm in MeCN in the presence of DIPEA, **Mes-Acr-BF$_4$** had undergone complete conversion to **Mes-Acr•** indicating the feasibility of this strategy. Indeed, in the presence of 1.2 equiv. of DIPEA and 10 mol% **Mes-Acr-BF$_4$**$^-$, 4-(tert)butylbromobenzene underwent hydrodebromination in 50% yield following irradiation at 390 nm for 13 hours (**Figure 5.13**, entry 1.). Increasing the loading of DIPEA to 3.0 equiv. resulted in an increase in yield, with the desired product formed in 81% yield under otherwise identical conditions (entry 2-3). Control experiments indicated that both **Mes-Acr-BF$_4$** and DIPEA are required for the reaction to proceed (entry 4-5). Additionally, 0% conversion to the desired dehalogenation product was observed following irradiation at 450 nm, highlighting the requirement of higher energy irradiation to reach maximum reducing ability in this system.

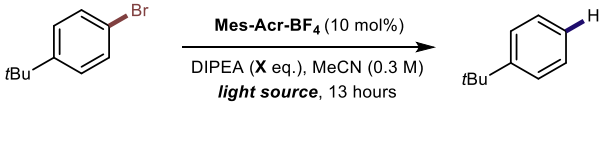

entry[a]	X	Light source	Yield
1	1.2	390 nm	50%
2	2.0	390 nm	65%
3	3.0	390 nm	81%
4[b]	1.2	390 nm	0
5	-	390 nm	0
6	1.2	450 nm	0

substrate	$E^{red}_{1/2}$ (vs. SCE)	Yield (390 nm)	Yield (467 nm)
X	> -2.7 V	90%	0%
X	-2.06 V	78%	34%
X	-1.58 V	72%	49%

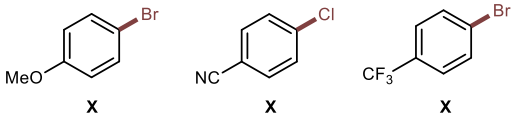

a: All reactions conducted on 0.1 mmol scale under air and analyzed by crude ^{1}H NMR using HMDSO as an internal standard
b: reaction conducted in the absence of **Mes-Acr-BF$_4$**

Figure 5.13: Initial optimization of reductive dehalogenation reaction and control experiments

To chemically probe the possibility of charge transfer to the *N*-phenyl ring, brominated acridinium **5.1** was prepared. In the presence of 3 equiv. DIPEA, **5.1** was completely converted to a mixture of debrominated acridinum **5.1a** and hydroacridine **5.1b** following irradiation at 390

nm for 18 hours (**Figure 5.14**). As aryl halide radical anions are known to quickly fragment to yield the corresponding aryl radicals, this experiment is indicative of the formation of radical anion character localized on the *N*-phenyl ring during excitation. The formation of hydroacridine may be the result of disproportionation of two acridine radicals, facilitated by light.

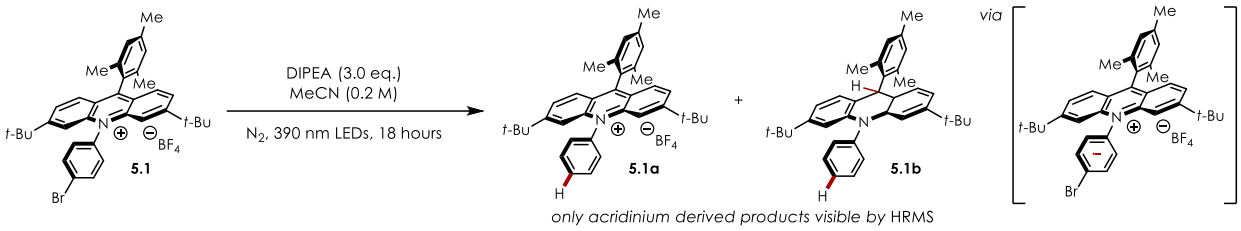

Figure 5.14: Intramolecular charge transfer promoted debromination of acridinium derivative

5.7: Scope of Reductive Reactions Facilitated by Photoexcited Mes-Acr•

To evaluate the competency of this radical species as a catalytic reductant, conditions for the reductive dehalogenation of aryl halides were developed (**Figure 5.15**). A variety of both electron-rich (**5.6-5.13**) and electron-poor (**5.14, 5.15**) aryl bromides afforded the desired hydrodebrominated products in good to excellent yields (NMR yields of products taken using HMDSO as an internal standard). It is of note that reductively recalcitrant aryl chlorides also participated efficiently in this reaction, in contrast to previously reported methods which are only effective for electron-poor (under visible light irradiation) or moderately electron rich aryl chlorides (under UVA irradiation).[141,142] A variety of both electron-donating (**5.16-5.20)** and electron-withdrawing (**5.21-5.24**) substituents were tolerated, with only slightly reduced yields in the case of electron-poor substrates. Substrates bearing ketone (**5.30**), carboxylic acid (**5.31**), and alcohol (**5.28**) functionalities all afforded the desired hydrodechlorinated products in good to excellent yield. Medicinally relevant pyridine (**5.25, 5.26**) and aryl carbamate (**5.27**) derivatives

were also efficient substrates for this transformation. When substrate (**5.23**), which bears a trifluoromethyl substituent, was subjected to the reaction conditions, partial hydrodefluorination (5%) to yield the corresponding difluoromethyl derivative was observed in addition to hydrodechlorination. In all other examples, no Birch-type products resulting from overreduction are detected. The *bis*-reduction of polyhalogenated compounds (**5.33**) and (**5.34**) gave the corresponding *bis*-hydrodebromination and *bis*-hydrodechlorination products in 58% yield and 46% yield, respectively. For compound **5.34**, 49% yield of the product resulting from *mono*-hydrodechlorination (**5.34b**) was observed in addition to the fully dechlorinated product.

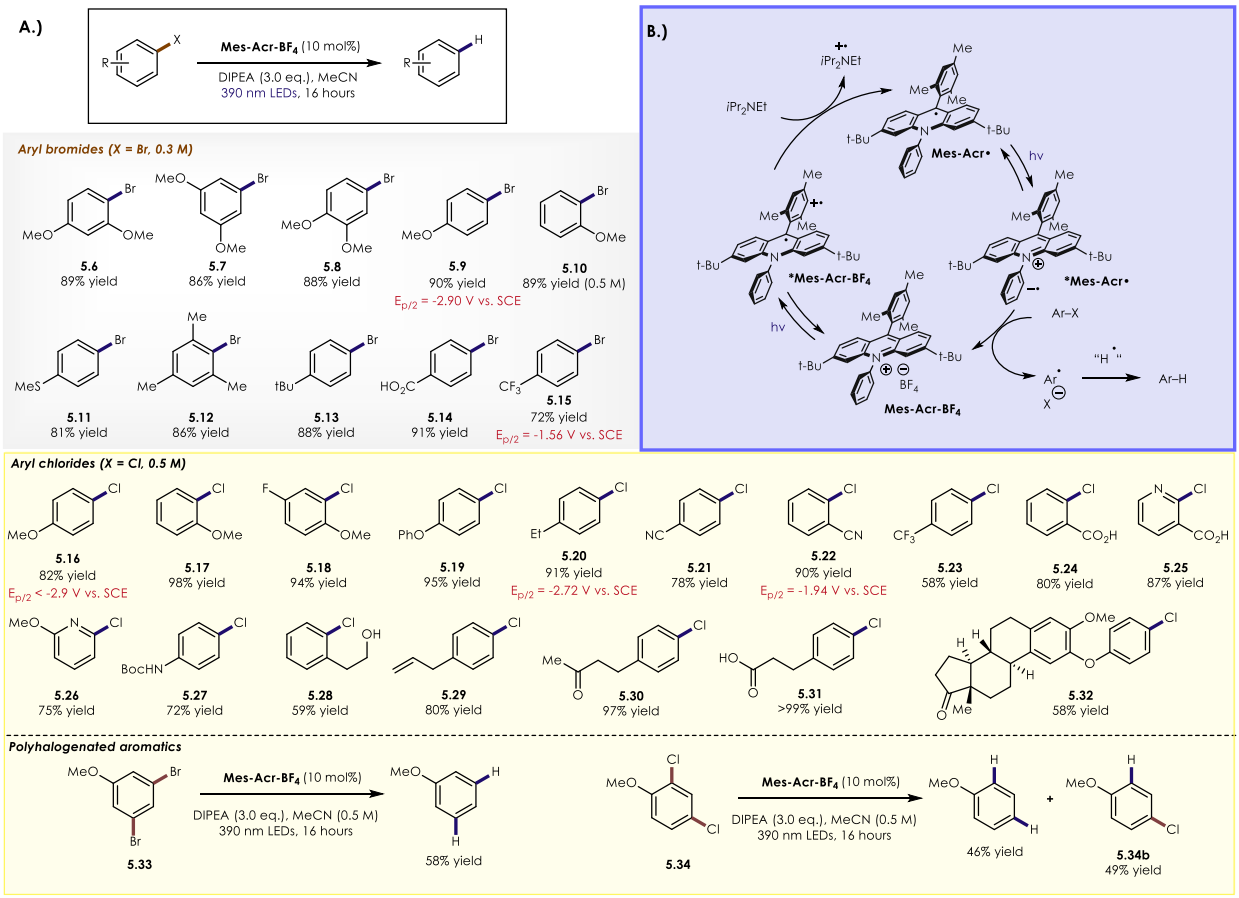

Figure 5.15: Scope of acridine radical catalyzed photoredox hydrodehalogenation

The reductive detosylation of amines was identified as another possible transformation, which may be facilitated by **Mes-Acr•** (**Figure 5.16**). Typically, strong acid, dissolving metal (Li/Mg), or low-valent transition metal reductions are employed in detosylation reactions.[143–145] A variety of electronically diverse tosylated aniline derivatives were smoothly converted to the desired free anilines in moderate to excellent yield. Interestingly, substrates containing aryl halides were tolerated under the reaction conditions. As this reaction is conducted at a significantly lower concentration of substrate compared to the reductive dehalogenation method (0.1 M vs. 0.5 M), the observed lack of aryl halide reduction may be a function of concentration. Esters (**5.43, 5.73**), free carboxylic acids (**5.44**), ketones (**5.48**), and free alcohols (**5.58**) were tolerated under the reaction conditions, showcasing the high functional group tolerance of this method relative to methods relying on harsh dissolving metal conditions. Benzylic (**5.52**) and secondary alkyl amines (**5.45, 5.53, 5.65-5.68**) were efficient substrates for this transformation as well. Medicinally-relevant heterocycles, including pyridines (**5.59**), indoles (**5.58**), pyrroles (**5.62**), pyrrolidines (**5.67**), indazoles (**5.63**), benzimidazoles (**5.64**), and morpholines (**5.65**) were deprotected in good to excellent yields, with no reduction of the aromatic system observed in all cases. Of note is the ability of this method to chemoselectively and efficiently deprotect tosyl-amines over mesyl protected-amines, as shown by the reaction of substrate **5.51**, yielding the desired detosylation product in 61% yield with no observed cleavage of the mesyl-amine.

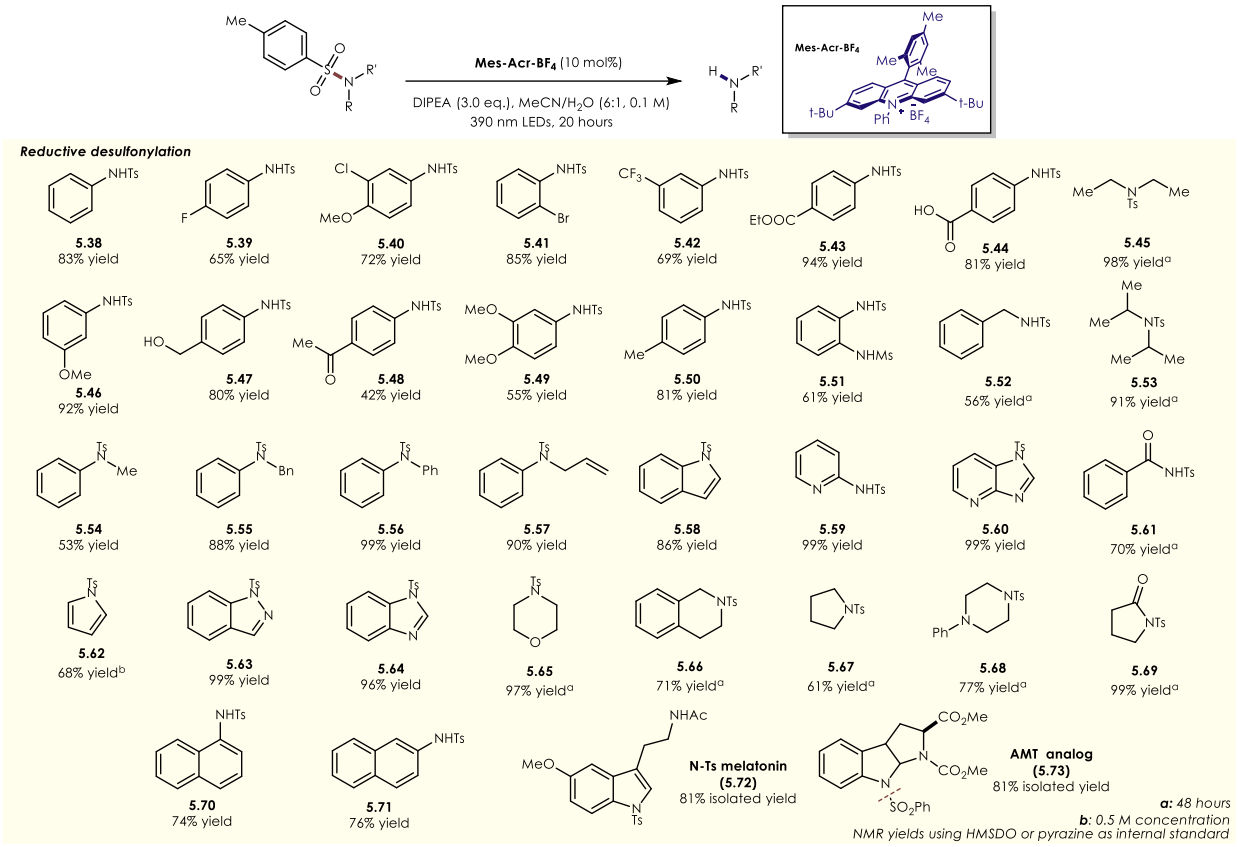

Figure 5.16: Scope of acridine radical catalyzed photoredox desulfonylation

Additionally, the reaction performed well on 1.28 g scale, with substrate **5.64** undergoing the desired detosylation in 92% yield when conducted in a standard round bottom flask irradiated with LED lamps (see appendix for experimental details).

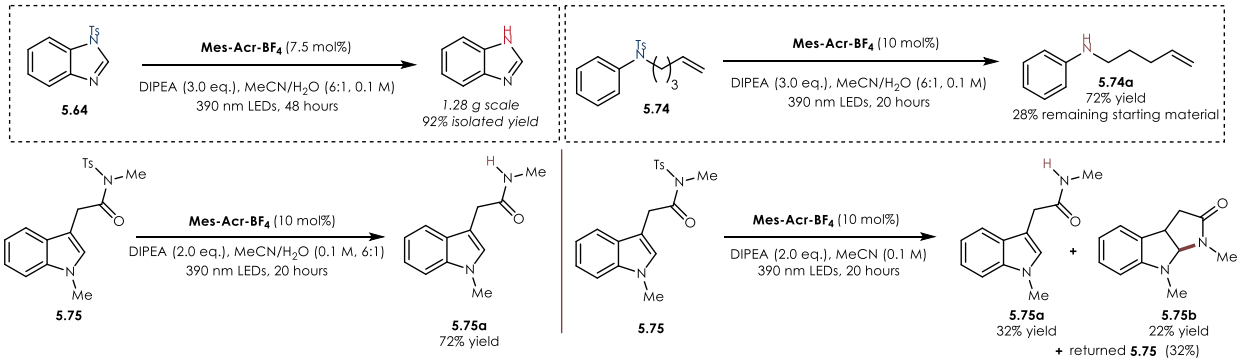

Figure 5.17: Gram-scale detosylation and initial mechanistic experiments probing hydrogen atom transfer

Efforts to intercept intermediates using Michael acceptors or substrates which may potentially undergo 5-exo-trig cyclization with a pendant alkene following radical generation failed to yield any products indicative of nitrogen centered radical generation (**Figure 5.17**). While these experiments cannot entirely exclude the formation of nitrogen-centered radicals during the transformation, the results indicate that any nitrogen-centered radicals formed undergo very rapid hydrogen atom transfer to yield the desulfonylation product, outcompeting other possible intramolecular or intermolecular processes in most cases. Substrate **5.75**, bearing a pendant Ts-amide, was detosylated in 72% yield in the presence of 2.0 equiv. DIPEA in a 6:1 MeCN/H_2O solvent system after 20 hours. Curiously, the removal of water from the solvent system leads to the formation of the desired detosylation product in 32% yield as well as a product corresponding to the cyclization of a punitive nitrogen-centered radical onto the indole core in 22% yield (32% remaining starting material). This result indicates that water may serve a critical role in accelerating the rate of HAT in this system.

Reductive deoxygenation of aryl ester and sulfonate derivatives is also observed under the reaction conditions, albeit in reduced yields. A brief screen of substituted anisole derivatives showed that decarbonylative cleavage to the corresponding phenol **5.77** was possible when using the corresponding phenolic trifluoroacetate ester as the substrate for reduction. The corresponding mesylate derivative afforded the deoxygenation product **5.76** in 36% yield, with 8% of the phenol product present as well. Benzylic alcohol derived mesylate **5.78** was deoxygenated to yield methylbenzoate in 47% yield, indicating that this process may applicable to both phenol and benzylic alcohol derivatives.

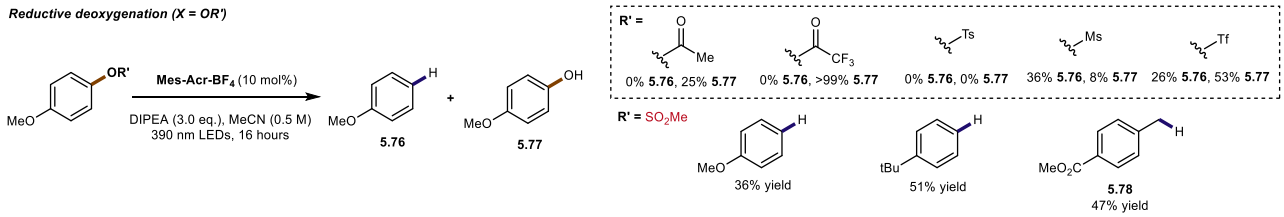

Figure 5.18: Initial investigations of reductive deoxygenation using Mes-Acr•

In conclusion, an acridine radical generated *in situ* from single electron reduction of an acridinium derivative may act as potent single electron reductant upon excitation with 390 nm light. Spectroscopic and computational investigations indicate the formation of at least two distinct excited states, one of which may be characterized as a TICT state. The development of chemoselective dehalogenation and desulfonylation reactions utilizing **Mes-Acr•** compliment the well-known oxidative chemistry associated with acridinium salts and highlight the potential for the development of other types of reactions based on excitation of organic radicals.

APPENDIX A: SUPPORTING INFORMATION FOR "GENERATION AND TRAPPING OF α-CARBAMYL RADICALS VIA ORGANIC PHOTOREDOX CATALYSIS"

A.1: General Information

Proton and carbon magnetic resonance spectra (^{1}H NMR and ^{13}C NMR) were recorded on a Bruker AVANCE III 600 CryoProbe (^{1}H NMR at 600 MHz, ^{13}C NMR at 151 MHz and ^{19}F NMR at 565 MHz) spectrometer with solvent resonance as the internal standard (^{1}H NMR: CDCl3 at 7.26 ppm; ^{13}C NMR: CDCl3 at 77.0 ppm). ^{1}H NMR data are reported as follows: chemical shift, multiplicity (s = singlet, d = doublet, t = triplet, dd = doublet of doublets, ddd = doublet of doublets of doublets, ddddd = doublet of doublets of doublets of doublets of doublets, dt = doublet of triplets, ddt = doublet of doublets of triplets, td = triplet of doublets, tt = triplet of triplets, m = multiplet, q = quartet), coupling constants (Hz), and integration. Electrochemical potentials were obtained with a standard set of conditions to main internal consistency. Cyclic voltammograms were collected with a Pine WaveNow Potentiostat. Data was analyzed using MATLAB by subtracting a background current prior to identifying the maximum current (C_p) and determining the potential ($E_{p/2}$) at half this value ($C_{p/2}$). The obtained value was referenced to Ag|AgCl and converted to SCE by subtracting 0.03 V. Infrared (IR) spectra were obtained using a Jasco 260 Plus Fourier transform infrared spectrometer. High Resolution Mass Spectra (HRMS) were obtained using a Thermo LTqFT mass spectrometer with electrospray ionization in positive or negative mode. Optical rotation values were determined using a Jasco DIP-1000 digital polarimeter. Flash chromatography was performed using SiliaFlash P60 silica gel (40-63 μm) purchased from Silicycle. Irradiation of photochemical reactions was carried out using 2 x 15W PAR38 Royal Blue Aquarium LED flood lamps Model# 6851 purchased from Ecoxotic with an output centered at a wavelength of approximately 455 nm. Irradiance at the reaction

vessel was determined using a ThorLabs Digital Optical Power and Energy Meter (part no. PM100D). The reactions were carried out in 2-dram borosilicate glass vials (purchased from Fisher Scientific, catalogue # 03-339- 22D) sealed with polypropylene caps equipped with Teflon coated septa (purchased through VWR international, Microliter Product # 15-0060K). All reagents were purchased from Sigma-Aldrich, Fisher Scientific, Oakwood Chemical or TCI corporation and were used without additional purification unless otherwise noted.

A.2: Electrochemical Data

Samples were prepared with 0.1 mmol of analyte in 5 mL of 0.1 M tetra-*N*-butylammonium hexafluorophosphate in dry, degassed acetonitrile. Measurements employed a glassy carbon working electrode, platinum wire counter electrode, 3.5 M NaCl silver-silver chloride reference electrode, and a scan rate of 100 mV/s. Reductions were measured by scanning potentials in the negative direction and oxidations in the positive direction.

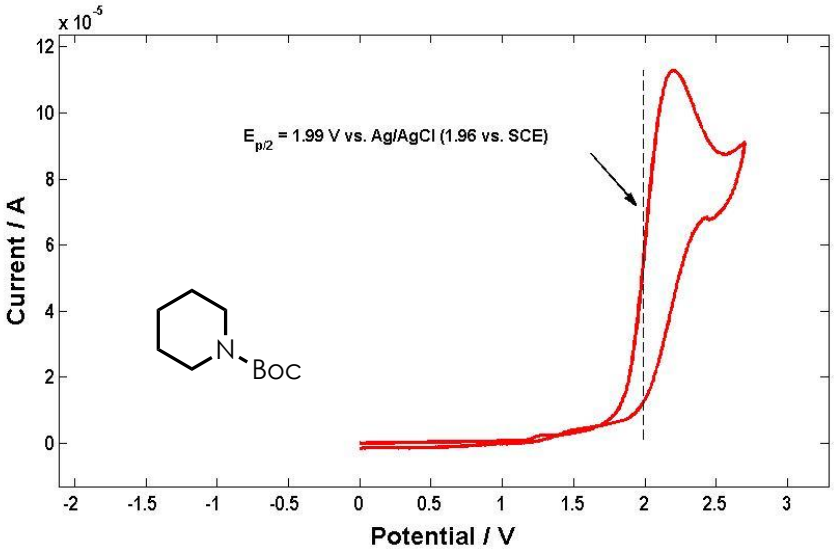

Figure A.1: Cyclic voltammagram for Boc-piperidine, collected in MeCN and referenced to SCE

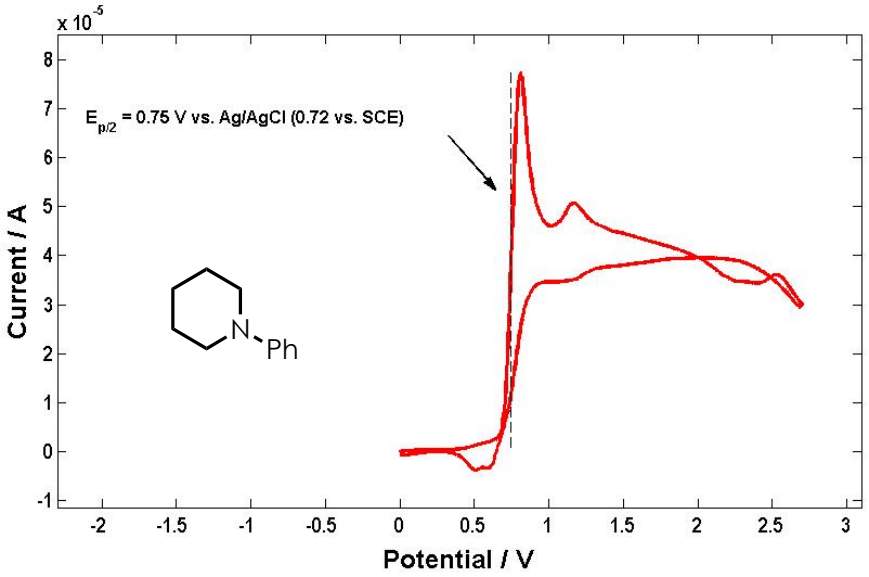

Figure A.2: Cyclic voltammagram for *N*-phenylpiperidine, collected in MeCN and referenced to SCE

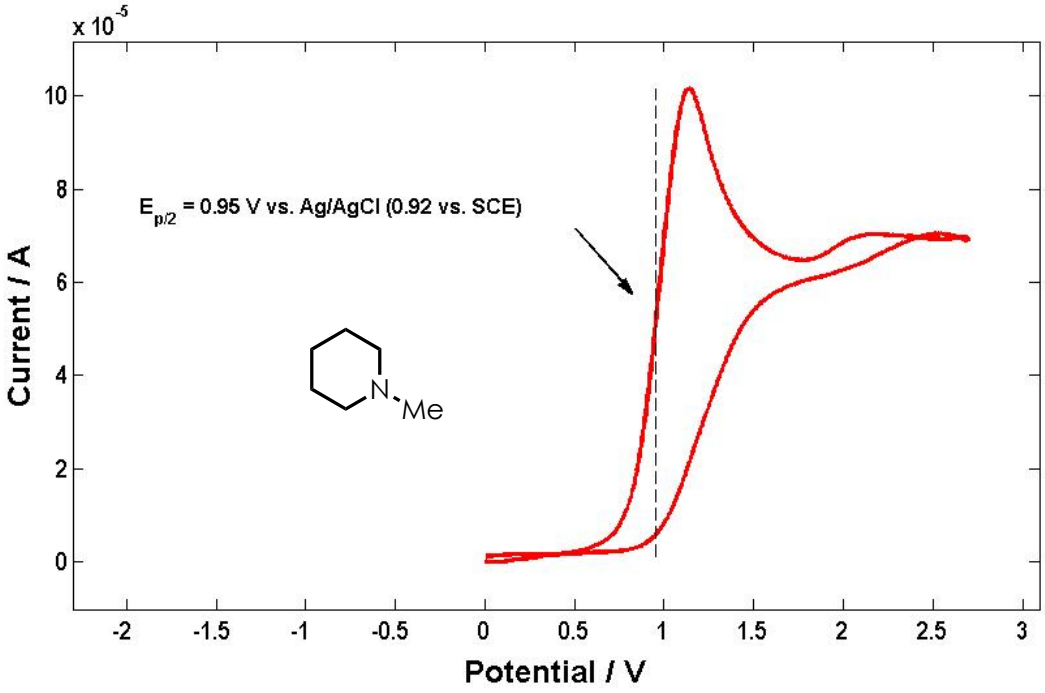

Figure A.3: Cyclic voltammagram for *N*-methylpiperidine, collected in MeCN and referenced to SCE

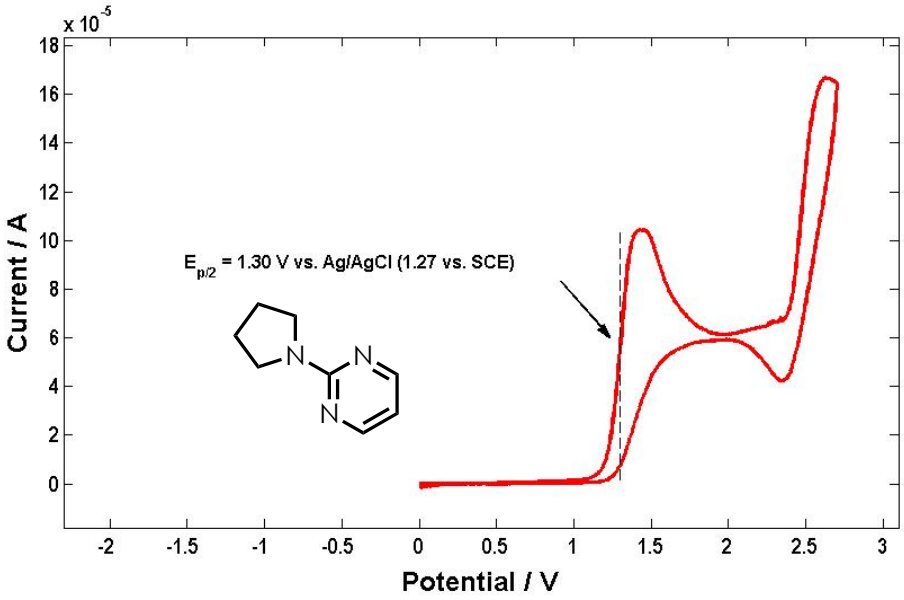

Figure A.4: Cyclic voltammagram for 2-(pyrrolidin-1-yl)pyrimidine, collected in MeCN and referenced to SCE

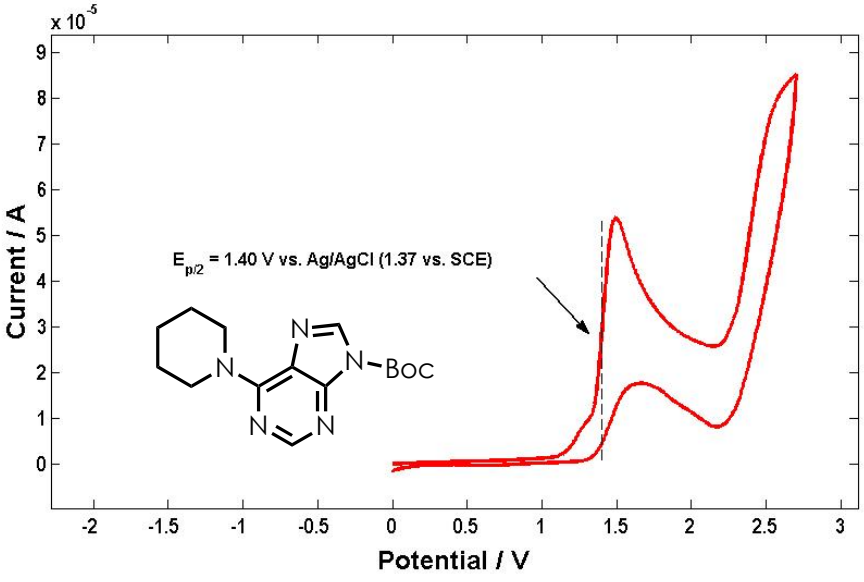

Figure A.5: Cyclic voltammagram for *tert*-butyl 6-(piperidin-1-yl)-9H-purine-9-carboxylate, collected in MeCN and referenced to SCE

A.3: Synthesis and Characterization of Catalyst and Substrates:

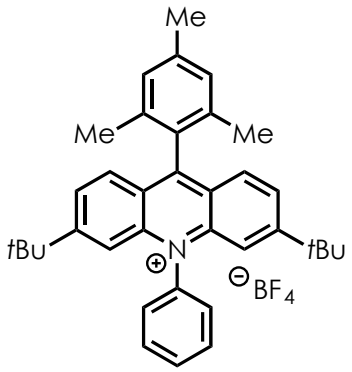

3,6-Di-*tert*-butyl-9-mesityl-10-phenylacridin-10-ium tetrafluoroborate prepared according to literature precedent: Analytical data matched that reported in the literature.[1]

^{1}H NMR (600 MHz, CDCl3) δ 7.99 (td, *J* = 7.5, 6.7, 1.3 Hz, 2H), 7.94 (s, 1H), 7.94 – 7.90 (m, 1H), 7.83 – 7.74 (m, 6H), 7.44 (dd, *J* = 1.5, 0.7 Hz, 2H), 7.19 (d, *J* = 1.2 Hz, 2H), 2.51 (s, 3H), 1.89 (s, 6H), 1.32 (s, 18H). **^{13}C NMR** (151 MHz, $CDCl_3$) δ 163.53, 162.26, 142.14, 140.15, 136.85, 136.17, 131.81, 131.60, 129.31, 128.93, 128.26, 128.03, 127.45, 124.04, 115.08, 36.67, 30.22, 21.32, 20.25. **^{19}F NMR** (565 MHz, $CDCl_3$) δ -150.85, -154.50.

Preparation of Amine Substrates:

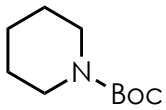

***tert*-Butyl piperidine-1-carboxylate** was prepared according to a published procedure; spectral data were in agreement with literature values.[146]

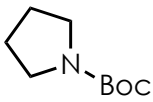

***tert*-Butyl pyrrolidine-1-carboxylate** was prepared according to a published procedure; spectral data were in agreement with literature values.[147]

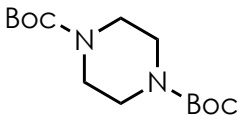

Di-*tert*-butyl piperazine-1,4-dicarboxylate was prepared according to the following procedure: Piperazine (10 mmol, 0.86 g) was dissolved in 70 mL of DCM. Et_3N (15 mmol, 2.1 mL) was added to the solution before di-*tert*-butyl dicarbonate (22 mmol, 4.8 g). The reaction mixture stirred overnight, before being concentrated and purified by column chromatography (10% EtOAc/hexane). Spectral data were in agreement with literature values.[148]

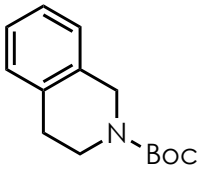

***tert*-Butyl 3,4-dihydroisoquinoline-2(1*H*)-carboxylate** was prepared according to a published procedure; spectral data were in agreement with literature values.[149]

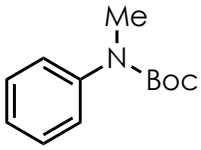

***tert*-Butyl methyl(phenyl)carbamate** was prepared according to a published procedure; spectral data were in agreement with literature values.[150]

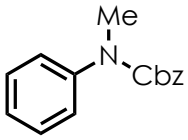

Benzyl methyl(phenyl)carbamate: was prepared according to a published procedure; spectral data were in agreement with literature values.[151]

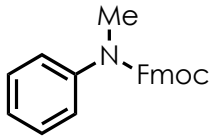

(9*H*-Fluoren-9-yl)methyl methyl(phenyl)carbamate: Fmoc-Cl (3.02 g, 11.7 mmol) in dioxane (20 mL) was added slowly to an ice-bath cooled solution of n-methylaniline (0.5 g, 4.7 mmol) in dioxane (50 mL) and 10 % $NaHCO_3$ (50 mL). The mixture was stirred in the ice-bath for 30 minutes and then warmed to room temperature where it was allowed to stir for 12 hours. The solution was poured into H_2O, and extracted with Et_2O (50 mL x 3). The organic layer was separated and washed with H_2O (3 mL). The organic layer was dried with $MgSO_4$ and concentrated in vacuo. Reaction mixture was purified by column chromatography (0-10% EtOAc/hexane) to give the desired compound (1.4 g, 4.4 mmol, 94%) as a white solid.

^{1}H NMR (600 MHz, chloroform-*d*) δ 7.79 (d, *J* = 7.6 Hz, 2H), 7.44 (dt, *J* = 13.0, 7.6 Hz, 5H), 7.39 – 7.20 (m, 6H), 4.48 (d, *J* = 6.9 Hz, 2H), 4.19 (s, 1H), 3.38 (s, 3H).

^{13}C NMR (151 MHz, $CDCl_3$) δ 155.57, 143.93, 143.18, 141.33, 129.08, 127.67, 127.01, 126.53, 125.20, 119.96, 67.66, 47.19, 37.87.

IR (thin film): 1700, 1596, 1497, 1341 1150, 756.

HRMS (+ESI): *m/z* calculated for [M+Na]+: 352.130830; found: 352.13019.

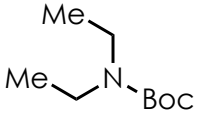

***tert*-Butyl diethylcarbamate** was prepared according to a published procedure; spectral data were in agreement with literature values.[152]

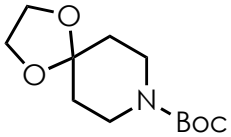

***tert*-Butyl 1,4-dioxa-8-azaspiro[4.5]decane-8-carboxylate** was prepared according to a published procedure; spectral data were in agreement with literature values.[153]

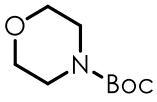

***tert*-Butyl morpholine-4-carboxylate** was prepared according to a published procedure; spectral data were in agreement with literature values.[154]

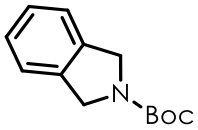

***tert*-Butyl isoindoline-2-carboxylate** was prepared according to the following procedure: Isoindoline (1.00 g, 8.39 mmol) was stirred with DCM (10 mL). Boc_2O (2.75 g, 12.6 mmol) was added in one portion, followed by triethylamine (1.8 mL, 12.6 mmol). The reaction mixture was allowed to stir overnight before being concentrated to yield a dark oil. The product was isolated *via* flash column chromatography (15% EtOAc/hexaneane) to yield the desired product as a white solid (2.28 g, quant.). Spectral data were in agreement with literature values.[155]

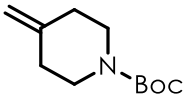

***tert*-Butyl 4-methylenepiperidine-1-carboxylate** was prepared according to the following procedure: Methyltriphenylphosphonium bromide (1.97 g, 5.52 mmol) was stirred with THF (20 mL) under nitrogen in a flame-dried flask. Potassium *tert*-butoxide (619 mg, 5.52 mmol) was added in one portion and the reaction mixture became a bright yellow color. The reaction mixture

was allowed to stir for 30 minutes at room temperature. *tert*-Butyl 4-oxopiperidine-1-carboxylate (1.00 g, 5.02 mmol) was then added in one portion and the yellow color disappeared. A white precipitate formed and the reaction mixture was allowed to stir overnight. The next day, the reaction mixture was concentrated and the desired product was isolated *via* flash column chromatography (5% EtOAc/hexaneane) as a clear oil (593 mg, 60% yield). Spectral data were in agreement with literature values.[10]

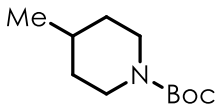

***tert*-Butyl 4-methylpiperidine-1-carboxylate** was prepared according to the following procedure: *tert*-Butyl 4-methylenepiperidine-1-carboxylate (300 mg, 1.52 mmol) was dissolved in methanol (10 mL) and sparged with argon for 10 minutes. A small portion of Pd/C was added to the flask and the resulting suspension was sparged with hydrogen for 10 minutes. The flask was then stirred for 24 hours under an atmosphere of hydrogen (balloon). The reaction mixture was then filtered through a celite pad and concentrated to yield the desired product as a clear oil (293 mg, 97% yield). Spectral data were in agreement with literature values.[156]

Di-*tert*-Butyl 3,4-dihydro-1H-pyrido[3,4-b]indole-2,9-dicarboxylate was prepared according to a published procedure; spectral data were in agreement with literature values.[157]

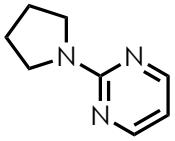

2-(Pyrrolidin-1-yl)pyrimidine was prepared according to a published procedure; spectral data were in agreement with literature values.[158]

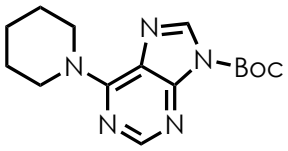

***tert*-Butyl 6-(piperidin-1-yl)-9*H*-purine-9-carboxylate** was prepared according to a published procedure; spectral data were in agreement with literature values.[159]

Preparation of Radical Acceptors

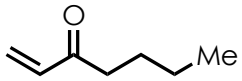

Hept-1-en-3-one was prepared according to a published procedure; spectral data were in agreement with literature values.[160]

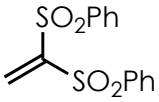

(Ethene-1,1-diyldisulfonyl)dibenzene was prepared according to a published procedure; spectral data were in agreement with literature values.[161]

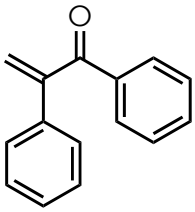

1,2-Diphenylprop-2-en-1-one was prepared according to a published procedure; spectral data were in agreement with literature values.[162]

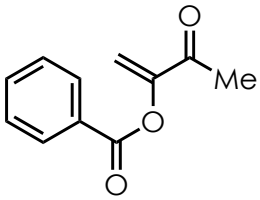

3-Oxobut-1-en-2-yl benzoate was prepared according to a published procedure; spectral data were in agreement with literature values.[163]

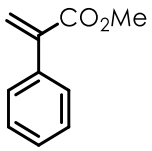

Methyl 2-phenylacrylate was prepared according to a published procedure; spectral data were in agreement with literature values.[164]

A.4: Reaction Optimization

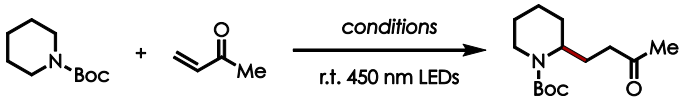

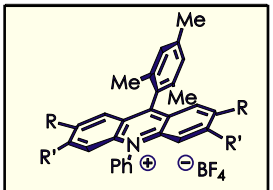

Catalyst 1: R = H, R' = tBu
Catalyst 2: R = R' = H
Catalyst 3: R = Me, R' = H

entry	catalyst	concentration	solvent	time	X:XX	yield	additive
1	2	0.1	DCE	20	1:1	< 5	-
2	3	0.1	DCE	20	1:1	< 5	-
3	1	0.1	DCE	20	1:1	33	-
4	1	0.1	DCE	20	1:2	39	-
5	1	0.1	DCE	20	1:3	45	-
6	1	0.1	DCE	20	1:4	43	-
7	1	0.1	MECN	20	1:3	28	-
8	1	0.1	$PhCF_3$	20	1:3	< 5	-
9	1	0.1	DCM	20	1:3	51	-
10	1	0.1	$MeNO_2$	20	1:3	13	-
11	1	0.05	DCM	20	1:3	42	-
12	1	0.033	DCM	20	1:3	35	-
13	1	0.025	DCM	20	1:3	42	-
14	2	0.1	DCM	20	1:3	< 5	-
15	3	0.1	DCM	20	1:3	< 5	-
16	1	0.1	DCE	20	2:1	57	-
17	1	0.1	DCE	20	3:1	68	-
18	1	0.1	DCE	20	4:1	65	-
19	1	0.1	DCM	1	3:1	31	-
20	1	0.1	DCM	2	3:1	57	-
21	1	0.1	DCM	3	3:1	58	-
22	1	0.1	DCM	6	3:1	79	-
23	1	0.1	DCM	9	3:1	63	-
24	1	0.1	DCM	12	3:1	71	-
25	1	0.1	DCM	18	3:1	72	-
26	1	0.1	DCM	36	3:1	58	-
27	1	0.05	DCM	20	1:3	33	HCO_2H
28	1	0.05	DCM	20	1:3	42	$MeCO_2H$
29	1	0.05	DCM	20	1:3	< 5	$TsOHÅEH_2O$
30	1	0.05	DCM	20	1:3	43	NH_4Cl
31	1	0.05	DCM	20	1:3	36	$NaBF_4$
32	1	0.05	DCM	20	1:3	28	$LiBF_4$
33	1	0.05	DCM	20	1:3	< 5	$Sc(OTf)_3$
34	1	0.05	DCM	20	1:3	23	$Zn(OTf)_2$
35	1	0.05	DCM	20	1:3	12	$Ce(OTf)_3$
36	1	0.05	DCM	20	1:3	12	2,6-lutidine
37	1	0.05	DCM	20	1:3	41	2,6-di-tert-butyl-4-methylpyridine
38	1	0.05	DCM	20	1:3	19	K_2CO_3
39	1	0.05	DCM	20	1:3	21	pH 9 buffer

A.5: Procedure and Data for Product Synthesis

Reaction Setup:

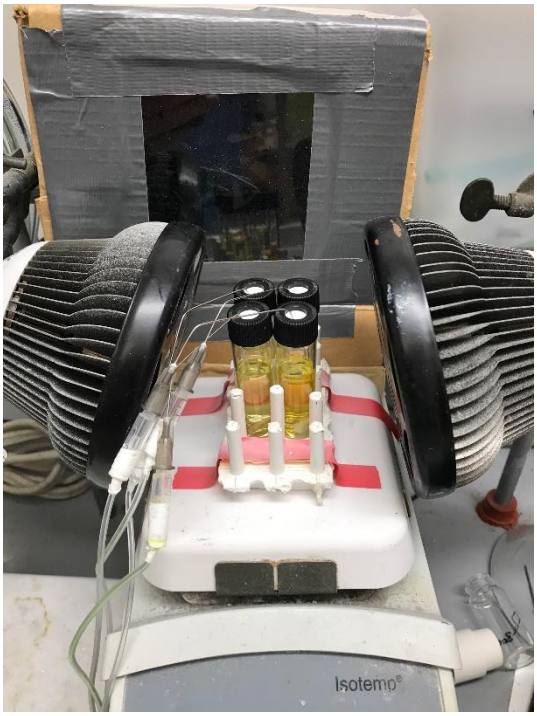

Light intensity at reaction site was determined to be 96mW/cm^2

General Procedure:

To a 1- or 2-dram vial charged with a Teflon-coated stir was added 3,6-Di-*tert*-Butyl-9-mesityl-*N*-phenylacridinium (2.89 mg, 0.005 mmol) and amine substrate (0.30 mmol). The vial was then sealed with a Teflon coated septum cap before 1 mL (0.10 M) of dichloromethane was added via syringe and the mixture sparged with N_2 for 5 minutes. The Michael acceptor was added (0.1 mmol) and the reactions were stirred for 6 hours under irradiation with 450 nm LEDs. After completion, the reaction mixture was concentrated in vacuo and purified using silica gel chromatography to afford the desired product.

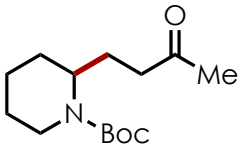

(±)-*tert*-Butyl-2-(3-oxobutyl)piperidine-1-carboxylate (2.2): Isolated by column chromatography (0-20% EtOAc/hexane), as a yellow oil, 21.2 mg, 83%. Analytical data matched that reported in the literature.[165]

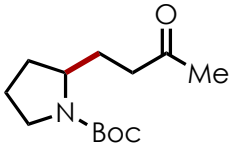

***tert*-Butyl (*S*)-2-(3-oxobutyl)pyrrolidine-1-carboxylate (2.3)**: Isolated by column chromatography (0-20% EtOAc/hexane), as a yellow oil, 21.0 mg, 87%. Analytical data matched that reported in the literature.[165]

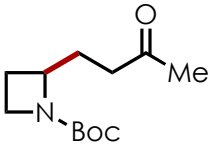

***tert*-Butyl (*R*)-2-(3-oxobutyl)azetidine-1-carboxylate (2.4)**: Isolated by column chromatography (0-20% EtOAc/hexane), as a colorless oil, 15.4 mg, 68%.

^{1}H NMR (600 MHz, chloroform-*d*) δ 4.22 (p, *J* = 6.5 Hz, 1H), 3.89 – 3.74 (m, 2H), 2.62 – 2.48 (m, 2H), 2.33 – 2.24 (m, 1H), 2.18 (s, 3H), 2.00 (ddq, *J* = 63.6, 14.5, 7.2 Hz, 2H), 1.83 (q, *J* = 9.3, 8.3 Hz, 1H), 1.45 (s, 9H).

^{13}C NMR (151 MHz, $CDCl_3$) δ 208.45, 156.86, 79.34, 61.33, 46.37, 39.42, 29.91, 29.70, 28.44, 21.79.

IR (thin film): 2971, 2929, 2892, 1603, 1363, 1249, 1134.

HRMS (+ESI): *m/z* calculated for [M+Na]+: 250.141395; found: 250.14130.

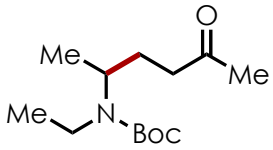

***tert*-Butyl (*S*)-ethyl(5-oxohexan-2-yl)carbamate (2.5)**: Isolated by column chromatography (0-20% EtOAc/hexane), as a yellow oil, 9.5 mg, 39%. Analytical data matched that reported in the literature.[166]

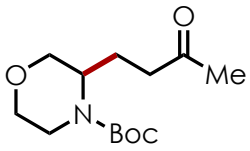

***tert*-Butyl (*R*)-3-(3-oxobutyl)morpholine-4-carboxylate (2.6)**: Isolated by column chromatography (40% EtOAc/hexane), as a yellow oil, 15.9 mg, 62%.

^{1}H NMR (500 MHz, chloroform-*d*) δ 3.94 – 3.86 (m, 1H), 3.80 – 3.70 (m, 2H), 3.64 (d, *J* = 11.7 Hz, 2H), 3.49 (dd, *J* = 11.6, 3.3 Hz, 1H), 3.35 (td, *J* = 11.9, 3.0 Hz, 1H), 3.03 (s, 1H), 2.50 – 2.24 (m, 2H), 2.08 (s, 3H), 1.76 (dtd, *J* = 13.0, 7.5, 5.4 Hz, 1H), 1.39 (s, 9H).

^{13}C NMR (151 MHz, chloroform-*d*) δ 207.71, 154.72, 80.01, 69.65, 66.91, 39.78, 36.63, 29.97, 29.69, 28.39, 24.68.

IR (thin film): 2971, 1686, 1409, 1364, 1165, 1119, 864

HRMS (+ESI): *m/z* calculated for [M+Na]+: 280.15208; found: 280.15229.

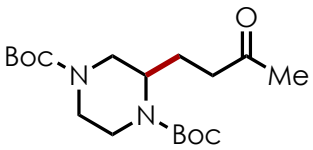

Di-*tert*-butyl (*R*)-2-(3-oxobutyl)piperazine-1,4-dicarboxylate (2.7): Isolated by column chromatography (0-20% EtOAc/hexane), as a white solid, 32.1 mg, 90%.

^{1}H NMR (600 MHz, chloroform-*d*) δ 4.21 – 3.69 (m, 4H), 2.83 (d, *J* = 135.3 Hz, 3H), 2.55 – 2.29 (m, 2H), 2.12 (d, *J* = 2.8 Hz, 3H), 1.95 – 1.79 (m, 1H), 1.79 – 1.68 (m, 1H), 1.50 – 1.35 (m, 18H).

^{13}C NMR (151 MHz, $CDCl_3$) δ 207.51, 154.91, 154.70, 80.07, 80.02, 47.20, 45.48, 43.95, 42.81, 39.62, 29.96, 28.35, 22.58.

IR (thin film): 2974, 1687, 1412, 1364, 1227, 1164, 865.

HRMS (+ESI): *m/z* calculated for [M+Na]+: 379.220922; found: 379.22077.

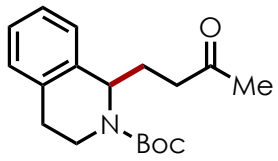

***tert*-Butyl 1-(3-oxobutyl)-3,4-dihydroisoquinoline-2(1*H*)-carboxylate (2.8)**: Isolated by column chromatography (5-25% EtOAc/hexane), as a colorless oil, 30.1 mg, 99%.

^{1}H NMR (600 MHz, chloroform-*d*) δ 7.24 – 7.14 (m, 3H), 7.11 (d, *J* = 5.9 Hz, 1H), 5.20 – 5.00 (m, 1H), 4.30 – 3.86 (m, 1H), 3.32 – 3.04 (m, 1H), 3.01 – 2.82 (m, 1H), 2.72 (d, *J* = 16.3 Hz, 1H), 2.63 (dt, *J* = 17.9, 7.5 Hz, 1H), 2.59 – 2.49 (m, 1H), 2.17 (s, 3H), 2.13 – 1.92 (m, 2H), 1.48 (s, 9H).

^{13}C NMR (151 MHz, $CDCl_3$) δ 208.13, 207.60, 155.19, 154.88, 137.79, 137.57, 134.26, 134.13, 129.07, 128.73, 127.33, 127.13, 126.52, 126.10, 80.04, 79.58, 54.02, 53.51, 40.23, 40.03, 38.33, 36.66, 30.21, 28.47.

IR (thin film): 2974, 1684, 1416, 1364, 1159, 748.

HRMS (+ESI): *m/z* calculated for [M+Na]+: 326.173244; found: 326.17301.

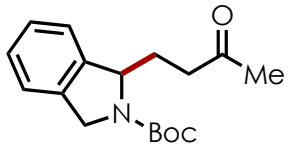

***tert*-Butyl-1-(3-oxobutyl)isoindoline-2-carboxylate (2.9)**: Isolated by column chromatography (15% EtOAc/hexane), as a yellow oil, 63.2 mg (0.3 mmol scale), 73%.

^{1}H NMR (400 MHz, chloroform-*d*) δ 7.45 – 7.05 (m, 4H), 5.21 – 5.11 (m, 1H), 4.75 (dd, *J* = 35.9, 14.9 Hz, 1H), 4.58 – 4.44 (m, 1H), 2.62 – 2.27 (m, 2H), 2.20 – 1.98 (m, 5H), 1.69 – 1.04 (m, 9H).

^{13}C NMR (151 MHz, chloroform-*d*) δ 208.46, 208.19, 154.55, 140.10, 140.02, 136.95, 136.66, 127.70, 127.62, 127.54, 127.47, 122.58, 122.43, 122.37, 80.08, 79.71, 62.21, 62.08, 52.54, 52.45, 38.60, 37.56, 29.88, 29.57, 29.16, 28.94, 28.52.

(Mixture of rotomers)

IR (thin film): 2976, 2360, 1712, 1367, 1276, 764

HRMS (+ESI): *m/z* calculated for [M+Na]+: 312.157594; found: 312.15741.

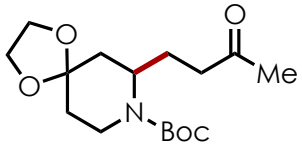

***tert*-Butyl 7-(3-oxobutyl)-1,4-dioxa-8-azaspiro[4.5]decane-8-carboxylate (2.10):** Isolated by column chromatography (10-50% EtOAc/hexane), as a orange oil, 23.5 mg, 32%.

^{1}H NMR (600 MHz, chloroform-*d*) δ 4.40 – 4.30 (m, 1H), 4.11 – 3.89 (m, 5H), 3.07 – 2.94 (m, 1H), 2.49 – 2.33 (m, 2H), 2.28 – 2.12 (m, 4H), 1.86 (dd, *J* = 13.7, 6.6 Hz, 1H), 1.75 (dtd, *J* = 14.8, 7.6, 4.9 Hz, 1H), 1.71 – 1.59 (m, 3H), 1.53 – 1.43 (m, 9H).

^{13}C NMR (151 MHz, $CDCl_3$) δ 208.34, 154.87, 107.16, 79.70, 77.23, 77.02, 76.80, 64.68, 63.85, 50.15, 40.59, 37.52, 34.63, 30.04, 28.44, 25.10.

IR (thin film): 2965, 1684, 1415, 1377, 1165, 1105.

HRMS (+ESI): *m/z* calculated for [M+Na]+: 314.196199; found: 314.19644.

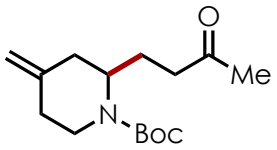

***tert*-Butyl 4-methylene-2-(3-oxobutyl)piperidine-1-carboxylate (2.11)**: Isolated by column chromatography (15% EtOAc/hexane), as a yellow oil, 8.2 mg, 31%.

^{1}H NMR (500 MHz, chloroform-*d*) δ 4.80 (dd, *J* = 44.1, 1.9 Hz, 1H), 4.45 – 3.76 (m, 2H), 2.75 (s, 1H), 2.36 (tdd, *J* = 17.7, 11.2, 5.8 Hz, 2H), 2.23 – 2.05 (m, 4H), 1.96 – 1.74 (m, 1H), 1.79 – 1.56 (m, 2H), 1.57 – 1.40 (m, 9H), 1.38 – 1.22 (m, 2H), 1.03 – 0.83 (m, 1H).

^{13}C NMR (151 MHz, chloroform-*d*) δ 175.92, 155.05, 154.77, 142.20, 111.13, 81.88, 79.65, 79.32, 70.09, 54.95, 50.43, 39.84, 38.56, 34.12, 30.06, 29.70, 28.46, 28.15, 28.04, 23.86, 20.76, 14.02. (Mixture of rotomers)

IR (thin film): 2924, 2362, 1687, 1412, 1261, 1162, 764

HRMS (+ESI): *m/z* calculated for [M+Na]+: 290.173244; found: 290.17302.

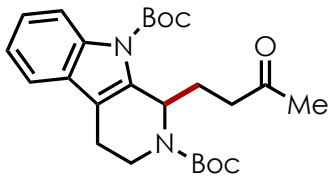

Di-*tert*-butyl (*R*)-1-(3-oxobutyl)-3,4-dihydro-1*H*-pyrido[3,4-*b*]indole-2,9-dicarboxylate (2.12): Isolated by column chromatography (30% EtOAc – 50% EtOAc/hexanes gradient), as a yellow solid, 17.7 mg, 20% (0.2 mmol scale).

^{1}H NMR (500 MHz, chloroform-*d*) δ 8.61 – 8.32 (m, 1H), 7.52 – 7.48 (m, 1H), 7.37 (d, *J* = 8.1 Hz, 1H), 7.19 (t, *J* = 7.6 Hz, 1H), 7.12 (t, *J* = 7.4 Hz, 1H), 5.30 – 5.12 (m, 1H), 4.57 – 4.24 (m,

1H), 3.24 – 3.02 (m, 1H), 2.91 – 2.67 (m, 3H), 2.59 (s, 1H), 2.31 – 2.19 (m, 3H), 2.00 – 1.92 (m, 1H), 1.51 (d, *J* = 11.9 Hz, 18H).

^{13}C NMR (151 MHz, , chloroform-*d*) δ 171.18, 155.47, 154.84, 135.96, 134.46, 133.93, 126.72, 121.74, 119.41, 118.00, 110.98, 108.76, 108.16, 80.22, 79.93, 60.42, 50.77, 50.18, 40.02, 38.77, 37.57, 30.13, 29.72, 28.49, 21.48, 21.08, 14.22. (Mixture of rotomers)

IR (thin film): 3009, 2360, 1689, 1276, 1261

HRMS (+ESI): *m/z* calculated for [M+Na]+: 465.236024; found: 465.23453.

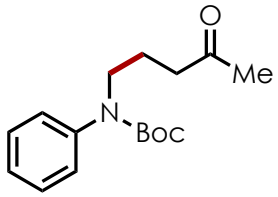

***tert*-Butyl (4-oxopentyl)(phenyl)carbamate (2.13)**: Isolated by column chromatography (5-20% EtOAc/hexane), as a yellow oil, 27.0 mg, 97%.

^{1}H NMR (600 MHz, chloroform-*d*) δ 7.35 (t, *J* = 7.7 Hz, 2H), 7.25 – 7.16 (m, 3H), 3.66 (t, *J* = 7.2 Hz, 2H), 2.47 (t, *J* = 7.3 Hz, 2H), 2.12 (s, 3H), 1.83 (p, *J* = 7.2 Hz, 2H), 1.44 (s, 9H).

^{13}C NMR (151 MHz, $CDCl_3$) δ 207.51, 154.91, 154.70, 80.07, 80.02, 77.27, 77.05, 47.20, 45.48, 43.95, 42.81, 39.62, 29.96, 28.35, 22.58.

IR (thin film): 2975, 1602, 1390, 1298, 1158, 756.

HRMS (+ESI): *m/z* calculated for [M+Na]+: 300.157544; found: 300.15728.

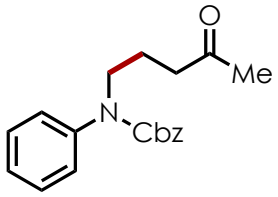

Benzyl (4-oxopentyl)(phenyl)carbamate (2.14): Isolated by column chromatography (0-30% EtOAc/hexane), as a yellow oil, 25.2 mg, 81%.

^{1}H NMR (600 MHz, chloroform-*d*) δ 7.41 – 7.18 (m, 10H), 5.16 (s, 2H), 3.72 (t, *J* = 7.1 Hz, 2H), 2.46 (t, *J* = 7.3 Hz, 2H), 2.08 (s, 3H), 1.88 – 1.76 (m, 2H).

^{13}C NMR (151 MHz, $CDCl_3$) δ 207.90, 155.49, 141.54, 136.65, 129.08, 128.40, 127.86, 127.55, 127.26, 126.81, 67.17, 49.58, 40.40, 29.91, 22.35.

IR (thin film): 2974, 1700, 1494, 1403, 1294, 697.

HRMS (+ESI): *m/z* calculated for [M+Na]+: 334.141396; found: 334.14086.

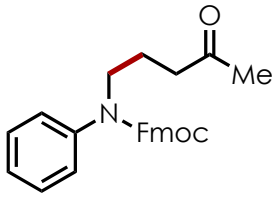

(9*H*-Fluoren-9-yl)methyl (4-oxopentyl)(phenyl)carbamate (2.15): Isolated by column chromatography (0-40% EtOAc/hexane), as white solid, 31.4 mg, 79%.

^{1}H NMR (600 MHz, chloroform-*d*) δ 7.74 (d, *J* = 7.6 Hz, 2H), 7.38 (ddt, *J* = 25.3, 17.6, 7.5 Hz, 6H), 7.27 – 7.14 (m, 5H), 4.60 – 4.24 (m, 2H), 4.13 (d, *J* = 38.2 Hz, 1H), 3.67 (s, 2H), 2.45 (s, 2H), 2.13 (s, 3H), 1.75 (d, *J* = 57.4 Hz, 2H).

^{13}C NMR (151 MHz, $CDCl_3$) δ 207.92, 155.52, 143.80, 141.27, 134.70, 129.19, 127.75, 127.58, 127.04, 126.91, 125.10, 119.84, 67.30, 49.56, 47.13, 40.45, 29.98, 22.31.

IR (thin film): 3084, 2946, 1702, 1405, 1295, 740.

HRMS (+ESI): *m/z* calculated for [M+Na]+: 422.172695; found: 422.17197.

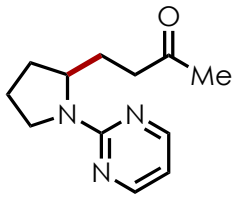

4-(1-(Pyrimidin-2-yl)pyrrolidin-2-yl)butan-2-one (2.16): Isolated by column chromatography (0-55% EtOAc/hexane), as an orange solid, 21.9 mg, 100%.

^{1}H NMR (600 MHz, chloroform-*d*) δ 8.24 (td, *J* = 4.0, 3.5, 1.6 Hz, 2H), 6.41 (tdd, *J* = 4.8, 4.0, 3.3, 1.6 Hz, 1H), 4.20 – 4.09 (m, 1H), 3.59 – 3.45 (m, 2H), 2.51 – 2.39 (m, 2H), 2.13 – 2.07 (m, 3H), 2.06 – 1.86 (m, 4H), 1.77 – 1.65 (m, 2H).

^{13}C NMR (151 MHz, $CDCl_3$) δ 208.68, 160.52, 157.51, 109.20, 56.69, 47.02, 40.70, 30.26, 29.69, 27.59, 23.34.

IR (thin film): 2691, 2872, 1711, 1580, 1494, 1338, 798.

HRMS (+ESI): *m/z* calculated for [M+H]+: 220.144439; found: 220.14434.

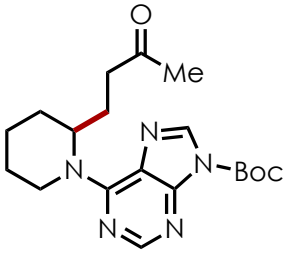

***tert*-Butyl (*S*)-6-(2-(3-oxobutyl)piperidin-1-yl)-9*H*-purine-9-carboxylate (2.17)**: Isolated by column chromatography (0-55% EtOAc/hexane), as a yellow oil, 22.6 mg, 60.5%.

^{1}H NMR (400 MHz, chloroform-*d*) δ 8.45 (s, 1H), 8.15 (s, 1H), 6.01 – 4.96 (m, 2H), 3.11 (s, 1H), 2.56 – 2.33 (m, 2H), 2.25 (dtt, *J* = 16.1, 11.7, 5.9 Hz, 1H), 2.04 (s, 3H), 1.69 (s, 16H).

^{13}C NMR (101 MHz, $CDCl_3$) δ 208.33, 154.49, 154.32, 150.99, 146.11, 136.46, 119.93, 86.22, 40.19, 30.03, 29.69, 29.13, 27.97, 25.86, 23.66, 19.20.

IR (thin film): 2931, 1749, 1714, 1580, 1258, 1138.

HRMS (+ESI): *m/z* calculated for [M+H]+: 374.218666; found: 374.21807.

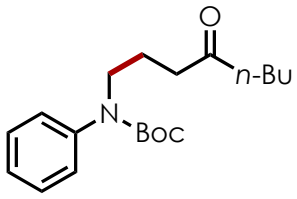

***tert*-Butyl (4-oxooctyl)(phenyl)carbamate (2.18)**: Isolated by column chromatography (0-8% EtOAc/hexane), as a colorless oil, 26.0 mg, 82.0%.

^{1}H NMR (600 MHz, chloroform-*d*) δ 7.34 (t, *J* = 7.8 Hz, 2H), 7.24 – 7.17 (m, 3H), 3.65 (t, *J* = 7.2 Hz, 2H), 2.44 (t, *J* = 7.3 Hz, 2H), 2.37 (t, *J* = 7.5 Hz, 2H), 1.83 (p, *J* = 7.3 Hz, 2H), 1.53 (p, *J* = 7.5 Hz, 2H), 1.34 – 1.25 (m, 3H), 0.90 (t, *J* = 7.4 Hz, 3H).

^{13}C NMR (151 MHz, $CDCl_3$) δ 210.42, 154.77, 142.34, 128.77, 127.02, 126.05, 80.13, 49.20, 42.57, 39.58, 28.32, 25.93, 22.60, 22.33, 13.85.

IR (thin film): 2957, 2931, 1693, 1389, 1365, 1298, 1157, 697.

HRMS (+ESI): *m/z* calculated for [M+Na]+: 342.203995; found: 342.20246.

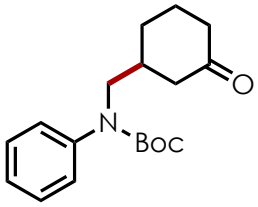

***tert*-Butyl (*S*)-((3-oxocyclohexyl)methyl)(phenyl)carbamate (2.19)**: Isolated by column chromatography (0-20% EtOAc/hexane), as a white solid, 16.2 mg, 53%.

^{1}H NMR (600 MHz, chloroform-*d*) δ 7.35 (t, *J* = 7.8 Hz, 2H), 7.25 – 7.21 (m, 1H), 7.19 (d, *J* = 7.8 Hz, 2H), 3.73 – 3.61 (m, 2H), 2.45 (ddt, *J* = 13.6, 4.0, 2.0 Hz, 1H), 2.36 (dddt, *J* = 14.2, 4.9, 3.4, 1.6 Hz, 1H), 2.27 (td, *J* = 13.5, 6.2 Hz, 1H), 2.05 (ddddd, *J* = 30.4, 15.8, 11.7, 7.5, 3.8 Hz, 3H), 1.90 (dtd, *J* = 13.6, 3.8, 1.9 Hz, 1H), 1.60 (tdt, *J* = 13.0, 8.3, 4.1 Hz, 3H), 1.43 (s, 10H).

^{13}C NMR (151 MHz, $CDCl_3$) δ 210.87, 154.94, 142.30, 128.89, 127.14, 126.26, 80.39, 77.23, 77.02, 76.81, 54.79, 45.68, 41.38, 38.14, 28.90, 28.29, 24.94.

IR (thin film): 2928, 1696, 1390, 1365, 1280, 1164, 698.

HRMS (+ESI): *m/z* calculated for [M+Na]+: 326.173244; found: 326.17313.

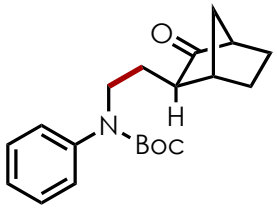

(±)-*tert*-Butyl (2-((1*R*,2*S*,4*S*)-3-oxobicyclo[2.2.1]heptan-2-yl)ethyl)(phenyl)carbamate (2.20): Isolated by column chromatography (0-20% EtOAc/hexane), as a colorless oil, 31.8mg, 100%.

^{1}H NMR (600 MHz, chloroform-*d*) δ 7.34 (t, *J* = 7.8 Hz, 2H), 7.25 – 7.14 (m, 3H), 3.75 (ddd, *J* = 14.5, 9.7, 5.1 Hz, 1H), 3.64 (ddd, *J* = 13.9, 9.4, 6.3 Hz, 1H), 2.66 – 2.58 (m, 2H), 2.03 – 1.90 (m, 2H), 1.82 (dtd, *J* = 13.1, 8.5, 5.3 Hz, 1H), 1.67 (dt, *J* = 10.3, 1.8 Hz, 1H), 1.63 – 1.56 (m, 3H), 1.53 – 1.35 (m, 11H).

^{13}C NMR (151 MHz, $CDCl_3$) δ 219.21, 154.64, 142.29, 128.81, 127.07, 126.12, 80.19, 51.33, 50.30, 48.69, 38.30, 37.12, 28.34, 25.35, 25.30, 21.21.

IR (thin film): 2964, 2358, 1743, 1696, 1391, 1154.

HRMS (+ESI): *m/z* calculated for [M+Na]+: 352.188894; found: 352.18875.

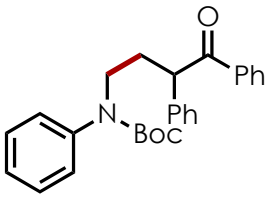

***tert*-Butyl (4-oxo-3,4-diphenylbutyl)(phenyl)carbamate (2.21)**: Isolated by column chromatography (0-8% EtOAc/hexane), as a white solid, 31.2 mg, 91%.

^{1}H NMR (600 MHz, chloroform-*d*) δ 7.97 – 7.87 (m, 2H), 7.51 – 7.45 (m, 1H), 7.38 (t, *J* = 7.8 Hz, 2H), 7.36 – 7.31 (m, 2H), 7.30 – 7.17 (m, 8H), 4.65 (t, *J* = 7.2 Hz, 1H), 3.78 – 3.59 (m, 2H), 2.54 – 2.41 (m, 1H), 2.15 – 2.00 (m, 1H), 1.38 (s, 9H).

^{13}C NMR (151 MHz, $CDCl_3$) δ 198.95, 154.69, 142.34, 139.14, 136.53, 132.85, 129.01, 128.79, 128.72, 128.45, 128.14, 127.12, 126.93, 125.98, 80.23, 51.00, 48.14, 32.69, 28.25.

IR (thin film): 2976, 2365, 1693, 1391, 1165, 755.

HRMS (+ESI): *m/z* calculated for [M+Na]+: 438.204544; found: 438.20440.

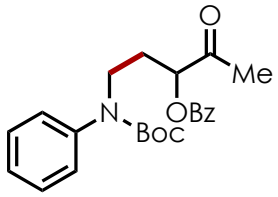

1-((*tert*-Butoxycarbonyl)(phenyl)amino)-4-oxopentan-3-yl benzoate (2.22): Isolated by column chromatography (0-21% EtOAc/hexane), as a colorless oil, 29.0mg, 73%.

^{1}H NMR (600 MHz, chloroform-*d*) δ 8.08 – 8.01 (m, 2H), 7.63 – 7.58 (m, 1H), 7.47 (t, *J* = 7.7 Hz, 2H), 7.34 (t, *J* = 7.8 Hz, 2H), 7.25 – 7.17 (m, 3H), 5.28 (dd, *J* = 9.2, 3.9 Hz, 1H), 3.88 (dddd, *J* = 33.7, 14.0, 8.6, 6.0 Hz, 2H), 2.33 – 2.06 (m, 5H), 1.43 (d, *J* = 5.1 Hz, 9H).

^{13}C NMR (151 MHz, $CDCl_3$) δ 204.72, 165.89, 154.53, 142.10, 133.46, 129.82, 129.16, 128.92, 128.47, 126.88, 126.26, 80.56, 76.85, 46.35, 29.18, 28.27, 26.08.

IR (thin film): 2975, 1718, 1693, 1270, 1164, 711.

HRMS (+ESI): *m/z* calculated for [M+Na]+: 420.178723; found: 420.17858.

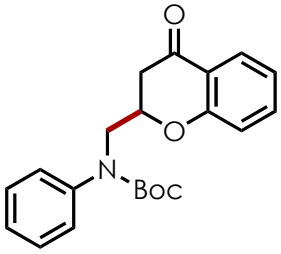

(±)-*tert*-Butyl-((4-oxochroman-2-yl)methyl)(phenyl)carbamate (2.23): Isolated by column chromatography (0-20% EtOAc/hexane), as a yellow solid, 23.0 mg, 65%.

^{1}H NMR (600 MHz, chloroform-*d*) δ 7.88 (dd, *J* = 7.8, 1.7 Hz, 1H), 7.50 – 7.44 (m, 1H), 7.37 (t, *J* = 7.7 Hz, 2H), 7.30 (s, 1H), 7.26 (d, *J* = 7.4 Hz, 1H), 7.02 (t, *J* = 7.5 Hz, 1H), 6.90 (d, *J* = 8.3 Hz, 1H), 4.70 (dtd, *J* = 12.6, 6.2, 3.5 Hz, 1H), 4.09 – 3.98 (m, 2H), 2.82 – 2.65 (m, 2H), 1.45 (s, 9H).

^{13}C NMR (151 MHz, $CDCl_3$) δ 191.47, 161.04, 154.78, 142.49, 136.02, 128.88, 127.34, 126.96, 126.48, 121.48, 120.98, 117.93, 80.88, 75.85, 53.34, 40.68, 28.27.

IR (thin film): 2975, 1689, 1463, 1365, 1148, 761.

HRMS (+ESI): *m/z* calculated for [M+Na]+: 376.152508; found: 376.15231.

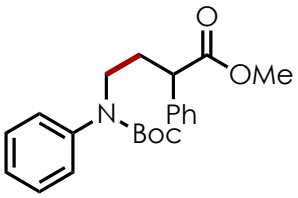

Methyl 4-((*tert*-butoxycarbonyl)(phenyl)amino)-2-phenylbutanoate (2.24): Isolated by column chromatography (10% EtOAc/hexane), as a clear oil, 25.3 mg, 69%.

^{1}H NMR (400 MHz, chloroform-*d*) δ 7.41 – 7.07 (m, 10H), 3.73 – 3.52 (m, 6H), 2.34 (dtd, *J* = 13.7, 8.3, 5.6 Hz, 1H), 2.16 – 2.00 (m, 1H), 1.44 (s, 9H).

^{13}C NMR (151 MHz, chloroform-*d*) δ 173.82, 154.59, 142.29, 138.43, 128.78, 128.71, 127.83, 127.37, 126.94, 126.03, 80.27, 52.06, 48.97, 48.06, 32.03, 28.31.

IR (thin film): 2976, 1734, 1694, 1390, 1158, 697

HRMS (+ESI): *m/z* calculated for [M+Na]+: 392.183610; found: 392.18361.

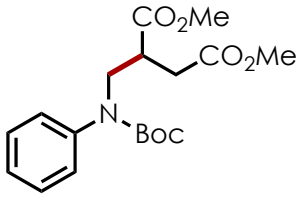

Dimethyl 2-(((*tert*-butoxycarbonyl)(phenyl)amino)methyl)succinate (2.25): Isolated by column chromatography (20% EtOAc/hexane), as a clear oil, 26.5 mg, 76%.

^{1}H NMR (600 MHz, chloroform-*d*) δ 7.35 (t, *J* = 7.6 Hz, 2H), 7.25 – 7.17 (m, 3H), 4.06 (dd, *J* = 14.2, 7.2 Hz, 1H), 3.87 (dd, *J* = 14.2, 6.6 Hz, 1H), 3.66 (s, 3H), 3.58 (s, 3H), 3.10 (ddd, *J* = 11.5, 9.2, 5.7 Hz, 1H), 2.77 (dd, *J* = 17.0, 9.3 Hz, 1H), 2.52 (dd, *J* = 17.0, 4.7 Hz, 1H), 1.43 (s, 9H).

^{13}C NMR (151 MHz, chloroform-*d*) δ 173.31, 171.93, 154.65, 141.75, 128.82, 127.30, 126.43, 51.99, 51.80, 50.80, 40.67, 33.35, 28.22.

IR (thin film): 2978, 1736, 1697, 1367, 1160, 751

HRMS (+ESI): *m/z* calculated for [M+Na]+: 374.157988; found: 374.15780

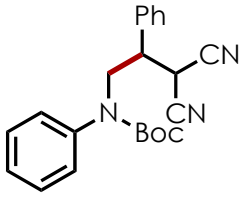

(±)-*tert*-Butyl-(3,3-dicyano-2-phenylpropyl)(phenyl)carbamate (2.26): Isolated by column chromatography (0-18% EtOAc/hexane), as a white solid, 33.8mg, 94%.

^{1}H NMR (600 MHz, chloroform-*d*) δ 7.43 – 7.36 (m, 3H), 7.36 – 7.27 (m, 4H), 7.25 (t, *J* = 7.4 Hz, 1H), 7.04 (d, *J* = 7.8 Hz, 2H), 4.42 (dd, *J* = 14.4, 8.0 Hz, 1H), 4.19 (d, *J* = 5.9 Hz, 1H), 4.13 (dd, *J* = 14.4, 7.0 Hz, 1H), 3.56 (q, *J* = 7.0 Hz, 1H), 1.44 (s, 9H).

^{13}C NMR (151 MHz, $CDCl_3$) δ 154.73, 141.34, 134.76, 129.21, 129.18, 129.11, 128.30, 126.91, 126.82, 112.00, 111.52, 81.55, 77.33, 77.12, 76.91, 51.50, 45.25, 28.21, 27.44.

IR (thin film): 2978, 1688, 1159, 1392, 1366, 2253, 697.

HRMS (+ESI): *m/z* calculated for [M+Na]+: 362.186303; found: 362.18776.

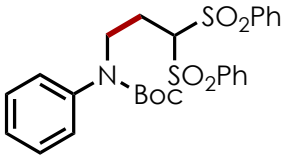

***tert*-Butyl (3,3-bis(phenylsulfonyl)propyl)(phenyl)carbamate (2.27)**: Isolated by column chromatography (20-50% EtOAc/hexane), as a white solid, 51.0 mg, 99%.

^{1}H NMR (600 MHz, chloroform-*d*) δ 7.86 (d, *J* = 7.8 Hz, 4H), 7.69 – 7.64 (m, 2H), 7.55 – 7.47 (m, 4H), 7.37 (t, *J* = 7.8 Hz, 2H), 7.30 – 7.24 (m, 1H), 7.21 – 7.14 (m, 2H), 4.96 (s, 1H), 4.04 (t, *J* = 5.9 Hz, 2H), 2.45 (q, *J* = 5.8 Hz, 2H), 1.44 (s, 9H).

^{13}C NMR (151 MHz, $CDCl_3$) δ 155.07, 142.42, 142.42, 137.72, 134.40, 129.61, 129.07, 128.98, 127.29, 126.37, 80.85, 80.23, 48.38, 28.26, 25.41.

IR (thin film): 2976, 1682, 1328, 1312, 1147, 1079, 728.

HRMS (+ESI): *m/z* calculated for [M+Na]+: 538.133429; found: 538.13377.

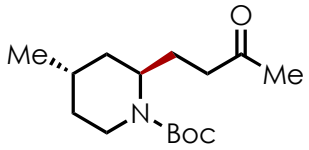

(±)-*tert*-Butyl-*trans*-4-methyl-2-(3-oxobutyl)piperidine-1-carboxylate (2.28): Isolated as a single diastereomer by column chromatography (5% EtOAc/hexane), as a yellow oil, 13.2 mg, 49%. Crude NMR showed >20:1 d.r.

^{1}H NMR (400 MHz, chloroform-*d*) δ 4.33 – 4.05 (m, 1H), 3.91 (dd, *J* = 69.9, 13.1 Hz, 1H), 2.67 (dt, *J* = 46.5, 16.7 Hz, 1H), 2.44 – 2.24 (m, 2H), 2.07 (d, *J* = 2.9 Hz, 3H), 1.94 – 1.87 (m, 1H), 1.76 – 1.42 (m, 3H), 1.38 (s, 9H), 1.18 (tq, *J* = 13.0, 5.7 Hz, 2H), 1.01 – 0.87 (m, 1H), 0.81 (d, *J* = 6.5 Hz, 3H).

^{13}C NMR (151 MHz, $CDCl_3$) δ 208.64, 208.62, 155.13, 79.39, 79.20, 50.53, 49.69, 40.55, 40.31, 39.32, 38.03, 37.70, 34.33, 34.08, 30.06, 30.05, 28.53, 25.48, 25.41, 24.30, 23.35, 22.34 (Mixture of rotomers).

IR (thin film): 2925, 1684, 1414, 1364, 1246, 1156, 1087.

HRMS (+ESI): *m/z* calculated for [M+Na]+: 292.188345; found: 292.18717.

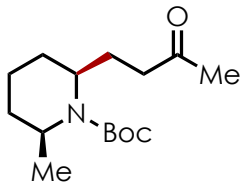

***tert*-Butyl (2*S*,6*S*)-2-methyl-6-(3-oxobutyl)piperidine-1-carboxylate ((*S*)-2.29)**: Isolated as a single diastereomer by column chromatography (0-20% EtOAc/hexane), as a colorless oil, 17.0 mg, 20%. HPLC analysis was performed on an Agilent 1200 Series PDA system equipped with Chiralpak IA column using a flow rate of 1 mL/min with a 95:5 ratio of hexanes and isopropanol as eluent. Retnetion time of the enantiopure sample matched that of the racemic standard. Starting material ee was 97% and ee of product after the completion of the reaction was 90%. Crude NMR showed >10:1 d.r. (other diastereomer not visible)

^{1}H NMR (600 MHz, chloroform-*d*) δ 4.33 (p, *J* = 7.1 Hz, 1H), 4.12 (qd, *J* = 7.5, 3.8 Hz, 1H), 2.55 – 2.47 (m, 1H), 2.41 (ddd, *J* = 17.4, 9.5, 5.4 Hz, 1H), 2.16 (s, 3H), 1.90 – 1.76 (m, 2H), 1.72 – 1.55 (m, 4H), 1.48 (s, 10H), 1.19 (d, *J* = 7.0 Hz, 3H).

^{13}C NMR (151 MHz, $CDCl_3$) δ 208.43, 155.40, 79.16, 49.27, 45.67, 41.47, 30.17, 29.97, 28.73, 28.51, 28.19, 20.54, 14.12.

IR (thin film): 2970, 2934, 1679, 1362, 1173, 1079.

HRMS (+ESI): *m/z* calculated for [M+Na]+: 292.188345; found: 292.18784.

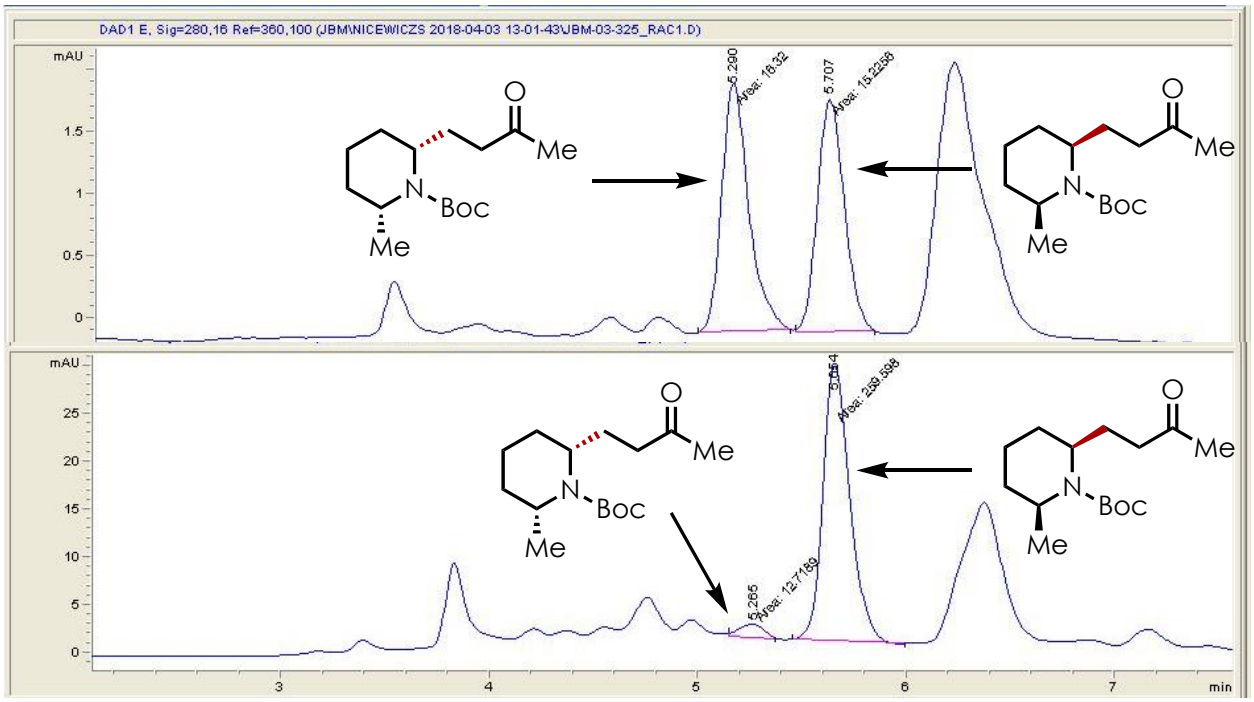
DAD1 E, Sig=280,16 Ref=360,100 (JBM\NICEWICZS 2018-04-03 13-01-43\JBM-03-325_RAC1.D)
mAU
5.290
Area: 16.32
5.707
Area: 15.2258
O
Me
N
Boc
Me
mAU
5.264
Area: 269.598
5.265
Area: 12.7189
min

Synthesis of monomorine I

30

(+)-*tert*-Butyl (2*S*,6*S*)-2-methyl-6-(3-oxoheptyl)piperidine-1-carboxylate (2.30): To a 2 dram vial was added *tert*-butyl (*S*)-2-methylpiperidine-1-carboxylate (59.8 mg, 0.3 mmol), catalyst 1 (2.87 mg, 0.005 mmol) and 1 mL of DCM. The solution was sparged with N_2 then irradiated with blue light. During irradiation, a degassed 1 mL solution of butyl vinyl ketone (11.2 mg, 0.1 mmol) and catalyst **1** (2.87 mg, 0.005 mmol) was added over 8 hours via syringe pump. The solution then stirred for an additional 2 hours under irradiation before being concentrated and purified by column chromatography (8% Et_2O/hexane) to give compound **30** as a single diastereomer (11:1 d.r. by crude NMR) as an orange oil (54% by NMR vs. HMDS).

^{1}H NMR (600 MHz, chloroform-*d*) δ 4.38 – 4.27 (m, 1H), 4.15 – 4.07 (m, 1H), 2.53 – 2.34 (m, 4H), 1.90 – 1.51 (m, 10H), 1.49 (s, 9H), 1.31 (ddt, *J* = 19.0, 11.6, 5.5 Hz, 3H), 1.19 (d, *J* = 7.0 Hz, 3H), 0.92 (t, *J* = 7.3 Hz, 3H).

^{13}C NMR (151 MHz, $CDCl_3$) δ 210.92, 155.39, 79.13, 42.64, 42.49, 40.56, 30.19, 28.82, 28.52, 28.17, 26.04, 23.33, 22.37, 20.52, 14.14, 13.86.

IR (thin film): 2932, 2871, 1712, 1680, 1362, 1174, 1079.

HRMS (+ESI): *m/z* calculated for [M+Na]+: 334.235298; found: 334.23522.

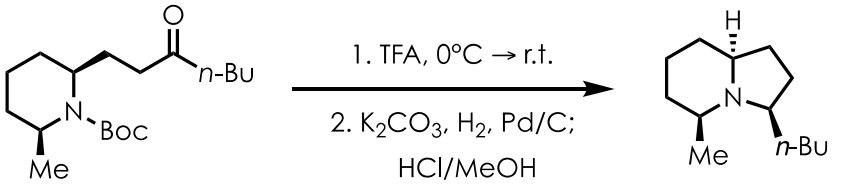

30 *(+)-monomorine I*

(+)-monomorine I: Compound 30 (65 mg, 0.077 mmol) was taken up in 1.2 mL of trifluoroacetic acid at 0 °C. The reaction was allowed to warm to room temperature where it stirred for an additional 6 hours. The reaction mixture was then concentrated in vacuo to afford the crude TFA salt.

The crude product was combined with K_2CO_3 (43.26 mg, 0.313 mmol) and 10 wt% palladium on carbon (10 mg, 9.4 μmol). The mixture was taken up in 10 mL of anhydrous MeOH and cooled to 0°C. The solution was then purged 3x with H_2 and allowed to warm to room temperature. The reaction then stirred for 14 hours under 1 atm of H_2 then passed through a silica plug and acidified with 2 mL of 3N methanolic HCl. The solution was concentrated in vacuo to give monomorine I hydrochloride as a white solid (45.4 mg, 93.8%). The HCl salt was purified by column chromatography (0-15% MeOH/DCM). $[\alpha]^{26}_D$ = +29.1 (*c* 0.0043, n-Hexane). The spectral data of the free base was in agreement with literature values. [29]

A.6: Stern Volmer Analysis

Emission lifetime measurements were taken at ambient temperature using a Edinburgh FLS920 spectrometer and fit to single exponential decay according to a modification of the method previously described by our laboratory.[167] Measurements were made by the time-correlated single photon counting (TCSPC) capability of the instrument with pulsed excitation light (444.2 nm, typical pulse width = 95 ps) generated by a Edinburgh EPL-445 ps pulsed laser diode operating at a repetition rate of 5 MHz. The maximum emission channel count rate was less than 5% of the

laser channel count rate, and each data set collected greater than 10000 counts on the maximum channel. The lifetime of fluorescence was determined by reconvolution fit with the instrument response function using the Edinburgh FS900 software. In all cases, after reconvolution, fluorescence decay was satisfactorily fit with a monoexponential function of the form:

$$\boldsymbol{I_t = I_0 e^{-t/\tau}}$$

where I is the intensity (counts), and τ is the mean lifetime of fluorescence.

Stern-Volmer analysis on the quenching of fluorescence lifetime was carried out in DCM with detection at 500 nm (15 nm bandwidth), where the concentration of acridinium was 1.6×10^{-5} M. The quenching constant was determined with quencher concentrations in the range of 0 M to 2.0×10^{-2} M. Bimolecular quenching constants, k_q, were determined from the corresponding Stern-Volmer constant.[30] Quenching constants were determined for ***Mes-Acr-BF$_4$*** with a representative Boc-amine. Comparison of UV-Vis absorption spectra taken before and after lifetime quenching studies verified that the acridinium was unchanged. UV-Vis spectra were taken on a Hewlett-Packard 8453 Chemstation spectrophotometer.

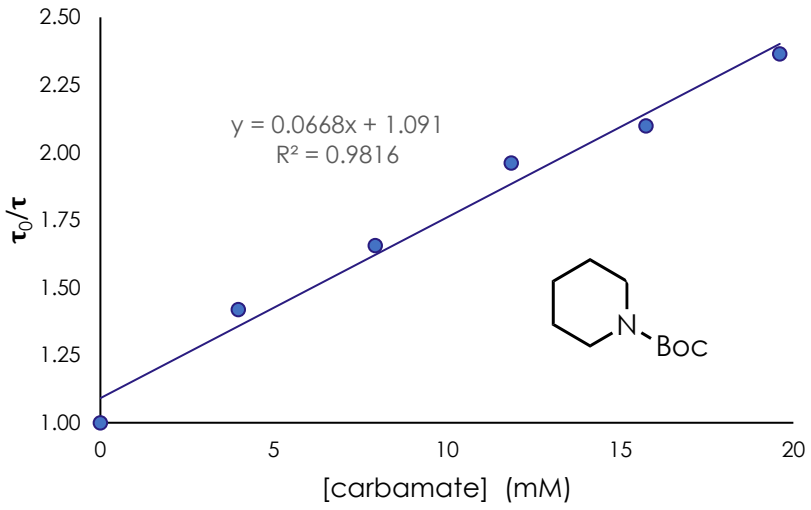

Figure A.4: Stern-Volmer plot for quenching of acridinium with *N*-Boc-piperidine

spike	catalyst concentration (M)	Quencher concentration (M)	lifetime (ns)	normalization
0	0.00016000	0.000000	14.9	1.000
1	0.00015936	0.003984	10.5	1.419
2	0.00015873	0.007937	9.0	1.656
3	0.00015810	0.011858	7.6	1.961
4	0.00015748	0.015748	7.1	2.099
5	0.00015686	0.019608	6.3	2.365

Raw Data

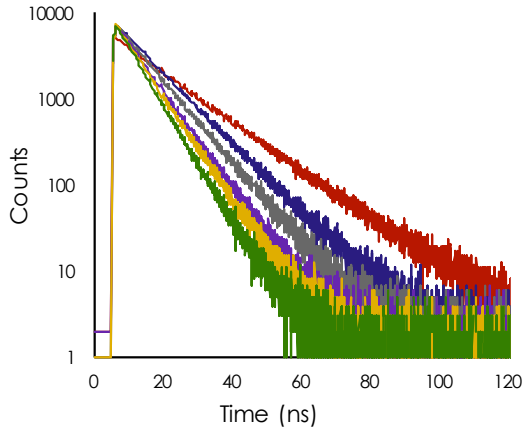

Normalized Data

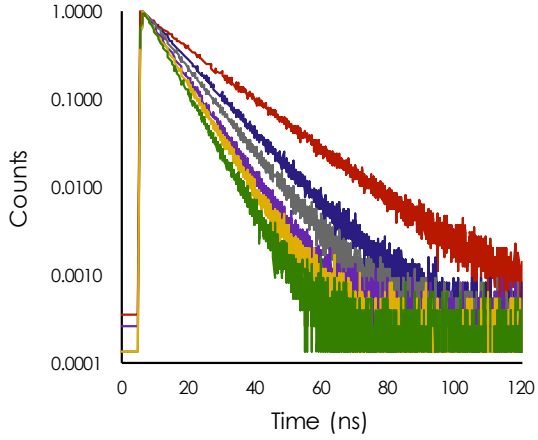

A.7: Photochemical Quantum Yield (Φ_r) Determination:

A flame-dried vial was charged with acridinium catalyst (0.005 mmol, 5 mol%), DCM (1 mL), Boc-piperidine (0.3 mmol) and methyl vinyl ketone (0.1 mmol). The reaction mixture was then sparged with nitrogen for 10 minutes before being sealed and irradiated using a single blue LED for 2 hours (see below).

After this time, the reaction mixture was concentrated and the yield of the desired product was determined by proton NMR using HMDS as an internal standard (18.5% yield). This process was repeated for a reaction time of 3 hours, resulting in a 35.1% yield of the desired alkylation product. The photon flux for this light source had been previously determined to be 1.50 x 10^{-6} mol photons s^{-1} after two trials (std. dev.=5 x10^{-8} mol photons s^{-1}) using potassium ferrioxalate as a chemical actinometer (see reference for details).[168]

Based on these values, the quantum yield (Φ_r) for this reaction was determined to be 0.19±0.03 % (n=2). This value suggests that a rapid chain mechanism is not the dominant pathway under these conditions.

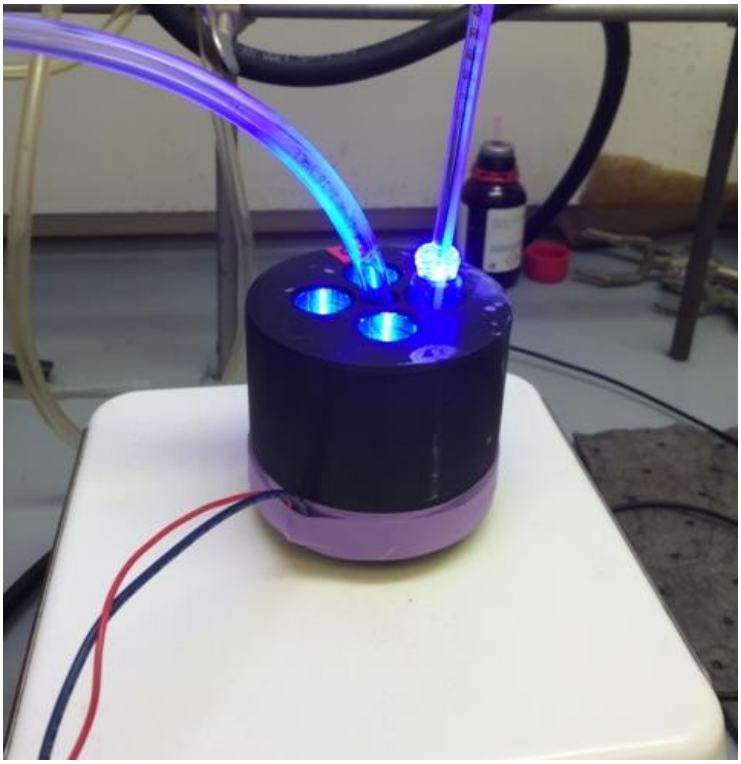

Figure A.5: Photoreactor setup used in the quantum yield determination studies

This photoreactor allows for irradiation using a single 450 nm LED to ensure consistent photon flux. Individual reaction vials (1-dram) can be placed into the LED slots. The same slot was used for photon flux measurements, and quantum yield determination. The reactor is cooled by flowing air through the reactor and out a heat sink mounted on the bottom. Reactor temperature was maintained below 40˚C throughout the reactions. Stirring is accomplished by setting the reactor on a standard stir plate.

CREE XT-E Royal Blue LEDs were used pre-soldered to MCPCB (metal core printed circuit board); purchased from www.rapidled.com (http://www.rapidled.com/cree-xt-e-royal-blue-led/)

A.8: Large Scale Flow Synthesis of *tert*-butyl (*R*)-(3,3-dicyano-2-phenylpropyl)(phenyl)carbamate

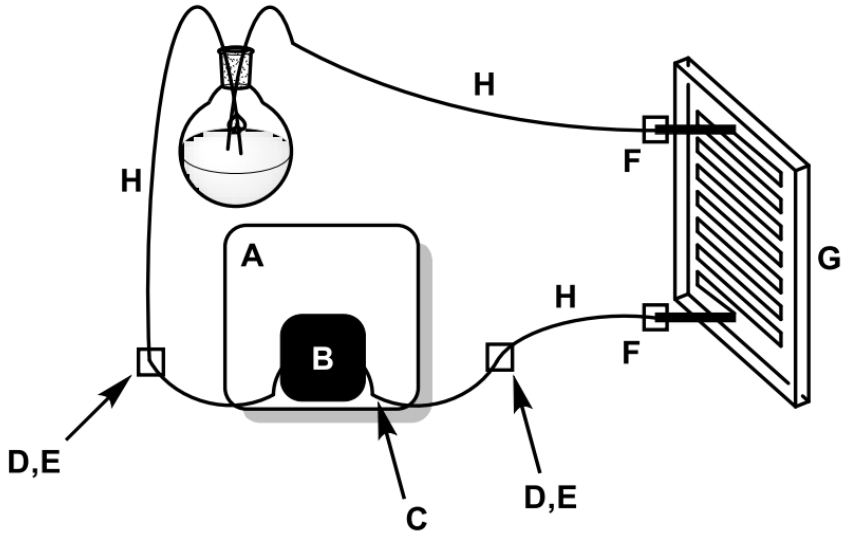

A. Masterflex L/S Variable-Speed Drive (Cole-Parmer # EW-07528-30)

B. Masterflex L/S Rigid PTFE-Tubing Pump Head (Cole-Parmer # EW-77390-00)

C. Masterflex PTFE-tubing 4mm O.D. (Cole-Parmer # EW-77390-50)

D. 4MM PTFE Male NPT Compression Adapter (Cole-Parmer # WU-31321-62)

E. 1/8” O.D. to 1/8” PTFE Female NPT Compression Adapter (Cole-Parmer # EW-31320-50)

F. 1/4-28 flangeless fitting/ferrule for 1/8" O.D. tubing (Sigma-Aldrich SUPELCO # 58686)

G. Microreactor (Little Things Factory Gmbh # XXL-ST-02)

H. PTFE Tubing 1/16” I.D., 1/8” O.D. (Cole-Parmer # WU-06605-27)

A flame-dried, 100 mL round bottom flask was charged with *tert*-butyl methyl(phenyl)carbamate (3.11 g, 15.0 mmol, 3 equiv.), benzylidenemalononitrile (771 mg, 5.00 mmol, 1 equiv.), 3,6-Di-*tert*-butyl-9-mesityl-10-phenylacridin-10-ium tetrafluoroborate (143 mg, 0.25 mmol, 0.05 equiv.) and dichloroethane (50 mL). Dichloroethane was used due to the potential volatility of dichloromethane, The resulting mixture was sparged with nitrogen for 20 minutes. The flow cell was purged with dichloroethane which was sparging with nitrogen prior to the introduction of the reaction mixture. Two 15W PAR38 blue LED floodlamps were positioned on either side of the microreactor (**G**). Tubing was introduced into the flask using a commercially available rubber septum which had been punctured. A nitrogen line was introduced into the headspace of the flask to ensure the complete exclusion of oxygen from the reaction mixture. The Masterflex L/S Variable-Speed Drive was set to 20 rpm and the occlusion bed of the pump head was adjusted as per the manufacturer's instructions. The floodlamps were then switched on and the reaction mixture was allowed to flow though the reactor for 18 hours. The temperature remained at ~35 ºC during the reaction, as measured at the center of the lamps, close to the flow cell using a conventional alcohol thermometer. At this point. TLC indicated that the reaction had reached completion. Solvent was removed under reduced pressure and the resulting residue was purified *via* flash column chromatography (10→15% EtOAc/hexanes), yielding the desired product as a pale yellow solid (95%, 1.71 g).

A.9: Computational Details:

All computations were performed in the Gaussian 16 software package,[23] and were performed at the UB3LYP level of theory [169,170] using the 6-311+G(d) basis set.[171,172] Bond dissociation energies were estimated by calculating the relative energy differences of the optimized geometries of the starting molecule and corresponding radical plus the energy of a hydrogen atom

in the gas phase. All obtained geometries were verified as minima by ensuring that they possess no negative vibrational frequencies. All transition states were verified by ensuring that they possessed one negative vibrational mode. Transition state energies were calculated using CPCM solvent modeling for dichloromethane/ pKa values for cation radicals were calculated using these computed bond dissociation energies and experimentally determined oxidation potentials according to the methods described by Arnold and coworkers.[28] The energy of a gas phase hydrogen atom was calculated to be -0.502156 hartrees. Visual representations of the optimized geometries of the ground state of Boc-piperidine and the corresponding radical, as well as their single point energies are given below. (Calculated BDE = 96.04 kcal/mol, Calculated cation radical pKa ~ 5

Boc-piperidine (Energy = -597.893854 Hartrees)

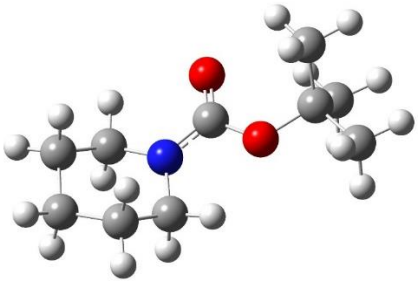

Boc-piperidine radical (Energy = -597.238650 Hartrees)

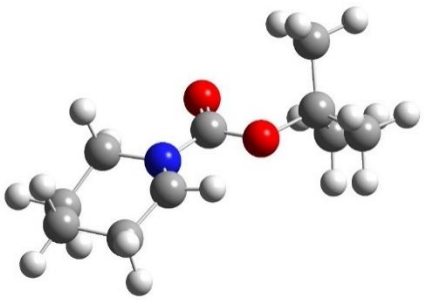

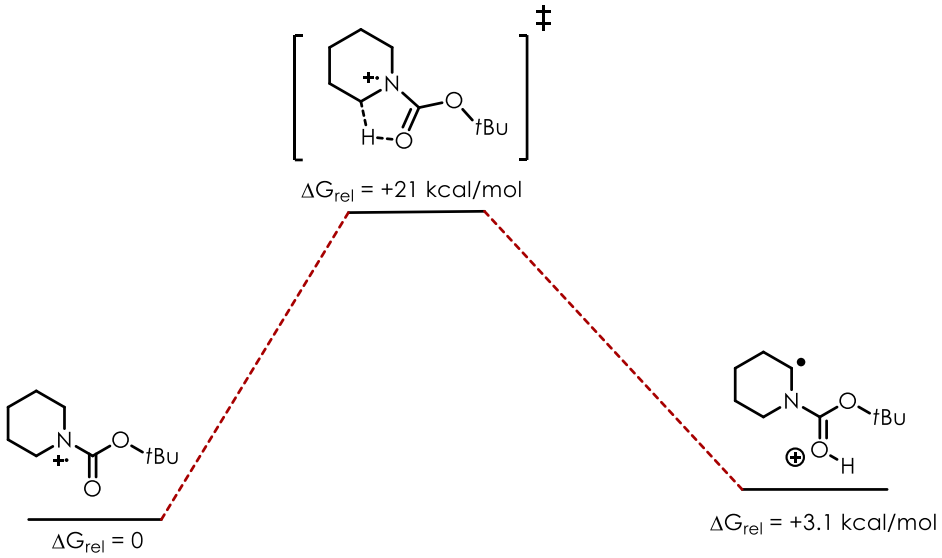

Figure A.6: Relative free energies for intramolecular deprotonation mechanism

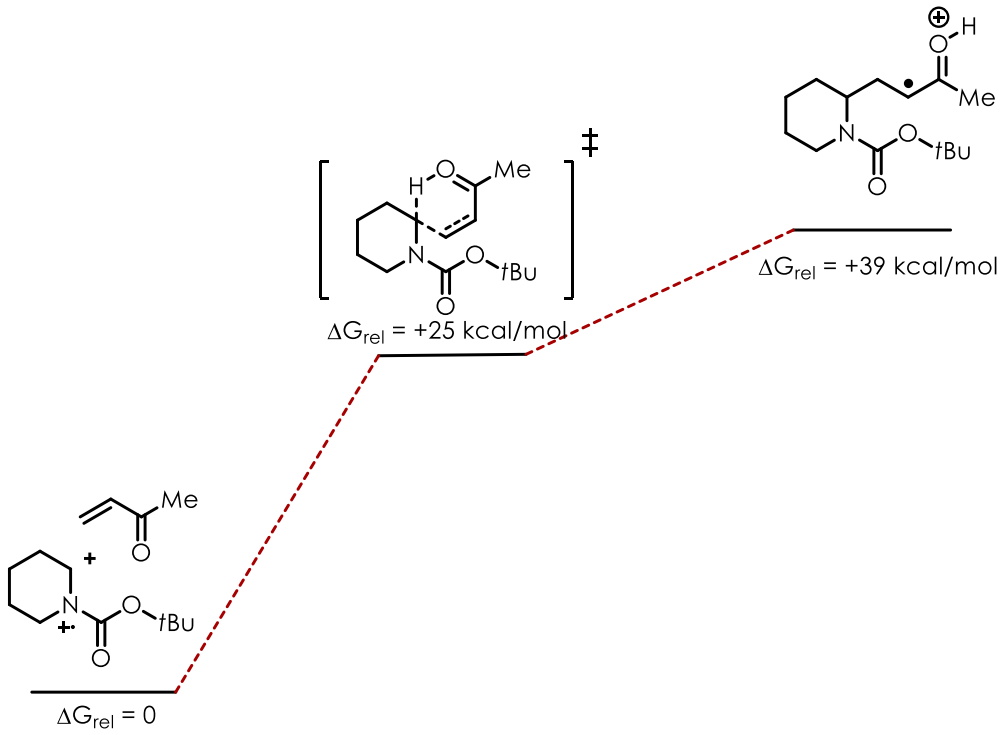

Figure A.7: Relative free energies for concerted alkylation/proton transfer mechanism with methyl vinyl ketone

Figure A.8: Overall free energy differences for possible intermolecular deprotonations of the carbamate cation radical

A.10: NMR Spectra for New Compounds

NMR data is available in the corresponding published supporting information, which is available online.[173]

APPENDIX B: SUPPORTING INFORMATION FOR "ANTI-MARKOVNIKOV HYDROAZIDATION OF ACTIVATED OLEFINS *VIA* ORGANIC PHOTOREDOX CATALYSIS"

B.1: General Information: Commercially available reagents were purchased from Sigma-Aldrich, Fischer Scientific or TCI Corporation and were used without further purification. Styrenes containing radical inhibitors were filtered through a small pad of silica gel to remove any inhibitors. Styrenes which appeared impure upon purchase/preparation were also purified by passing them through a short pad of silica. Solvents were used as received unless otherwise noted.

TMS-azide was used as received and stored in a refrigerator.

WARNING: TMS-azide is an acutely toxic reagent and should be treated with extreme care. When scaling up reactions, ensure that all waste is kept basic to prevent the formation of hydrazoic acid at any point during work-up. Please familiarize yourself with the handling of this hazardous reagent before attempting any of the reactions disclosed within.

General Analytical Information: Proton and carbon (^{1}H and ^{13}C) magnetic resonance spectra were collected on a Bruker AVANCE III 600 CryoProbe (^{1} H NMR at 600 MHz and ^{13}C NMR at 151 MHz) spectrometer or Bruker AVANCE III 500 (^{1} H NMR at 500 MHz and ^{13}C NMR at 126 MHz) spectrometer. Unless otherwise noted, spectra are referenced to chloroform-d (^{1} H NMR at 7.26 ppm and ^{13}C at 77.16 ppm) and reported as parts per million. ^{1}H NMR data are reported as follows: chemical shift, multiplicity (s = singlet, d = doublet, t = triplet, dd = doublet of doublets, ddd = doublet of doublets of doublets, ddddd = doublet of doublets of doublets of doublets of doublets, dt = doublet of triplets, ddt = doublet of doublets of triplets, td = triplet of doublets, tt = triplet of triplets, m = multiplet, q = quartet), coupling constants (Hz), and integration

High Resolution Mass Spectra (HRMS) were obtained via direct infusion using a Thermo LTQ FT mass spectrometer with positive mode electrospray ionization or APCI. Low resolution mass spectra were obtained using an Agilent Technologies 5977E MSD GC/MS unit with electron impact (EI) ionization.

Flash chromatography was performed using SiliaFlash P60 silica gel (40-63 μm) purchased from Silicycle.

General Photoreactor Configuration: All photochemical reactions were conducted using a SynLED Parallel Photoreactor, available for purchase from Sigma-Aldrich (item number: **Z742680).** The unit has bottom-lit LEDS (465-470 nm) with 130-140 lm intensity and a built-in cooling fan. The measured temperature range was 35 - 40°C. The reactor was fit to an IKA magnetic stirrer with round plate (item number: Z645052). Small stir bars are sometimes required for efficient stirring when using 2 dram vials.

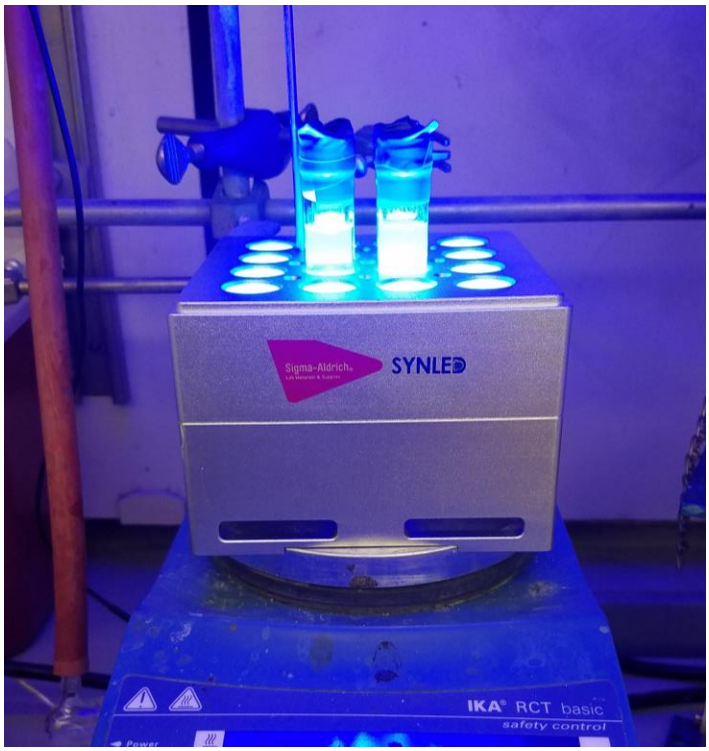

General Procedure for Photochemical Reactions: A flame-dried 2-dram borosilicate vial (purchased from Fisher Scientific, catalogue # 03-339-22D), equip with a stir bar, was charged with 3,6-Di-*tert*-butyl-9-mesityl-10-phenylacridin-10-ium tetrafluoroborate (0.01 equiv., 0.01

mmol) and 2,5,6-triisopropylthiophenol (0.10 mmol, 0.20 equiv.). For solid/non-volatile substrates, the substrate (0.50 mmol) was then added. 2,2,2-trifluoroethanol (5.0 mL) was added and vials were capped tightly with a Teflon lined phenolic resin septum cap (purchased through VWR international, Microliter Product # 15-0060K). The reaction mixture was the sparged by bubbling with nitrogen or argon for 5 minutes. Trimethylsilylazide (0.625 mmol, 1.25 equiv.) was then added *via* microliter syringe. Prior to irradiation, vials were sealed with Teflon tape and electrical tape to ensure maximal oxygen exclusion. The reaction vial was then placed into the reactor and irradiated for 18 hours unless otherwise noted. Following irradiation, the reaction mixture was concentrated under reduced pressure and the desired products were isolated *via* flash column chromatography (see substrate/product details for solvent information). Unless otherwise noted, all reaction yields are reported as the average of two separate trials (including chromatography).

B.2: Catalyst and Substrate Synthesis:

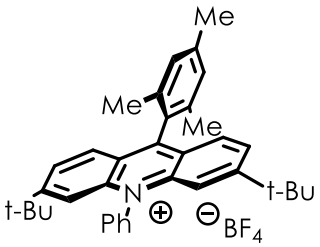

3,6-Di-*tert*-butyl-9-mesityl-10-phenylacridin-10-ium tetrafluoroborate was prepared according to published procedure.[93]Spectral data matched that reported in the literature.

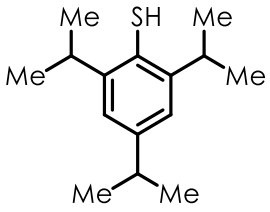

2,4,6-triisopropylbenzenethiol was prepared according to the procedure of Knowles and coworkers. Spectral data matched that reported in the literature.[174]

General procedure for preparation of beta-methylstyrene derived substrates:

In a flame-dried round bottom flask under an atmosphere of nitrogen, ethyltriphenylphosphonium iodide (1.1 equiv.) was stirred with THF (0.5 M) and cooled to 0 ºC using an ice/water bath. Potassium *tert*-butoxide (1.1 equiv.) was added portionwise across several minutes, resulting in the formation of a vibrant orange suspension. This suspension was stirred at 0 ºC for one hour. Following this, the corresponding benzaldehyde derivative (1.0 equiv.) was added, either by syringe for liquid aldehydes or portionwise for solid aldehydes. As the aldehyde was added, the bright orange color gradually faded, accompanied by the formation of a white precipitate. To simplify purification, the addition of aldehyde should be halted upon the complete disappearance of color. The reaction mixture was stirred and allowed to warm to RT overnight (12-18 hours). After ensuring that the reaction had reached completion by TLC, the reaction mixture was concentrated under reduced pressure to remove THF. Following this, the resulting crude mixture was loaded onto silica gel. The desired product was isolated *via* flash column chromatography (typically using hexane as the eluent). In some cases, distillation is also an effective purification method for more volatile substrates. Styrenes are typically isolated as a mixture of (E)- and (Z)-isomers. This isomeric mixture can be used in the hydroazidation reaction with no effect on yield or reaction efficiency.

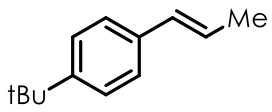

1-(*tert*-butyl)-4-(prop-1-en-1-yl)benzene

The alkene was prepared according to the general procedure.

Spectral data matches those previously reported.[175]

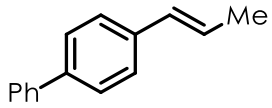

4-(prop-1-en-1-yl)-1,1'-biphenyl

The alkene was prepared according to the general procedure.

Spectral data matched that reported in the literature.[176]

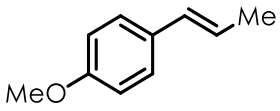

1-methoxy-4-(prop-1-en-1-yl)benzene

The alkene was purchased commercially and used with no additional purification.

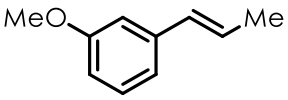

1-methoxy-3-(prop-1-en-1-yl)benzene

The alkene was prepared according to the general procedure.

Spectral data matched that reported in the literature.[177]

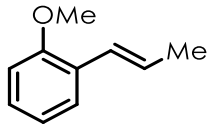

1-methoxy-2-(prop-1-en-1-yl)benzene

The alkene was prepared according to the general procedure.

Spectral data matched that reported in the literature.[178]

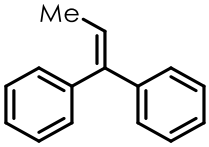

prop-1-ene-1,1-diyldibenzene

The alkene was prepared according to a modified general procedure. Instead of potassium *tert*-butoxide, n-butyllithium (1.6 M in hexanes) was used in the deprotonation step, per literature precedent.[179]

Spectral data matched that reported in the literature.[179]

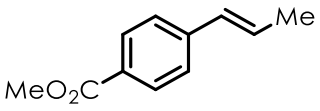

methyl 4-(prop-1-en-1-yl)benzoate

The alkene was purchased commercially and used with no additional purification.

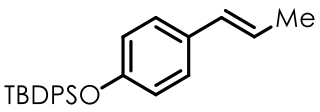

***tert*-butyldiphenyl(4-(prop-1-en-1-yl)phenoxy)silane**

The alkene was prepared from the corresponding aldehyde according to the general procedure. The desired product was isolated as a pale yellow semi-solid following purification by flash column chromatography (60% yield, 1.24 g). NMR data is given for mixture of alkene isomers.

^{1}H NMR (600 MHz, chloroform-d) δ 7.79 – 7.67 (m, 5H), 7.57 – 7.49 (m, 1H), 7.48 – 7.33 (m, 9H), 7.26 – 7.17 (m, 2H), 7.13 – 6.99 (m, 2H), 6.71 (ddt, J = 27.1, 8.6, 2.3 Hz, 2H), 6.36 – 6.20 (m, 1H), 6.10 – 5.46 (m, 1H), 1.91 – 1.79 (m, 3H), 1.14 – 1.08 (m, 9H).

^{13}C NMR (151 MHz, chloroform-*d*) δ 154.68, 154.21, 135.82, 135.64, 134.93, 133.06, 130.00, 129.90, 129.44, 127.89, 127.39, 126.74, 125.13, 119.80, 119.45, 27.42, 26.64, 19.68, 19.60

HRMS (APCI, positive mode): calculated: 373.1982, found: 373.1983 (M+H)

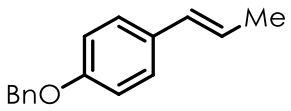

1-(benzyloxy)-4-(prop-1-en-1-yl)benzene

The alkene was prepared in two steps starting from 4-hydroxybenzaldehyde. 4-hydroxybenzaldehyde (2.00 g, 16.4 mmol), potassium carbonate (2.94 g, 21.3 mmol), benzyl bromide (3.08 g, 18.0 mmol) were stirred together in DMF (10 mL) and the mixture was heated at 60 ºC for one hour. At this time, the mixture was cooled to RT and poured onto water. The resulting mixture was extracted with diethyl ether. The ethereal extracts were washed with brine, dried with magnesium sulfate, and concentrated under reduced pressure to yield the crude product as an oil (60% yield, 2.07 g). This material was used in the next step without further

purification. The aldehyde was converted to the alkene product according to the general procedure. The desired product was isolated as a clear oil following purification by column chromatography (66% yield, 1.44 g).

Spectral data matched that reported in the literature.[180]

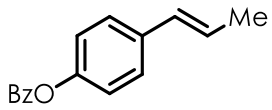

4-(prop-1-en-1-yl)phenyl benzoate

The alkene was prepared in two steps starting from 4-hydroxybenzaldehyde. 4-hydroxybenzaldehyde (1.50 g, 12.0 mmol), triethylamine (2.5 mL, 18 mmol) and dichloromethane (35 mL) were stirred together in a flame-dried RBF and cooled to 0 ºC using an ice/water bath. Benzoyl chloride (2.1 mL, 18 mmol) was added dropwise and the reaction mixture was stirred and warmed to RT overnight. The next day, the reaction mixture was quenched with sodium bicarbonate and extracted with dichloromethane (3 x 30 mL). The combined organic washings were washed with brine, dried with sodium sulfate, and concentrated under reduced pressure to yield the desired product as a yellow oil (quant.). The crude material was used in the next step according to the general procedure to prepare the alkene. The final product was isolated as a clear oil (62% yield, 1.31 g). Spectral data matched that reported in the literature.[181]

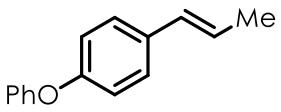

1-phenoxy-4-(prop-1-en-1-yl)benzene

The alkene was prepared according to the general procedure using the corresponding, known aldehyde. The desired product was isolated as a pale yellow oil following flash column chromatography as a 2.7:1 ratio of Z/E alkene isomers. NMR data is given for mixture of alkene isomers.

^{1}H NMR (600 MHz, chloroform-d) δ 7.40 – 7.27 (m, 4H), 7.11 (t, J = 7.7 Hz, 1H), 7.07 – 6.98 (m, 2H), 6.98 – 6.93 (m, 2H), 6.40 (t, J = 14.6 Hz, 1H), 6.17 (dq, J = 19.4, 6.6 Hz, 1H), 5.77 (dq, J = 11.6, 7.2 Hz, 1H), 1.92 (d, J = 7.1 Hz, 1.5H), 1.89 (d, J = 6.8 Hz, 1.5H).

^{13}C NMR (151 MHz, chloroform-d) δ 157.50, 157.35, 156.07, 155.75, 133.44, 132.91, 130.32, 130.26, 129.86, 129.83, 129.18, 127.19, 126.26, 124.99, 123.34, 123.22, 119.17, 118.97, 118.80, 118.65, 18.63, 14.78.

HRMS (APCI, positive mode): calculated: 211.1174, found: 211.1117 (M+H)

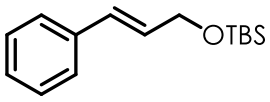

***tert*-butyl(cinnamyloxy)dimethylsilane**

The substrate was prepared with a previously reported method.[182]

Spectral data matched that reported in the literature.[182]

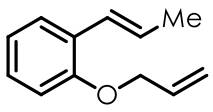

1-(allyloxy)-2-(prop-1-en-1-yl)benzene

The corresponding aldehyde starting material was prepared from salicylaldehyde according to a previously reported procedure.[183] The alkene was prepared according to the general procedure. The desired product was isolated as a pale yellow oil following purification by flash column chromatography (100% hexane) (813 mg, 76% yield).

Spectral data matched those previously reported.[184]

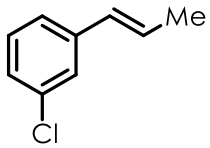

1-chloro-3-(prop-1-en-1-yl)benzene

The alkene was prepared according to the general procedure.

Spectral data matched that reported in the literature.[185]

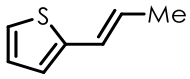

2-(prop-1-en-1-yl)thiophene

The alkene was prepared according to the general procedure.

Spectral data (^{1}H NMR) matched that reported in the literature.[186]

^{13}C NMR (151 MHz, chloroform-*d*) δ 175.70, 136.39, 131.02, 128.52, 128.05, 63.84, 28.13.

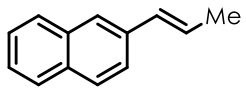

2-(prop-1-en-1-yl)naphthalene

The alkene was prepared according to the general procedure.

Spectral data matched that reported in the literature.[187]

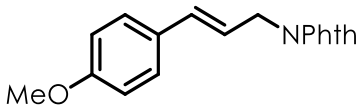

(*E*)-2-(3-(4-methoxyphenyl)allyl)isoindoline-1,3-dione

Substrate was prepared according to a previously published procedure. Spectral data matched that reported in the literature.[184]

HRMS (APCI, positive mode): calculated: 294.1125, found: 294.1126 (M+H)

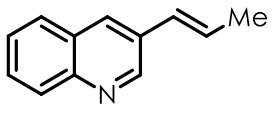

(*E*)-3-(prop-1-en-1-yl)quinoline

The alkene was prepared according to the general procedure.

Spectral data matched that reported in the literature.[188]

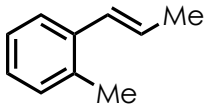

(*E*)-1-methyl-2-(prop-1-en-1-yl)benzene

The alkene was prepared according to the general procedure.

Spectral data matched that reported in the literature.[178]

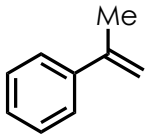

prop-1-en-2-ylbenzene

The alkene was purchased commercially and used without additional purification.

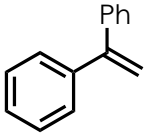

ethene-1,1-diyldibenzene

The alkene was purchased commercially and used without additional purification.

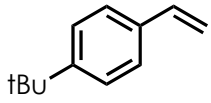

1-(*tert*-butyl)-4-vinylbenzene

The alkene was purchased commercially and used without additional purification.

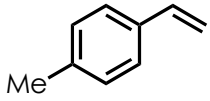

1-methyl-4-vinylbenzene

The alkene was purchased commercially and used without additional purification.

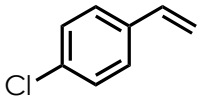

1-chloro-4-vinylbenzene

The alkene was purchased commercially and used without additional purification.

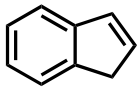

1*H*-indene

The alkene was purchased commercially and used without additional purification.

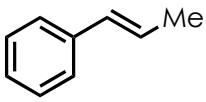

(*E*)-prop-1-en-1-ylbenzene

The alkene was purchased commercially and used without additional purification.

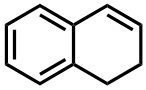

1,2-dihydronaphthalene

The alkene was purchased commercially and used without additional purification.

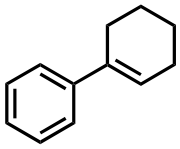

2,3,4,5-tetrahydro-1,1'-biphenyl

The alkene was purchased commercially and used without additional purification.

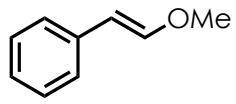

(*E*)-(2-methoxyvinyl)benzene

The alkene was purchased commercially and used without additional purification.

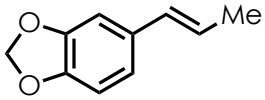

(*E*)-5-(prop-1-en-1-yl)benzo[*d*][1,3]dioxole

The alkene was purchased commercially and used without additional purification.

B.3: Hydroazidation Product Characterization (0.5 mmol scale):

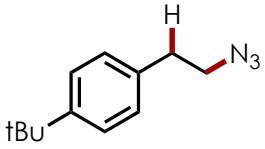

1-(2-Azidoethyl)-4-(*tert*-butyl)benzene (3.1): Following irradiation, the crude reaction mixture was concentrated under reduced pressure. HMDSO was added as an internal standard and the resulting mixture was dissolved in deuterated chloroform and analyzed by NMR. Integration relative to the internal standard showed the product was formed in 43% yield (n=2).

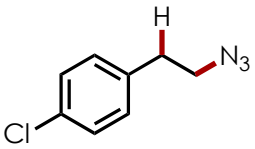

1-(2-Azidoethyl)-4-chlorobenzene (3.2): Following irradiation, the crude reaction mixture was concentrated under reduced pressure. HMDSO was added as an internal standard and the resulting mixture was dissolved in deuterated chloroform and analyzed by NMR. Spectral data matched those previously reported. (22% yield, n =2).[189]

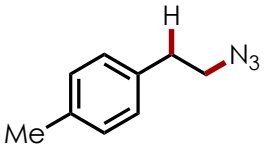

1-(2-Azidoethyl)-4-methylbenzene (3.3): Following irradiation, the crude reaction mixture was concentrated under reduced pressure. HMDSO was added as an internal standard and the resulting mixture was dissolved in deuterated chloroform and analyzed by NMR. Spectral data matched those previously reported. (22% yield, n =2).[189]

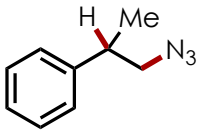

(1-Azidopropan-2-yl)benzene (3.4): Following irradiation, the crude reaction mixture was concentrated under reduced pressure. HMDSO was added as an internal standard and the resulting mixture was dissolved in deuterated chloroform and analyzed by NMR. Spectral data matched those previously reported. (49% yield, n =2).[190]

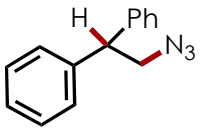

(2-Azidoethane-1,1-diyl)dibenzene (3.5): Following irradiation, the crude reaction mixture was concentrated under reduced pressure. HMDSO was added as an internal standard and the resulting mixture was dissolved in deuterated chloroform and analyzed by NMR. Spectral data matched those previously reported (ELI LILLY AND COMPANY - WO2005/821, 2005, A1), (24% yield, n =2).

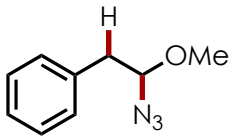

(2-Azido-2-methoxyethyl)benzene (3.6): The desired product was isolated as a pale yellow oil following purification by flash column chromatography (100% hexane → 5% EtOAc/hexane gradient).

^{1}H NMR (400 MHz, chloroform-*d*) δ 7.45 – 6.98 (m, 5H), 4.49 (t, *J* = 6.0 Hz, 1H), 3.47 (s, 3H), 3.07 (dd, *J* = 14.0, 6.2 Hz, 1H), 2.99 (dd, *J* = 14.0, 5.8 Hz, 1H).

^{13}C NMR (151 MHz, chloroform-*d*) δ 135.79, 129.65, 128.65, 127.11, 94.67, 56.96, 41.25.

MS (EI): calculated: 177.090, found: 177.00 (M^{+})

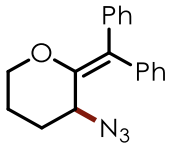

3-Azido-2-(diphenylmethylene)tetrahydro-2*H*-pyran (3.7): The desired product was isolated as a pale yellow oil following purification by flash column chromatography (100% hexane → 5% EtOAc/hexane gradient).

^{1}H NMR (600 MHz, chloroform-*d*) δ 7.36 (dd, *J* = 8.1, 6.7 Hz, 2H), 7.32 – 7.25 (m, 5H), 7.25 – 7.17 (m, 3H), 4.31 (t, *J* = 3.2 Hz, 1H), 4.27 (ddt, *J* = 11.0, 4.5, 1.9 Hz, 1H), 3.80 (ddd, *J* = 12.4, 11.0, 2.8 Hz, 1H), 2.29 – 2.17 (m, 1H), 1.97 – 1.90 (m, 1H), 1.88 – 1.80 (m, 1H), 1.63 – 1.51 (m, 1H).

^{13}C NMR (151 MHz, chloroform-*d*) δ 146.89, 139.35, 138.66, 130.67, 129.86, 128.61, 127.91, 127.49, 127.37, 126.99, 70.09, 56.02, 28.66, 20.37.

HRMS (APCI, positive mode): calculated: 264.1310, found: 264.1382 ($M+H, -N_2$)

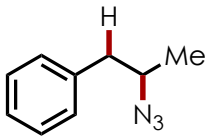

(2-Azidopropyl)benzene (3.9): Following irradiation, the crude reaction mixture was concentrated under reduced pressure to yield a yellow oil. HMDSO was added as an internal standard and the resulting mixture was dissolved in $CDCl_3$ and analyzed by ^1H NMR to determine yield (98% yield, n=2). Spectral data matched those previously reported.[191]

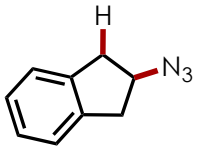

2-Azido-2,3-dihydro-1*H*-indene (3.10): Following irradiation, the crude reaction mixture was concentrated under reduced pressure and dry loaded onto silica gel. The desired product was isolated as a pale yellow oil following column chromatography (100% hexane → 1% EtOAc/hex, 52% yield, n=3). Spectral data matched those previously reported.[192]

^{1}H NMR (500 MHz, chloroform-*d*) δ 7.29 (dd, *J* = 5.3, 3.5 Hz, 2H), 7.26 – 7.17 (m, 2H), 4.40 (dt, *J* = 11.1, 6.7, 4.4 Hz, 1H), 3.28 (dd, *J* = 16.2, 6.7 Hz, 2H), 3.06 (dd, *J* = 16.2, 4.4 Hz, 2H).

^{13}C NMR (126 MHz, chloroform-*d*) δ 140.23, 127.10, 124.77, 61.86, 39.09.

MS (EI): calculated: 159.08, found: 159.10

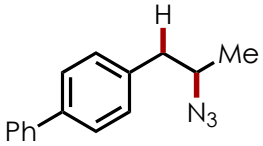

4-(2-Azidopropyl)-1,1'-biphenyl (3.11): Following irradiation, the crude reaction mixture was concentrated under reduced pressure and dry loaded onto silica gel. The desired product was

isolated as a pale yellow oil following column chromatography (100% hexane → 1% EtOAc/hex, 97% yield, n=2). Spectral data matches those previously reported.

^{1}H NMR (600 MHz, chloroform-*d*) δ 7.63 (dd, *J* = 26.1, 7.7 Hz, 4H), 7.49 (t, *J* = 7.6 Hz, 2H), 7.39 (t, *J* = 7.4 Hz, 1H), 7.32 (d, *J* = 7.8 Hz, 2H), 3.77 (h, *J* = 6.6 Hz, 1H), 2.92 (dd, *J* = 13.7, 7.3 Hz, 1H), 2.82 (dd, *J* = 13.7, 6.4 Hz, 1H), 1.35 (d, *J* = 6.5 Hz, 3H).

^{13}C NMR (151 MHz, chloroform-*d*) δ 140.90, 139.73, 136.91, 129.79, 128.84, 127.29, 127.10, 59.04, 42.24, 19.22.

HRMS (APCI, positive mode): calculated 210.1277, found: 210.1278 (M+H, -N_2)

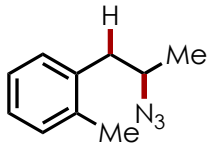

1-(2-Azidopropyl)-2-methylbenzene (3.12): The desired product was isolated as a clear oil following purification by flash chromatography (100% hexane, 76% yield, n=2).

^{1}H NMR (500 MHz, chloroform-*d*) δ 7.26 – 7.12 (app s., 4H), 3.72 (m, 1H), 2.92 (dd, *J* = 13.7, 7.4 Hz, 1H), 2.77 (dd, *J* = 13.7, 6.6 Hz, 1H), 2.38 (s, 3Hu), 1.33 (d, *J* = 6.5 Hz, 3H).

^{13}C NMR (126 MHz, chloroform-*d*) δ 136.40, 136.19, 130.53, 130.20, 126.95, 126.11, 58.36, 39.87, 19.65, 19.42.

HRMS (APCI, positive mode): calculated: 193.1447, found: 193.1423 (M+NH_4)

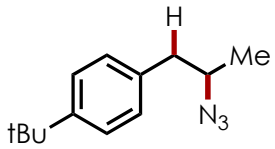

1-(2-Azidopropyl)-4-(*tert*-butyl)benzene (3.13): Following irradiation, the crude reaction mixture was concentrated under reduced pressure and dry loaded onto silica gel. The desired

product was isolated as a pale yellow oil following column chromatography (100% hexane → 1% EtOAc/hex, 51% yield, n=2). Spectral data matched those previously reported.[191]

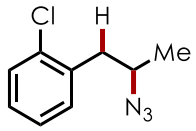

1-(2-Azidopropyl)-2-chlorobenzene (3.14): Following irradiation, the crude reaction mixture was concentrated under reduced pressure and dry loaded onto silica gel. The desired product was isolated as a pale yellow oil following column chromatography (100% hexane → 3% EtOAc/hex, 64% yield, n=2).

^{1}H NMR (600 MHz, chloroform-*d*) δ 7.40 (dd, *J* = 7.2, 1.9 Hz, 1H), 7.28 (dd, *J* = 7.1, 2.3 Hz, 1H), 7.25 – 7.19 (m, 2H), 3.85 (h, *J* = 6.7 Hz, 1H), 3.00 – 2.84 (m, 2H), 1.33 (d, *J* = 6.5 Hz, 3H).
^{13}C NMR (151 MHz, chloroform-*d*) δ 135.70, 134.32, 131.85, 129.74, 128.42, 126.95, 57.57, 40.40, 19.43.

MS (EI): calculated: 195.056, found: 195.05 (M^{+})

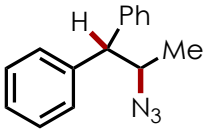

(2-Azidopropane-1,1-diyl)dibenzene (3.15): Following irradiation, the crude reaction mixture was concentrated under reduced pressure and dry loaded onto silica gel. The desired product was isolated as a clear oil following column chromatography (100% hexane → 1% EtOAc/hex, 66% yield, n=2). Spectral data matched those previously reported.[193]

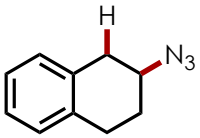

2-Azido-1,2,3,4-tetrahydronaphthalene (3.16): Following irradiation, the crude reaction mixture was concentrated under reduced pressure and dry loaded onto silica gel. The desired product was isolated as a clear oil following column chromatography (100% hexane → 1% EtOAc/hex, 81% yield, n=2). Spectral data matched those previously reported.[194]

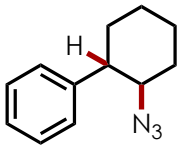

(2-Azidocyclohexyl)benzene (3.17): Following irradiation, the crude reaction mixture was concentrated under reduced pressure and dry loaded onto silica gel. The desired product was isolated as a clear oil following column chromatography (100% hexane → 1% EtOAc/hex, 81% yield, n=2) as a single diastereomer. Spectral data matched those previously reported.[195]

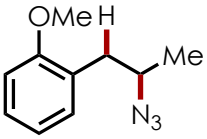

1-(2-Azidopropyl)-2-methoxybenzene (3.18): The desired product was isolated as a clear oil following column chromatography (100% hexane → 1% EtOAc/hex, 75% yield, n=2)

^{1}H NMR (600 MHz, chloroform-*d*) δ 7.24 (td, *J* = 7.8, 1.7 Hz, 1H), 7.14 (dd, *J* = 7.4, 1.7 Hz, 1H), 6.91 (td, *J* = 7.4, 1.1 Hz, 1H), 6.86 (dd, *J* = 8.1, 1.0 Hz, 1H), 3.83 (s, 3H), 3.81 – 3.72 (m, 1H), 2.85 (dd, *J* = 13.3, 7.3 Hz, 1H), 2.76 (dd, *J* = 13.4, 6.6 Hz, 1H), 1.24 (d, *J* = 6.5 Hz, 3H).

^{13}C NMR (151 MHz, chloroform-*d*) δ 157.66, 131.32, 128.23, 126.35, 120.55, 110.38, 57.73, 55.35, 37.51, 19.48

MS (EI): calculated: 191.106, found: 191.10 (M^+)

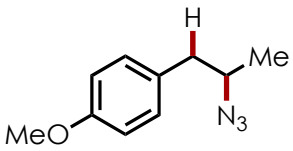

1-(2-Azidopropyl)-4-methoxybenzene (3.19): . The desired product was isolated as a clear oil following column chromatography (100% hexane → 1% EtOAc/hex, 90% yield, n=2)

^{1}H NMR (500 MHz, chloroform-*d*) δ 7.12 (d, *J* = 8.6 Hz, 2H), 6.85 (d, *J* = 8.6 Hz, 2H), 3.80 (s, 3H), 3.64 (h, *J* = 6.6 Hz, 1H), 2.77 (dd, *J* = 13.8, 7.3 Hz, 1H), 2.67 (dd, *J* = 13.8, 6.4 Hz, 1H), 1.25 (d, *J* = 6.5 Hz, 3H).

^{13}C NMR (151 MHz, chloroform-*d*) δ 158.52, 130.39, 129.92, 114.01, 59.36, 55.39, 41.80, 19.18

MS (EI): calculated: 191.106, found: 191.10 (M^+)

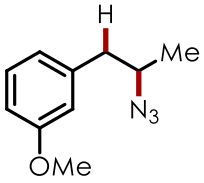

1-(2-Azidopropyl)-3-methoxybenzene (3.20): . The desired product was isolated as a clear oil following column chromatography (100% hexane → 1% EtOAc/hex, 80% yield, n=2)

^{1}H NMR (500 MHz, chloroform-*d*) δ 7.23 (t, *J* = 7.9 Hz, 1H), 6.89 – 6.68 (m, 3H), 3.81 (s, 3H), 3.68 (p, *J* = 6.6 Hz, 1H), 2.82 (dd, *J* = 13.6, 7.3 Hz, 1H), 2.70 (dd, *J* = 13.6, 6.5 Hz, 1H), 1.27 (d, *J* = 6.5 Hz, 3H).

^{13}C NMR (126 MHz, chloroform-*d*) δ 159.77, 139.47, 129.62, 121.76, 115.22, 112.04, 59.07, 55.32, 42.72, 19.31

MS (EI): calculated: 191.106, found: 191.05 (M^+)

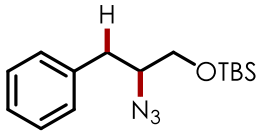

(2-Azido-3-phenylpropoxy)(*tert*-butyl)dimethylsilane (3.21): Following irradiation, the crude reaction mixture was concentrated under reduced pressure. HMDSO was added as an internal standard and the sample was dissolved in deuterated chloroform and analyzed by NMR. Integration relative to the internal standard showed that the product was formed in 39% yield (n = 2).

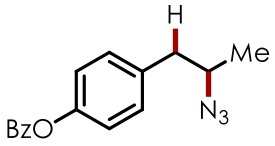

4-(2-Azidopropyl)phenyl benzoate (3.22): Following irradiation, the crude reaction mixture was concentrated under reduced pressure and dry loaded onto silica gel. The desired product was isolated as a clear oil following purification by column chromatography (5 % EtOAc/hexane to 30 % EtOAc/hex, 62% yield, n =2).

^{1}H NMR (600 MHz, chloroform-*d*) δ 8.20 (dd, *J* = 8.3, 1.4 Hz, 2H), 7.68 – 7.60 (m, 1H), 7.58 – 7.44 (m, 2H), 7.32 – 7.24 (m, 2H), 7.17 (d, *J* = 8.4 Hz, 2H), 3.71 (h, *J* = 6.6 Hz, 1H), 2.86 (dd, *J* = 13.7, 7.3 Hz, 1H), 2.75 (dd, *J* = 13.7, 6.4 Hz, 1H), 1.29 (d, *J* = 6.5 Hz, 3H).

^{13}C NMR (151 MHz, chloroform-*d*) δ 165.19, 149.76, 135.39, 133.60, 130.33, 130.17, 129.56, 128.58, 121.72, 58.96, 41.97, 19.12.

HRMS (APCI, positive mode): calculated: 254.1175, found: 254.1175 ($M+H, -N_2$)

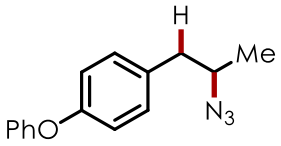

1-(2-Azidopropyl)-4-phenoxybenzene (3.23): The desired product was isolated as a clear oil following purification by column chromatography (100% hexane → 1 % EtOAc/Hexane, 91% yield, n=2)

^{1}H NMR (600 MHz, chloroform-*d*) δ 7.38 – 7.30 (m, 2H), 7.16 (d, *J* = 8.5 Hz, 2H), 7.13 – 7.06 (m, 1H), 7.01 (dd, *J* = 8.7, 1.1 Hz, 2H), 6.96 (d, *J* = 8.5 Hz, 2H), 3.77 – 3.47 (m, 1H), 2.80 (dd, *J* = 13.8, 7.4 Hz, 1H), 2.72 (dd, *J* = 13.8, 6.3 Hz, 1H), 1.28 (d, *J* = 6.5 Hz, 3H).

^{13}C NMR (151 MHz, chloroform-*d*) δ 157.31, 156.03, 132.62, 130.57, 129.72, 123.18, 118.96, 118.78, 59.14, 41.87, 19.16.

HRMS (APCI, positive mode): calculated: 226.1226, found: 226.1227 ($M+H, -N_2$)

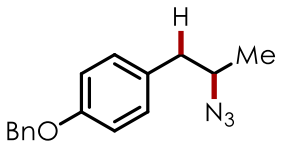

1-(2-Azidopropyl)-4-(benzyloxy)benzene (3.24): The desired product was isolated as clear oil and purified using column chromatography (1 % EtOAc/hexane, Yield: 91 %, n =2).

^{1}H NMR (500 MHz, chloroform-*d*) δ 7.44 (d, *J* = 6.9 Hz, 2H), 7.39 (t, *J* = 7.4 Hz, 2H), 7.33 (t, *J* = 7.2 Hz, 1H), 7.12 (d, *J* = 8.6 Hz, 2H), 6.93 (d, *J* = 8.6 Hz, 2H), 5.05 (s, 2H), 3.64 (h, *J* = 6.7 Hz, 1H), 2.77 (dd, *J* = 13.8, 7.3 Hz, 1H), 2.67 (dd, *J* = 13.8, 6.4 Hz, 1H), 1.25 (d, *J* = 6.5 Hz, 3H).

^{13}C NMR (151 MHz, chloroform-d) δ 157.69, 137.07, 130.29, 130.12, 128.59, 127.95, 127.49, 114.87, 70.06, 59.20, 41.71, 19.05.

HRMS (APCI, positive mode): calculated: 240.1383, found: 240.1383 ($M+H, -N_2$)

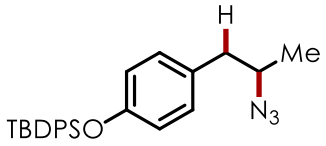

(4-(2-Azidopropyl)phenoxy)(*tert*-butyl)diphenylsilane (3.25): The desired product was isolated as clear oil following purification by column chromatography (100 % pentane to 100 % hexane, 76% yield, n=2)

^{1}H NMR (500 MHz, chloroform-*d*) δ 7.71 (dd, *J* = 6.8, 1.3 Hz, 4H), 7.47 – 7.38 (m, 2H), 7.36 (d, *J* = 8.0 Hz, 4H), 6.91 (d, *J* = 8.5 Hz, 2H), 6.70 (d, *J* = 8.5 Hz, 2H), 3.57 (h, *J* = 6.6 Hz, 1H), 2.69 (dd, *J* = 13.8, 7.2 Hz, 1H), 2.58 (dd, *J* = 13.8, 6.5 Hz, 1H), 1.18 (d, *J* = 6.5 Hz, 3H), 1.09 (s, 9H).

^{13}C NMR (151 MHz, chloroform-*d*) δ 154.40, 135.53, 132.99, 130.17, 130.01, 129.84, 127.73, 119.69, 59.21, 41.80, 26.53, 19.47, 19.04

HRMS (APCI, positive mode): calculated: 388.2018, found: 388.2090 ($M+H, -N_2$)

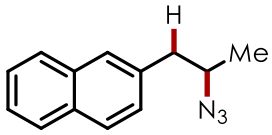

2-(2-Azidopropyl)naphthalene (3.26): The desired product was isolated as a clear oil following purification by column chromatography (100% hexane → 2% EtOAc/hexane, 67% yield, n=2). Spectral data matched those previously reported.[196]

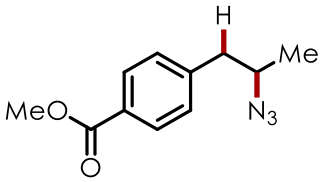

Methyl 4-(2-azidopropyl)benzoate (3.27): The desired product was isolated as clear oil and purified using column chromatography (100 % hexane, 70% yield, n=2)

^{1}H NMR (600 MHz, chloroform-*d*) δ 7.99 (d, *J* = 8.2 Hz, 2H), 7.28 (d, *J* = 8.1 Hz, 2H), 3.91 (s, 3H), 3.72 (h, *J* = 6.5 Hz, 1H), 2.87 (dd, *J* = 13.7, 7.5 Hz, 1H), 2.79 (dd, *J* = 13.7, 6.2 Hz, 1H), 1.28 (d, *J* = 6.5 Hz, 3H).

^{13}C NMR (151 MHz, chloroform-*d*) δ 166.94, 143.11, 129.82, 129.35, 128.74, 58.65, 52.08, 42.54, 19.21.

HRMS (APCI, positive mode): calculated: 192.1019, found: 192.1019(M+H, -N_2)

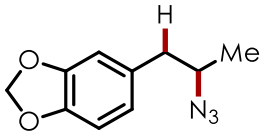

5-(2-Azidopropyl)benzo[d][1,3]dioxole (3.28): The desired product was isolated as a pale yellow oil following purification by column chromatography (100% hexane → 3% EtOAc/hex, 92% yield, n =2). Spectral data matched those previously reported.[51]

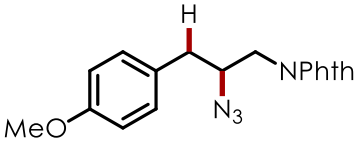

2-(2-Azido-3-(4-methoxyphenyl)propyl)isoindoline-1,3-dione (3.29): The desired product was isolated as a clear oil following purification by flash chromatography (100% hexane → 1% EtOAc/hexane gradient, 87% yield, n=2).

^{1}H NMR (500 MHz, chloroform-*d*) δ 7.83 (dd, *J* = 5.4, 3.0 Hz, 1H), 7.70 (dd, *J* = 5.4, 3.0 Hz, 1H), 7.16 (d, *J* = 8.6 Hz, 1H), 6.83 (d, *J* = 8.6 Hz, 1H), 3.99 (tt, *J* = 8.6, 5.1 Hz, 1H), 3.82 (dd, *J* = 14.0, 8.9 Hz, 1H), 3.75 (s, 2H), 3.70 (dd, *J* = 14.0, 4.6 Hz, 1H), 2.88 (dd, *J* = 14.2, 5.5 Hz, 1H), 2.81 (dd, *J* = 14.2, 8.4 Hz, 1H).

^{13}C NMR (126 MHz, chloroform-*d*) δ 168.08, 158.60, 134.17, 131.78, 130.16, 128.44, 123.44, 114.08, 61.52, 55.19, 41.20, 38.01.

HRMS (APCI, positive mode): calculated: 337.1295, found: 337.1295 (M+H)

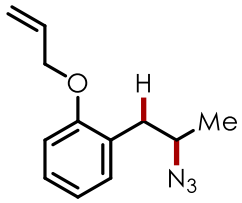

1-(Allyloxy)-2-(2-azidopropyl)benzene (3.30): The desired product was isolated as a clear oil following purification by flash chromatography (100% hexane → 1% EtOAc/hexane gradient, 71% yield, n = 2).

^{1}H NMR (600 MHz, chloroform-*d*) δ 7.30 – 7.24 (m, 1H), 7.21 (dd, *J* = 7.4, 1.7 Hz, 1H), 6.96 (td, *J* = 7.4, 1.1 Hz, 1H), 6.89 (dd, *J* = 8.2, 1.0 Hz, 1H), 6.11 (ddd, *J* = 17.3, 10.3, 5.0 Hz, 1H), 5.46 (dd, *J* = 17.3, 1.7 Hz, 1H), 5.33 (dd, *J* = 10.3, 1.5 Hz, 1H), 4.68 – 4.46 (m, 2H), 3.85 (h, *J* = 6.7 Hz, 1H), 2.95 (dd, *J* = 13.3, 7.3 Hz, 1H), 2.85 (dd, *J* = 13.3, 6.7 Hz, 1H), 1.29 (d, *J* = 6.6 Hz, 3H).

^{13}C NMR (151 MHz, chloroform-*d*) δ 156.62, 133.42, 131.39, 128.12, 126.59, 120.73, 117.08, 111.63, 68.67, 57.75, 37.57, 19.42.

HRMS (APCI, positive mode): calculated: 190.1226, found: 190.1226 (M+H, -N_2)

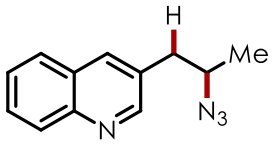

3-(2-Azidopropyl)quinoline (3.31): The desired product was isolated as a clear oil following purification by column chromatography (3% EtOAc/hexane to 30% EtOAc/hexane, 55% yield, n =2)

^{1}H NMR (600 MHz, chloroform-*d*) δ 8.79 (d, *J* = 2.2 Hz, 1H), 8.10 (d, *J* = 8.4 Hz, 1H), 8.04 – 7.95 (m, 1H), 7.82 – 7.76 (m, 1H), 7.70 (ddd, *J* = 8.4, 6.9, 1.5 Hz, 1H), 7.55 (ddd, *J* = 8.1, 6.9, 1.2 Hz, 1H), 3.85 – 3.78 (m, 1H), 2.98 (dd, *J* = 14.1, 7.4 Hz, 1H), 2.94 (dd, *J* = 14.0, 6.0 Hz, 1H), 1.35 (d, *J* = 6.5 Hz, 3H).**^{13}C NMR (151 MHz, chloroform-*d*)** δ 151.91, 147.16, 135.82, 130.48, 129.18, 127.93, 126.83, 58.57, 39.79, 19.15.

HRMS (APCI, positive mode): calculated: 185.1073, found: 185.1074 ($M+H, -N_2$)

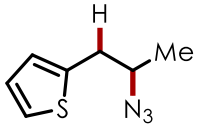

2-(2-Azidopropyl)thiophene (3.32): Following irradiation, the reaction mixture was concentrated under reduced pressure to yield a red oil. This oil was dissolved in deuterated chloroform and HMDSO was added as an internal standard. Yield was then determined *via* NMR spectroscopy (65% yield, n =2). **^{1}H NMR (600 MHz, chloroform-*d*)** δ 7.21 (dd, *J* = 5.1, 1.2 Hz, 1H), 6.98 (dd, *J* = 5.1, 3.4 Hz, 1H), 6.91 – 6.88 (m, 1H), 3.74 (h, *J* = 6.6 Hz, 1H), 3.03 (dd, *J* = 14.7, 7.1 Hz, 1H), 2.98 (dd, *J* = 14.7, 6.1 Hz, 1H), 1.32 (d, *J* = 6.5 Hz, 3H).

^{13}C NMR (151 MHz, chloroform-*d*) δ 139.72, 126.99, 126.33, 124.48, 59.03, 36.67, 19.09.

MS (EI): calculated: 167.051, found: 167.05 (M^+)

B.4: NMR Spectra for New Compounds

NMR data is available in the corresponding published supporting information, which is available online.[197]

APPENDIX C: SUPPORTING INFORMATION FOR "REGIOSELECTIVE ARENE C–H ALKYLATION *VIA* ORGANIC PHOTOREDOX CATALYSIS"

C.1: General Information:

Reagent Information: Commercially available reagents were purchased from Sigma-Aldrich, Fischer Scientific or TCI Corporation and were used without further purification. Solvents used in photochemical reactions were dried *via* distillation over compatible drying agent (typically calcium hydride or activated 4Å molecular sieves). Dry solvents were then degassed *via* freeze-pump-thaw (4 cycles or until no bubbling was visible during thawing). Solvents were then stored in a nitrogen filled glovebox (O_2 levels < 10 ppm) and dispensed within the glovebox.

Analytical Information: Proton and carbon (^{1}H and ^{13}C) magnetic resonance spectra were collected on a Bruker AVANCE III 600 CryoProbe (^{1} H NMR at 600 MHz and ^{13}C NMR at 151 MHz) spectrometer or Bruker AVANCE III 500 (^{1} H NMR at 500 MHz and ^{13}C NMR at 126 MHz) spectrometer. Unless otherwise noted, spectra are referenced to chloroform-*d* (^{1} H NMR at 7.26 ppm and ^{13}C at 77.16 ppm) and reported as parts per million. ^{1}H NMR data are reported as follows: chemical shift, multiplicity (s = singlet, d = doublet, t = triplet, dd = doublet of doublets, ddd = doublet of doublets of doublets, ddddd = doublet of doublets of doublets of doublets of doublets, dt = doublet of triplets, ddt = doublet of doublets of triplets, td = triplet of doublets, tt = triplet of triplets, m = multiplet, q = quartet), coupling constants (Hz), and integration

High resolution mass spectra (HRMS) were obtained *via* direct infusion using a Thermo LTQ FT mass spectrometer with positive mode electrospray ionization, via gas chromatography using an Exactive GC gas chromatographic system in positive mode chemical ionization, equipped with a

Trace 1300 SSL injector and TriPlus RSH autosampler, or via liquid chromatography using Waters Acquity H-class liquid

Electrochemical potentials were obtained with a standard set of conditions to main internal consistency. Cyclic voltammograms were collected with a Pine WaveNow Potentiostat. Data was analyzed using MATLAB by subtracting a background current prior to identifying the maximum current (Cp) and determining the potential ($E_{p/2}$) at half this value ($_{Cp/2}$). The obtained value was referenced to Ag|AgCl and converted to SCE by subtracting 0.03 V. Samples were prepared with 0.1 mmol of analyte in 5 mL of 0.1 M tetra-(N)-butylammonium hexafluorophosphate in dry, degassed acetonitrile. Measurements employed a glassy carbon working electrode, platinum wire counter electrode, 3.5 M NaCl silver-silver chloride reference electrode, and a scan rate of 100 mV/s. Reductions were measured by scanning potentials in the negative direction and oxidations in the positive direction.

Flash chromatography was performed using SiliaFlash P60 silica gel (40-63 μm) purchased from Silicycle.

General Photoreactor Configuration: All photochemical reactions were conducted using a SynLED Parallel Photoreactor, available for purchase from Sigma-Aldrich (item number: **Z742680).** The unit has bottom-lit LEDS (465-470 nm) with 130-140 lm intensity and a built-in cooling fan. The measured temperature range was 35 - 40°C. The reactor was fit to an IKA magnetic stirrer with round plate (item number: Z645052). Small stir bars are sometimes required for efficient stirring when using 2 dram vials. All reaction mixtures were kept under a positive pressure of nitrogen *via* an inlet needle which was routed to a standard Shlenk line, equip with a nitrogen source which feeds through a desiccant tube (Dririte/$CaCl_2$).

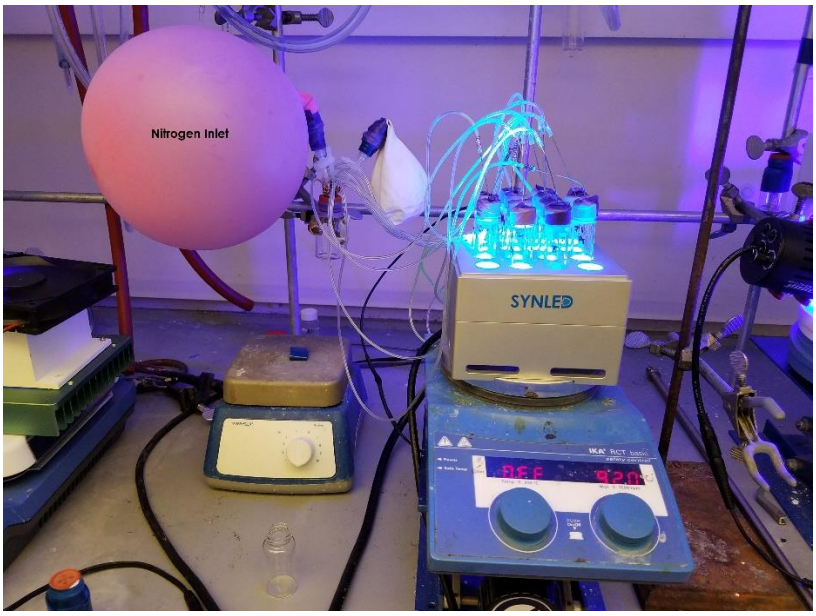

Figure C.1: General photoreactor configuration

General Procedure for Photochemical Reactions: A flame-dried 2 dram borosilicate vial (purchased from Fisher Scientific, catalogue # 03-339-22D), equip with a stir bar, was charged with 3,6-di-*tert*-butyl-9-mesityl-10-phenylacridin-10-ium tetrafluoroborate (0.05 equiv, 0.01 mmol). For solid/non-volatile substrates, the substrate (0.20 mmol) was then added. The vial was moved into a nitrogen filled glovebox (<10 ppm O_2) and acetonitrile (1.0 mL) and TFE (1.0 mL) were added via syringe. Ethyl diazoacetate (or other liquid diazo- compounds) was added via a microliter syringe (0.20 mmol, 1.0 equiv.). Vials were capped tightly with a Teflon lined phenolic resin septum cap (purchased through VWR international, Microliter Product # 15-0060K) and moved out of the glovebox. Prior to irradiation, vials were sealed with electrical tape to ensure maximal oxygen exclusion. The reaction vial was then placed into the reactor and equip with a nitrogen inlet needle. The reactions were irradiated for 18 hours unless otherwise noted. Following irradiation, the reaction mixture was concentrated under reduced pressure and the desired products were isolated *via* flash column chromatography (see substrate/product details for solvent

information). *Unless otherwise noted, all reaction yields and regioisomer ratios are reported as the average of two separate trials (including chromatography).* As regioisomers were extremely difficult to separate by conventional silica gel chromatography, NMR data for each regioisomer was determined from the mixture of compounds, utilizing 2-D NMR when required for peak assignments

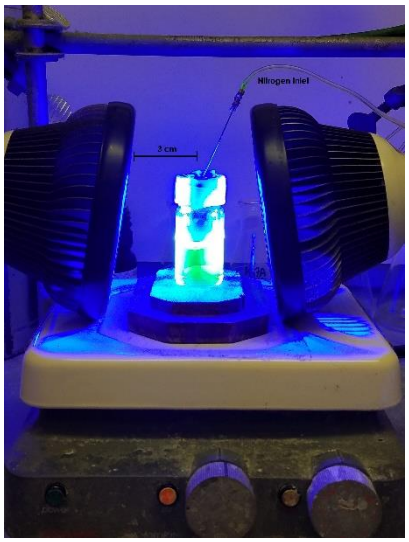

General Procedure for Batch Reaction: A flame-dried 20 mL borosilicate vial (purchased from Chemglass Life Sciences, catalogue # CG-4904-01), equipped with a stir bar was charged with 3,6-di-*tert*-butyl-9-mesityl-10-phenylacridin-10-ium tetrafluoroborate (0.05 equiv, 0.05 mmol). The vial was sealed with the PTFE faced septa and was then put under an inert atmosphere by evacuating under vacuum and refilling with nitrogen three times. A 1:1 mixture of MeCN and TFE was sparged to remove oxygen for fifteen minutes, then was transferred to the vial via cannula. Mesitylene (1.0 equiv., 1.0 mmol) and ethyldiazoacetate (1.0 equiv., 1.0 mmol) were added via microsyringe. Prior to irradiation, vials were sealed with electrical tape to ensure maximal oxygen exclusion. The reaction vial was then placed into the reactor and equip with a nitrogen inlet needle. The reactions were irradiated for 18 hours. Following irradiation, the reaction mixture was concentrated under reduced pressure and the desired products were isolated *via* flash column chromatography (see substrate/product details for solvent information). General Photoreactor Information: The photoreactor consists of two Par38 Royal Blue Aquarium LED lamps (Model #6851) angled towards the reaction wells for maximum LED exposure. The wells were placed on

top of a stir plate for and the reactions were cooled with a fan. The measured temperature with cooling was 26 °C.

C.2: Large Scale Flow Synthesis of Ethyl Mesitylacetate:

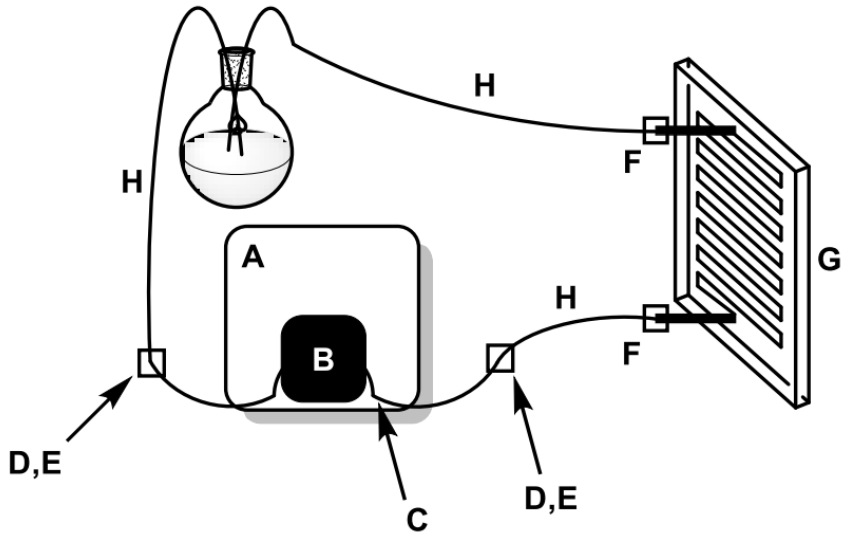

Figure C.2: Flow reactor schematic

A. Masterflex L/S Variable-Speed Drive (Cole-Parmer # EW-07528-30)

B. Masterflex L/S Rigid PTFE-Tubing Pump Head (Cole-Parmer # EW-77390-00)

C. Masterflex PTFE-tubing 4mm O.D. (Cole-Parmer # EW-77390-50)

D. 4MM PTFE Male NPT Compression Adapter (Cole-Parmer # WU-31321-62)

E. 1/8” O.D. to 1/8” PTFE Female NPT Compression Adapter (Cole-Parmer # EW31320-50)

F. 1/4-28 flangeless fitting/ferrule for 1/8" O.D. tubing (Sigma-Aldrich SUPELCO # 58686)

G. Microreactor (Little Things Factory Gmbh # XXL-ST-02)

H. PTFE Tubing 1/16” I.D., 1/8” O.D. (Cole-Parmer # WU-06605-27)

Procedure: A flame-dried, 100 mL pear flask was charged with 3,6-di-*tert*-butyl-9-mesityl-10-phenylacridin-10-ium tetrafluoroborate (143 mg, 0.05 Eq, 250 µmol) and degassed 1**:**1 MeCN:TFE (50 mL) . The resulting mixture was sparged with argon for five minutes. Ethyl 2-diazoacetate (571 mg, 528 µL, 1.00 Eq, 5.00 mmol) and mesitylene (601 mg, 696 µL, 1.00 Eq, 5.00 mmol) were added via microsyringe. The flow cell was purged with 1:1 MeCN:TFE which was sparging with nitrogen prior to the introduction of the reaction mixture. Two 15W PAR38 blue LED floodlamps were positioned on either side of the microreactor (**G**). Tubing was introduced into the flask using a commercially available rubber septum which had been punctured. A nitrogen line was introduced into the headspace of the flask to ensure the complete exclusion of oxygen from the reaction mixture. The Masterflex L/S Variable-Speed Drive was set to 15 rpm and the occlusion bed of the pump head was adjusted as per the manufacturer's instructions. The floodlamps were then switched on and the reaction mixture was allowed to flow though the reactor for 18 hours. The temperature remained at ~35 ºC during the reaction, as measured at the center of the lamps, close to the flow cell using a conventional alcohol thermometer. Solvent was removed under reduced pressure and the resulting residue was purified via flash column chromatography (0 → 5% EtOAc/hexanes), yielding the desired product as a colorless oil (45%, 0.46 g).

C.3: Electrochemical Data: Samples were prepared with 0.1 mmol of analyte in 5 mL of 0.1 M tetra-n-butylammonium hexafluorophosphate in dry, degassed acetonitrile. Measurements employed a glassy carbon working electrode, platinum wire counter electrode, 3.5 M NaCl silver-silver chloride reference electrode, and a scan rate of 100 mV/s. Reductions were measured by scanning potentials in the negative direction and oxidations in the positive direction.

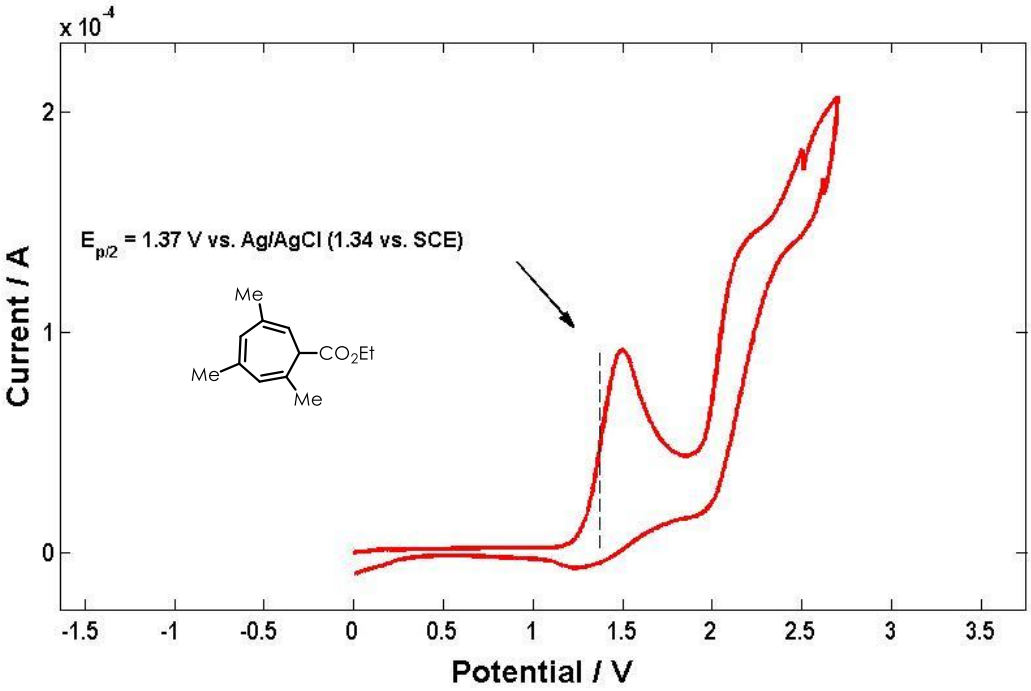
x 10^-4
2
1
0
Current / A
E_p/2 = 1.37 V vs. Ag/AgCl (1.34 vs. SCE)
Me
Me
Me
CO2Et
-1.5
-1
-0.5
0
0.5
1
1.5
2
2.5
3
3.5
Potential / V

C.4: Optimization Data:

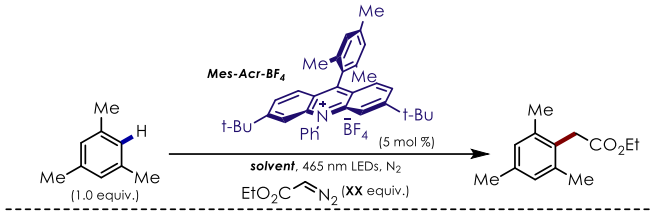

solvent (0.1 M)	*equiv. ethyl diaozacetate*	*yield*
MeOH	1.0	11%
MeCN	1.0	54%
DCE	1.0	31%
TFE	1.0	74%
TFE	2.0	31%
TFE	3.0	9.4%
TFE	4.0	<5%
TFE/MeCN	1.0	76%

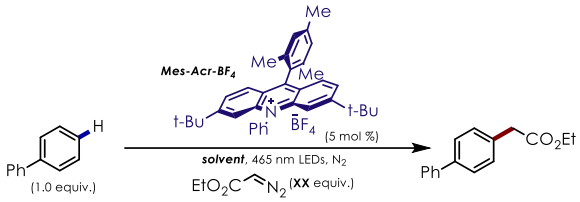

solvent	*equiv. ethyl diaozacetate*	*yield*
DCE/TFE (0.1 M), 1:1	1.0	56%
DCE/TFE (0.1 M), 1:2	1.0	36%
DCE/TFE (0.1 M), 2:1	1.0	21%
MeCN/TFE (0.1 M), 1:1	1.2	25%
MeCN/TFE (0.1 M), 1:1	1.4	16%
MeCN/TFE (0.1 M), 1:1	1.6	10%
MeCN/TFE (1:1), 1.25 eq. substrate	1.0	35%
MeCN/TFE (1:1), 1.50 eq. substrate	1.0	28%
MeCN/TFE (1:1), 1.75 eq. substrate	1.0	31%
MeCN/TFE (1:1), 2.00 eq. substrate	1.0	30%

Figure C.3: Results of optimization of C–H alkylation reaction

C.5: Catalyst and Substrate Synthesis:

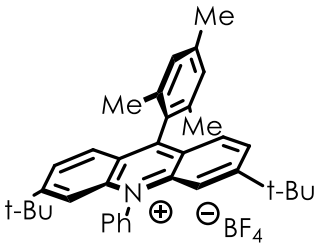

3,6-Di-*tert*-butyl-9-mesityl-10-phenylacridin-10-ium tetrafluoroborate was prepared according to literature precedent. Spectral data matched that reported in the literature. [93]

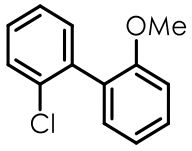

2-Chloro-2'-methoxy-1,1'-biphenyl was prepared according to literature precedent. Spectral data matched that reported in the literature.[198]

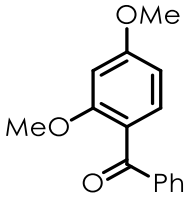

(2,4-Dimethoxyphenyl)(phenyl)methanone was prepared according to literature precedent. Spectral data matched that reported in the literature.[93]

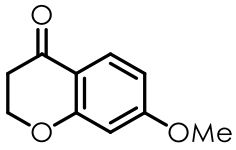

7-Methoxychroman-4-one was prepared according to literature precedent. Spectral data matched that reported in the literature.[199]

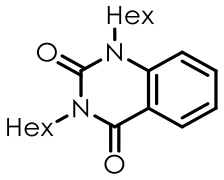

1,3-Dihexanoylquinazoline-2,4(1H,3H)-dione was prepared according to literature precedent. Spectral data matched that reported in the literature.[198]

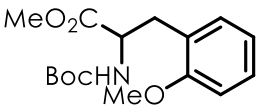

Methyl 2-((*tert*-butoxycarbonyl)amino)-3-(2-methoxyphenyl)propanoate was prepared according to literature precedent. Spectral data matched that reported in the literature.[200]

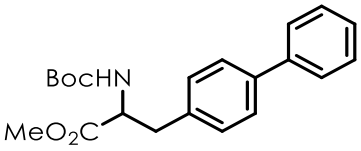

Methyl 3-([1,1'-biphenyl]-4-yl)-2-((*tert*-butoxycarbonyl)amino) propanoate was prepared according to literature precedent. Spectral data matched that reported in the literature.[200]

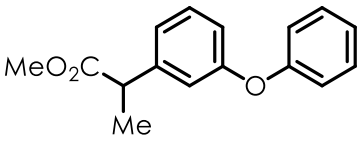

Methyl 2-(3-phenoxyphenyl)propanoate was prepared according to literature precedent. Spectral data matched those previously reported in the literature.[201]

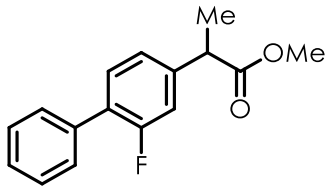

Methyl 2-(2-fluoro-[1,1'-biphenyl]-4-yl)propanoate: A flame dried 25 mL RBF was charged with potassium carbonate (1.44 g, 5.1 Eq, 10.4 mmol), 2-(2-fluoro-[1,1'-biphenyl]-4-yl)propanoic acid (0.500 g, 1.00 Eq, 2.05 mmol) and DMF (5 mL). The reaction solution was cooled to 0 °C. Iodomethane (0.4 mL, 3.1 Equiv., 6.36 mmol) was added dropwise over 5 minutes. The reaction was allowed to warm to room temperature while stirring overnight. The next day, resulting reaction mixture was quenched with a saturated sodium bicarbonate solution. The organics were extracted with EtOAc (3x 15 mL), washed with brine (2x 30 mL) then a LiCl aqueous solution (2x 30 mL). The organics were combined, dried over magnesium sulfate, filtered and concentrated to give the crude mixture. This was purified via flash column chromatography with 5% EtOAc in Hexanes to give the pure product, a clear oil (0.3868 g, 73%). Spectral data matched that reported in the literature.[202]

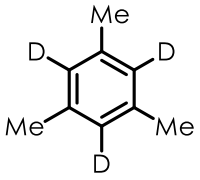

***d*$_3$-Mesitylene** was prepared according to literature precedent. Spectral data matched that reported in the literature. The final product was calculated to be 95.3% deuterated by using ^{1}H NMR integration of the methyl relative to residual aromatic protons with HMDSO as an internal standard.[203]

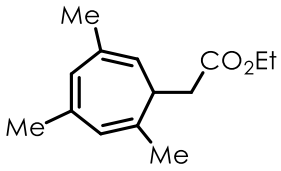

Ethyl 2-(2,4,6-trimethylcyclohepta-2,4,6-trien-1-yl)acetate was prepared according to literature precedent. Spectral data matched that reported in the literature.[100]

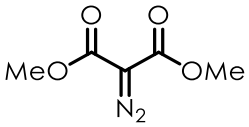

Dimethyl 2-diazomalonate was prepared according to literature precedent. Spectral data matched that reported in the literature.[204,205]

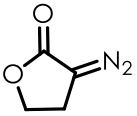

3-Diazodihydrofuran-2(*3H*)-one was prepared according to literature precedent. Spectral data matched that reported in the literature.[206]

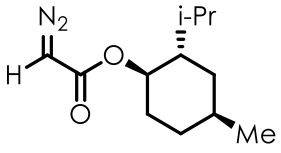

(–)-Menthyl 2-diazoacetate was prepared according to literature precedent. Spectral data matched that reported in the literature.[207]

C.6: Procedure and Data for Product Synthesis

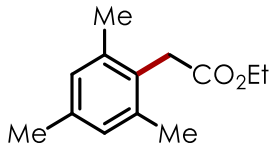

Ethyl 2-mesitylacetate (4.1a): Isolated by column chromatography (0-5% EtOAc in Hexanes) as a colorless oil, 76% yield. Spectral data matched reported literature values.[208]

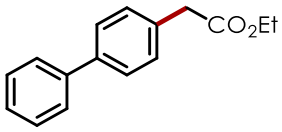

Ethyl 2-([1,1'-biphenyl]-4-yl)acetate (4.2a): The desired product was isolated as a white solid, 42% yield, Spectral data matched reported literature values.[209]

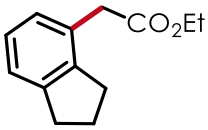

Ethyl 2-(2,3-dihydro-1H-inden-4-yl)acetate (4.3a): The desired product was isolated as a clear oil following flash column chromatography (3% EtOAc in hexanes) (24% yield) (NMR data for each individual isomer is not able to be reported due to overlapping signals. Regioisomeric ratio = 1:5 based on NMR ratios)

^{1}H NMR (500 MHz, chloroform-*d*) δ 7.17 (d, *J* = 7.7 Hz, 1H), 7.15 (s, 1H), 7.04 (d, *J* = 7.7 Hz, 1H), 4.15 (q, *J* = 7.1 Hz, 2H), 3.58 (s, 2H), 2.89 (q, *J* = 7.1 Hz, 4H), 2.10 – 2.00 (m, 2H), 1.26 (t, *J* = 7.2 Hz, 3H).

^{13}C NMR (151 MHz, chloroform-*d*) δ 172.07, 144.71, 143.06, 131.81, 127.01, 125.27, 124.39, 60.82, 41.27, 32.79, 32.54, 25.50, 14.23.

HRMS: Calculated (M+H): 205.1223; found: 205.1230

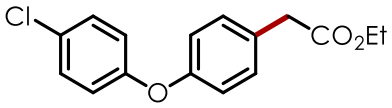

Ethyl 2-(4-(4-chlorophenoxy)phenyl)acetate (4.4a, major product): The desired product was isolated as a clear oil following column chromatography (5% EtOAc in hexanes) as a clear oil (36% yield, n = 2) in 4:1 ratio of para:ortho products. NMR characterization is given below for the major isomer.

^{1}H NMR (500 MHz, chloroform-*d*) δ 7.31 – 7.25 (m, 5H), 6.99 – 6.93 (m, 4H), 4.18 (q, *J* = 7.1 Hz, 2H), 3.61 (s, 2H), 1.28 (t, *J* = 7.1 Hz, 3H).

^{13}C NMR (151 MHz, chloroform-*d*) δ 171.67, 155.93, 155.87, 130.74, 129.72, 129.40, 120.05, 119.49, 118.97, 60.97, 40.60, 14.22.

HRMS: Calculated (M+H): 291.0782; found: 291.0793

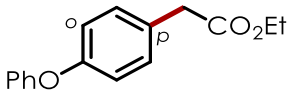

Ethyl 2-(4-phenoxyphenyl)acetate (4.5a, major product): Isolated by column chromatography (5% EtOAc in Hexanes) as a colorless oil, 29% yield (n=2), 5:1(para:ortho).

Para Isomer: **^{1}H NMR** (600 MHz, chloroform-d) δ 1.25 – 1.29 (m, 3H), 3.59 (s, 2H), 4.16 (q, J = 7.1 Hz, 2H), 6.94 – .96 (d, J = 8.3 Hz, 2H), 7.01 (d, J = 8.0 Hz, 2H), 7.09 (t J = 7.4 Hz, 1H), 7.21 – 7.27 (d, J = 8.1 Hz, 2H), 7.32 (t, J = 7.7, 5.5 Hz, 2H). **^{13}C NMR (151 MHz, chloroform-d)** δ 171.85, 157.26, 156.41, 130.70, 129.85, 123.38, 119.02, 119.01, 61.04, 40.74, 31.10, 14.33. **HRMS:** Calculated (M+H): 257.1172; found: 257.1151

Ortho Isomer: **^{1}H NMR (600 MHz, chloroform-d)** δ 1.17 (t, J = 7.1 Hz, 3H), 3.68 (s, 2H), 4.07 (q, J = 7.1 Hz, 2H), 6.88 (d, J = 8.1 Hz, 1H), 6.94 – 6.98 (app d, 1H), 7.09 (app t, 2H), 7.21 – 7.27

(m, 2H), 7.32 (3, 3H). **^{13}C NMR (151 MHz, chloroform-d)** δ 171.54, 157.44, 155.19, 131.61, 129.77, 129.04, 128.75, 126.19, 123.78, 123.14, 118.43, 60.91, 36.07, 14.27. **HRMS:** Calculated (M+H): 257.1172; found: 257.1151

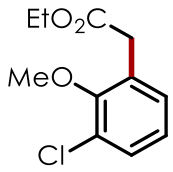

Ethyl 2-(3-chloro-2-methoxyphenyl)acetate (4.6a): Isolated by column chromatography (10 to 30% EtOAc in Hexanes) as a colorless oil, 47% yield (n=2).

^{1}H NMR (600 MHz, chloroform-d) δ 1.25 (d, J = 7.0 Hz, 3H), 3.52 (s, 2H), 3.89 (s, 3H), 4.15 (q, J = 7.1 Hz, 2H), 6.88 (d, J = 8.4 Hz, 1H), 7.14 (dd, J = 8.3, 2.1 Hz, 1H), 7.30 (d, J = 2.1 Hz, 1H). **^{13}C NMR (151 MHz, chloroform-d)** δ 171.54, 154.20, 131.15, 128.69, 127.29, 122.43, 112.14, 77.37, 77.16, 61.14, 56.30, 40.28, 14.32. **HRMS:** Calculated (M+H): 229.0625; found: 229.0516

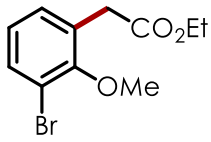

Ethyl 2-(3-bromo-2-methoxyphenyl)acetate (4.7a): Isolated by column chromatography (10% EtOAc in Hexanes) as a colorless oil, 33% yield (n=2).

^{1}H NMR (600 MHz, chloroform-d) δ 1.25 (t, J = 7.1 Hz, 4H), 3.52 (s, 2H), 3.88 (s, 3H), 4.15 (q, J = 7.1 Hz, 2H), 6.85 (d, J = 8.4 Hz, 1H), 7.19 (dd, J = 8.4, 2.2 Hz, 1H), 7.47 (d, J = 2.2 Hz, 1H). **^{13}C NMR (151 MHz, chloroform-d)** δ 171.53, 155.07, 134.15, 129.45, 127.74, 111.96, 111.64, 61.13, 56.38, 40.15, 14.31. **HRMS:** Calculated (M+Na): 294.9940; found: 294.9951

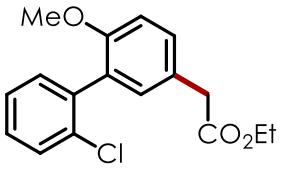

Ethyl 2-(2'-chloro-6-methoxy-[1,1'-biphenyl]-3-yl)acetate (4.8a): Isolated by column chromatography (10 % EtOAc in Hexanes) as a white solid, 55%. Spectra obtained as a mixture of rotational isomers.

^{1}H NMR (600 MHz, chloroform-d) δ 1.28 (br app t, 3H), 3.63 (br s, 2H), 3.81 (br s, 3H), 4.14 – 4.26 (br app q, 2H), 6.98 (app d, J = 8.7, 3.8 Hz, 1H), 7.16 (s, 1H), 7.28 – 7.40 (m, 4H), 7.49 (app d, 1H). **^{13}C NMR (151 MHz, chloroform-d)** δ 172.00, 156.84, 155.96, 137.84, 137.56, 134.05, 134.00, 132.03, 131.82, 131.79, 131.09, 130.16, 129.49, 129.43, 128.71, 128.66, 126.55, 126.03, 120.46, 111.17, 111.07, 60.98, 55.86, 55.76, 40.60, 31.11, 14.35. **HRMS:** Calculated (M+H); 305.0938, found: 305.0941

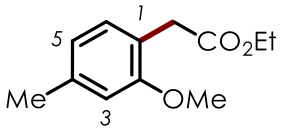

Ethyl 2-(2-methoxy-4-methylphenyl)acetate (4.9a, major isomer): The desired product was isolated as a mixture of three regioisomers following purification by column chromatography (7% EtOAc in hexane) as a clear oil, 57% yield (n = 2), 3.5:1.8:1.0 (***1:5:3***) (n=2).

*Regioisomer (1):***^{1}H NMR (500 MHz, chloroform-*d*)** δ 7.06 (d, *J* = 7.5 Hz, 1H), 6.73 (d, *J* = 7.5 Hz, 1H), 6.69 (app. s, 1H), 4.15 (q, *J* = 7.0 Hz, 2H), 3.80 (s, 3H), 3.58 (s, 2H), 2.35 (s, 3H), 1.25 (t, *J* = 7.1 Hz, 3H). **^{13}C NMR (151 MHz, chloroform-d)** 172.27, 157.42, 138.60, 130.67, 125.21, 121.14, 111.51, 60.69, 55.45, 35.83, 21.73, 14.36. **HRMS:** Calculated (M+H): 209.1172; found: 209.1160

Regioisomer (5): **^{1}H NMR (500 MHz, chloroform-*d*)** δ 7.11 (d, *J* = 8.3 Hz, 1H), 6.74 (d, *J* = 8.3 Hz, 1H), 6.69 (s, 1H), 4.15 (q, *J* = 7.1 Hz, 2H), 3.78 (s, 3H), 3.56 (s, 2H), 2.29 (s, 3H), 1.25 (t, *J* = 7.1 Hz, 3H).

^{13}C NMR (151 MHz, chloroform-*d*) δ 172.02, 158.75, 138.32, 131.24, 120.18, 116.05, 111.22, 60.69, 55.29, 38.56, 20.05, 14.33. **HRMS:** Calculated (M+H): 209.1172; found: 209.1160

Regioisomer (3): **^{1}H NMR (500 MHz, chloroform-*d*)** δ 7.15 (t, *J* = 7.9 Hz, 1H), 6.81 (d, *J* = 8.5 Hz, 1H), 6.72 (d, *J* = 8.1 Hz, 1H), 4.15 (q, *J* = 7.1 Hz, 2H), 3.80 (s, 3H), 3.70 (s, 2H), 2.29 (s, 3H), 1.25 (t, *J* = 7.1 Hz, 3H). **^{13}C NMR (151 MHz, chloroform-*d*)** δ 172.01, 157.74, 138.38, 127.80, 121.98, 111.22, 108.19, 60.89, 55.73, 32.09, 29.84, 14.29. **HRMS:** Calculated (M+H): 209.1172; found: 209.1160

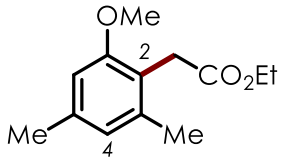

Ethyl 2-(2-methoxy-4,6-dimethylphenyl)acetate (4.10a, major isomer): The desired product was isolated as a mixture of two regioisomers following purification by column chromatography (3% EtOAc in hexane) as a clear oil , 48% yield (n = 2), 6.0:1.0 (***2:4***).

Regioisomer (2): **^{1}H NMR (500 MHz, chloroform-*d*)** δ 6.64 (s, 1H), 6.57 (s, 1H), 4.15 (q, *J* = 7.1 Hz, 2H), 3.79 (s, 3H), 3.65 (s, 2H), 2.31 (s, 3H), 2.25 (s, 3H), 1.25 (t, *J* = 7.1 Hz, 3H). **^{13}C NMR (126 MHz, chloroform-*d*)** δ 172.15, 157.69, 137.82 (d, *J* = 49.3 Hz), 123.41, 119.00, 113.55, 109.25, 60.61, 55.72, 31.84, 21.65, 19.78, 14.38. **HRMS:** Calculated (M+H): 223.1328; found: 223.1337

Regioisomer (4): **^{1}H NMR (500 MHz, chloroform-*d*)** δ 6.61 (s, 2H), 4.14 (q, *J* = 7.1 Hz, 2H), 3.77 (s, 3H), 3.61 (s, 2H), 2.31 (s, 6H), 1.25 (t, *J* = 7.1 Hz, 3H). **^{13}C NMR (126 MHz, chloroform-*d*)** δ 171.79, 158.18, 138.61, 124.17, 119.00, 60.79, 55.18, 34.90, 29.84, 20.75. **HRMS:** Calculated (M+H): 223.1328; found: 223.1337

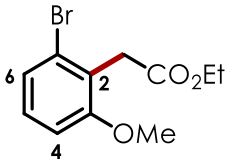

Ethyl 2-(2-bromo-6-methoxyphenyl)acetate (4.11a, major isomer): Isolated by column chromatography (10% EtOAc in Hexanes) as a colorless oil, 47% yield as a mixture of three regioisomers, 2.7:2.0:1.0 (**4:6:2**) (n=2)

Regioisomer (4): **^{1}H NMR (500 MHz, chloroform-*d*)** δ 1.25 (t, 3H), 3.56 (s, 2H), 3.80 (s, 3H), 4.12 – 4.20 (q, 2H), 6.99 (s 1H), 7.05 (m, 2H).

Regioisomer (6): **^{1}H NMR (500 MHz, chloroform-*d*)** δ 1.25 (t, 3H), 3.71 (s, 2H), 3.78 (s, 3H), 4.12 – 4.20 (q, 2H), 6.83 (dd, J = 8.5, 2.8 Hz, 1H), 7.04-7.20 (m, 2H).

Regioisomer (2): **^{1}H NMR (500 MHz, chloroform-*d*)** δ 1.25 (t, 3H), 3.81 (3, 2H), 3.87 (s, 2H), 4.12 – 4.20 (q, 2H), 7.04-7.20 (m, 3H).

^{13}C NMR (126 MHz, chloroform-*d*) δ 171.45, 171.07, 170.93, 159.32, 158.66, 158.24, 132.04, 131.90, 129.16, 126.45, 126.23, 125.30, 124.79, 123.90, 123.59, 122.39, 121.72, 118.09, 114.21, 113.75, 109.57, 77.16, 61.11, 60.89, 55.83, 55.66, 40.92, 35.71, 14.35, 14.34. **HRMS:** Calculated (M+H): 273.0120; found: 273.0128

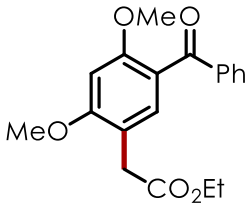

Ethyl 2-(5-benzoyl-2,4-dimethoxyphenyl)acetate (4.12a): Isolated by column chromatography (20 to 30% EtOAc in Hexanes) as a white solid, 31% yield (n=2).

^{1}H NMR (600 MHz, chloroform-d) δ 1.23 – 1.26 (t, 3H), 3.55 (s, 2H), 3.72 (s, 3H), 3.90 (s, 3H), 4.14 (q, J = 7.2 Hz, 2H), 6.49 (s, 1H), 7.29 (s, 1H), 7.41 (t, J = 7.6 Hz, 2H), 7.51 (t, J = 7.4 Hz, 1H), 7.75 – 7.80 (d, J = 7.1 Hz, 2H). **^{13}C NMR (151 MHz, chloroform-d)** δ 195.51, 171.76, 161.17, 159.31, 138.97, 133.39, 132.43, 129.83, 129.80, 128.11, 120.46, 115.37, 95.30, 60.79, 55.96, 55.83, 35.32, 14.35. **HRMS:** Calculated (M+H): 329.1383; found: 329.1395

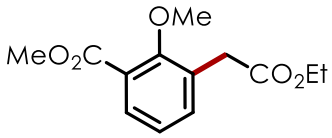

Methyl 3-(2-ethoxy-2-oxoethyl)-2-methoxybenzoate (4.13a): The desired product was isolated as a single regioisomer following purification by column chromatography as a white solid (15% EtOAc in hexanes → 20% EtOAc in hexanes), 63% yield (n = 2)

^{1}H NMR (500 MHz, chloroform-*d*) δ 1.25 (d, J = 1.6 Hz, 4H), 3.63 (s, 2H), 3.88 (d, J = 2.8 Hz, 6H), 4.16 (q, J = 7.2 Hz, 2H), 6.89 (d, J = 8.6 Hz, 1H), 7.88 (d, J = 2.2 Hz, 1H), 7.98 (dd, J = 8.6, 2.2 Hz, 1H). **^{13}C NMR** δ 171.47, 166.95, 161.44, 132.64, 131.07, 123.37, 122.44, 109.98, 77.16, 60.91, 55.84, 52.05, 36.12, 29.85, 14.36. **HRMS:** Calculated (M+H): 253.1070; found : 253.1071

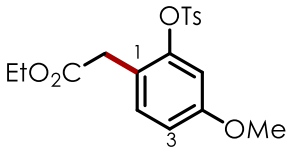

Ethyl 2-(4-methoxy-2-(tosyloxy)phenyl)acetate (4.14a, major isomer): The desired product was isolated as a mixture of two regioisomers following purification by column chromatography (15% EtOAc/in hexanes) as clear oil, 33% yield (n = 2), 2.3:1.0 (**1:3**) (n=2).

Regioisomer 1: **^{1}H NMR (500 MHz, chloroform-d)** δ 7.72 (d, *J* = 8.2 Hz, 2H), 7.32 (d, *J* = 8.2 Hz, 2H), 7.04 (d, *J* = 8.2 Hz, 1H), 6.55 (d, *J* = 2.3 Hz, 1H), 6.44 (dd, *J* = 8.2, 2.3 Hz, 1H), 4.21 – 4.10 (m, 2H), 3.70 (s, 3H), 3.54 (s, 2H), 2.44 (s, 3H), 1.23 (t, *J* = 7.2 Hz, 3H). **^{13}C NMR (126 MHz, chloroform-d)**: δ 171.36, 158.08, 149.61, 145.36, 131.98, 131.03, 129.74, 128.61, 122.17, 113.76, 105.50, 60.76, 55.65, 35.47, 21.74, 14.20 **HRMS:** Calculated (M+H): 365.1053; found: 365.106

Regioisomer 3: **^{1}H NMR (500 MHz, chloroform-d)**: δ 7.77 (d, *J* = 8.2 Hz, 2H), 7.34 (d, *J* = 8.2 Hz, 2H), 7.17 (d, *J* = 8.5 Hz, 1H), 6.78 (dd, *J* = 8.5, 2.4 Hz, 1H), 6.60 (d, *J* = 2.6 Hz, 1H), 4.17 – 4.03 (m, 2H), 3.70 (s, 3H), 3.41 (s, 2H), 2.45 (s, 3H), 1.29 – 1.13 (m, 3H).f**^{13}C NMR (126 MHz, chloroform-d)**: δ 171.28, 159.69, 148.81, 145.93, 133.13, 132.75, 130.22, 128.87, 120.15, 113.53, 108.49, 61.28, 55.85, 35.25, 22.09, 14.51. **HRMS:** Calculated (M+H): 365.1053; found: 365.1063

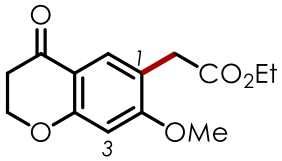

Ethyl 2-(4-methoxy-2-(tosyloxy)phenyl)acetate (4.15a, major isomer): Isolated by column chromatography (30% EtOAc in Hexanes) as a white solid, 50% yield, 3.8:1 (***1:3***) (n=2).

Regioisomer 1: **^{1}H NMR (600 MHz, chloroform-d)** δ 1.25 (t, J = 7.1 Hz, 3H), 2.75 (t, 2H), 3.54 (s, 2H), 3.84 (s, 3H), 4.15 (q, 2H), 4.52 (t, 2H), 6.39 (s, 1H), 7.70 (s, 1H). **^{13}C NMR (151 MHz, chloroform-d)** δ 190.54, 171.57, 164.06, 163.55, 129.49, 118.05, 114.67, 99.05, 67.60, 60.89, 56.06, 37.49, 35.57, 14.37. **HRMS:** Calculated (M+H): 287.0889; found: 287.0898

Regioisomer 3: **^{1}H NMR (600 MHz, chloroform-d)** δ 1.25 (app t, 3H), 2.75 (app t, 2H), 3.66 (s, 2H), 3.88 (s, 3H), 4.15 (app q, 2H), 4.52 (app t, 2H), 6.63 (d, J = 8.9 Hz, 1H), 7.89 (d, J = 8.8 Hz, 1H). **^{13}C NMR (151 MHz, chloroform-d)** δ 191.17, 171.60, 163.44, 160.96, 128.07, 115.79, 110.96, 104.81, 67.53, 60.82, 56.16, 37.59, 28.74, 14.40. **HRMS:** Calculated (M+H): 287.0889; found: 287.0898

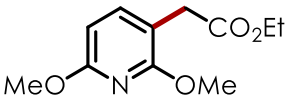

Ethyl 2-(2,6-dimethoxypyridin-3-yl)acetate (4.16a): The desired product was isolated as clear oil following purification by column chromatography (5% EtOAc in hexanes), 21% yield(n=2). **^{1}H NMR (500 MHz, chloroform-*d*)** δ 7.40 (d, *J* = 7.9 Hz, 1H), 6.29 (d, *J* = 7.9 Hz, 1H), 4.17 (q, *J* = 7.1 Hz, 2H), 3.95 (s, 3H), 3.92 (s, 3H), 3.52 (s, 2H), 1.27 (t, *J* = 7.1 Hz, 3H). **^{13}C NMR (151 MHz, chloroform-*d*)** δ 171.88, 162.40, 160.64, 141.93, 108.03, 100.44, 60.87, 53.71, 53.53, 34.65, 14.36. **HRMS:** Calculated (M+H): 226.1073; found: 226.1077

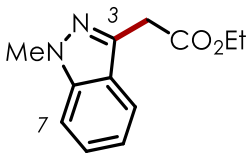

Ethyl 2-(1-methyl-1H-indazol-3-yl)acetate (4.17a, major isomer): The desired product was isolated as a mixture of regioisomers following purification by column chromatography (15% EtOAc in hexanes → 20% EtOAc in hexanes) as a white solid, 23% yield (n =2), 10:1 (**3:7**).

Spectral data for minor isomer is not reported due to the low concentration of this product in the obtained mixture (some signals corresponding to this product are visible in proton NMR data and were used to determine the ratio of regioisomers).

Regioisomer 3: **^{1}H NMR (500 MHz, chloroform-*d*)**: δ 7.71 (d, *J* = 8.1 Hz, 1H), 7.47 – 7.32 (m, 2H), 7.15 (t, *J* = 7.5 Hz, 1H), 4.18 (q, *J* = 7.2 Hz, 2H), 4.04 (s, 3H), 4.00 (s, 2H), 1.25 (t, *J* = 7.1 Hz, 3H). **^{13}C NMR (126 MHz, chloroform-*d*)** δ 170.54, 137.88, 126.52, 122.97, 120.65, 120.43, 109.15, 61.27, 35.50, 33.76, 29.84, 14.33. **HRMS:** Calculated (M+H): 219.1128; found: 219.1138

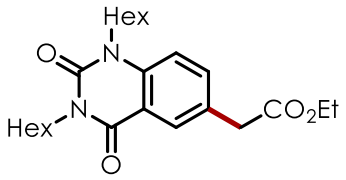

Ethyl 2-(1,3-dihexanoyl-2,4-dioxo-1,2,3,4-tetrahydroquinazolin-6-yl)acetate (4.18a): Isolated by column chromatography (0 to 10% EtOAc in Hexanes) as a colorless oil, 13% yield (n=2).

^{1}H NMR (600 MHz, chloroform-d) δ 0.87 – 0.90 (m, 6H), 1.26 (d, J = 7.1 Hz, 3H), 1.30 – 1.37 (m, 12H), 1.65 – 1.73 (m, 5H), 3.67 (s, 2H), 4.05 – 4.11 (m, 4H), 4.15 – 4.18 (m, 2H), 7.14 (d, J = 8.6 Hz, 1H), 7.60 (dd, J = 8.6, 2.3 Hz, 1H), 8.11 (d, J = 2.2 Hz, 1H). **^{13}C NMR (151 MHz, chloroform-d)** δ 171.31, 161.68, 150.77, 138.99, 136.12, 129.70, 128.83, 115.89, 114.02, 61.30, 43.95, 42.11, 40.38, 31.67, 31.61, 27.91, 27.42, 26.80, 26.62, 22.73, 22.72, 14.34, 14.22, 14.17. **HRMS:** Calculated (M+H): 445.2333; found: 445.2322

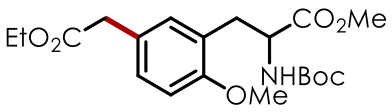

Methyl 2-((*tert*-butoxycarbonyl)amino)-3-(5-(2-ethoxy-2-oxoethyl)-2-methoxyphenyl)propanoate (4.19a): Isolated by column chromatography (20% EtOAc in Hexanes) as a clear oil , 37% yield (n=2).

^{1}H NMR (600 MHz, chloroform-d) δ 1.25 (t, J = 7.1 Hz, 3H), 1.38 (s, 9H), 3.04 (dd, J = 6.7, 3.1 Hz, 1H), 3.51 (s, 2H), 3.70 (s, 3H), 3.81 (s, 3H), 4.13 (q, J = 7.1 Hz, 2H), 4.48 (q, J = 7.3 Hz, 1H), 5.23 (d, J = 7.8 Hz, 1H), 6.81 (d, J = 8.3 Hz, 1H), 7.00 (d, J = 2.3 Hz, 1H), 7.14 (d, J = 2.3 Hz, 1H). **^{13}C NMR (151 MHz, chloroform-d)** δ 172.97, 171.94, 156.84, 155.38, 132.20, 129.27, 126.30, 124.93, 110.60, 79.70, 60.95, 55.55, 54.22, 52.22, 40.56, 32.88, 28.41, 14.34. **HRMS:** Calculated (M+Na): 418.1836; found: 418.1847

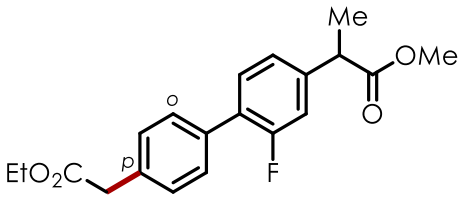

Methyl 2-(4'-(2-ethoxy-2-oxoethyl)-2-fluoro-[1,1'-biphenyl]-4-yl)propanoate (4.20a, major isomer): Isolated by column chromatography (10% EtOAc in Hexanes) as a white solid , 28% yield (n=2), 7.2:1 (**p:o**). Spectral data for minor isomer is not reported due to the low concentration of this product in the obtained mixture (some signals corresponding to this product are visible in proton NMR data and were used to determine the ratio of regioisomers).

^{1}H NMR (600 MHz, chloroform-*d*) δ 7.51 – 7.47 (m, 2H), 7.39 (d, *J* = 7.9 Hz, 1H), 7.36 (d, *J* = 8.3 Hz, 2H), 7.14 (dd, *J* = 7.9, 1.8 Hz, 1H), 7.11 (dd, *J* = 11.5, 1.8 Hz, 1H), 4.17 (q, *J* = 7.1 Hz, 2H), 3.76 (q, *J* = 7.1 Hz, 1H), 3.70 (s, 3H), 3.66 (s, 2H), 1.53 (d, *J* = 7.1 Hz, 3H), 1.27 (d, *J* = 7.1

Hz, 3H). **^{13}C NMR (151 MHz, chloroform-*d*)** δ 174.58, 171.66, 159.81 (d, *J* = 248.3 Hz), 141.91 (d, *J* = 7.7 Hz), 134.38, 133.72, 130.87 (d, *J* = 3.9 Hz), 129.51, 129.23 (d, *J* = 2.8 Hz), 127.57 (d, *J* = 13.7 Hz), 123.67 (d, *J* = 3.3 Hz), 115.37 (d, *J* = 23.6 Hz), 61.11, 52.39, 45.03, 41.23, 18.57, 14.33. **HRMS:** Calculated (M+Na): 367.1316; found: 367.1332

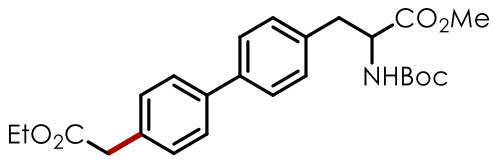

Methyl 2-((*tert*-butoxycarbonyl)amino)-3-(4'-(2-ethoxy-2-oxoethyl)-[1,1'-biphenyl]-4-yl)propanoate (4.21a): Isolated by column chromatography (20% EtOAc in Hexanes) as a white solid, 17% yield.

^{1}H NMR (600 MHz, chloroform-d) δ 1.26 (t, J = 7.3 Hz, 3H), 1.42 (s, 9H), 3.05 – 3.20 (m, 2H), 3.65 (s, 2H), 3.74 (s, 3H), 4.17 (d, J = 7.1 Hz, 2H), 4.62 (q, J = 6.6 Hz, 1H), 5.01 (d, J = 8.5 Hz, 1H), 7.19 (d, J = 7.8 Hz, 2H), 7.35 (d, J = 7.8 Hz, 2H), 7.48 – 7.59 (m, 4H). **^{13}C NMR (151 MHz, chloroform-d)** δ 172.49, 171.75, 155.23, 139.66, 139.62, 135.17, 133.30, 129.87, 129.82, 127.29, 127.29, 80.12, 61.10, 54.49, 52.44, 41.17, 38.11, 28.44, 14.35. **HRMS:** Calculated (M+Na): 464.2043; found: 464.2057

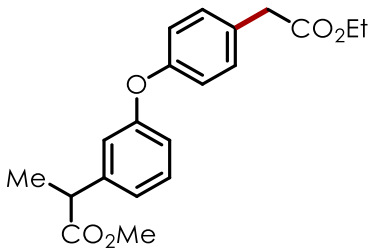

Methyl 2-(3-(4-(2-ethoxy-2-oxoethyl)phenoxy)phenyl)propanoate (4.22a, major isomer): Isolated by column chromatography (4% EtOAc in Hexanes) as a white semisolid in a 2:1

mixture of para/ortho isomers, 32% yield (n=2). NMR data is reported for the mixture of isomers – some trace impurities are present

^{1}H NMR (600 MHz, chloroform-*d*): δ 7.39 – 7.17 (m, 6H), 7.15 – 6.95 (m, 7H), 6.92 – 6.88 (m, 1H), 6.87 – 6.78 (m, 1H), 4.18 (q, *J* = 7.2 Hz, 2H), 4.10 (dq, *J* = 9.5, 7.1 Hz, 1H), 3.73 – 3.63 (m, 8H), 3.61 (s, 2H), 1.50 (d, *J* = 7.1 Hz, 3H), 1.45 (d, *J* = 7.2 Hz, 1H), 1.28 (dd, *J* = 8.8, 5.5 Hz, 3H), 1.19 (td, *J* = 7.2, 3.1 Hz, 2H).

^{13}C NMR (151 MHz, chloroform-*d*): δ 174.79, 174.72, 171.84, 171.51, 157.53, 157.44, 156.17, 155.04, 142.60, 142.52, 141.42, 141.39, 130.72, 129.96, 129.90, 129.86, 129.79, 126.12, 125.04, 123.82, 123.13, 122.87, 122.42, 122.21, 119.05, 118.26, 118.21, 117.43, 61.05, 60.94, 52.25, 45.37, 45.15, 40.74, 36.04, 35.72, 18.63, 18.57, 14.32, 14.26.

HRMS: Calculated (M+Na): 365.1359; found: 365.1367

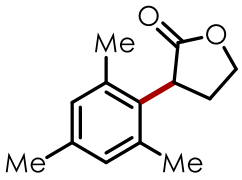

3-Mesityldihydrofuran-2(*3H*)-one (4.1b):Isolated by column chromatography (10% EtOAc in Hexanes) as a colorless oil, 61% yield (n=2). Spectral data matched reported literature values.[210]

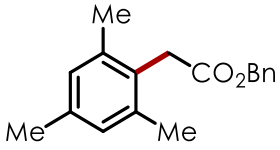

Benzyl 2-mesitylacetate (4.1c):Isolated by column chromatography (0-5% EtOAc in Hexanes) as a colorless oil, 44% yield (n=2).

^{1}H NMR (600 MHz, chloroform-d) δ 2.27 (s, 3H), 2.28 (s, 6H), 3.71 (s, 2H), 5.13 (s, 2H), 6.87 (s, 2H), 7.30 – 7.39 (m, 5H). **^{13}C NMR (151 MHz, chloroform-d)** δ 171.48, 137.13, 136.66, 136.13, 129.03, 128.63, 128.58, 128.25, 128.15, 66.56, 53.58, 35.15, 22.29, 20.37. **HRMS:** Calculated (M+Na): 291.1355; found: 291.1365

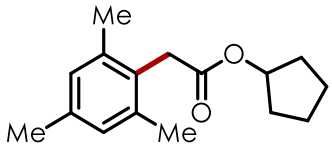

Cyclopentyl 2-mesitylacetate (4.1d):Isolated by column chromatography (0-5% EtOAc in Hexanes) as a colorless oil, 39% yield (n=2).

^{1}H NMR (600 MHz, chloroform-d) δ 1.26 – 1.32 (m, 2H), 1.57 (m, 2H), 1.66 (m, 4H), 1.79 – 1.85 (m, 2H), 2.26 (s, 3H), 2.29 (s, 6H), 3.60 (s, 2H), 5.16 (dt, J = 6.0, 3.4 Hz, 1H), 6.86 (s, 2H). **^{13}C NMR (151 MHz, chloroform-d)**) δ 171.43, 137.06, 136.41, 128.99, 128.94, 77.43, 35.50, 32.76, 23.80, 21.03, 20.35. **HRMS:** Calculated (M+H): 269.1511; found: 269.1515

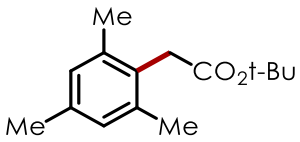

***tert*-Butyl 2-mesitylacetate (4.1e):** Isolated by column chromatography (0-5% EtOAc in Hexanes) as a colorless oil, 57% yield (n=2). Spectral data matched reported literature values.[211]

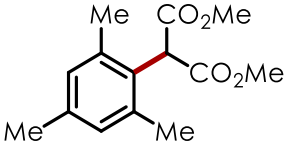

Dimethyl 2-mesitylmalonate (4.1f): Isolated by column chromatography (0-10% EtOAc in Hexanes) as a colorless oil, 19% yield (n=2). Spectral data matched reported literature values.[212]

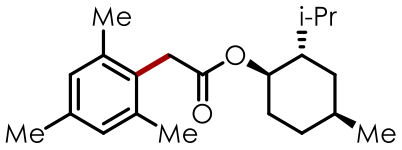

(–)-(1R,2S,4S)-2-isopropyl-4-methylcyclohexyl 2-mesitylacetate (4.1g): Isolated by column chromatography (0-2.5% EtOAc in Hexanes, stained with CAM) as a colorless oil, 45% yield (n=2).

^{1}H NMR (600 MHz, chloroform-d) δ 0.70 (d, J = 7.0 Hz, 3H), 0.84 (d, J = 7.1 Hz, 3H), 0.89 (d, J = 6.6 Hz, 3H), 0.91 – 1.07 (m, 3H), 1.32 (t, J = 11.6 Hz, 1H), 1.46 (dd, J = 16.8, 10.5 Hz, 1H), 1.65 (dt, J = 13.8, 7.6 Hz, 2H), 1.74 (d, J = 2.5 Hz, 1H), 1.98 (d, J = 11.4 Hz, 1H), 2.27 (d, J = 15.2 Hz, 9H), 3.63 (d, J = 3.0 Hz, 2H), 4.67 (td, J = 10.9, 4.4 Hz, 1H), 6.85 (s, 2H).**^{13}C NMR (151 MHz, chloroform-d)** δ 171.19, 137.02, 136.39, 129.00, 128.90, 74.54, 47.17, 40.91, 35.46, 34.35, 31.48, 26.26, 23.42, 22.17, 21.03, 20.87, 20.32, 16.32. **HRMS:** Calculated(M+Na): 339.2294; found: 339.2164

C.7: Computational Details

All computations were performed using the Gaussian 9 software package at the UB3LYP level of theory using the 6-31+G(d) basis set with solvation in dichloromethane evaluated in a self-consistent reaction field (SCRF) with the PCM model. All obtained geometries were verified as minima by ensuring that they possess no negative vibrational frequencies. Transition states were calculated using the QST2 method. All transition states were verified as local maxima by ensuring that they possessed one negative vibrational mode, and confirming that this vibrational mode corresponds to the bond forming/bond breaking event in question. Transition states were confirmed using IRC calculations, which resulted in optimized product and starting material geometries which matched those submitted in the QST2 calculation. Free energies at 298.15 K were calculated using scaled vibrational frequencies. In cases where rotational isomers may exist, verification of the minimized geometry was accomplished by conducting a scan of dihedral angles corresponding to the proposed rotamers and comparing these energies to those of the previously optimized geometry.

Cartesian coordinates, thermally corrected free energies, and entropy values for all optimized geometries are given below. The complete computed reaction pathway is illustrated below for reference. All values of Gibbs free energy are given in kcal/mol, relative to the starting structure (neutral ethyl diazoacetate and mesitylene). Images were generated using the CYLview program.

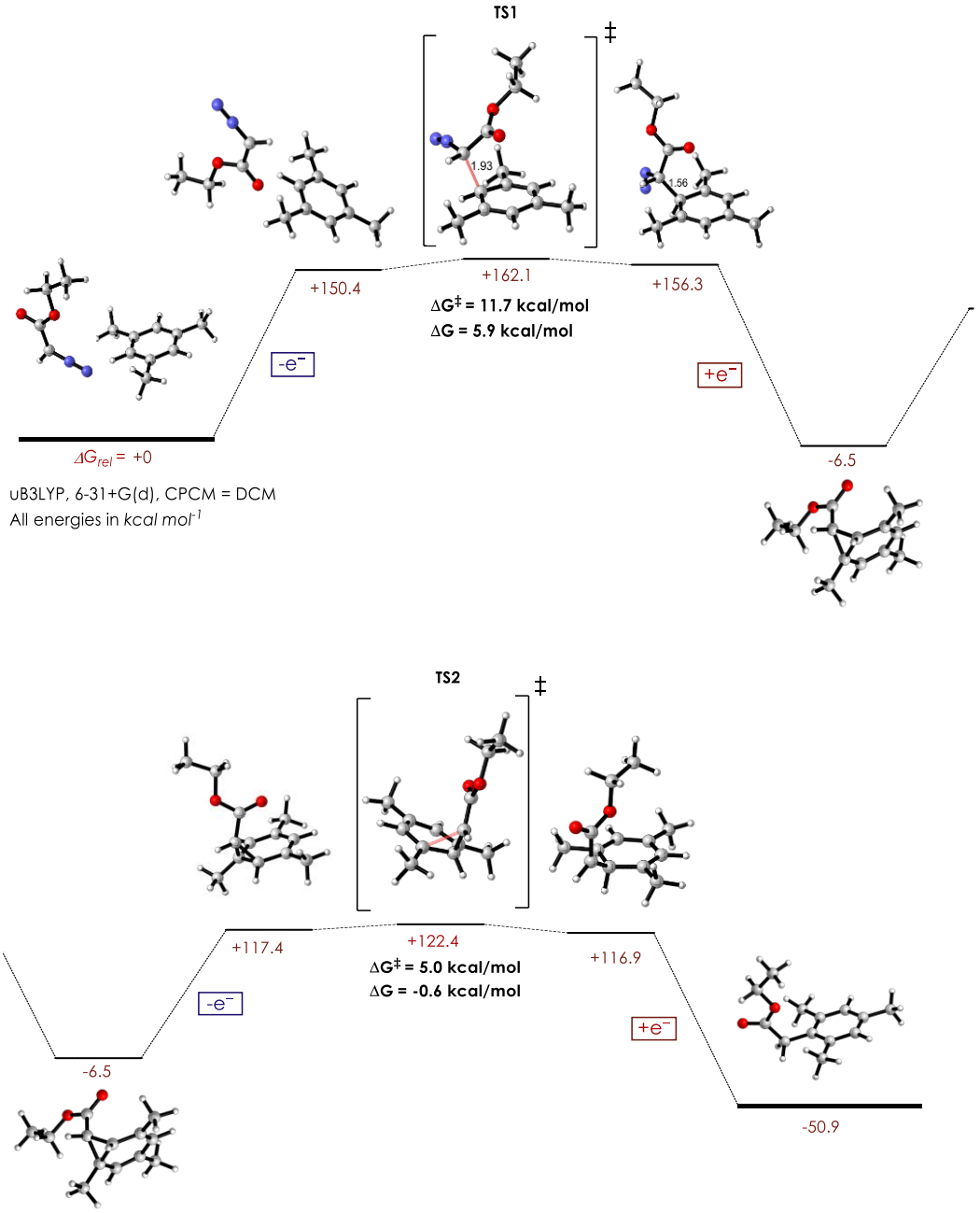

Figure C.4: Overall computed free energy profile and associated activation energies

C.8: Optimized DFT reactant geometries and coordinates:

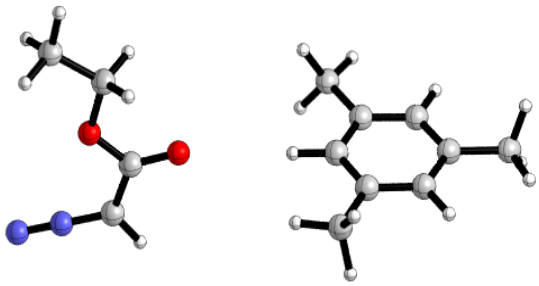

EE + Thermal Free Energy Correction: -765.961078 Hartree, Entropy = 178.382 cal mol^{-1} K^{-1}

Tag	Symbol	Bond	Angle	Dihedral	X	Y	Z
1	C				-2.8314	0.6297	-1.0443
2	C	1.3979453			-4.2293	0.6308	-1.0331
3	C	1.4070432	121.494371		-4.9567	-0.007	-0.0114
4	C	1.3979455	118.474882	-0.0264526	-4.2494	-0.652	1.0074
5	C	1.4068836	121.50354	-0.0043475	-2.8428	-0.6729	1.0264
6	C	1.3982139	118.575327	0.0239836	-2.1504	-0.0291	-0.0037
7	H	1.0891737	119.315148	-179.975486	-4.7686	1.1367	-1.8328
8	H	1.0893248	119.303927	-179.980573	-4.799	-1.1504	1.805
9	H	1.0891301	119.382134	179.991935	-1.0613	-0.037	-0.0019
10	C	1.5131722	120.34408	179.909472	-6.4697	0.0121	-0.0239
11	H	1.0974324	111.316676	58.7053679	-6.8668	-0.4393	-0.942
12	H	1.0949723	111.373904	179.137364	-6.8828	-0.5389	0.8274
13	H	1.0975553	111.30313	-60.4865316	-6.8559	1.0385	0.0206
14	C	1.5132252	120.289995	-179.903435	-2.105	-1.3813	2.1416
15	H	1.0948338	111.386738	-179.269218	-1.0203	-1.296	2.0199
16	H	1.0974698	111.318552	-58.820444	-2.3679	-0.964	3.122
17	H	1.0975728	111.293648	60.3435463	-2.3572	-2.4491	2.171
18	C	1.5131921	121.115363	-179.915883	-2.0577	1.32	-2.1464
19	H	1.0975477	111.305651	119.589115	-1.4155	2.1146	-1.7454
20	H	1.0973677	111.332443	-121.226278	-1.4025	0.6163	-2.6753
21	H	1.0950701	111.379665	-0.7843466	-2.7299	1.772	-2.8833
22	C	5.8080126	116.677148	-161.532206	3.4085	-1.5376	-0.7494
23	H	1.0812335	66.8278606	75.0517232	2.7133	-2.2822	-1.1118
24	N	1.3085539	176.129169	-108.744412	4.6836	-1.7983	-0.8853
25	N	1.1361286	179.815074	2.4982451	5.7915	-2.0214	-1.0018
26	C	1.4528567	55.3678731	-104.672843	2.9646	-0.2973	-0.1367
27	O	1.2264522	122.871675	0.2591099	1.7804	-0.0133	0.0089
28	O	1.3488259	112.842776	-179.705781	3.9882	0.4931	0.2465
29	C	1.4556175	117.088947	-179.988084	3.6473	1.762	0.873
30	H	1.0939604	108.312402	59.425263	3.0578	1.5546	1.7709

31	H	1.0937974	108.334889	-58.2063726	3.0304	2.3355	0.1752
32	C	1.5161178	107.49944	-179.408067	4.9461	2.473	1.1989
33	H	1.0957083	109.187348	-179.906547	4.721	3.434	1.6747
34	H	1.0951741	111.138892	-60.5499745	5.5569	1.8826	1.8901
35	H	1.0951996	111.129048	60.7354875	5.5283	2.6671	0.2918

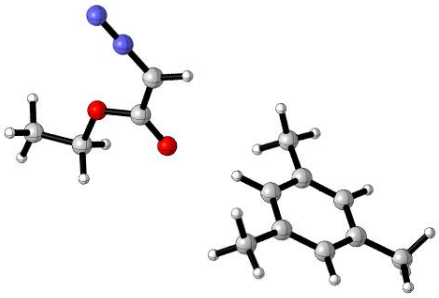

EE + Thermal Free Energy Correction: -765.721331 Hartree, Entropy = 168.135 cal mol^{-1} K^{-1}

Tag	**Symbol**	**Bond**	**Angle**	**Dihedral**	**X**	**Y**	**Z**
1	C				2.4923	-0.3682	-1.1956
2	C	1.3770628			3.8691	-0.3422	-1.2025
3	C	1.4425676	121.49107		4.6224	-0.0073	-0.0187
4	C	1.4172257	119.833028	0.0867703	3.9424	0.3022	1.1856
5	C	1.3795927	120.526324	-0.0536421	2.5638	0.2871	1.2357
6	C	1.4255578	117.31832	-0.0432968	1.8381	-0.0513	0.0307
7	H	1.0864864	120.370938	179.949901	4.4184	-0.5763	-2.1102
8	H	1.0854367	119.064372	179.91617	4.5216	0.5511	2.0692
9	H	1.0897462	119.104039	-179.964942	0.7491	-0.0636	0.0691
10	C	1.4855863	118.907732	-179.793059	6.1061	0.0078	-0.092
11	H	1.1006635	109.84654	59.5459508	6.4355	0.7372	-0.8476
12	H	1.0911833	112.616357	-178.541665	6.5711	0.2487	0.8653
13	H	1.0998057	110.078575	-56.1597082	6.4767	-0.9662	-0.4435
14	C	1.4955955	122.904211	179.96908	1.7924	0.604	2.4772
15	H	1.0981272	110.358564	-121.235198	1.1557	-0.2453	2.7586
16	H	1.0921543	111.746441	0.1028779	2.4525	0.8438	3.3136
17	H	1.0980545	110.40585	121.471736	1.1172	1.4521	2.3024
18	C	1.5038114	122.832704	179.967373	1.6772	-0.7123	-2.4116
19	H	1.0965233	110.639557	121.204285	1.0382	-1.5815	-2.2153
20	H	1.0965571	110.620908	-120.327047	1.0152	0.1194	-2.6808
21	H	1.0927596	111.32077	0.4059232	2.3172	-0.9376	-3.2682
22	C	4.8995908	116.186916	155.822942	-2.7522	1.622	-0.337
23	H	1.0810984	60.8476395	-83.2998258	-1.9288	2.3115	-0.461
24	N	1.309962	176.368218	-29.2728119	-3.9593	2.1007	-0.5095
25	N	1.1353217	179.865642	129.331106	-5.0065	2.5132	-0.6584
26	C	1.4509076	61.5765857	99.8849116	-2.5512	0.2264	0.0051

27	O	1.2286856	122.888926	3.2527502	-1.4381	-0.2651	0.1757
28	O	1.3460335	112.988167	-176.74778	-3.7042	-0.4597	0.1131
29	C	1.4563057	117.291715	179.972746	-3.6111	-1.8726	0.4535
30	H	1.0937992	108.280538	59.1070736	-3.099	-1.9606	1.416
31	H	1.0938441	108.290227	-58.5105672	-3.0072	-2.3707	-0.3105
32	C	1.5160303	107.449337	-179.693563	-5.0234	-2.421	0.5084
33	H	1.095701	109.186871	-179.995096	-4.9865	-3.486	0.7633
34	H	1.0951558	111.138836	-60.6303961	-5.6177	-1.906	1.2706
35	H	1.0951245	111.127185	60.6428809	-5.5252	-2.3168	-0.4594

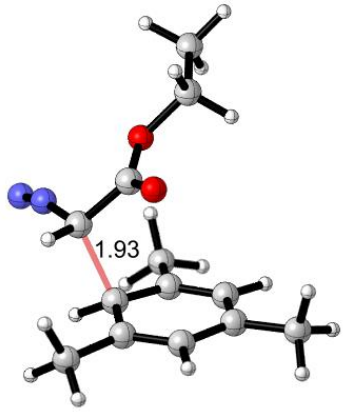

EE + Thermal Free Energy Correction: -765.702786 Hartree, Entropy = 147.572 cal mol^{-1} K^{-1}

Tag	**Symbol**	**Bond**	**Angle**	**Dihedral**	**X**	**Y**	**Z**
1	C				2.1384	0.8982	-0.4187
2	C	1.3782901			2.6678	-0.3689	-0.5365
3	C	1.4148372	121.888552		2.2408	-1.4369	0.2874
4	C	1.4171957	119.106886	-2.9265527	1.2858	-1.1844	1.3036
5	C	1.3785091	122.055699	2.6816757	0.7177	0.059	1.4811
6	C	1.4622644	118.84203	-3.6913651	1.0494	1.1222	0.5311
7	H	1.0871799	119.355436	178.256309	3.4582	-0.5511	-1.2604
8	H	1.0873544	118.608076	-174.538812	1.0303	-1.9886	1.9894
9	H	1.0930193	114.443933	150.558225	1.0141	2.1316	0.9489
10	C	1.4982058	120.25809	177.960282	2.8083	-2.8104	0.0975
11	H	1.0950725	111.571765	34.9095902	3.8619	-2.7733	-0.1987
12	H	1.0937144	112.013148	157.485179	2.7123	-3.4219	0.9992
13	H	1.1003018	109.647116	-83.2239554	2.2682	-3.3253	-0.7111
14	C	1.5038322	121.660613	-176.79262	-0.2412	0.3354	2.6061
15	H	1.0983805	111.383155	-100.239516	-1.283	0.3136	2.2588
16	H	1.0936006	111.002108	18.9477031	-0.1497	-0.4183	3.3932
17	H	1.0964852	111.639009	139.834488	-0.067	1.3215	3.0528

18	C	1.5039584	121.565671	177.662869	2.634	2.0401	-1.2627
19	H	1.1006897	111.61391	94.2721226	2.0222	2.1702	-2.1684
20	H	1.095809	111.909943	-145.200286	2.6189	2.9895	-0.7157
21	H	1.093566	110.979263	-24.1772342	3.6566	1.8588	-1.6052
22	C	1.9335286	103.333808	-108.290364	-0.4905	1.3814	-0.6091
23	H	1.0886907	101.162199	-36.5698147	-0.0477	1.9274	-1.4404
24	N	1.3800972	110.683841	-151.605865	-1.4217	2.193	0.0064
25	N	1.1370628	161.108199	-0.7233826	-1.93	2.8509	0.7821
26	C	1.5249687	109.35231	81.5879116	-1.0311	0.0236	-1.0446
27	O	1.2082218	120.258876	-73.0879192	-0.4323	-0.6371	-1.8599
28	O	1.327982	111.965179	105.680491	-2.1547	-0.2904	-0.4102
29	C	1.4759505	116.938925	178.769945	-2.7894	-1.5735	-0.7697
30	H	1.0931441	107.257652	62.7270371	-2.0872	-2.3682	-0.5045
31	H	1.0927286	107.291673	-54.0000946	-2.9288	-1.5745	-1.8535
32	C	1.5131756	107.542564	-175.598121	-4.0952	-1.6649	-0.0106
33	H	1.0954346	108.865925	179.76595	-4.5876	-2.6097	-0.2653
34	H	1.0947563	111.532573	-61.1059669	-3.9327	-1.6482	1.0719
35	H	1.0945203	111.317803	60.7483004	-4.7704	-0.8468	-0.2804

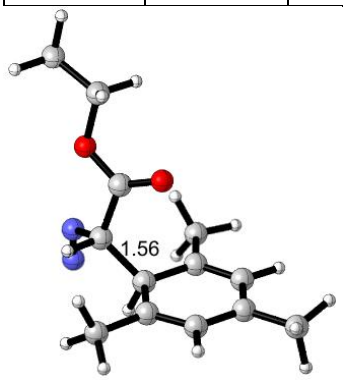

EE + Thermal Free Energy Correction: --765.712026 Hartree, Entropy = 147.378 cal mol^{-1} K^{-1}

Tag	**Symbol**	**Bond**	**Angle**	**Dihedral**	**X**	**Y**	**Z**
1	C				1.6479	0.5892	-1.238
2	C	1.3708142			2.7071	-0.2731	-1.1211
3	C	1.4158383	121.85199		3.0417	-0.8827	0.1122
4	C	1.413806	120.229357	-0.0488609	2.2787	-0.6105	1.2709
5	C	1.3718338	121.955306	1.3702504	1.1859	0.2183	1.2425
6	C	1.5025677	119.961947	1.083929	0.8202	0.9291	-0.0309
7	H	1.0862827	119.518834	-178.193455	3.3186	-0.4909	-1.9921
8	H	1.0859286	118.64706	-179.619014	2.5619	-1.0872	2.2046
9	H	1.1130014	104.448605	111.325704	1.0501	1.9992	0.1711
10	C	1.4925473	119.646978	-178.324561	4.2281	-1.7848	0.192
11	H	1.100867	108.645619	82.462328	5.1316	-1.168	0.3151
12	H	1.0926745	112.030757	-158.816714	4.1714	-2.4618	1.0478
13	H	1.0941356	111.471796	-35.0561817	4.3581	-2.3581	-0.7308
14	C	1.496324	120.292139	-179.064093	0.4173	0.4971	2.4957

15	H	1.0963693	112.041879	-123.332071	-0.643	0.2372	2.3945
16	H	1.0918031	110.838964	-2.5903042	0.8251	-0.069	3.3355
17	H	1.0974565	110.564152	117.885674	0.4564	1.5658	2.7422
18	C	1.4995111	120.437607	178.2209	1.3459	1.2479	-2.5508
19	H	1.0992346	110.781767	97.6158932	0.555	0.7045	-3.087
20	H	1.0953388	112.055191	-142.355645	1.0069	2.2817	-2.4239
21	H	1.0927318	110.572982	-20.8910516	2.2292	1.2449	-3.1941
22	C	1.5610366	111.661109	-137.410945	-0.7052	0.939	-0.3624
23	H	1.0931429	109.844002	-32.0626706	-0.8583	1.2612	-1.3957
24	N	1.5437928	113.812007	-144.464601	-1.5025	2.0165	0.4035
25	N	1.1671294	124.337793	18.6878311	-1.0244	2.9515	0.9128
26	C	1.5314808	113.845812	87.5967374	-1.3782	-0.4295	-0.222
27	O	1.2168458	121.83863	-13.4689257	-0.7317	-1.4553	-0.1196
28	O	1.3233494	111.916182	168.971355	-2.6972	-0.3396	-0.2804
29	C	1.4683383	117.24089	177.452528	-3.4598	-1.5927	-0.2156
30	H	1.0928997	107.678784	57.537024	-3.1893	-2.0981	0.7149
31	H	1.0929828	107.597761	-59.7815607	-3.1487	-2.2129	-1.0601
32	C	1.5140109	107.381807	178.89096	-4.929	-1.2315	-0.2723
33	H	1.0955715	108.920624	179.935119	-5.5229	-2.151	-0.2267
34	H	1.0947462	111.173836	-60.8302306	-5.2131	-0.5969	0.5733
35	H	1.0948158	111.176612	60.7088653	-5.1727	-0.7113	-1.2043

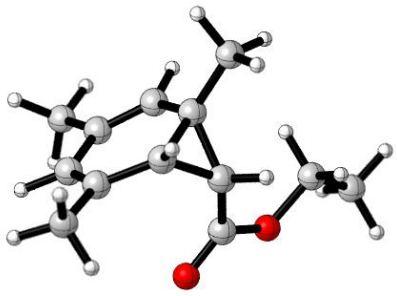

EE + Thermal Free Energy Correction: -656.428463 Entropy = 127.753 cal mol^{-1} K^{-1}

For N_2, EE + Thermal Free Energy Correction: -109.543015, Entropy = 45.784 cal mol^{-1} K^{-1}

Tag	**Symbol**	**Bond**	**Angle**	**Dihedral**	**X**	**Y**	**Z**
1	C				2.1905	-0.7204	0.0888
2	C	1.3525966			2.2677	0.5113	0.6424
3	C	1.4615547	122.846152		1.3637	1.6012	0.2804
4	C	1.3548539	120.088711	-1.788194	0.4192	1.4122	-0.6724
5	C	1.4851548	123.329038	3.4302192	0.1875	0.1082	-1.3444
6	C	1.4852258	120.260168	-3.2268858	1.112	-1.0386	-0.8815
7	H	1.0889539	119.468635	179.738405	3.0612	0.7293	1.3556
8	H	1.0895722	119.932408	-173.20021	-0.1791	2.2541	-1.0194
9	H	1.0900808	114.413831	149.247678	1.3879	-1.7751	-1.6363

10	C	1.509532	117.760416	-178.668935	1.5724	2.9389	0.948
11	H	1.0982662	111.031353	55.3588229	2.6001	3.297	0.8004
12	H	1.094916	111.623671	176.255425	0.8856	3.6966	0.5568
13	H	1.0983309	110.980213	-63.1548997	1.4162	2.8657	2.0327
14	C	1.5209846	115.401952	-145.402935	-0.2243	0.1916	-2.8062
15	H	1.0975011	111.098753	-61.2730536	-1.173	0.7317	-2.9192
16	H	1.0967084	110.462096	58.3347218	0.5367	0.7244	-3.3891
17	H	1.0956239	111.37854	178.37953	-0.3497	-0.8052	-3.2433
18	C	1.5044539	122.991908	174.406424	3.1923	-1.8078	0.3669
19	H	1.0989178	110.995181	120.1863	2.7056	-2.6874	0.8108
20	H	1.0995094	110.927495	-121.570459	3.669	-2.1498	-0.563
21	H	1.0948878	111.642399	-0.7679511	3.9779	-1.4681	1.0497
22	C	1.5156268	123.979928	-64.8982979	-0.3621	-1.0671	-0.5303
23	H	1.0892036	114.175788	-150.099083	-0.9486	-1.7672	-1.1238
24	C	1.4995738	123.737229	-7.7752192	-0.8875	-0.9427	0.8687
25	O	1.2183937	124.877458	-26.6670589	-0.2761	-1.2609	1.8734
26	O	1.354157	117.450139	156.1843	-2.1562	-0.4946	1.0215
27	C	1.4536881	122.205117	-3.0785448	-2.9726	-0.0798	-0.1075
28	H	1.0946165	109.085583	61.5345772	-3.1129	-0.932	-0.78
29	H	1.0929866	109.007277	-57.4688897	-2.456	0.7188	-0.646
30	C	1.5174417	107.260242	-178.082453	-4.3002	0.4001	0.4491
31	H	1.0958492	109.364314	-179.812425	-4.9463	0.7192	-0.3765
32	H	1.0951225	111.00383	-60.3047524	-4.8092	-0.4008	0.9957
33	H	1.0951823	110.942782	60.7002415	-4.1572	1.2506	1.1241

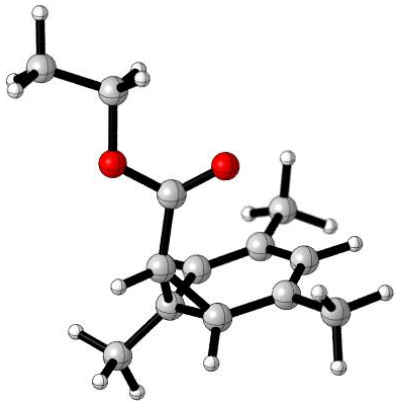

EE + Thermal Free Energy Correction: -656.230901, Entropy = 133.065 cal mol^{-1} K^{-1}

Tag	**Symbol**	**Bond**	**Angle**	**Dihedral**	**X**	**Y**	**Z**
1	C				1.8941	-0.0233	1.176
2	C	1.3946688			2.0964	1.0763	0.3423
3	C	1.4128173	122.747468		1.696	1.0921	-1.0125
4	C	1.3982269	118.927461	-1.6664998	1.1021	-0.0513	-1.5556

5	C	1.459282	124.010155	1.8448254	0.828	-1.2674	-0.797
6	C	1.4691442	120.40021	-1.2226164	1.2171	-1.2251	0.6703
7	H	1.0865283	118.484438	179.333836	2.5907	1.953	0.7517
8	H	1.08777	118.84834	-175.720788	0.8586	-0.0631	-2.6157
9	H	1.088291	115.23433	150.20038	1.5219	-2.1601	1.1364
10	C	1.5012273	120.094224	179.174387	1.9267	2.3155	-1.8514
11	H	1.0951268	110.941141	43.2447311	2.9251	2.7291	-1.6741
12	H	1.0927781	111.75603	165.247959	1.8116	2.1034	-2.9172
13	H	1.0983077	109.766756	-74.8858559	1.202	3.0946	-1.5792
14	C	1.5226179	116.210583	-148.523152	0.8967	-2.5748	-1.5744
15	H	1.0951883	110.533715	-60.0044425	0.1696	-2.5734	-2.3934
16	H	1.0948268	110.154693	60.0615119	1.898	-2.711	-1.9957
17	H	1.0936384	110.902889	179.833738	0.6806	-3.4272	-0.9242
18	C	1.4879317	121.606068	176.867612	2.3871	-0.0387	2.5798
19	H	1.0987035	109.910317	124.147916	1.5536	-0.2395	3.2669
20	H	1.0991138	109.869229	-119.48827	3.0998	-0.8642	2.7164
21	H	1.0916727	112.351543	2.2139842	2.8684	0.8999	2.8611
22	C	1.5272754	120.8033	-68.355421	-0.2677	-1.1948	0.3139
23	H	1.0855813	114.824127	-151.310307	-0.7824	-2.1442	0.4244
24	C	1.501354	123.707093	-5.6907103	-1.1598	-0.0127	0.5606
25	O	1.218747	125.6598	-2.2768204	-0.8267	1.0287	1.099
26	O	1.3363185	109.615121	178.513059	-2.3908	-0.2787	0.1138
27	C	1.4624684	117.177679	179.128878	-3.4045	0.7606	0.2901
28	H	1.0934216	107.923763	59.9677402	-3.0676	1.6533	-0.2439
29	H	1.0934734	107.882002	-57.3376583	-3.4659	0.9922	1.357
30	C	1.5149553	107.516129	-178.687772	-4.7101	0.2217	-0.2577
31	H	1.0956175	109.054239	-179.977962	-5.4893	0.9826	-0.1383
32	H	1.0950336	111.178115	-60.6915326	-4.6238	-0.0166	-1.323
33	H	1.0949806	111.155181	60.736236	-5.0236	-0.6781	0.2818

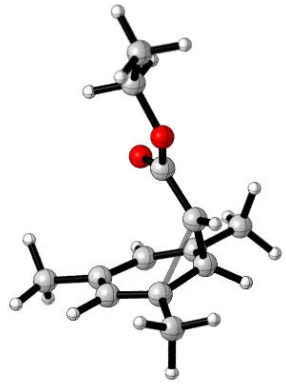

EE + Thermal Free Energy Correction: -656.222938, Entropy = 132.556 cal mol^{-1} K^{-1}

Tag	Symbol	Bond	Angle	Dihedral	X	Y	Z

1	C				1.6035	-0.7726	-1.1515
2	C	1.3692158			2.1361	-1.1817	0.0417
3	C	1.4247543	121.9435191		2.0987	-0.3601	1.2051
4	C	1.4050636	120.0638744	-6.4743177	1.6272	0.9607	1.1192
5	C	1.4008963	121.9421731	-1.1497609	1.2058	1.5198	-0.0942
6	C	1.4956469	117.8850954	11.204704	1.0259	0.6027	-1.2619
7	H	1.0866137	119.4918209	-179.9916417	2.5567	-2.1801	0.1255
8	H	1.0873379	118.945785	-174.5297238	1.69	1.6	1.9965
9	H	1.0955779	113.7072362	-147.9972727	1.2444	1.0713	-2.2278
10	C	1.4958718	119.2322297	174.2787556	2.5817	-0.9154	2.5074
11	H	1.0962927	111.0867943	45.4073486	3.5325	-1.4464	2.3814
12	H	1.0925622	112.4391578	168.1845407	2.6988	-0.1438	3.272
13	H	1.0999133	109.2018966	-71.8499715	1.856	-1.6548	2.8768
14	C	1.50542	120.7784982	-161.702642	1.0967	3.0123	-0.258
15	H	1.0947865	111.9317423	-48.9636677	0.5448	3.4749	0.5666
16	H	1.098747	108.3570029	69.3059031	2.1105	3.4359	-0.2538
17	H	1.0930608	112.8121631	-172.1171816	0.6285	3.3019	-1.2023
18	C	1.4927853	123.1308698	-175.8086415	1.5467	-1.645	-2.3615
19	H	1.099006	110.2473848	119.8649172	0.5041	-1.7895	-2.6776
20	H	1.098427	110.9038332	-122.2562258	2.0697	-1.1774	-3.2067
21	H	1.0922489	111.8147255	-0.6256521	1.987	-2.627	-2.1749
22	C	1.5154833	83.9386751	102.9223311	-0.4485	0.7452	-0.9417
23	H	1.0838058	117.263299	82.0760457	-0.9556	1.6257	-1.3188
24	C	1.4774941	125.9917766	-100.6179356	-1.2763	-0.2343	-0.208
25	O	1.2205815	125.0596943	-0.6001977	-0.8768	-1.301	0.2306
26	O	1.3380262	109.409345	-179.9852086	-2.5294	0.2251	-0.1131
27	C	1.4657003	116.9864859	178.1345787	-3.5068	-0.6412	0.5521
28	H	1.0940538	107.6060106	60.5788102	-3.1615	-0.8033	1.5775
29	H	1.0940279	107.6652947	-56.0016734	-3.5053	-1.6038	0.0322
30	C	1.5140262	107.6218226	-177.7590228	-4.8507	0.0535	0.4921
31	H	1.0955601	109.0614991	-179.9011877	-5.6005	-0.5746	0.9856
32	H	1.094702	111.3091417	-60.6476376	-4.8226	1.0193	1.0067
33	H	1.094561	111.2750525	60.8707807	-5.1686	0.2147	-0.5428

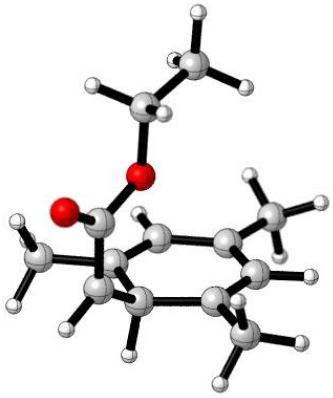

EE + Thermal Free Energy Correction: -656.231844 Hartree, Entropy = 136.631 cal mol^{-1} K^{-1}

Tag	Symbol	Bond	Angle	Dihedral	X	Y	Z
1	C				-0.8735	-0.6706	-1.3578
2	C	1.3708583			-1.8882	0.2421	-1.2289
3	C	1.4162185	121.6639963		-2.4349	0.5724	0.0351
4	C	1.4171854	120.6482837	-0.0098826	-1.9439	-0.0376	1.2163
5	C	1.3704012	121.7166703	-0.2115535	-0.9348	-0.9642	1.1827
6	C	1.5061419	119.6986493	4.0158623	-0.3789	-1.4129	-0.1442
7	H	1.0861999	119.6139215	-176.8324931	-2.2789	0.7387	-2.1124
8	H	1.0862726	118.6466813	179.1363948	-2.3772	0.2503	2.1699
9	H	1.1110047	102.2652736	103.1235337	-0.8469	-2.4124	-0.2719
10	C	1.4919685	119.7734549	-178.7560946	-3.5575	1.5511	0.1239
11	H	1.1011149	108.4087832	91.1835968	-4.5073	0.9964	0.0725
12	H	1.0935964	111.7196864	-151.0245485	-3.5506	2.0896	1.0757
13	H	1.0930725	111.914575	-26.9792925	-3.5486	2.2588	-0.7091
14	C	1.4944602	121.8575981	179.3091334	-0.4043	-1.5982	2.4277
15	H	1.0922755	111.3377348	10.1773217	-1.0319	-1.3653	3.2908
16	H	1.0961886	111.2479653	132.2124217	-0.3307	-2.6865	2.319
17	H	1.098691	110.1599213	-109.8183473	0.6115	-1.2343	2.6347
18	C	1.4941082	121.8135206	-178.8810488	-0.2776	-1.0034	-2.6869
19	H	1.0988808	109.996802	107.8487683	0.7305	-0.5731	-2.7651
20	H	1.0960364	111.3641529	-134.1599697	-0.1672	-2.0863	-2.8151
21	H	1.0923951	111.3360823	-11.9241265	-0.8813	-0.6031	-3.5046
22	C	1.5130629	114.1756044	-143.2889863	1.1139	-1.6595	-0.1344
23	H	1.0829738	120.2924874	-113.7626901	1.5014	-2.6683	-0.2051
24	C	1.4563018	123.3369005	66.8528995	2.1003	-0.5943	-0.0196
25	O	1.2282202	122.8751251	179.4737741	3.3102	-0.805	-0.0031
26	O	1.3474081	112.8458741	-0.5373503	1.5418	0.629	0.0648
27	C	1.4585335	117.002264	-179.9978723	2.4494	1.7646	0.1831
28	H	1.0937831	108.0025783	58.281016	3.1123	1.7596	-0.6869
29	H	1.0938459	107.9834694	-58.8920249	3.0552	1.6205	1.0824
30	C	1.5151972	107.7930003	179.6949924	1.6091	3.0234	0.2548

31	H	1.0956504	109.057892	179.9898798	2.2718	3.8913	0.3444
32	H	1.0950955	111.1985588	-60.7619894	1.0034	3.1472	-0.6491
33	H	1.0950783	111.2109484	60.73248	0.9458	3.0079	1.126

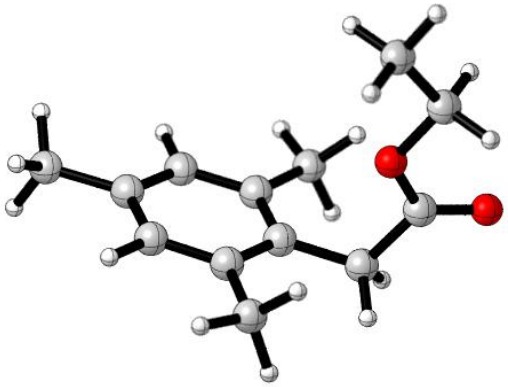

EE + Thermal Free Energy Correction: -656.499163 Hartree, Entropy = 134.337 cal mol^{-1} K^{-1}

Tag	Symbol	Bond	Angle	Dihedral	X	Y	Z
1	C				1.0842	1.2883	-0.3026
2	C	1.4011245			2.2955	0.8641	-0.8647
3	C	1.3996053	121.9064235		2.924	-0.3195	-0.461
4	C	1.3994295	117.8058541	0.4188111	2.2981	-1.0864	0.5282
5	C	1.4020468	122.0623604	-0.3715496	1.0856	-0.6978	1.1152
6	C	1.4113239	119.234435	0.0681857	0.4716	0.5027	0.6985
7	H	1.0887802	118.8409328	179.7666483	2.7578	1.4748	-1.6385
8	H	1.0887323	119.158669	179.4725568	2.7634	-2.0157	0.8526
9	C	1.5123169	121.0808633	-178.3994892	4.2493	-0.7415	-1.0548
10	H	1.0987263	111.0978792	88.5846947	5.0896	-0.3177	-0.4878
11	H	1.0955362	111.4435719	-151.8846898	4.3653	-1.8308	-1.0418
12	H	1.0956613	111.442287	-30.9081029	4.3514	-0.3989	-2.0905
13	C	1.5149145	118.9508385	179.9119703	0.4689	-1.5829	2.1788
14	H	1.0944632	110.5808539	-2.9576164	1.0666	-2.4889	2.3194
15	H	1.0981282	111.9454729	116.6578467	0.41	-1.0759	3.1511
16	H	1.096597	111.9162079	-123.0135301	-0.5489	-1.8931	1.9135
17	C	1.5143287	119.2082199	-179.9565256	0.4571	2.5791	-0.7861
18	H	1.0974012	112.1449747	121.7522783	-0.5545	2.4245	-1.1824
19	H	1.0980552	111.9073463	-118.216056	0.373	3.3206	0.0194
20	H	1.094324	110.703263	1.6978704	1.0582	3.0262	-1.5838
21	C	1.5166364	120.8590637	-179.5297039	-0.8347	0.9635	1.3161
22	H	1.0962497	110.6450361	21.382819	-0.9851	0.4958	2.2961
23	C	1.5251944	117.0543302	-99.3675838	-2.1113	0.6796	0.5313
24	O	1.221144	123.3157415	-153.1760852	-3.1225	1.3574	0.6275
25	O	1.3406312	113.2218907	28.9257311	-2.0257	-0.4138	-0.2397
26	C	1.4562357	117.2129474	177.668561	-3.2151	-0.7957	-0.9881

27	H	1.0938847	108.2506226	58.2310132	-3.4974	0.0414	-1.6332
28	H	1.0940167	108.2695893	-59.1321229	-4.0264	-0.9726	-0.2758
29	C	1.5162621	107.5918196	179.5258777	-2.875	-2.0397	-1.7855
30	H	1.0958641	109.2751407	-179.9323576	-3.7534	-2.3513	-2.3619
31	H	1.0952966	111.1204562	-60.5238783	-2.0552	-1.8476	-2.486
32	H	1.0952769	111.1434126	60.6623744	-2.587	-2.8653	-1.1259
33	H	1.0939632	111.4227273	138.61141	-0.8308	2.0417	1.5011

C.9: Fluorescence Quenching and Isotope Labeling Studies

Emission lifetime and Stern-Volmer experiments: Emission lifetime measurements were taken at ambient temperature using a Edinburgh FLS920 spectrometer and fit to single exponential according to the methods previously described by our laboratory.[119] The fluorescence of **Mes-Acr-Ph** in 1:1 MeCN:TFE was observed as a single exponential decay. Stern-Volmer analysis on the quenching of fluorescence lifetime was carried at a 1.5×10^{-6} M concentration of Mes-Acr-Ph. The quenching constant was determined with varying quencher concentrations in the range of 0-1.0×10^{-2} M. Bimolecular quenching constant, k_q, was determined from the corresponding Stern-Volmer constant.

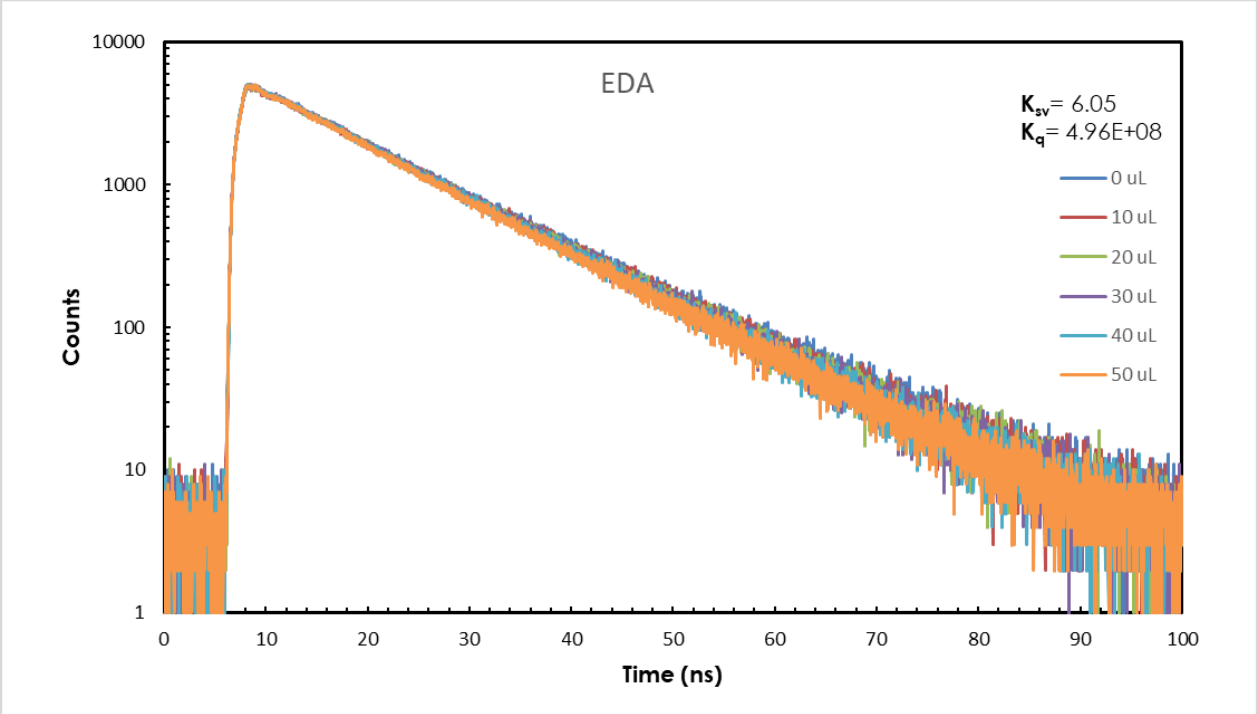

Figure C.5: Fluorescence decay obtained by time-correlated single photon counting of 3,6-di-*tert*-butyl-9-mesityl-10-phenylacridinium tetrafluoroborate in 1:1 MeCN:TFE with quenching by ethyl diazoacetate (concentration range: 0 - 1.0×10^{-2} M)

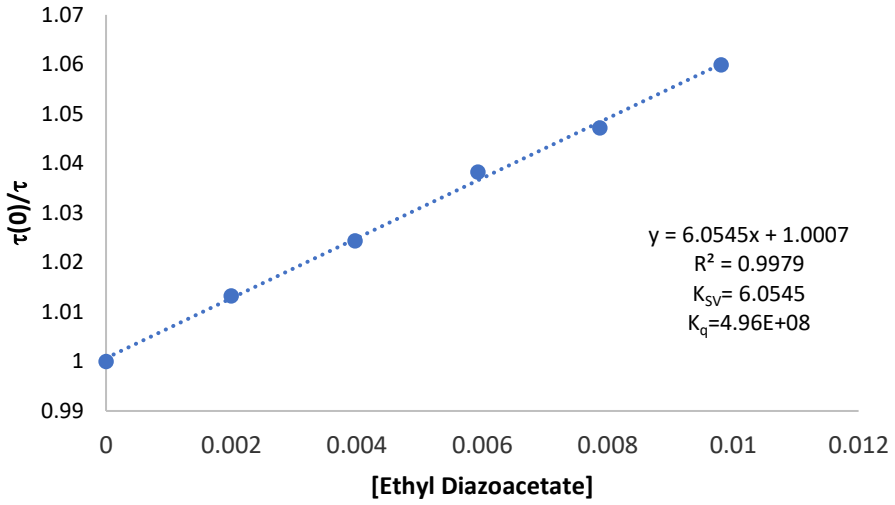

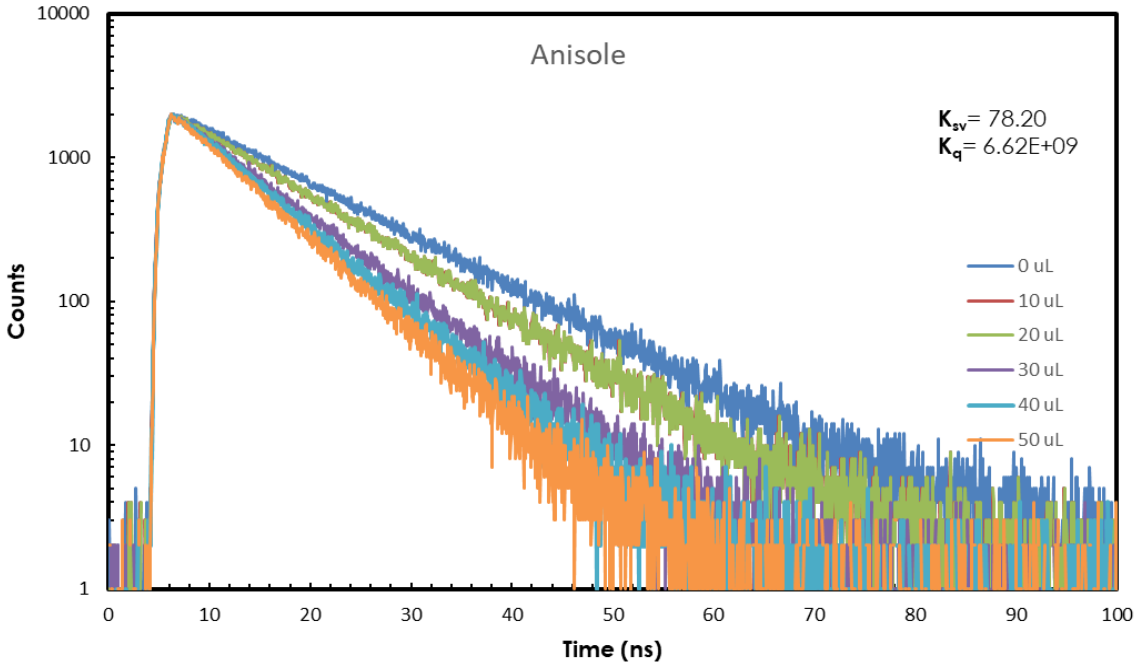

Figure C.6: Fluorescence decay obtained by time-correlated single photon counting of 3,6-di-*tert*-butyl-9-mesityl-10-phenylacridinium tetrafluoroborate in 1:1 MeCN:TFE with quenching by anisole (concentration range: 0 - 1.0x10^{-2} M)

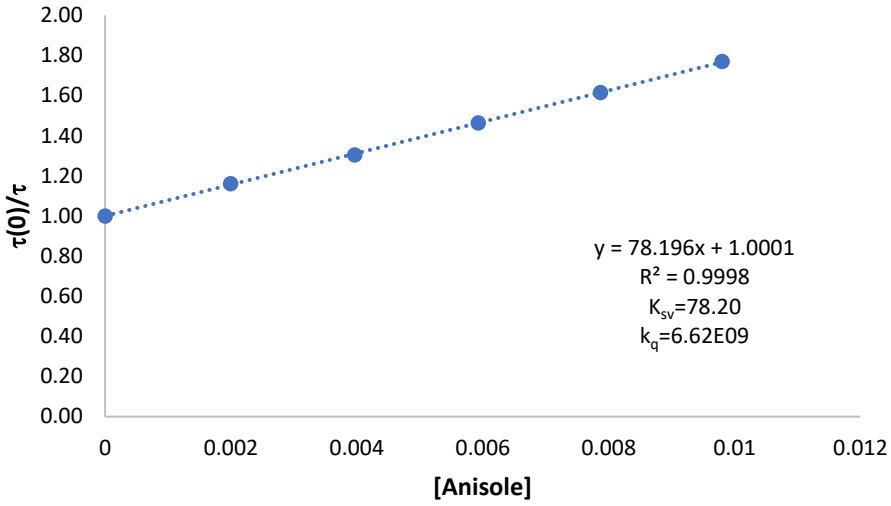

Figure C.7: Stern-Volmer analysis of the fluorescence quenching of 3,6-di-*tert*-butyl-9-mesityl-10-phenylacridinium tetrafluoroborate in 1:1 MeCN:TFE with quenching by anisole (concentration range: 0 - 1.0x10^{-2} M.)

C.10: Deuterium labeling and control experiments

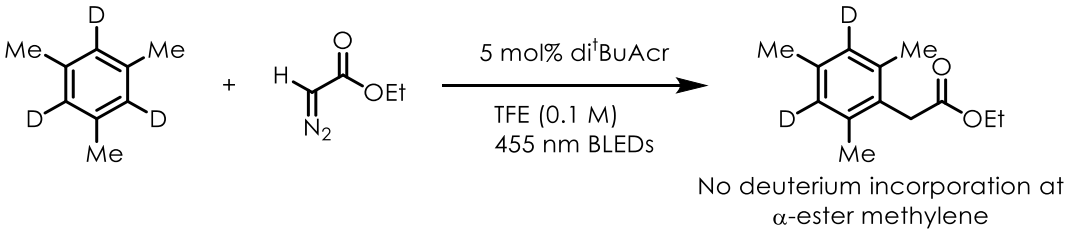

The reaction was prepared according to the general conditions with d_3-Mesitylene as the substrate. The crude reaction was analyzed by NMR and GC-MS and showed no deuterium incorporation at the alpha-ester methylene position.

Deuterium is incorporated from d_1- 2,2,2-trifluoroethanol

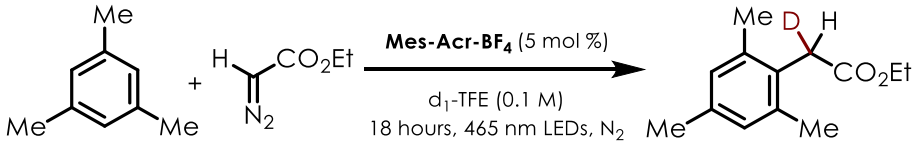

The reaction was prepared according to the general conditions using *d*$_1$-2,2,2 trifluoroethanol. The reaction was analyzed by NMR and GCMS. The major product observed was mono deuteration. Minor di- and non-deuterated product was observed, which is believed to be from enolate equilibration of the monodeuterated product in the final protonation step.

No Deuterium exchage from d_1 TFE occurs once product is formed

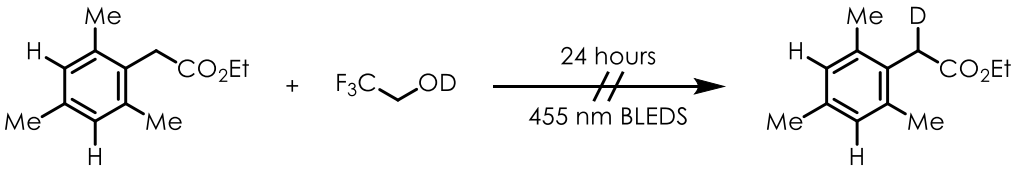

Ethyl 2-mesitylacetate (0.100 mmol, 20.6 mg) were added to a 2 dram vial equipped with a stir bar. The vial was moved to a nitrogen filled glovebox (<10 ppm O_2) and and 0.50 mL 2,2,2,-trifluoroethan-1-ol-*d* was added. The vial was capped tightly with a Teflon-lined phenolic resin septum cap (purchased through VWR international, Microliter Product # 15-0060K) and moved out of the glovebox. Prior to irradiation, vials were sealed with electrical tape to ensure maximal oxygen exclusion. The reaction vial was then placed into the reactor and equip with a nitrogen inlet needle. The reactions were irradiated for 18 hours to mimic any heating throughout the reaction. The reaction was concentrated and analyzed by ^{1}H NMR which showed no deuterium incorporation.

Full Conversion to the Desired Product When Subjecting the Intermediate Cycloheptatriene

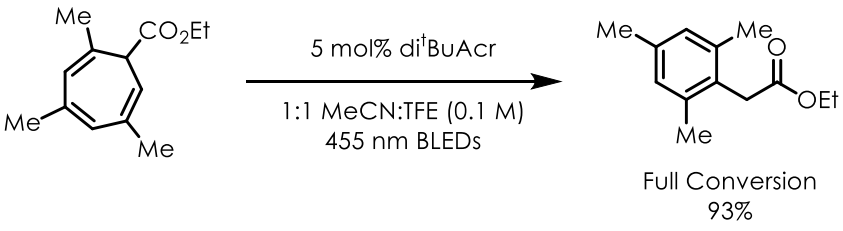

The reaction was prepared according to the general conditions with ethyl 2-(2,4,6-trimethylcyclohepta-2,4,6-trien-1-yl)acetate as the substrate. The reaction was analyzed by ^{1}H NMR which showed full conversion to the desired product (93% yield). Spectra data matched those previously reported.

Without the Photoredox Catalyst, No Ring Opening is Observed

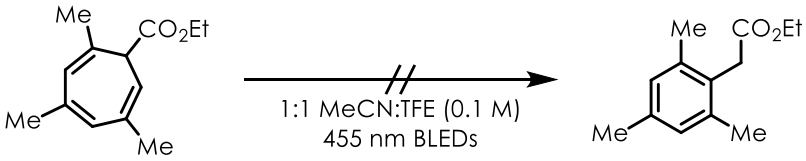

The reaction was prepared according to the general conditions with ethyl 2-(2,4,6-trimethylcyclohepta-2,4,6-trien-1-yl)acetate as the substrate and without 5 mol% acridinum catalyst. The reaction was analyzed by ^{1}H NMR which gave only returned starting material with no ethyl 2-mesitylacetate observed. Spectra data matched those previously reported.

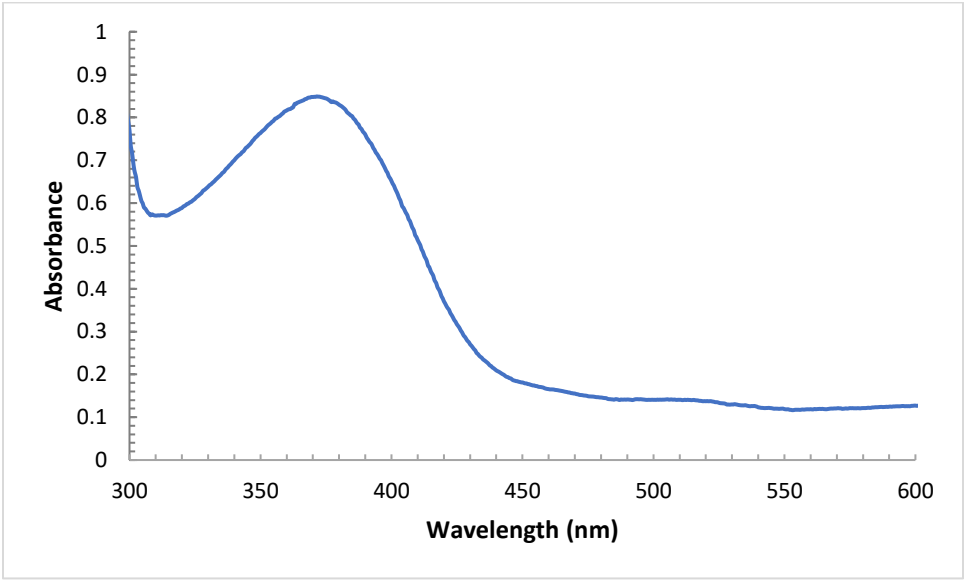

Figure C.8: UV-Vis absorbance spectrum of a 0.5 mM solution of ethyl diazoacetate in 1:1 MeCN:TFE

C.11: NMR Spectra for New Compounds

NMR data is available in the corresponding published supporting information, which is available online.[213]

APPENDIX D: SUPPORTING INFORMATION FOR "DISCOVERY AND CHARACTERIZATION OF ACRIDINE RADICAL PHOTOREDUCTANTS"

D.1: General Information

Methods and Materials: Proton and carbon magnetic resonance spectra (^{1}H NMR and ^{13}C NMR) were recorded on a Bruker AVANCE III 600 CryoProbe (^{1}H NMR at 600 MHz, ^{13}C NMR at 151 MHz and ^{19}F NMR at 565 MHz) spectrometer or Bruker AVANCE III 500 (^{1} H NMR at 500 MHz and ^{13}C NMR at 126 MHz) spectrometer with solvent resonance as the internal standard (1H NMR: CDCl3 at 7.26 ppm; 13C NMR: CDCl3 at 77.0 ppm). ^{1}H NMR data are reported as follows: chemical shift, multiplicity (s = singlet, d = doublet, t = triplet, dd = doublet of doublets, ddd = doublet of doublets of doublets, ddddd = doublet of doublets of doublets of doublets of doublets, dt = doublet of triplets, ddt = doublet of doublets of triplets, td = triplet of doublets, tt = triplet of triplets, m = multiplet, q = quartet), coupling constants (Hz), and integration. High Resolution Mass Spectra (HRMS) were obtained via direct infusion using a Thermo LTQ FT mass spectrometer with positive mode electrospray ionization.

Flash chromatography was performed using SiliaFlash P60 silica gel (40-63 μm) purchased from Silicycle. Irradiation of photochemical reactions was carried out using materials purchased from RapidLED. Ultraviolet UVA LEDs (390-400 nm) were mounted upon a NanoTank heatsink and attached to 40o focusing lenses attached to a 3D printed frame that held 1 dram and 2 dram vials above each lens. Reactions were cooled using GDSTIME 3000rpm 12cm by 12cm fans placed on top of the reactor. Stirring was achieved by placing the assembled reactor on a stir plate.

All reactions were performed in 1 dram vials and were run under air unless otherwise specified. Alternatively, reactions performed at longer wavelength were irradiated from the side at 1–2 cm by a single 467nm Kessil floodlamp with an average intensity of 288mW/cm2 (measured

from 1 cm distance). The spectral bandwidth of the 467nm Kessil lamp was estimated to be ± 40 nm.

EPR spectra were acquired on a JEOL FA-100 spectrometer operating at X–band (9.5 GHz) using a TE011 cylindrical microwave resonator with 100 kHz field modulation. UV-vis spectra were collected using a Cary50 Bio spectrophotometer. All fluorescence measurements were collected using an Edinburgh FLS920 Spectrometer.

Cyclic voltammograms were collected using a Pine WaveNow Potentiostat. Samples were prepared with 0.05 mmol of substrate in 5 mL of 0.1 M tetra-n-butylammonium hexafluorophosphate (tBAPF6) in dry, degassed acetonitrile. Measurements employed a glass carbon working electrode, platinum wire counter electrode, 3.5 M NaCl silver-silver chloride pseudo-reference electrode, and a typical scan rate of 100 mV/s. Data analysis was performed in Excel where the $E_{1/2}$ (or $E_{p/2}$ for irreversible redox events) was found and referenced to Ag|AgCl. This value was then converted to SCE by subtraction of 0.03 V.

Commercially available reagents were purchased from Sigma-Aldrich, Acros, Alfa Aesar, or TCI, Matrix Scientific, Combi-Blocks, Oakwood Chemical, Chem Impex International, and Fisher Scientific and were used as received unless otherwise noted. Diethyl ether (Et_2O), dichloromethane (DCM), tetrahydrofuran (THF), toluene (PhMe), and dimethylformamide (DMF) were dried by passing through activated alumina under nitrogen prior to use. Other common solvents and chemical reagents were purified by standard published methods as noted or used as received. All catalyst and substrate syntheses were run under a nitrogen atmosphere unless specified otherwise.

Catalyst Synthesis:

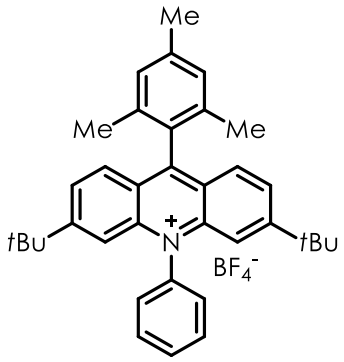

3,6-Di-*tert*-butyl-9-mesityl-10-phenylacridin-10-ium tetrafluoroborate prepared according to literature precedent: Analytical data matched that reported in the literature.[1]

^{1}H NMR (600 MHz, $CDCl_3$) δ 7.99 (td, *J* = 7.5, 6.7, 1.3 Hz, 2H), 7.94 (s, 1H), 7.94 – 7.90 (m, 1H), 7.83 – 7.74 (m, 6H), 7.44 (dd, *J* = 1.5, 0.7 Hz, 2H), 7.19 (d, *J* = 1.2 Hz, 2H), 2.51 (s, 3H), 1.89 (s, 6H), 1.32 (s, 18H). **^{13}C NMR** (151 MHz, $CDCl_3$) δ 163.53, 162.26, 142.14, 140.15, 136.85, 136.17, 131.81, 131.60, 129.31, 128.93, 128.26, 128.03, 127.45, 124.04, 115.08, 36.67, 30.22, 21.32, 20.25. **^{19}F NMR** (565 MHz, $CDCl_3$) δ -150.85, -154.50.

D.2: Preparation of Benzenesulfonamide Substrates

General Procedure for preparation of *N*-Ts-Amine Derivatives (Procedure A): To a solution of the appropriate amine (2.0 mmol, 1.0 eq) in pyridine (5 mL) was added *p*-toluenesulfonyl chloride (421 mg, 1.1 mmol) at 0 °C. After the solution was stirred at ambient temperature for 2−3 hours, pyridine was removed *via* rotary evaporation and the reaction mixture was poured into water. The product was extracted with CH_2Cl_2 (three times), dried over dry Na_2SO_4, and concentrated in vacuo. The residue was purified by silica gel column chromatography with hexane/ethyl acetate (5/1) as the eluent to give the corresponding product (65%-100% yield).

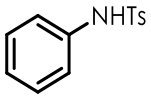

4-Methyl-*N*-phenylbenzenesulfonamid*e* (5.38) was prepared according to General Procedure A; spectral data were in agreement with literature values.[146]

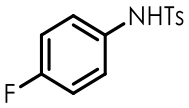

***N*-(4-fluorophenyl)-4-methylbenzenesulfonamide (5.39)** was prepared according to General Procedure A; spectral data were in agreement with literature values.[214]

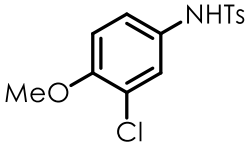

***N*-(3-chloro-4-methoxyphenyl)-4-methylbenzenesulfonamide (5.40)** was prepared according to General Procedure A and isolated as a white solid.

^{1}H NMR (400 MHz, $CDCl_3$) δ (ppm) = 7.65 (d, J=8.3 Hz, 2H), 7.26 (d, J =8.0 Hz, 2H), 7.13 (d, J = 2.6 Hz, 1H), 6.99 (dd, J = 8.8 Hz, J = 2.7 Hz, 1H), 6.91 (s, 1H), 6.79 (dd, J = 8.8 Hz, 1H), 3.86 (s, 3H), 2.41 (s, 3H); **^{13}C NMR** (101 MHz, $CDCl_3$) δ (ppm) = 153.3 (s), 144.0 (s), 135.7 (s), 129.7 (s), 129.5 (s), 127.3 (s), 125.5 (s), 122.9 (s), 122.7 (s), 112.3 (s), 56.3 (s), 21.6 (s); **HRMS** calculated for $C_{14}H_{15}ClNO_3S$ ($M + H^+$): 312.0456, found: 312.0437.

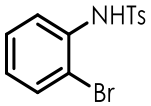

***N*-(2-bromophenyl)-4-methylbenzenesulfonamide (5.41)** was prepared according to General Procedure A; spectral data were in agreement with literature values.[215]

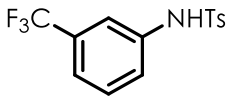

4-Methyl-*N*-(3-(trifluoromethyl)phenyl)benzenesulfonamide (5.42) was prepared according to General Procedure A; spectral data were in agreement with literature values.[216]

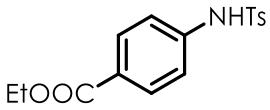

4-((4-Methylphenyl)sulfonamido)phenyl propionate (5.43) was prepared according to General Procedure A; spectral data were in agreement with literature values.[217]

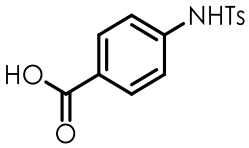

4-((4-Methylphenyl)sulfonamido)benzoic acid (5.44) was prepared according to Procedure B; spectral data were in agreement with literature values.[218]

Procedure B: 4-((4-Methylphenyl)sulfonamido)phenyl propionate (80 mg, 0.25 mmol) was placed in a 25 mL RBF. 2N NaOH (4 mL) was added dropwise. The mixture was left stirring at ambient temperature for 2 hours. 2 N HCl (5 mL) was added dropwise untill a white precipitate crashed out. The solid was filtered through a sinter funnel and dried under high vacuum. The product was isolated as a white solid (20 mmol, 80%). Analytical data matched that reported in the literature.

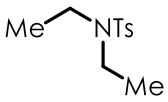

***N,N*-diethyl-4-methylbenzenesulfonamide (5.45)** was prepared according to General Procedure A; spectral data were in agreement with literature values.[219]

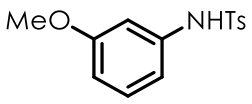

***N*-(3-methoxyphenyl)-4-methylbenzenesulfonamide (5.46)** was prepared according to General Procedure A; spectral data were in agreement with literature values.[220]

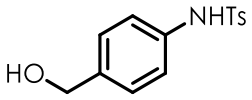

***N*-(4-(hydroxymethyl)phenyl)-4-methylbenzenesulfonamide (5.47)** was prepared according to Procedure C and isolated as a white solid.

Procedure C: 4-((4-Methylphenyl)sulfonamido)phenyl propionate (70 mg, 0.22 mmol) was placed in a 25 mL RBF and dissolved in 10 mL dry THF. The mixture was stirred at 0 °C for 10 minutes. Lithium aluminium hydride (33 mg, 0.88 mmol) was added portionwise over 5 minutes. The mixture was left stirring at 0 °C for 2 hours. The reaction mixture then was quenched with water (10 mL), extracted with ethyl acetate (3 x 10 mL). The combined organic extracts were washed with brine (20 mL), dried with anhydrous Na_2SO_4, and concentrated in vacuo. The residue was purified by silica gel column chromatography with hexane/ethyl acetate (4/1) as the eluent to give the corresponding product as a white solid (54 mg, 0.20 mmol, 88%).

^{1}H NMR (400 MHz, acetonitrile-d_3) δ (ppm) = 7.68 (d, J = 8.3 Hz, 2H), 7.37 – 7.29 (m, 2H), 7.22 (d, J = 8.6 Hz, 2H), 7.10 (d, J = 8.5 Hz, 2H), 4.49 (s, 2H), 2.37 (s, 3H). **^{13}C NMR** (101 MHz, Acetonitrile-d_3) δ (ppm) = 144.1(s), 138.7(s), 136.4(s), 136.3(s), 129.7(s), 127.7(s), 127.1(s), 120.8(s), 63.1(s), 20.6(s); **HRMS** calculated for $C_{14}H_{15}NO_3SNa$ ($M + Na^+$): 300.0670, found: 300.0649.

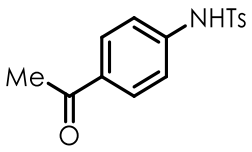

***N*-(4-acetylphenyl)-4-methylbenzenesulfonamide (5.48)** was prepared according to General Procedure A; spectral data were in agreement with literature values.[220]

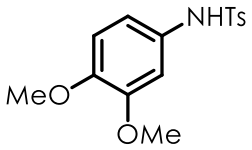

***N*-(3,4-dimethoxyphenyl)-4-methylbenzenesulfonamide (5.49)** was prepared according to General Procedure A; spectral data were in agreement with literature values.[221]

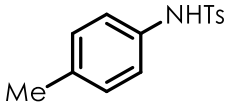

4-Methyl-*N*-(*p*-tolyl)benzenesulfonamide (5.50) was prepared according to General Procedure A; spectral data were in agreement with literature values.[146]

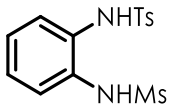

4-Methyl-*N*-(2-(methylsulfonamido)phenyl)benzenesulfonamide (5.51):

A solution of phenylene-1,2-diamine (150 mg, 1.31 mmol, 1.0 eq) in CH_2Cl_2 (8 mL) and pyridine (10 mL) was treated with MsCl (162 mg, 1.41 mmol, 1.02 eq) at 0° C and stirred for 30 min. The mixture was then treated with TsCl (270 mg, 1.41 mmol, 1.02 eq), stirred for 12 h at room temperature, and the solvent removed *via* rotary evaporation. After the addition of water, the precipitate was filtered off and crystallized from EtOH to afford the desired product (388 mg, 82% yield).

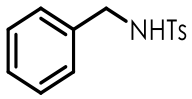

***N*-benzyl-4-methylbenzenesulfonamide (5.52)** was prepared according to General Procedure A; spectral data were in agreement with literature values.[220]

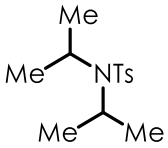

***N,N*-diisopropyl-4-methylbenzenesulfonamide (5.53)** was prepared according to General Procedure A; spectral data were in agreement with literature values.[222]

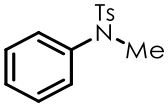

***N*,4-dimethyl-*N*-phenylbenzenesulfonamide (5.54)** was prepared according to General Procedure A; spectral data were in agreement with literature values.[146]

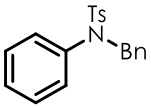

***N*-benzyl-4-methyl-*N*-phenylbenzenesulfonamide (5.55)** was prepared according to General Procedure A; spectral data were in agreement with literature values.[223]

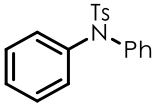

4-methyl-*N*,*N*-diphenylbenzenesulfonamide (5.56) was prepared according to General Procedure A; spectral data were in agreement with literature values.[224]

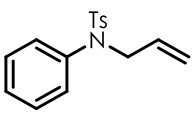

***N*-allyl-4-methyl-*N*-phenylbenzenesulfonamide (5.57)** was prepared according to General Procedure A; spectral data were in agreement with literature values.[225]

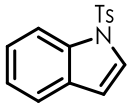

1-Tosyl-1*H*-indole (5.58) was prepared according to General Procedure A; spectral data were in agreement with literature values.[226]

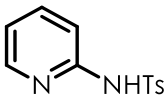

4-Methyl-n-(pyridin-2-yl)benzenesulfonamide (5.59) was prepared according to General Procedure A; spectral data were in agreement with literature values.[220]

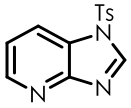

1-Tosyl-1*H*-imidazo[4,5-*b*]pyridine (5.60) was prepared according to General Procedure A: white solid, 98% yield.

^{1}H NMR (400 MHz, $CDCl_3$) δ (ppm) = 8.61 (m, 2H), 8.19 (dd, J =8.2 Hz, 1.6 Hz, 1H), 7.88 (d, J = 8.5 Hz, 2H), 7.43-7.27 (m, 3H), 2.39 (s, 3H); **^{13}C NMR** (101 MHz, $CDCl_3$) δ (ppm) = 156.2 (s), 147.0 (s), 146.9 (s), 143.4 (s), 134.1 (s), 130.6 (s), 127.3 (s), 123.7 (s), 120.9 (s), 120.5 (s), 21.7 (s); **HRMS** calculated for $C_{13}H_{12}N_3O_2S$ ($M + H^+$): 274.0645, found: 274.0629.

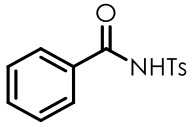

***N*-tosylbenzamide (5.61):**

To a solution of the appropriate benzoic acid (2.00 mmol, 1.0 equiv) in THF (10, 0.2 M) were sequentially added TsNCO (467 μL, 3.00 mmol, 1.5 equiv) and NEt_3 (400 μL, 3.0 mmol, 1.5 equiv) at room temperature. The mixture was then heated to 60 °C. After being stirred at 60 °C for 3 hours, the reaction mixture was cooled to room temperature and the solvent was removed by rotary evaporator. The residue was diluted with EtOAc (10 mL) and washed with 1.0 N HCl (10 mL). The organic layer was washed with brine, dried over Na_2SO_4, and concentrated in vacuo. The residue was purified by column chromatography on silica gel and then recrystallization from MeOH to give the corresponding product; spectral data were in agreement with literature values.[227]

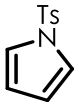

1-Tosyl-1*H*-pyrrole (5.62): Pyrrole (134 mg, 2.00 mmol) as a solution in THF (2 mL) was added to a suspension of NaH (120 mg as a 60% suspension in mineral oil, 3.00 mmol) in THF (2 mL) and stirred for 30 min. Tosyl chloride (419 mg, 2.20 mmol) was added as a solution in THF (2 mL) and stirred for 3 hours . Water was slowly added, and the organic layer was separated, dried over Na_2SO_4, and concentrated. The residue was purified by flash column chromatography on silica gel (288 mg, 1.30 mmol, 65%); spectral data were in agreement with literature values.[228]

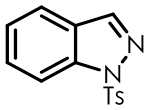

1-Tosyl-1*H*-indazole (5.63) was prepared according to General Procedure A; spectral data were in agreement with literature values.[229]

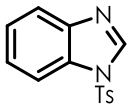

1-Tosyl-1*H*-benzo[*d*]imidazole (5.64) was prepared according to General Procedure A; spectral data were in agreement with literature values.[230]

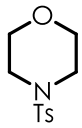

4-Tosylmorpholine (5.65) was prepared according to General Procedure A; spectral data were in agreement with literature values.[231]

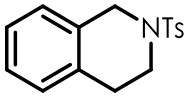

2-Tosyl-1,2,3,4-tetrahydroisoquinoline (5.66) was prepared according to General Procedure A; spectral data were in agreement with literature values.[223]

1-Tosylpyrrolidine (5.67) was prepared according to General Procedure A; spectral data were in agreement with literature values.[232]

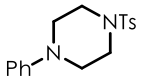

1-Phenyl-4-tosylpiperazine (5.68) was prepared according to General Procedure A; spectral data were in agreement with literature values.[233]

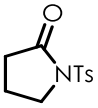

1-Tosylpyrrolidin-2-one (5.69): To a stirred solution of *n*-BuLi (2.5 M in hexanes, 1.68 mL, 4.2 mmol) in THF (4.0 mL), under argon at -78 °C, was added dropwise a solution of 2-pyrrolidinone (4.0 mmol) in THF (2.0 mL) over 5 min. The mixture was stirred for 30 min and a solution of the *p*-toluenesulfonyl chloride (4.4 mmol) in THF (2.0 mL) was then added. After 30 min stirring at -78 °C, the mixture was slowly warmed to room temperature and stirred overnight. The reaction was then quenched by addition of saturated aqueous NH_4Cl (12 mL). The aqueous layer was extracted with EtOAc (3 x 8 mL) and the combined organic layers were washed with brine (2 x 16 mL). The organic extracts were dried over Na_2SO_4, filtered and concentrated. The residue was purified by flash chromatography (1:4 EtOAc/hexane) as the eluent to give the corresponding product as a white solid (766 mg, 80%); spectral data were in agreement with literature values.[233]

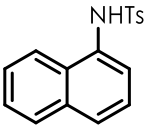

4-Methyl-*N*-(naphthalen-1-yl)benzenesulfonamide (5.70) was prepared according to General Procedure A; spectral data were in agreement with literature values.[220]

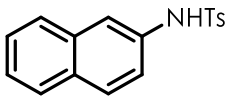

4-Methyl-*N*-(naphthalen-2-yl)benzenesulfonamide (5.71) was prepared according to General Procedure A; spectral data were in agreement with literature values.[234]

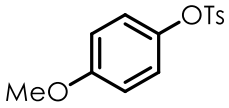

4-Methoxyphenyl 4-methylbenzenesulfonate: To a solution of paramethoxyphenol (2.00 mmol) in dichloromethane (80 mL), was added triethylamine (0.75 mL) and trimethylamine hydrochloride (0.05 mmol) was added. *p*-toluenesulfonyl chloride was added portionwise at room temperature. After stirring overnight, the mixture was quenched with water and stirred for 3 hours. The mixture was extracted with ethyl acetate (10 mL) and the organic layer was washed with water (10 mL), 10% aqueous HCl (3 x10 mL), water (2 x10 mL), saturated aqueous $NaHCO_3$, and brine (2 x 5 mL). The organic layer was dried over Na_2SO and the solvent was evaporated under vacuum. Flash chromatography on silica gel (hexane: ethyl acetate = 20:1 to 4:1) yielded the desired aromatic tosylate; spectral data were in agreement with literature values.[235]

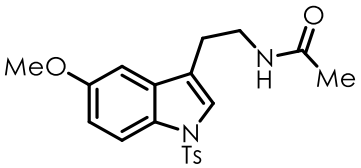

***N*-(2-(5-methoxy-1-tosyl-1*H*-indol-3-yl)ethyl)acetamide (5.72)**: To a stirred solution of melatonin (116 mg, 0.50 mmol, 1.0 eq) in CH_2Cl_2 (5 mL) were sequentially added n-Bu_4PF_6 (96.9 mg, 0.25 mmol, 0.5 eq) and KOH (84.2 mg, 1.5 mmol, 3.0 eq) at 0 °C. The resulting mixture was stirred at room temperature for 5 min before addition of TsCl (205 mg, 0.55 mmol, 1.1 eq). The reaction mixture was allowed to stir at room temperature for 2 days. Water was added, and the

mixture was extracted with EtOAc (3 x 10 mL). The combined organic phases were washed with brine, dried over Na_2SO_4, filtered and concentrated under reduced pressure. The residue was purified by flash column chromatography (DCM/Methanol = 50:1) to give the corrresponding tryptophan derivative (166 mg, 85% yield) ; spectral data were in agreement with literature values.[236]

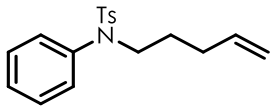

4-Methyl-*N*-(pent-4-en-1-yl)-*N* -phenylbenzenesulfonamide (5.74): 4-methyl-*N*-phenylbenzenesulfonamide (170 mg, 0.69 mmol, 1 equiv.) was dissolved in DMF (7 mL). Then, 5-bromo-1-pentene (164 mg, 1.10 mmol, 1.6 eq) and K_2CO_3 (190 mg, 1.37 mmol, 2.0 equiv) were subsequently added to the solution and the reaction mixture was heated overnight at 80 °C. Once the reaction was complete, as indicated by TLC, water (7 mL) and EtOAc (7 mL) were added to the reaction mixture. The aqueous phase was extracted with ethyl acetate (3 x 5 mL) and the combined organic layers were washed with H_2O (3 x 5 mL), brine (2 x 5 mL), dried over Na_2SO_4, and filtered and concentrated under reduced pressure. The crude residue was purified by flash chromatography on silica gel (1:4 EtOAc/hexane) and the product was obtained as a white solid in 81% yield (176 mg, 0.56 mmol).

^{1}H NMR (400 MHz, $CDCl_3$) δ (ppm) = 7.54-7.45 (m, 2H), 7.36-7.30 (m, 3H), 7.26 (d, J = 8.1, 2H), 7.09-7.03 (m, 2H), 5.75 (ddt, J = 16.9 Hz, J = 10.1 Hz, J = 6.6 Hz, 1H), 5.02-4.92 (m, 2H), 3.59-3.52 (m, 2H), 2.44 (s, 3H), 2.16-2.06 (m, 2H), 1.54 (p, J = 7.3 Hz, 2H); **^{13}C NMR** (101 MHz, $CDCl_3$) δ (ppm) = 143.3 (s), 139.2 (s), 137.5 (s), 135.3 (s), 129.4 (s), 129.0 (s), 128.8 (s), 127.8 (s), 115.3 (s), 50.0 (s), 30.5 (s), 27.5 (s), 21.6 (s); **HRMS** calculated for $C_{18}H_{22}NO_2S$ ($M + H^+$): 316.1366, found: 316.1348.

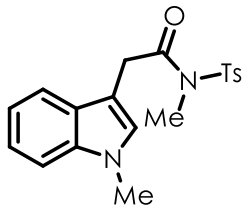

***N*-methyl-2-(1-methyl-1*H*-indol-3-yl)-*N*-tosylacetamide (5.75)**

^{1}H NMR (400 MHz, $CDCl_3$) δ (ppm) = 7.77 (d, J = 8.1 Hz, 2H), 7.41 (dd, J = 8.0, 1.1 Hz, 1H), 7.31 (m, 3H), 7.27 – 7.21 (m, 1H), 7.10 (td, J = 7.4, 7.0, 1.0 Hz, 1H), 6.94 (s, 1H), 4.17 (s, 2H), 3.74 (s, 3H), 3.35 (s, 3H), 2.47 (s, 3H).

^{13}C NMR (101 MHz, $CDCl_3$) δ (ppm) = 171.6 (s), 144.8 (s), 136.8 (s), 136.3 (s), 129.8 (s), 128.1 (s), 127.64 (s), 127.56 (s), 121.8 (s), 119.3 (s), 118.8 (s), 109.3 (s), 106.0 (s), 33.48 (s), 33.5 (s), 32.7 (s), 21.7 (s); **HRMS** calculated for $C_{19}H_{21}N_2O_3S$ ($M + H^+$): 357.1273, found: 357.1238.

Step I: To a stirred suspension of NaH (2.28 g, 57 mmol, 5.0 eq) in THF (50 mL) at 0 °C was added a solution of 1*H*-indol-3-ylacetic acid (2.0 g, 11.4 mmol, 1.0 eq) in THF (20 mL). After stirring the mixture for 30 min at 0 °C, a solution of iodomethane (2.35 mL, 37.6 mmol, 3.3 eq) in THF (20 mL) was added dropwise. The mixture was allowed to slowly reach RT and stirring was continued for 16 hours. The reaction mixture was then cooled to 0 °C and excess hydride was carefully destroyed by slow addition of MeOH with vigorous stirring, followed by cold water until a clear yellow solution resulted. The mixture was then diluted with diethyl ether. The aqueous phase was separated, acidified with 6 N HCl and extracted with CH_2Cl_2. The combined CH_2Cl_2 extracts were dried (Na_2SO_4) and concentrated under reduced pressure. Hexane was then added slowly until a brown colored solid completely precipitated out. The crude solid was recrystallised from EtOH to give the desired product (1.8 g, 90%) as a pale brown solid, spectral data were in agreement with literature values.[237]

Step II: To a flask that contained a solution of 2-(1-methyl-1*H*-indole-3-yl)acetic acid (416 mg, 2.2 mmol, 1.1 eq), DMAP (537 mg, 4.4 mmol) and EDCI (844 mg, 4.4 mmol) in DCM was added *p*-toluenesulfonamide (343 mg, 2.0 mmol, 1.0 eq) across 5 minutes at RT. The reaction mixture was stirred for 12 hours, then cooled to 0 °C and acidified to pH = 1 with the addition of 10% HCl, followed by extraction with DCM. The combined organic layers were washed with brine, dried over Na_2SO_4 and concentrated in vacuo. The residue was purified by flash chromatography (1:2 EtOAc/hexane) to afford 2-(1-methyl-1*H*-indol-3-yl)-n-tosylacetamide as a white solid (564 mg, 1.65 mmol, 82% yield), spectral data were in agreement with literature values.[238]

Step III: To a suspension of 2-(1-methyl-1*H*-indol-3-yl)-*N*-tosylacetamide (342 mg, 1.0 mmol, 1.0 eq) and potassium carbonate (272 mg, 2.0 mmol, 2.0 eq) in DMF (3 mL) was added iodomethane (564 mg, 4.0 mmol, 4.0 eq) at room temperature under N_2. After stirring the reaction mixture for 4 hours at room temperature, the mixture was diluted by adding CH_2Cl_2 (15 mL), washed with brine, and then extracted with CH_2Cl_2 (3 x 15 mL). The combined organic layers were dried over Na_2SO_4, filtered, and concentrated in vacuo. The crude residue was purified by flash column chromatography on silica gel (1:4 EtOAc/hexane) to afford the desired product as a white solid (324 mg, 0.91 mmol, 91% yield).

D.3: General Procedure for Photoredox Detosylation Reaction

To a 1-dram vial charged with a Teflon-coated stir was added 3,6-Di-*tert*-butyl-9-mesityl-*N*-phenylacridinium (5.78 mg, 0.01 mmol, 0.10 eq) and the corresponding benzenesulfonamide derivative substrate (0.10 mmol, 1.0 eq). The solid mixture was dissolved with 1 mL (0.1 M) solvent (acetonitrile/water = 6:1) then sealed with a Teflon coated septum cap before *N*,n-diisopropylethylamine (53 ul, 0.30 mmol, 3.0 eq) was added via syringe and the mixture was sparged with N_2 for 5 minutes. The reactions were stirred for 20 hours or 48 hours under irradiation with 390 nm LEDs. After completion, the reaction mixture was concentrated in vacuo then the yield was detected by one of two methods: 1) the desired product was isolated by flash column chromatography; or 2) the reaction mixture was dissolved in $CDCl_3$ followed with addition of hexamethyldisiloxane (3.5 ul, 0.10 mmol, 1.0 eq) or pyrazine (8.0 mg, 0.10 mmol, 1.0 eq) as an internal standard, and the yield of the desired product was determined *via* proton NMR.

D.4: General Procedure for Gram Scale Detosylation

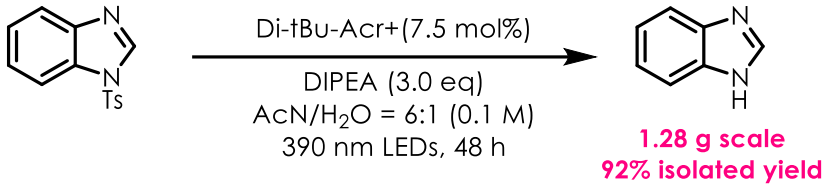

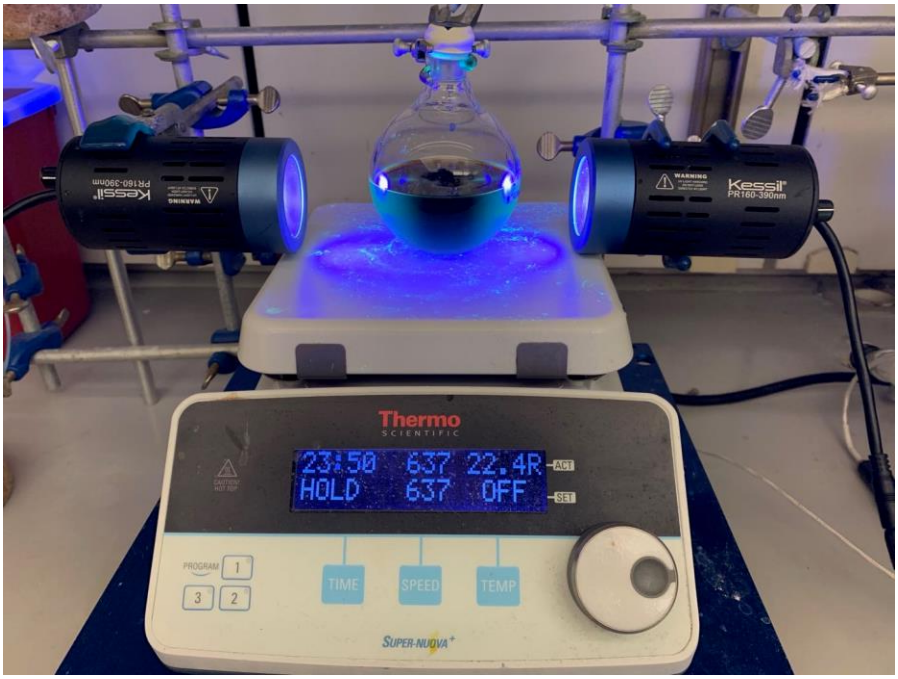

Figure D.1: Reaction apparatus for gram-scale reaction

A flame-dried, 250 mL round bottom flask was charged with 1-tosyl-1H-benzo[d]imidazole (3.20 g, 11.8 mmol, 1.0 equiv.), DIPEA (4.56 g, 35.3 mmol, 3.0 equiv.), 3,6-di-*tert*-butyl-9-mesityl-10-phenylacridin-10-ium tetrafluoroborate (505 mg, 0.881 mmol, 0.075 equiv.), MeCN (100 mL) and water (17 mL). The resulting mixture was sparged with nitrogen for 20 minutes. Kessil PR160 – 390 nm lamps were used to irradiate the reaction vessel at a distance of 5.0 cm from the walls of the flask. TLC indicated that the reaction had reached completion after 48 hours of irradiation. Solvent was removed under reduced pressure and the resulting residue was dissolved in 100 mL ethyl acetate and was washed with saturated Na_2CO_3 (100 mL) and brine (100 mL) and dried with

anhydrous Na_2SO_4. Solvent was removed under reduced pressure and the resulting residue purified via flash column chromatography (20% EtOAc/hexanes to 100% EtOAc), yielding the desired product as a white solid (92%, 1.28 g). **^{1}H NMR** (400 MHz, DMSO-d_6) δ (ppm) = 12.51 (s, 1H), 8.25 (s, 1H), 7.87 – 7.39 (m, 2H), 7.20 (dt, J = 6.2, 3.5 Hz, 2H), 3.48 (s, 1H).

D.5: General Procedure for Dehalogenation

To a 1-dram vial charged with a Teflon-coated stir bar was added 3,6-di-*tert*-butyl-9-mesityl-*N*-phenylacridinium (5.78 mg, 0.01 mmol, 0.10 eq) and the corresponding halogenated substrate (0.10 mmol, 1.0 eq). The solid mixture was dissolved with 0.13 mL (0.5 M) acetonitrile, then sealed with a Teflon coated septum cap before *N*,*N*-diisopropylethylamine (53 ul, 0.30 mmol, 3.0 eq) was added via syringe and the mixture sparged with N_2 for 5 minutes. The reactions were stirred for 16 hours under irradiation with 390 nm LEDs. After completion, the reaction mixture was dissolved with $CDCl_3$ followed by the addition of hexamethyldisiloxane (3.5 ul, 0.10 mmol, 1.0 eq) as the internal standard. Yields of the desired product were then calculated using crude proton NMR spectra.

D.6: Optimization of Detosylation Reaction

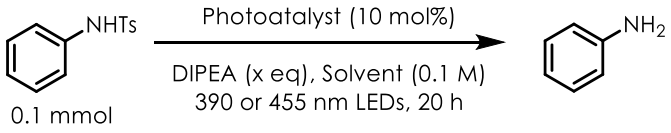

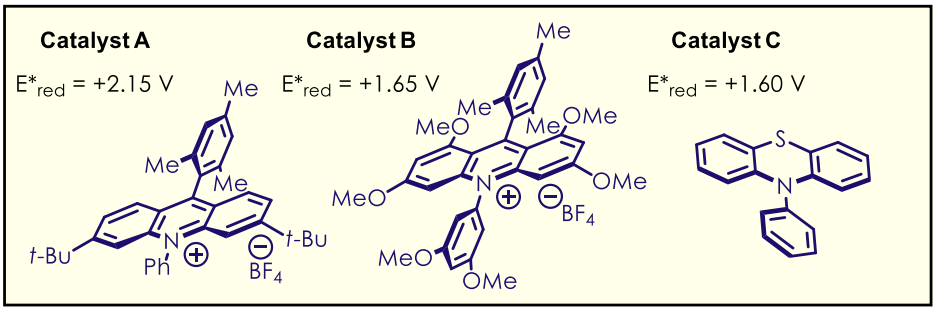

Entry	Photoatalyst	Solvent	LEDs	DIPEA	Yield[α]
1	Cat. A	AcN	455 nm	3.0 eq	< 5%
2	Cat. A	AcN	390 nm	3.0 eq	62%
3	Cat. A	AcN/H_2O = 4:1	390 nm	3.0 eq	79%
4	Cat. A	AcN/H_2O = 6:1	390 nm	3.0 eq	83%
5	Cat. A	AcN/H_2O = 10:1	390 nm	3.0 eq	68%
6	Cat. A	AcN/H_2O = 2:1	390 nm	3.0 eq	11%
7	Cat. A	AcN/H_2O = 6:1	455 nm	3.0 eq	< 5%
8	Cat. B	AcN/H_2O = 6:1	390 nm	3.0 eq	51%
9	$Ir(ppy)_3$	AcN/H_2O = 6:1	390 nm	3.0 eq	< 5%
10	Cat. C	AcN/H_2O = 6:1	390 nm	3.0 eq	< 5%
11	Cat. A	AcN/H_2O = 6:1	/	3.0 eq	0%
12	/	AcN/H_2O = 6:1	390 nm	3.0 eq	< 5%
13	Cat. A	AcN/H_2O = 6:1	390 nm	/	0%

α: NMR yield using hexamethyldisiloxane (HMDSO) as internal standard.

D.7: Optimization of Hydrodehalogenation Reaction

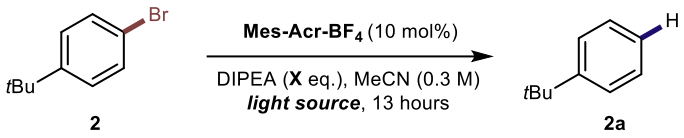

entry[a]	X	wavelength	Yield
1	1.2	390 nm	50%
2	2.0	390 nm	65%
3	3.0	390 nm	81%
4[b]	1.2	390 nm	0
5	-	390 nm	0
6	1.2	450 nm	0

substrate	$E^{red}_{1/2}$ (vs. SCE)	Yield (390 nm)	Yield (467 nm)
3	-2.9 V	90%	0%
4	-2.06 V	78%	34%
5	-1.58 V	72%	49%

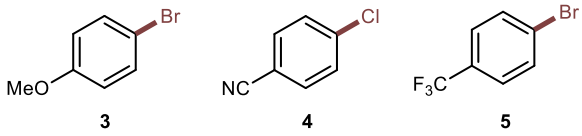

a: All reactions conducted on 0.1 mmol scale under air and analyzed by crude ^{1}H NMR using HMDSO as an internal standard
b: reaction conducted in the absence of **Mes-Acr-BF$_4$**

D.8: Deuterium labeling Experiment

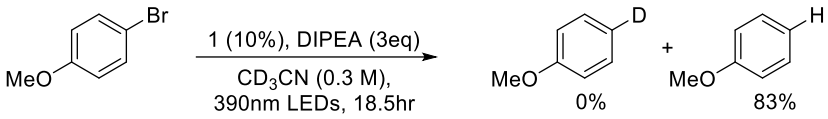

In a 1-dram vial with charged with a Teflon-coated stir bar were combined 4-bromoanisole (13µl, 0.1mmol, 1.0 equiv.), **Mes-Acr-BF$_4$** (5.7 mg, 0.01 mmol, 0.1 equiv.), DIPEA (52 µl, 0.3 mmol, 3.0 equiv.), and deuterated acetonitrile (CD_3CN, 0.3 mL). The vial was sealed with a septum cap and irradiated with 390 nm LEDs for 16 hours. ^{1}H NMR analysis of the reaction mixture showed the formation of anisole in 83% yield with 18% returned starting material and no deuterium incorporation into the product. GC-MS also confirms no deuterium incorporation. This result indicates that hydrogen atom transfer between a punitive aryl radical and the acetonitrile solvent is unlikely to be a dominant path in this system.

D.9: Scope of Aromatic Sulfonamides in Desulfonylation Reaction

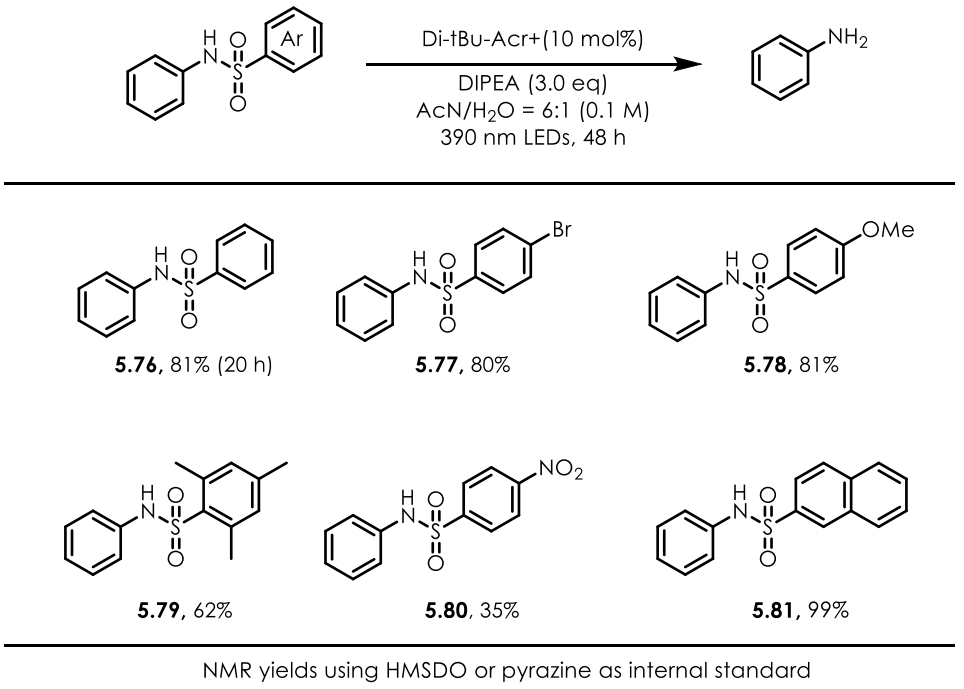

NMR yields using HMSDO or pyrazine as internal standard

D.10: Electron Paramagnetic Resonance (EPR) Measurements

In a nitrogen-filled glovebox, a solution of acridinium **Mes-Acr-BF_4** (54μM in CH_3CN) was reduced to acridine radical **Acr-Mes•** by addition of excess cobaltocene. The solution was removed from the glovebox and an EPR spectrum obtained as shown below.

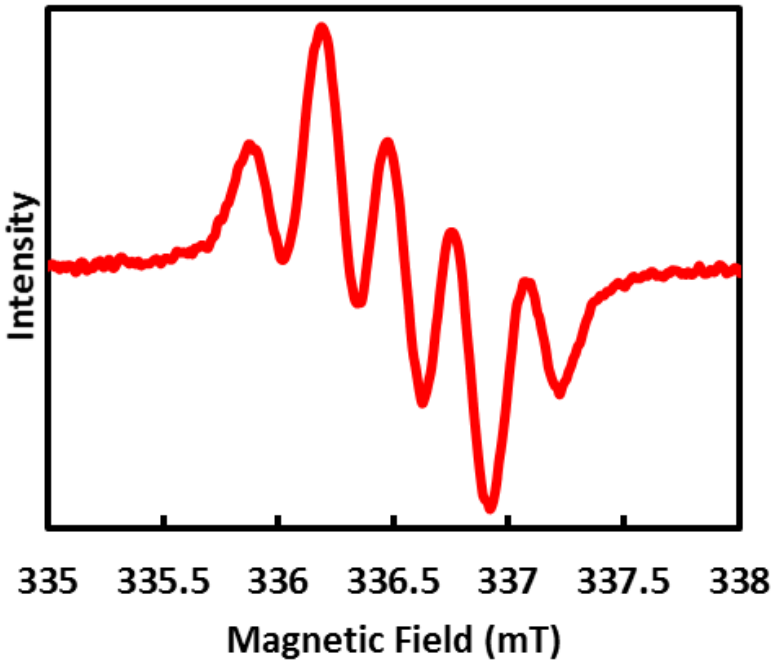

Figure D.2: EPR spectrum of Acr-Mes•

D.11: Electrochemical Measurements

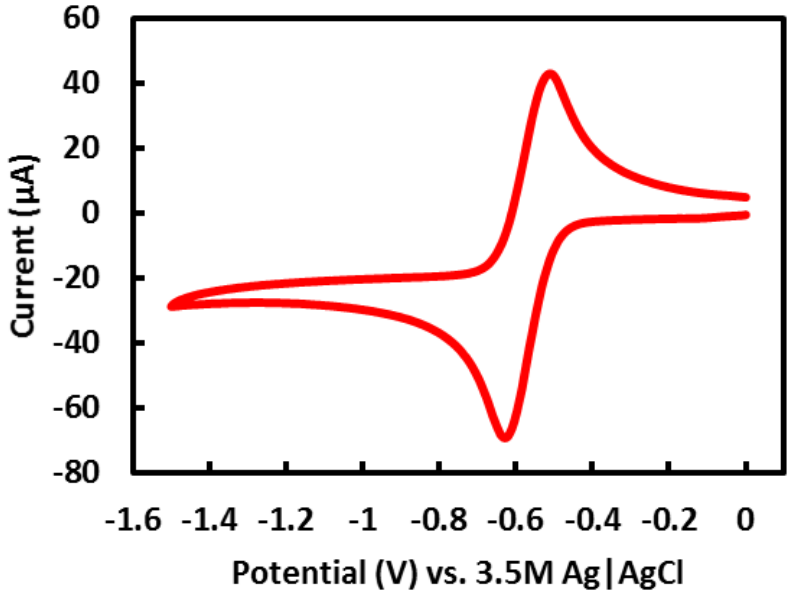

Figure D.3: Cyclic voltammogram of Acr-Mes-BF_4 in acetonitrile (scan rate = 100 mV/s). The ground state oxidation potential of Acr-Mes• is determined from the observed half peak potential to be -0.60 V vs. SCE.

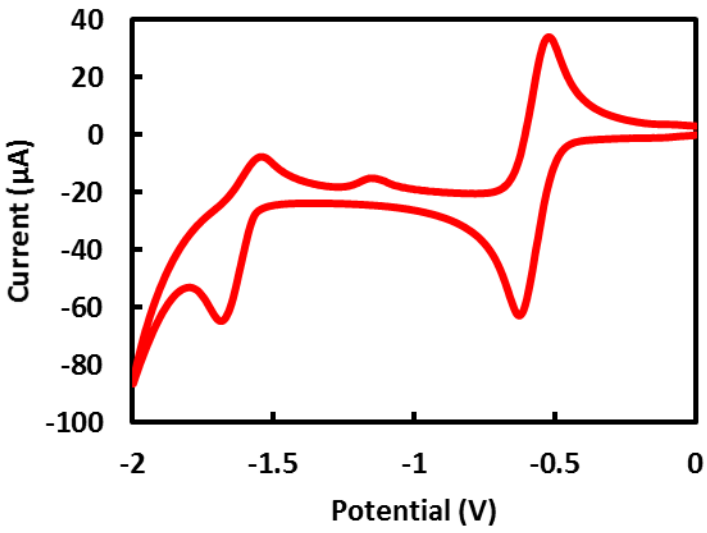

Figure D.4: Cyclic voltammogram of Acr-Mes-BF4 in acetonitrile showing the redox wave for reduction of Acr-Mes• to the corresponding anionic species. The corresponding half peak potential for this redox event was determined to be -1.64 V vs. SCE

D.12: Spectral Data and Analysis

Generation of Acr-Mes• via photoreaction of Acr-Mes-BF_4 and DIPEA:

A solution of **Acr-Mes-BF_4** (50 µM) in acetonitrile was prepared in a nitrogen filled glovebox. Excess DIPEA (~52 µl) was added to this in a quartz cuvette. The cuvette was sealed and brought out of the glovebox and an absorption spectrum recorded. The solution was then irradiated with 450 nm LEDs and absorption spectra recorded at intervals. Clean reduction of **Acr-Mes-BF_4** to **Acr-Mes•** was observed after short irradiation (~60 seconds to full conversion).

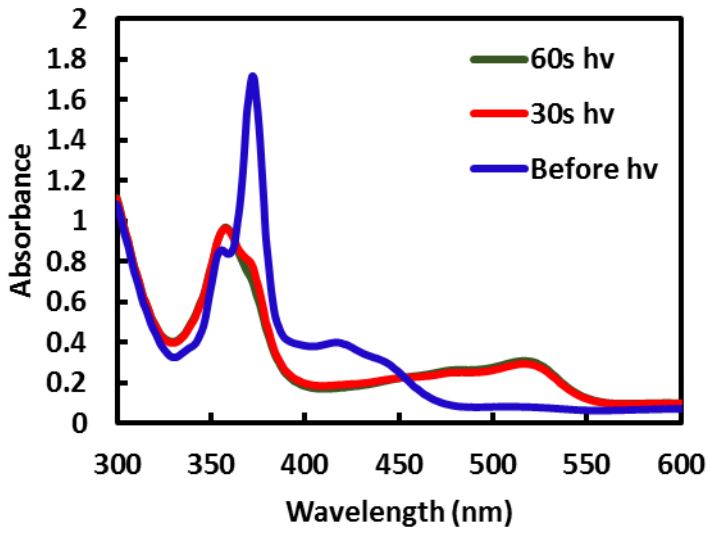

Figure D.5: Absorption spectra of Acr-Mes-BF_4 in the presence of excess DIPEA prior to irradiation (blue) and Acr-Mes• generated by 450 nm irradiation for 30 seconds (red) and for 60 seconds (green)

D.12.1: Fluorescence experiments

Samples for emission studies were prepared as follows: Acridinium **(Acr-Mes-BF_4)** was brought into a nitrogen filled glovebox and a stock solution in acetonitrile was prepared. This solution was reduced to **Acr-Mes•** with the addition of cobaltocene. A portion of this sample was taken and diluted to the desired concentration with hexane, after which the sample was passed through alumina to remove excess cobaltocene, cobaltocenium, and any remaining **Acr-Mes-BF_4**. The solution was transferred to a cuvette and sealed with a Teflon stopper or septum screw cap. The sample was then removed from the glovebox and absorption and emission spectra were collected. All emission and excitation data for **Acr-Mes•** were collected for a sample with an optical density of 0.80 at 512 nm except for the emission acquired at 484 nm excitation which was collected for a sample with an optical density of 0.27 at 512 nm.

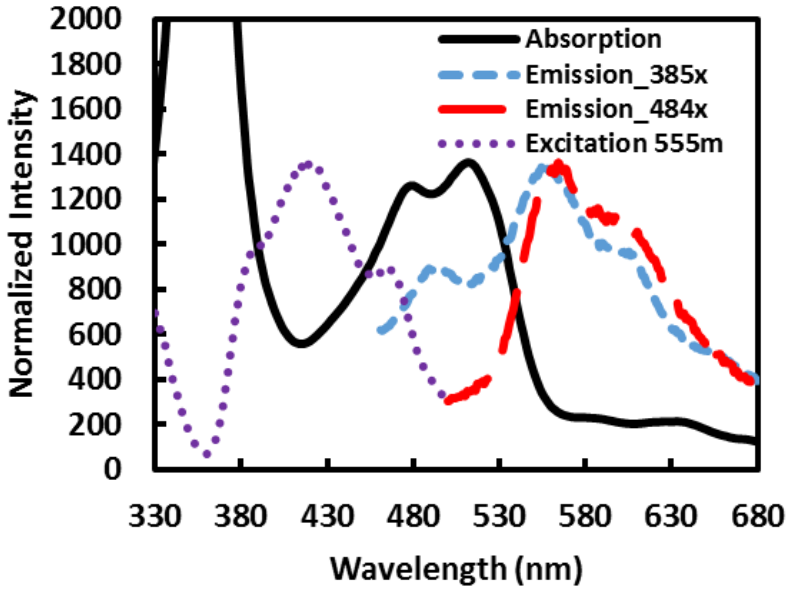

Figure D.6: Normalized absorption, emission, and excitation spectra of Acr-Mes• in hexanes. Excitation of the low energy absorption results in normal mirror like emission (red trace). Excitation at 385 nm reveals the new high energy emission band (blue trace)

The spectral wavelengths between 400–450 nm are obscured by a solvent Raman feature and were removed. The excitation spectrum is obtained by monitoring the emission intensity at 555 nm (purple trace).

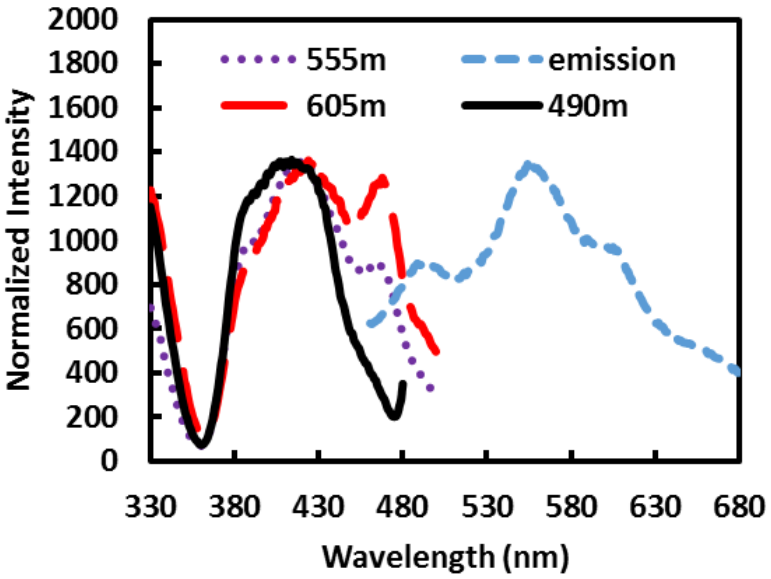

Figure D.7: Excitation spectra collected from Acr-Mes• by monitoring at different emission wavelengths. The emission generated by excitation at 385 nm is shown for comparison (blue trace)

As the emission represents the contributions of both emissive excited states, the excitation spectra are wavelength dependent and related to the relative population of each excited state at the chosen wavelength.

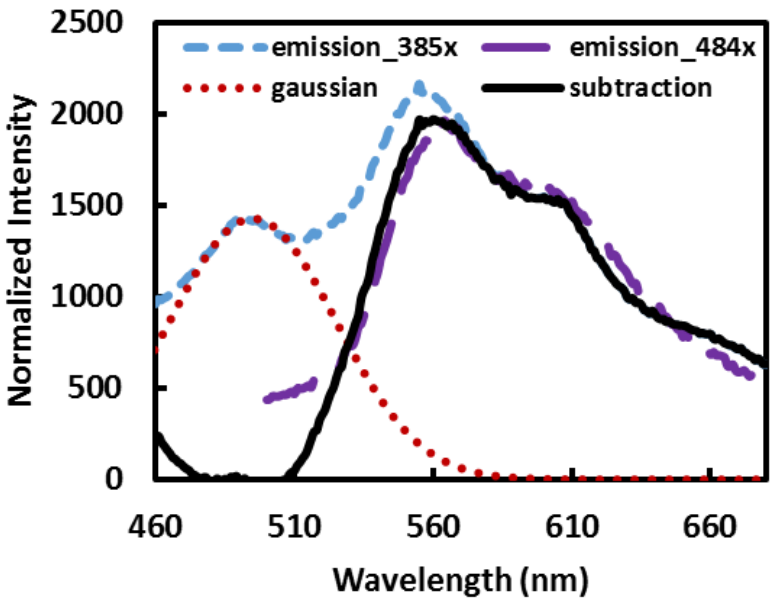

Figure D.8: Spectral deconvolution of the emission generated upon 385 nm excitation (blue trace). The high energy emission is fitted to a Gaussian distribution (red trace) and subtracted from the emission spectrum.

The subtraction (black trace) is compared to the emission spectrum (purple trace) obtained upon excitation only of the low energy absorption band.

D.12.2: Determination of excited state oxidation potentials for Acr-Mes•

The electronic energies of the two emissive excited states of **Acr-Mes•** were estimated from the absorption, emission, and excitation spectra as follows. E_{exc} for D_1 was estimated by averaging the energies of the lowest energy absorption maximum and the highest energy emission maximum observed upon 484 nm excitation. However, a similar estimation of E_{TICT} by comparison of the high energy absorption and emission maxima is believed to significantly overestimate the energy of this excited state, particularly as the transition at the absorption maximum does not appear to result in population of the TICT state (compare absorption and excitation spectra). Instead, E_{TICT} is estimated by averaging the energies of the emission maximum

near 490 nm and the maximum of the corresponding excitation spectrum monitored at this wavelength.

$$\mathrm{E_{D_1}} = \frac{2.42\ \mathrm{eV}\ (512\mathrm{nm}) + 2.20\ \mathrm{eV}\ (564\mathrm{nm})}{2} = 2.31\ \mathrm{eV}$$

$$\mathrm{E^*_{ox_{D1}}} = -0.60\ \mathrm{V\ vs.\ SCE} - 2.31\ \mathrm{eV} = -2.91\ \mathrm{V\ vs.\ SCE}$$

$$\mathrm{E_{TICT}} = \frac{2.99\ \mathrm{eV}\ (414\mathrm{nm}) + 2.52\ \mathrm{eV}\ (492\mathrm{nm})}{2} = 2.76\ \mathrm{eV}$$

$$\mathrm{E^*_{ox_{TICT}}} = -0.60\ \mathrm{V\ vs.\ SCE} - 2.76\ \mathrm{eV} = -3.36\ \mathrm{V\ vs.\ SCE}$$

D.12.3: Absorption and emission spectroscopy data

Methods: All spectroscopic experiments are conducted with a 1 mm path length cuvette. Linear absorption spectra are collected using an HP 8453 UV-Vis-NIR spectrometer. Fluorescence spectra are collected using an Edinburgh Instruments Xe900 fluorescence spectrometer with excitation and emission wavelengths indicated in Figures S1-S4. In all cases, the excitation monochromator was set to 5 nm bandwidth, while the emission monochromator was set to 3 nm bandwidth.

Ultrafast transient absorption experiments are conducted with a Coherent Libra laser (45 fs pulses, 4 mJ output, 1 kHz repetition rate, 800 nm fundamental). Approximately 100 nJ of the 800nm light is focused onto a BBO crystal to produce the 400nm pump pulses. The continuum probe pulses are generated by focusing ~2 μJ of the 800 nm fundamental onto a sapphire window (3mm thick). The 400 nm pump pulse is attenuated with a neutral density filter to achieve between 130-200 nJ pump energy at the sample position, depending on the signal strength. Both pump and probe pulses are then relayed to the sample using all reflective optics. The pump is focused to a FWHM spot size of ~140 μm at the sample position, and the size of the probe is adjusted to match that of the

pump. The transmitted probe is detected using a CMOS array detector synchronized to the repetition rate of the laser. The pump beam is passed through a chopper wheel operating at 500 Hz in order to acquire spectra with pump-on and pump-off on a shot-to-shot basis. For a single point in the delay line, 400 differences were collected; ultrafast transient absorption signals were averaged for 40-60 scans of the delay line.

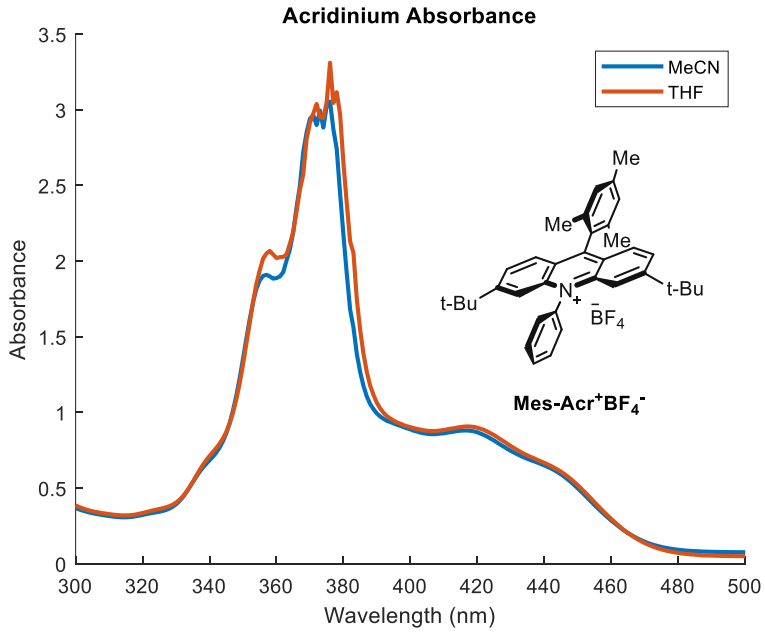

Figure D.9: Steady state absorbance of Acr-Mes-BF_4

(path length = 1 mm, concentration = 2.5 mM)

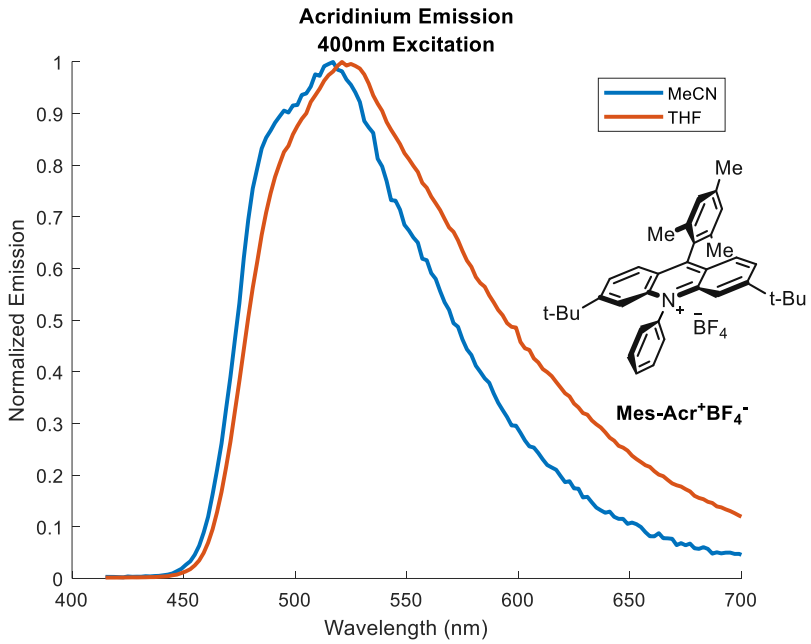

Figure D.10: Emission spectra of Acr-Mes- BF_4

(path length = 1 mm, concentration = 2.5 mM)

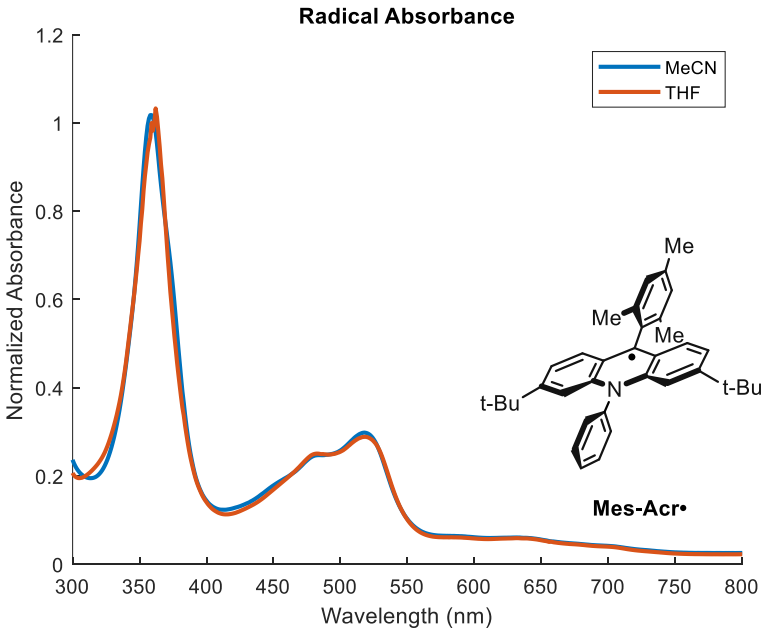

Figure D.11: Steady state absorbance of radical Acr-Mes•

(path length = 1 mm, concentration = 2.5 mM)

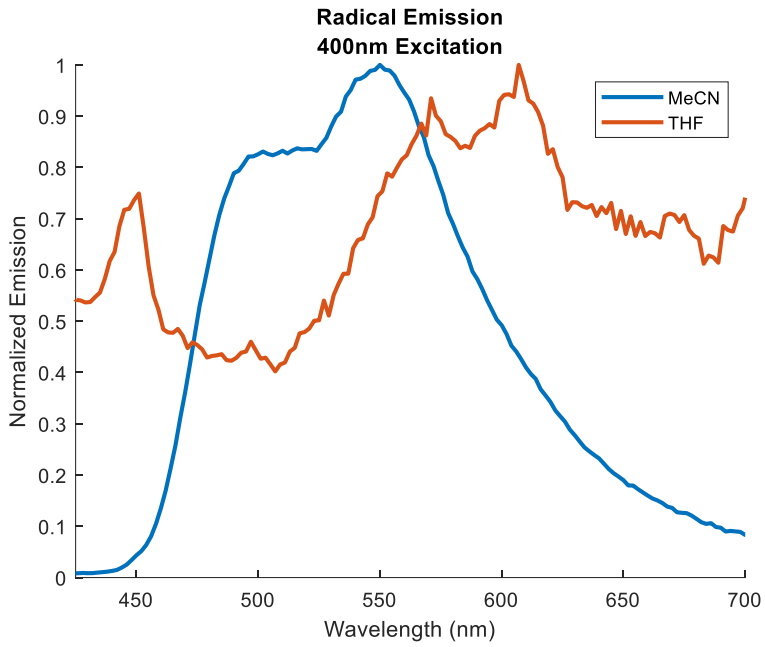

Figure D.12: Emission spectra of radical Acr-Mes•

(path length = 1 mm, concentration = 2.5 mM)

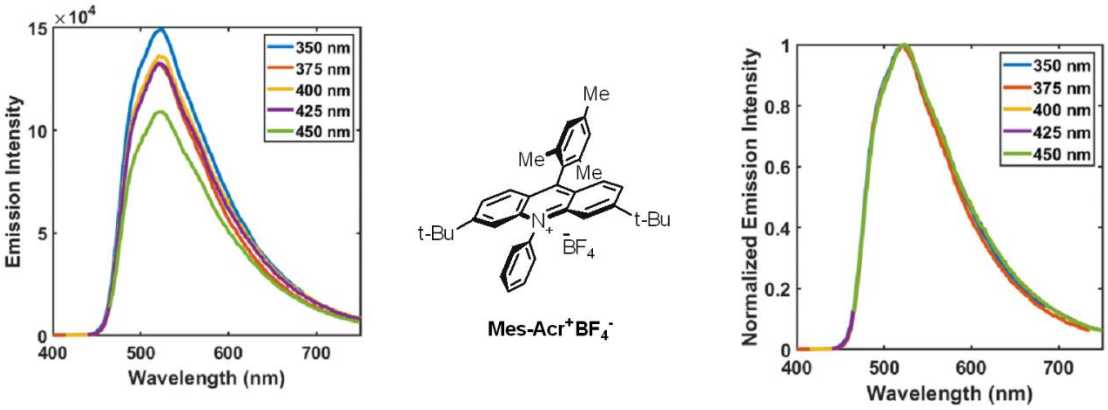

Figure D.13: Emission spectra obtained for acridinium Mes-Acr^{+}BF$_4^{-}$ in THF with variable excitation wavelength (see legends). Neither the raw (left) or normalized (right) spectra present evidence of anti-Kasha behavior.

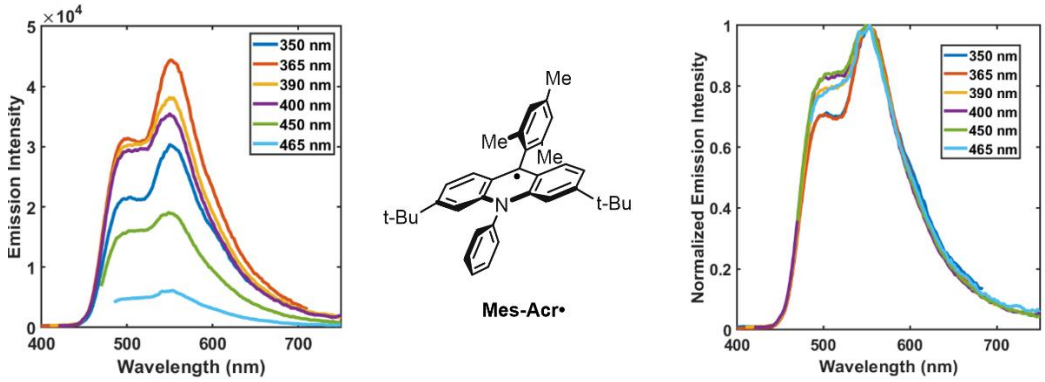

Figure D.14: Emission spectra obtained for the acridine radical Mes-Acr• in acetonitrile with variable excitation wavelength (see legends). Two main peaks at ~ 510 and 550 nm present different intensity ratios depending on the excitation wavelength

When the spectra are normalized to the 550 nm peak (right panel), the linewidth of the peaks also depends on the excitation wavelength.

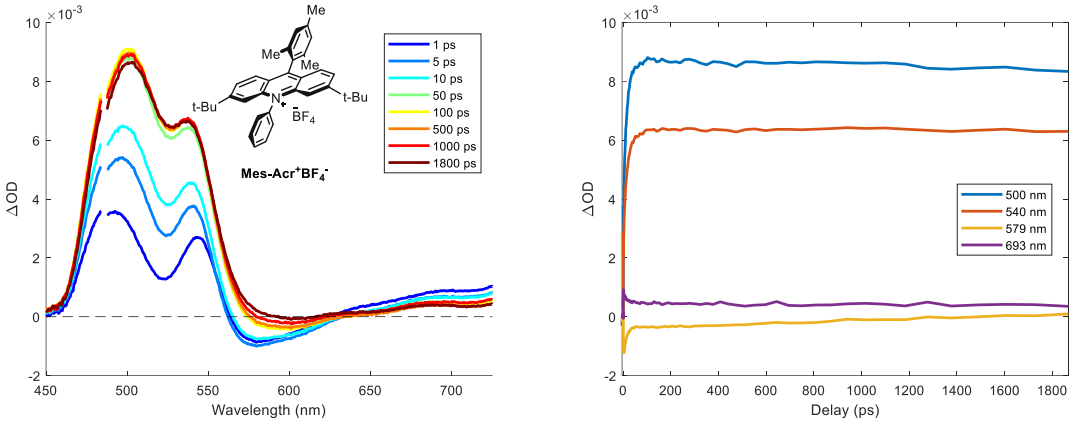

Figure D.15: Transient absorption spectra collected for acridinium in MeCN

Discontinuities in the spectra result from laser scatter over the course of the experiment. In both cases, prominent excited state absorption (ESA; $\Delta A>0$) resonances are apparent at early pump-probe delay times. The growth of these features with delay (see legends) suggests a growing excited state population. The negative feature ~575 nm corresponds to the excited state emission

of this species, the full lineshape of which is likely obscured by interference with the strong ESA features.

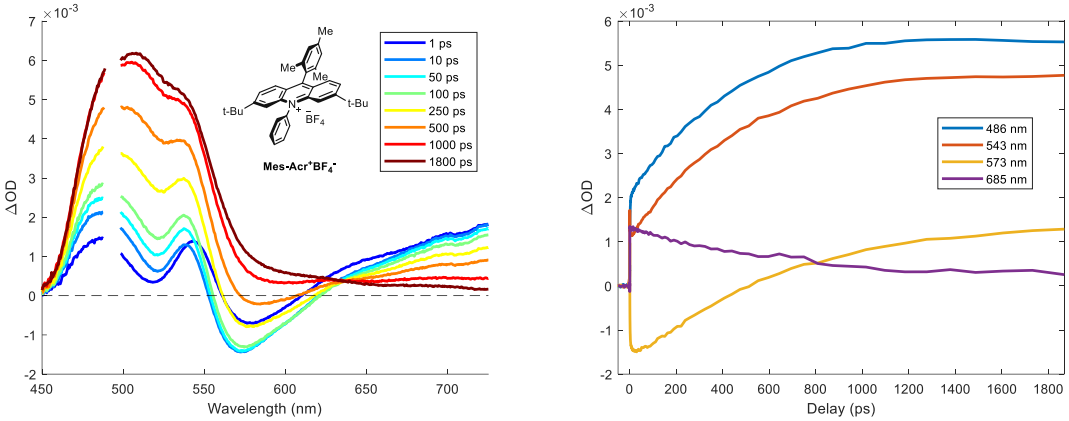

Figure D.16: Transient absorption spectra collected for acridinium in THF

Discontinuities in the spectra result from laser scatter over the course of the experiment. In both cases, prominent excited state absorption (ESA; ΔA>0) resonances are apparent at early pump-probe delay times. The growth of these features with delay (see legends) suggests a growing excited state population. The negative feature ~575 nm corresponds to the excited state emission of this species, the full lineshape of which is likely obscured by interference with the strong ESA features.

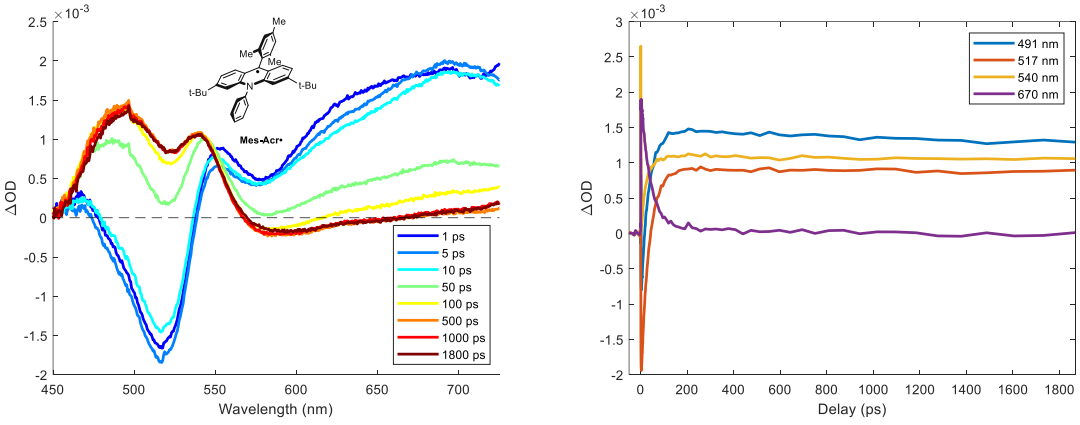

Figure D.17: Transient absorption spectra collected for Mes-Acr• in MeCN

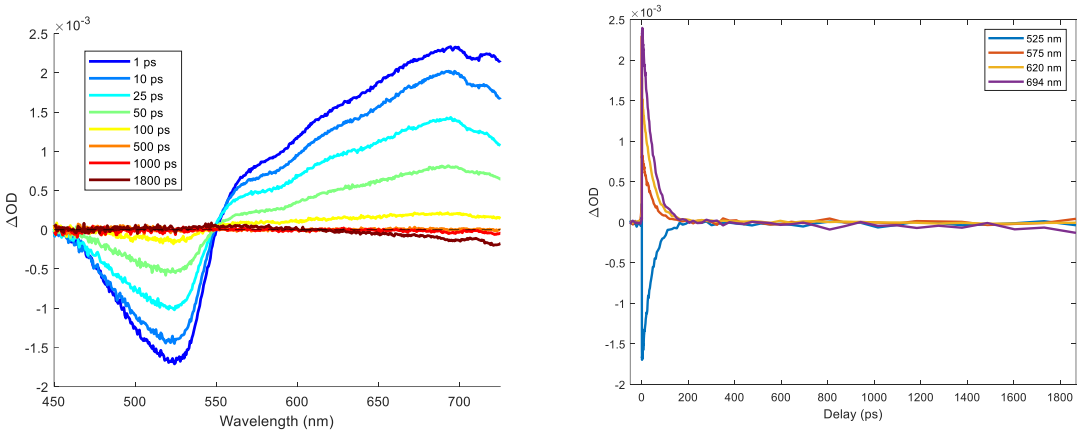

Figure D.18: Transient absorption spectra for Mes-Acr• in THF

D.13: Computational data

All calculations were performed using Q-Chem 4.[239] The molecular geometries are optimized at the wb97x-d/cc-pVDZ level of theory. Spectral calculations were completed using a screened range separated hybrid (SRSH) functional based TD-DFT method, where polarity of the medium is screened in both long and short ranges of the functional parameter. Energies calculated using SRSH-TDDFT more accurately reflect experimentally determined values, compared with the traditional B3LYP functional.[130–132]

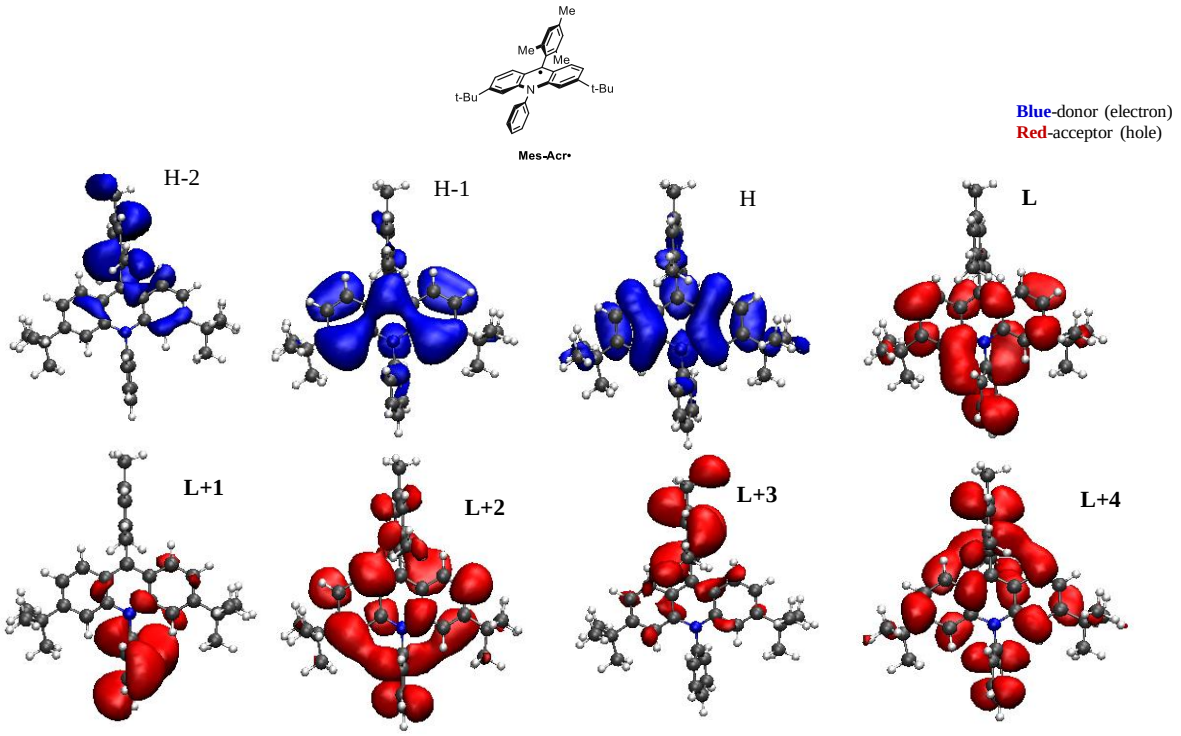

Figure D.19: Frontier orbital plots and energies (in eV) for calculated Mes-Acr• excited states

B3LYP state, energy & OS	SRSH TDDFT state, energy & OS	Experimental values (eV)
$\mathbf{D_1}$ (1), 2.16 (OS=0.016) $\mathbf{D_2}$ (2), 2.49 (OS=0.0003) $\mathbf{D_3}$ (3), 2.51 (OS=0.045)	$\mathbf{D_1}$ (1), 2.29 (0.016) $\mathbf{D_2}$ (2), 2.75 (0.07) $\mathbf{D_3}$ (3), 2.78 (0.0002) $\mathbf{D_4}$ (4), 2.92 (0.049)	D_1^*, 2.31 $\mathbf{D_{CT}}$, 2.76

Figure D.20: Calculated excited state energies using B3LYP and SRSH TD-DFT methods

D.14: Mechanistic Experiments

D.14.1: Wavelength dependent chemoselectivity experiments

In the presence of 1.2 equiv. of DIPEA and 10 mol% **Mes-Acr$^+$BF$_4^-$**, 4-(tert)butylbromobenzene (**2**) underwent hydrodebromination in 50% yield following irradiation at 390 nm for 13 hours (**Figure 5**, entry 1.). Increasing the loading of DIPEA to 3.0 equiv. resulted in an increase in yield, with the desired product **2a** formed in 81% yield under otherwise identical conditions (entry 2-3). Control experiments indicated that both **Mes-Acr$^+$BF$_4^-$** and DIPEA are required for the reaction to proceed (entry 4-5). Additionally, 0% conversion to the desired dehalogenation product was observed following irradiation at 450 nm, highlighting the requirement of higher energy irradiation in this system. To further examine the wavelength dependent chemoselectivity of this transformation, a series of aryl halides possessing varied reduction potentials were subject to the reaction conditions under various irradiation wavelengths.

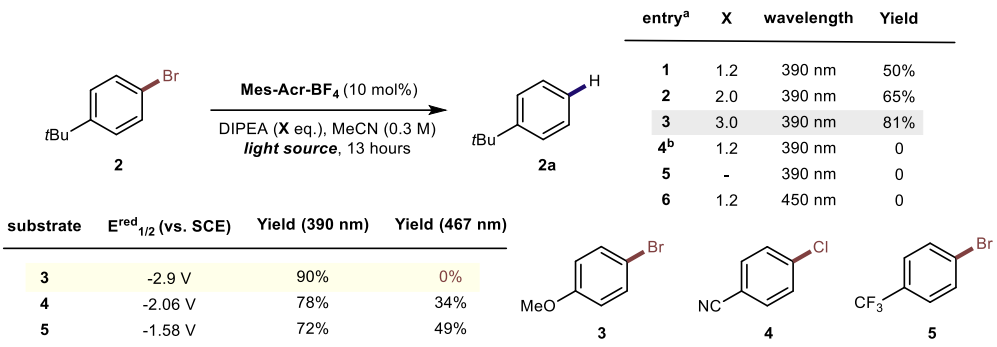

entry[a]	X	wavelength	Yield
1	1.2	390 nm	50%
2	2.0	390 nm	65%
3	3.0	390 nm	81%
4[b]	1.2	390 nm	0
5	-	390 nm	0
6	1.2	450 nm	0

substrate	$E^{red}_{1/2}$ (vs. SCE)	Yield (390 nm)	Yield (467 nm)
3	-2.9 V	90%	0%
4	-2.06 V	78%	34%
5	-1.58 V	72%	49%

a: All reactions conducted on 0.1 mmol scale under air and analyzed by crude ^{1}H NMR using HMDSO as an internal standard
b: reaction conducted in the absence of **Mes-Acr-BF$_4$**

Figure D.21: Optimization of acridine radical-catalyzed hydrodehalogenation reaction and summary of wavelength specific chemoselectivity

Substrates **4** and **5** afforded the corresponding dehalogenation products in 34% and 49% yield respectively following irradiation at 467 nm for 16 hours under otherwise identical reaction conditions. Switching the wavelength of irradiation from 467 nm to 390 nm resulted in increased yields of the desired product in both cases. Substrate **3**, possessing a reduction potential of -2.9 V vs. SCE was converted to the desired product in 90% yield following irradiation at 390 nm. Interestingly, irradiation at 467 nm did not result in any formation of the desired product, only affording unreacted starting material. This result highlights the relative reducing abilities of the multiple excited states of **Mes-Acr•.** When irradiating at 467 nm, the lower energy **D$_1$** excited state is populated, allowing for productive electron transfer to substrates with reduction potentials less negative than ~ -2.91 V vs. SCE. As the potential of **3** is very close to this value, the driving force for electron transfer is expected to be small. In contrast to this, population of the **TICT** state *via* irradiation at 390 nm allows for the reduction of substrates with reduction potentials less negative than -3.36 V vs. SCE and **3** is efficiently converted to the corresponding dehalogenated product.

D.14.2: Radical trapping experiments

Efforts to intercept nitrogen centered radical intermediates using Michael acceptors or substrates which may undergo 5-exo-trig cyclization with a pendant alkene failed to yield any products indicative of nitrogen centered radical generation. While these experiments cannot entirely exclude the formation of nitrogen-centered radicals during the transformation, the results indicate that any nitrogen-centered radicals formed undergo very rapid hydrogen atom transfer to yield the desulfonylation product, outcompeting other possible intramolecular or intermolecular processes in most cases. Substrate **72**, bearing a pendant Ts-amide, was detosylated in 72% yield in the presence of 2.0 equiv. DIPEA in a 6:1 MeCN/H_2O solvent system after 20 hours. Curiously, the removal of water from the solvent system leads to the formation of the desired detosylation product in 32% yield as well as a product corresponding to the cyclization of a punitive amidyl radical onto the indole core in 22% yield (32% remaining SM). This result indicates that water may serve a critical role in accelerating the rate of HAT in this system.

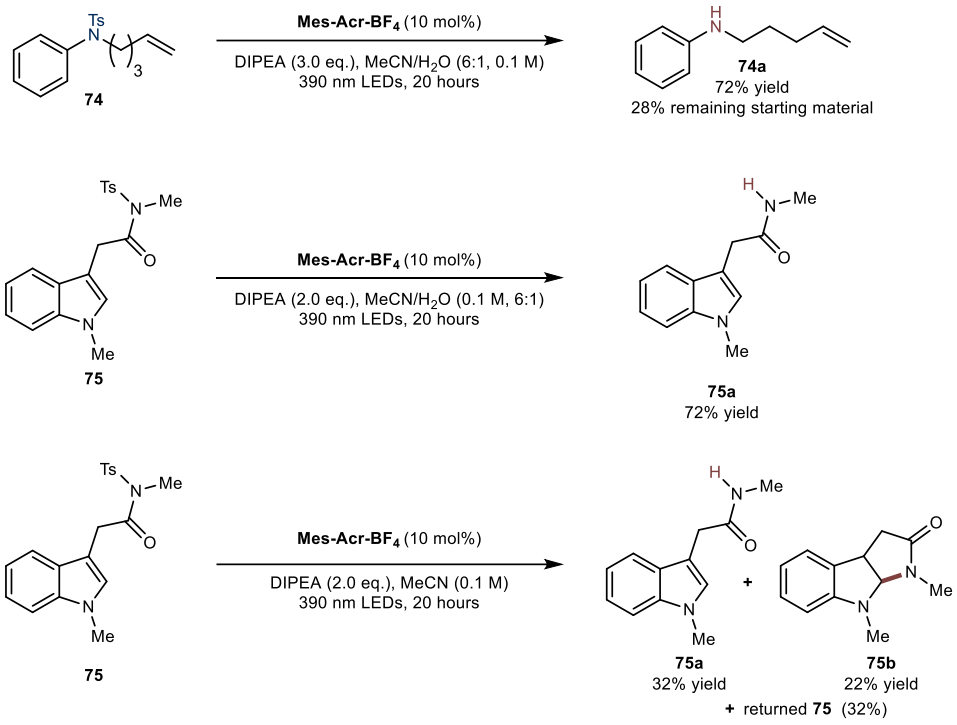

Figure D.22: Attempted radical trapping experiments

D.15: NMR Spectra for New Compounds

NMR data is available in the corresponding published supporting information, which is available online.[240]

REFERENCES

[1] K. J. Romero, M. S. Galliher, D. A. Pratt, C. R. J. Stephenson, *Chem. Soc. Rev.* **2018**, *47*, 7851–7866.

[2] M. Tomanik, I. T. Hsu, S. B. Herzon, *Angew. Chem. Int. Ed.* **2021**, *60*, 1116–1150.

[3] K. Hung, X. Hu, T. J. Maimone, *Nat. Prod. Rep.* **2018**, *35*, 174–202.

[4] C. K. Prier, D. A. Rankic, D. W. C. MacMillan, *Chem. Rev.* **2013**, *113*, 5322–5363.

[5] D. A. Nicewicz, D. W. C. MacMillan, *Science* **2008**, *322*, 77–80.

[6] E. Vitaku, D. T. Smith, J. T. Njardarson, *J. Med. Chem.* **2014**, *57*, 10257–10274.

[7] Z. Lu, S. S. Stahl, *Org. Lett.* **2012**, *14*, 1234–1237.

[8] R. Ebule, S. Mudshinge, M. H. Nantz, M. S. Mashuta, G. B. Hammond, B. Xu, *J. Org. Chem.* **2019**, *84*, 3249–3259.

[9] Y. Ju, R. S. Varma, *J. Org. Chem.* **2006**, *71*, 135–141.

[10] W. F. Bailey, P. Beak, S. T. Kerrick, S. Ma, K. B. Wiberg, *J. Am. Chem. Soc.* **2002**, *124*, 1889–1896.

[11] K. R. Campos, A. Klapars, J. H. Waldman, P. G. Dormer, C. Chen, *J. Am. Chem. Soc.* **2006**, *128*, 3538–3539.

[12] T. Shono, Y. Matsumura, K. Tsubata, Y. Sugihara, S. Yamane, T. Kanazawa, T. Aoki, *J. Am. Chem. Soc.* **1982**, *104*, 6697–6703.

[13] P. Magnus, C. Hulme, W. Weber, *J. Am. Chem. Soc.* **1994**, *116*, 4501–4502.

[14] J. Yoshida, S. Suga, S. Suzuki, N. Kinomura, A. Yamamoto, K. Fujiwara, *J. Am. Chem. Soc.* **1999**, *121*, 9546–9549.

[15] S. Suga, S. Suzuki, J. Yoshida, *J. Am. Chem. Soc.* **2002**, *124*, 30–31.

[16] T. Shono, *Tetrahedron* **1984**, *40*, 811–850.

[17] A. G. Condie, J. C. González-Gómez, C. R. J. Stephenson, *J. Am. Chem. Soc.* **2010**, *132*, 1464–1465.

[18] C. K. Prier, D. A. Rankic, D. W. C. MacMillan, *Chem. Rev.* **2013**, *113*, 5322–5363.

[19] L. Ruiz Espelt, E. M. Wiensch, T. P. Yoon, *J. Org. Chem.* **2013**, *78*, 4107–4114.

[20] S. Zhu, A. Das, L. Bui, H. Zhou, D. P. Curran, M. Rueping, *J. Am. Chem. Soc.* **2013**, *135*, 1823–1829.

[21] A. Das, I. Ghosh, B. König, *Chem Commun* **2016**, *52*, 8695–8698.

[22] L. Ruiz Espelt, I. S. McPherson, E. M. Wiensch, T. P. Yoon, *J. Am. Chem. Soc.* **2015**, *137*, 2452–2455.

[23] Y. Miyake, Y. Ashida, K. Nakajima, Y. Nishibayashi, *Chem. Commun.* **2012**, *48*, 6966.

[24] C. K. Prier, D. W. MacMillan, *Chem. Sci.* **2014**, *5*, 4173–4178.

[25] C. Le, Y. Liang, R. W. Evans, X. Li, D. W. C. MacMillan, *Nature* **2017**, *547*, 79–83.

[26] H. Roth, N. Romero, D. Nicewicz, *Synlett* **2016**, *27*, 714–723.

[27] A. R. White, L. Wang, D. A. Nicewicz, *Synlett* **2019**, *30*, 827–832.

[28] A. M. de P. Nicholas, D. R. Arnold, *Can. J. Chem.* **1982**, *60*, 2165–2179.

[29] J. Du, L. R. Espelt, I. A. Guzei, T. P. Yoon, *Chem. Sci.* **2011**, *2*, 2115.

[30] A. Fürst, Pl. A. Plattner, *Helv. Chim. Acta* **1949**, *32*, 275–283.

[31] Y. L. Chow, C. J. Colón, J. N. S. Tam, *Can. J. Chem.* **1968**, *46*, 2821–2825.

[32] D. J. Hart, *J. Am. Chem. Soc.* **1980**, *102*, 397–398.

[33] S. S. Libendi, Y. Demizu, O. Onomura, *Org Biomol Chem* **2009**, *7*, 351–356.

[34] T. Shono, Y. Matsumura, K. Tsubata, K. Uchida, *J. Org. Chem.* **1986**, *51*, 2590–2592.

[35] J. Quick, C. Mondello, M. Humora, T. Brennan, *J. Org. Chem.* **1978**, *43*, 2705–2708.

[36] M. M. Nebe, S. Zinn, T. Opatz, *Org. Biomol. Chem.* **2016**, *14*, 7084–7091.

[37] N. P. Schepp, L. J. Johnston, *J. Am. Chem. Soc.* **1996**, *118*, 2872–2881.

[38] D. R. Arnold, X. Du, J. Chen, *Can. J. Chem.* **1995**, *73*, 307–318.

[39] D. Crich, M. Shirai, S. Rumthao, *Org. Lett.* **2003**, *5*, 3767–3769.

[40] L. J. Johnston, N. P. Schepp, *Pure Appl. Chem.* **1995**, *67*, 71–78.

[41] L. J. Johnston, N. P. Schepp, *J. Am. Chem. Soc.* **1993**, *115*, 6564–6571.

[42] D. S. Hamilton, D. A. Nicewicz, *J. Am. Chem. Soc.* **2012**, *134*, 18577–18580.

[43] T. M. Nguyen, N. Manohar, D. A. Nicewicz, *Angew. Chem. Int. Ed Engl.* **2014**, *53*, 6198–6201.

[44] K. A. Margrey, D. A. Nicewicz, *Acc. Chem. Res.* **2016**, *49*, 1997–2006.

[45] L. Liang, D. Astruc, *Coord. Chem. Rev.* **2011**, *255*, 2933–2945.

[46] S. Bräse, C. Gil, K. Knepper, V. Zimmermann, *Angew. Chem. Int. Ed.* **2005**, *44*, 5188–5240.

[47] M. Meldal, C. W. Tornøe, *Chem. Rev.* **2008**, *108*, 2952–3015.

[48] M. Aldhoun, A. Massi, A. Dondoni, *J. Org. Chem.* **2008**, *73*, 9565–9575.

[49] C. I. Schilling, N. Jung, M. Biskup, U. Schepers, S. Bräse, *Chem. Soc. Rev.* **2011**, *40*, 4840.

[50] G. W. Breton, K. A. Daus, P. J. Kropp, *J. Org. Chem.* **1992**, *57*, 6646–6649.

[51] J. Waser, H. Nambu, E. M. Carreira, *J. Am. Chem. Soc.* **2005**, *127*, 8294–8295.

[52] I. Tsuchimochi, Y. Kitamura, H. Aoyama, S. Akai, K. Nakai, T. Yoshimitsu, *Chem. Commun.* **2018**, *54*, 9893–9896.

[53] Alfred. Hassner, Fred. Boerwinkle, *J. Am. Chem. Soc.* **1968**, *90*, 216–218.

[54] U. Biermann, U. Linker, J. O. Metzger, *Eur. J. Lipid Sci. Technol.* **2013**, *115*, 94–100.

[55] P. Zhang, W. Sun, G. Li, L. Hong, R. Wang, *Chem. Commun.* **2015**, *51*, 12293–12296.

[56] J. Wang, W. Yu, *Chem. – Eur. J.* **2019**, *25*, 3510–3514.

[57] G. H. Lonca, D. Y. Ong, T. M. H. Tran, C. Tejo, S. Chiba, F. Gagosz, *Angew. Chem. Int. Ed.* **2017**, *56*, 11440–11444.

[58] H. Li, S.-J. Shen, C.-L. Zhu, H. Xu, *J. Am. Chem. Soc.* **2019**, *141*, 9415–9421.

[59] A. Shulgin, A. Shulgin, *PIHKAL: A Chemical Love Story*, Transform Press, **1991**.

[60] O. Brede, F. David, S. Steenken, *J. Chem. Soc. Perkin Trans. 2* **1995**, 23.

[61] M. S. Workentin, N. P. Schepp, L. J. Johnston, D. D. M. Wayner, *J. Am. Chem. Soc.* **1994**, *116*, 1141–1142.

[62] E. Vitaku, D. T. Smith, J. T. Njardarson, *J. Med. Chem.* **2014**, *57*, 10257–10274.

[63] S. D. Roughley, A. M. Jordan, *J. Med. Chem.* **2011**, *54*, 3451–3479.

[64] T. Ishiyama, J. Takagi, K. Ishida, N. Miyaura, N. R. Anastasi, J. F. Hartwig, *J. Am. Chem. Soc.* **2002**, *124*, 390–391.

[65] J. Oyamada, M. Nishiura, Z. Hou, *Angew. Chem. Int. Ed.* **2011**, *50*, 10720–10723.

[66] A. Yokota, Y. Aihara, N. Chatani, *J. Org. Chem.* **2014**, *79*, 11922–11932.

[67] F. Minisci, R. Bernardi, F. Bertini, R. Galli, M. Perchinummo, *Tetrahedron* **1971**, *27*, 3575–3579.

[68] I. B. Seiple, S. Su, R. A. Rodriguez, R. Gianatassio, Y. Fujiwara, A. L. Sobel, P. S. Baran, *J. Am. Chem. Soc.* **2010**, *132*, 13194–13196.

[69] S. C. Fosu, C. M. Hambira, A. D. Chen, J. R. Fuchs, D. A. Nagib, *Chem* **2019**, *5*, 417–428.

[70] J. W. Beatty, J. J. Douglas, K. P. Cole, C. R. J. Stephenson, *Nat. Commun.* **2015**, *6*, 1–6.

[71] J. Li, J. Chen, R. Sang, W.-S. Ham, M. B. Plutschack, F. Berger, S. Chabbra, A. Schnegg, C. Genicot, T. Ritter, *Nat. Chem.* **2020**, *12*, 56–62.

[72] F. Berger, M. B. Plutschack, J. Riegger, W. Yu, S. Speicher, M. Ho, N. Frank, T. Ritter, *Nature* **2019**, *567*, 223–228.

[73] C. K. Prier, D. A. Rankic, D. W. C. MacMillan, *Chem. Rev.* **2013**, *113*, 5322–5363.

[74] D. Lapointe, K. Fagnou, *Chem. Lett.* **2010**, *39*, 1118–1126.

[75] S. I. Gorelsky, D. Lapointe, K. Fagnou, *J. Am. Chem. Soc.* **2008**, *130*, 10848–10849.

[76] D. Kalyani, K. B. McMurtrey, S. R. Neufeldt, M. S. Sanford, *J. Am. Chem. Soc.* **2011**, *133*, 18566–18569.

[77] Z. Yu, Y. Li, P. Zhang, L. Liu, J. Zhang, *Chem. Sci.* **2019**, *10*, 6553–6559.

[78] A. Conde, G. Sabenya, M. Rodríguez, V. Postils, J. M. Luis, M. M. Díaz-Requejo, M. Costas, P. J. Pérez, *Angew. Chem. Int. Ed.* **2016**, *55*, 6530–6534.

[79] M. P. Doyle, R. Duffy, M. Ratnikov, L. Zhou, *Chem. Rev.* **2010**, *110*, 704–724.

[80] I. Rivilla, B. P. Gómez-Emeterio, M. R. Fructos, M. M. Díaz-Requejo, P. J. Pérez, *Organometallics* **2011**, *30*, 2855–2860.

[81] A. DeAngelis, V. W. Shurtleff, O. Dmitrenko, J. M. Fox, *J. Am. Chem. Soc.* **2011**, *133*, 1650–1653.

[82] F. Hu, Y. Xia, C. Ma, Y. Zhang, J. Wang, *Chem. Commun.* **2015**, *51*, 7986–7995.

[83] D. V. Vorobyeva, M. M. Vinogradov, Y. V. Nelyubina, D. A. Loginov, A. S. Peregudov, S. N. Osipov, *Org. Biomol. Chem.* **2018**, *16*, 2966–2974.

[84] X. Yu, S. Yu, J. Xiao, B. Wan, X. Li, *J. Org. Chem.* **2013**, *78*, 5444–5452.

[85] E. Tayama, T. Yanaki, H. Iwamoto, E. Hasegawa, *Eur. J. Org. Chem.* **2010**, *2010*, 6719–6721.

[86] Z. Yu, B. Ma, M. Chen, H.-H. Wu, L. Liu, J. Zhang, *J. Am. Chem. Soc.* **2014**, *136*, 6904–6907.

[87] Z. Wang, A. G. Herraiz, A. M. del Hoyo, M. G. Suero, *Nature* **2018**, *554*, 86–91.

[88] I. D. Jurberg, H. M. L. Davies, *Chem. Sci.* **2018**, *9*, 5112–5118.

[89] E. Brachet, T. Ghosh, I. Ghosh, B. König, *Chem. Sci.* **2015**, *6*, 987–992.

[90] D. P. Hari, P. Schroll, B. König, *J. Am. Chem. Soc.* **2012**, *134*, 2958–2961.

[91] K. A. Margrey, A. Levens, D. A. Nicewicz, *Angew. Chem. Int. Ed Engl.* **2017**, *56*, 15644–15648.

[92] N. A. Romero, K. A. Margrey, N. E. Tay, D. A. Nicewicz, *Science* **2015**, *349*, 1326–1330.

[93] J. B. McManus, D. A. Nicewicz, *J. Am. Chem. Soc.* **2017**, *139*, 2880–2883.

[94] Ł. W. Ciszewski, J. Durka, D. Gryko, *Org. Lett.* **2019**, *21*, 7028–7032.

[95] J. D. Griffin, M. A. Zeller, D. A. Nicewicz, *J. Am. Chem. Soc.* **2015**, DOI 10.1021/jacs.5b07770.

[96] P. K. Mandal, J. S. McMurray, *J. Org. Chem.* **2007**, *72*, 6599–6601.

[97] J. A. Greenberg, T. Sammakia, *J. Org. Chem.* **2017**, *82*, 3245–3251.

[98] A. C. Cope, H. L. Holmes, O. House, in *Org. React.*, **1957**, pp. 107–331.

[99] F. J. Sarabia, E. M. Ferreira, *Org. Lett.* **2017**, *19*, 2865–2868.

[100] W. D. Mackay, J. S. Johnson, *Org. Lett.* **2016**, *18*, 536–539.

[101] G. Maier, *Angew. Chem. Int. Ed. Engl.* **1967**, *6*, 402–413.

[102] O. Hammerich, V. D. Parker, in *Adv. Phys. Org. Chem.*, Elsevier, **1984**, pp. 55–189.

[103] V. D. Parker, *Acc. Chem. Res.* **1984**, *17*, 243–250.

[104] J. Mattay, *Synthesis* **1989**, *1989*, 233–252.

[105] A. Bauer, F. Westkämper, S. Grimme, T. Bach, *Nature* **2005**, *436*, 1139–1140.

[106] M. A. Fox, *Photochem. Photobiol.* **1990**, *52*, 617–627.

[107] S. Fukuzumi, *Pure Appl. Chem.* **2007**, *79*, 981–991.

[108] N. A. Romero, D. A. Nicewicz, *Chem. Rev.* **2016**, *116*, 10075–10166.

[109] L. J. Johnston, *Chem. Rev.* **1993**, *93*, 251–266.

[110] B. R. Arnold, J. C. Scaiano, W. G. McGimpsey, *J. Am. Chem. Soc.* **1992**, *114*, 9978–9982.

[111] J. C. Scaiano, M. Tanner, D. Weir, *J. Am. Chem. Soc.* **1985**, *107*, 4396–4403.

[112] A. Samanta, K. Bhattacharyya, P. K. Das, P. V. Kamat, D. Weir, G. L. Hug, *J. Phys. Chem.* **1989**, *93*, 3651–3656.

[113] D. Weir, J. C. Scaiano, *Chem. Phys. Lett.* **1986**, *128*, 156–159.

[114] C. Scordilis-Kelley, *J. Electrochem. Soc.* **1992**, *139*, 694.

[115] I. Ghosh, T. Ghosh, J. I. Bardagi, B. König, *Science* **2014**, *346*, 725–728.

[116] M. Neumeier, D. Sampedro, M. Májek, V. A. de la Peña O'Shea, A. Jacobi von Wangelin, R. Pérez-Ruiz, *Chem. – Eur. J.* **2018**, *24*, 105–108.

[117] H. Kim, H. Kim, T. H. Lambert, S. Lin, *J. Am. Chem. Soc.* **2020**, *142*, 2087–2092.

[118] N. G. W. Cowper, C. P. Chernowsky, O. P. Williams, Z. K. Wickens, *J. Am. Chem. Soc.* **2020**, *142*, 2093–2099.

[119] N. A. Romero, D. A. Nicewicz, *J. Am. Chem. Soc.* **2014**, *136*, 17024–17035.

[120] T. U. Connell, C. L. Fraser, M. L. Czyz, Z. M. Smith, D. J. Hayne, E. H. Doeven, J. Agugiaro, D. J. D. Wilson, J. L. Adcock, A. D. Scully, D. E. Gómez, N. W. Barnett, A. Polyzos, P. S. Francis, *J. Am. Chem. Soc.* **2019**, *141*, 17646–17658.

[121] C. Lu, M. Fujitsuka, A. Sugimoto, T. Majima, *J. Phys. Chem. C* **2017**, *121*, 4558–4563.

[122] J. A. Christensen, B. T. Phelan, S. Chaudhuri, A. Acharya, V. S. Batista, M. R. Wasielewski, *J. Am. Chem. Soc.* **2018**, *140*, 5290–5299.

[123] J.-C. Gumy, E. Vauthey, *J. Phys. Chem. A* **1997**, *101*, 8575–8580.

[124] G. Brancato, G. Signore, P. Neyroz, D. Polli, G. Cerullo, G. Abbandonato, L. Nucara, V. Barone, F. Beltram, R. Bizzarri, *J. Phys. Chem. B* **2015**, *119*, 6144–6154.

[125] A. P. Demchenko, V. I. Tomin, P.-T. Chou, *Chem. Rev.* **2017**, *117*, 13353–13381.

[126] Z. Peng, Z. Wang, Z. Huang, S. Liu, P. Lu, Y. Wang, *J. Mater. Chem. C* **2018**, *6*, 7864–7873.

[127] S. Scuppa, L. Orian, A. Donoli, S. Santi, M. Meneghetti, *J. Phys. Chem. A* **2011**, *115*, 8344–8349.

[128] J. W. Verhoeven, H. J. van Ramesdonk, H. Zhang, M. M. Groeneveld, A. C. Benniston, A. Harriman, *Int. J. Photoenergy* **2005**, *7*, 103–108.

[129] S. Fukuzumi, K. Ohkubo, T. Suenobu, K. Kato, M. Fujitsuka, O. Ito, *J. Am. Chem. Soc.* **2001**, *123*, 8459–8467.

[130] S. Bhandari, B. D. Dunietz, *J. Chem. Theory Comput.* **2019**, *15*, 4305–4311.

[131] Y. Song, A. Schubert, E. Maret, R. K. Burdick, B. D. Dunietz, E. Geva, J. P. Ogilvie, *Chem. Sci.* **2019**, *10*, 8143–8153.

[132] S. Bhandari, M. S. Cheung, E. Geva, L. Kronik, B. D. Dunietz, *J. Chem. Theory Comput.* **2018**, *14*, 6287–6294.

[133] B. Maiti, A. Schubert, S. Sarkar, S. Bhandari, K. Wang, Z. Li, E. Geva, R. J. Twieg, B. D. Dunietz, *Chem. Sci.* **2017**, *8*, 6947–6953.

[134] T. Shida, *Electronic Absorption Spectra of Radical Ions*, Elsevier, Amsterdam ; New York, **1988**.

[135] C. Kerzig, M. Goez, *Phys. Chem. Chem. Phys.* **2015**, *17*, 13829–13836.

[136] C. Kerzig, X. Guo, O. S. Wenger, *J. Am. Chem. Soc.* **2019**, *141*, 2122–2127.

[137] I. Ghosh, T. Ghosh, J. I. Bardagi, B. König, *Science* **2014**, *346*, 725–728.

[138] S. O. Poelma, G. L. Burnett, E. H. Discekici, K. M. Mattson, N. J. Treat, Y. Luo, Z. M. Hudson, S. L. Shankel, P. G. Clark, J. W. Kramer, C. J. Hawker, J. Read de Alaniz, *J. Org. Chem.* **2016**, *81*, 7155–7160.

[139] E. H. Discekici, N. J. Treat, S. O. Poelma, K. M. Mattson, Z. M. Hudson, Y. Luo, C. J. Hawker, J. R. de Alaniz, *Chem. Commun.* **2015**, *51*, 11705–11708.

[140] J. M. R. Narayanam, J. W. Tucker, C. R. J. Stephenson, *J. Am. Chem. Soc.* **2009**, *131*, 8756–8757.

[141] H. Yin, Y. Jin, J. E. Hertzog, K. C. Mullane, P. J. Carroll, B. C. Manor, J. M. Anna, E. J. Schelter, *J. Am. Chem. Soc.* **2016**, *138*, 16266–16273.

[142] S. O. Poelma, G. L. Burnett, E. H. Discekici, K. M. Mattson, N. J. Treat, Y. Luo, Z. M. Hudson, S. L. Shankel, P. G. Clark, J. W. Kramer, C. J. Hawker, J. Read de Alaniz, *J. Org. Chem.* **2016**, *81*, 7155–7160.

[143] T. Javorskis, E. Orentas, *J. Org. Chem.* **2017**, *82*, 13423–13439.

[144] N. Shohji, T. Kawaji, S. Okamoto, *Org. Lett.* **2011**, *13*, 2626–2629.

[145] E. Alonso, D. J. Ramón, M. Yus, *Tetrahedron* **1997**, *53*, 14355–14368.

[146] N. Takasu, K. Oisaki, M. Kanai, *Org. Lett.* **2013**, *15*, 1918–1921.

[147] N. J. Taylor, E. Emer, S. Preshlock, M. Schedler, M. Tredwell, S. Verhoog, J. Mercier, C. Genicot, V. Gouverneur, *J. Am. Chem. Soc.* **2017**, *139*, 8267–8276.

[148] B. Deb, S. Debnath, A. Deb, D. K. Maiti, S. Majumdar, *Tetrahedron Lett.* **2017**, *58*, 629–633.

[149] J. H. Schrittwieser, V. Resch, S. Wallner, W.-D. Lienhart, J. H. Sattler, J. Resch, P. Macheroux, W. Kroutil, *J. Org. Chem.* **2011**, *76*, 6703–6714.

[150] M. Chen, Z.-H. Ren, Y.-Y. Wang, Z.-H. Guan, *J. Org. Chem.* **2015**, *80*, 1258–1263.

[151] M. S. McCammant, S. Thompson, A. F. Brooks, S. W. Krska, P. J. H. Scott, M. S. Sanford, *Org. Lett.* **2017**, *19*, 3939–3942.

[152] A. Millet, D. Dailler, P. Larini, O. Baudoin, *Angew. Chem. Int. Ed.* **2014**, *53*, 2678–2682.

[153] M. Minakawa, Y. M. A. Yamada, Y. Uozumi, *RSC Adv* **2014**, *4*, 36864–36867.

[154] R. Varala, S. Nuvula, S. R. Adapa, *J. Org. Chem.* **2006**, *71*, 8283–8286.

[155] B. Bagh, D. L. J. Broere, V. Sinha, P. F. Kuijpers, N. P. van Leest, B. de Bruin, S. Demeshko, M. A. Siegler, J. I. van der Vlugt, *J. Am. Chem. Soc.* **2017**, *139*, 5117–5124.

[156] T. Qin, L. R. Malins, J. T. Edwards, R. R. Merchant, A. J. E. Novak, J. Z. Zhong, R. B. Mills, M. Yan, C. Yuan, M. D. Eastgate, P. S. Baran, *Angew. Chem. Int. Ed.* **2017**, *56*, 260–265.

[157] E. J. Cochrane, L. A. Hassall, I. Coldham, *J. Org. Chem.* **2015**, *80*, 5964–5969.

[158] H. Kawada, P. F. Kador, *J. Med. Chem.* **2015**, *58*, 8796–8805.

[159] T. I. Aarhus, U. F. Fritze, M. Hennum, L.-L. Gundersen, *Tetrahedron Lett.* **2014**, *55*, 5748–5750.

[160] M. C. McLeod, G. Singh, J. N. Plampin, D. Rane, J. L. Wang, V. W. Day, J. Aubé, *Nat. Chem.* **2014**, *6*, 133–140.

[161] A. Quintard, A. Alexakis, C. Mazet, *Angew. Chem. Int. Ed.* **2011**, *50*, 2354–2358.

[162] V. Gembus, J.-J. Bonnet, F. Janin, P. Bohn, V. Levacher, J.-F. Brière, *Org. Biomol. Chem.* **2010**, *8*, 3287.

[163] R. Sanabria, R. Herrera, R. Aguilar, C. González-Romero, H. A. Jiménez-Vázquez, F. Delgado, B. C. Söderberg, J. Tamariz, *Helv. Chim. Acta* **2008**, *91*, 1807–1827.

[164] F.-X. Felpin, K. Miqueu, J.-M. Sotiropoulos, E. Fouquet, O. Ibarguren, J. Laudien, *Chem. - Eur. J.* **2010**, *16*, 5191–5204.

[165] R. K. Dieter, C. M. Topping, L. E. Nice, *J. Org. Chem.* **2001**, *66*, 2302–2311.

[166] S. Angioni, D. Ravelli, D. Emma, D. Dondi, M. Fagnoni, A. Albini, *Adv. Synth. Catal.* **2008**, *350*, 2209–2214.

[167] N. A. Romero, D. A. Nicewicz, *J. Am. Chem. Soc.* **2014**, *136*, 17024–17035.

[168] J. D. Griffin, C. L. Cavanaugh, D. A. Nicewicz, *Angew. Chem. Int. Ed.* **2017**, *56*, 2097–2100.

[169] A. D. Becke, *J. Chem. Phys.* **1993**, *98*, 5648–5652.

[170] C. Lee, W. Yang, R. G. Parr, *Phys. Rev. B* **1988**, *37*, 785–789.

[171] R. Krishnan, J. S. Binkley, R. Seeger, J. A. Pople, *J. Chem. Phys.* **1980**, *72*, 650–654.

[172] A. D. McLean, G. S. Chandler, *J. Chem. Phys.* **1980**, *72*, 5639–5648.

[173] J. B. McManus, N. P. R. Onuska, D. A. Nicewicz, *J. Am. Chem. Soc.* **2018**, *140*, 9056–9060.

[174] Q. Zhu, D. E. Graff, R. R. Knowles, *J. Am. Chem. Soc.* **2018**, *140*, 741–747.

[175] K. Michigami, T. Mita, Y. Sato, *J. Am. Chem. Soc.* **2017**, *139*, 6094–6097.

[176] R. Kumar, A. Sharma, N. Sharma, V. Kumar, A. K. Sinha, *Eur. J. Org. Chem.* **2008**, *2008*, 5577–5582.

[177] X.-L. Lu, M. Shannon, X.-S. Peng, H. N. C. Wong, *Org. Lett.* **2019**, *21*, 2546–2549.

[178] K. Nakayama, N. Maeta, G. Horiguchi, H. Kamiya, Y. Okada, *Org. Lett.* **2019**, *21*, 2246–2250.

[179] M. Brown, R. Kumar, J. Rehbein, T. Wirth, *Chem. – Eur. J.* **2016**, *22*, 4030–4035.

[180] J. H. Shin, E. Y. Seong, H. J. Mun, Y. J. Jang, E. J. Kang, *Org. Lett.* **2018**, *20*, 5872–5876.

[181] A. E. Díaz-Álvarez, P. Crochet, V. Cadierno, *Tetrahedron* **2012**, *68*, 2611–2620.

[182] J. Yu, S. Y. Ko, *Tetrahedron Asymmetry* **2012**, *23*, 650–654.

[183] F. Miege, C. Meyer, J. Cossy, *Angew. Chem. Int. Ed.* **2011**, *50*, 5932–5937.

[184] C. Chen, S. Jin, Z. Zhang, B. Wei, H. Wang, K. Zhang, H. Lv, X.-Q. Dong, X. Zhang, *J. Am. Chem. Soc.* **2016**, *138*, 9017–9020.

[185] G. W. Kabalka, D. Tejedor, N.-S. Li, R. R. Malladi, S. Trotman, *Tetrahedron* **1998**, *54*, 15525–15532.

[186] M. Lara, F. G. Mutti, S. M. Glueck, W. Kroutil, *Eur. J. Org. Chem.* **2008**, *2008*, 3668–3672.

[187] D. Srimani, G. Leitus, Y. Ben-David, D. Milstein, *Angew. Chem. Int. Ed.* **2014**, *53*, 11092–11095.

[188] F. Berthiol, H. Doucet, M. Santelli, *Synthesis* **2005**, *2005*, 3589–3602.

[189] T. Suzuki, Y. Ota, M. Ri, M. Bando, A. Gotoh, Y. Itoh, H. Tsumoto, P. R. Tatum, T. Mizukami, H. Nakagawa, S. Iida, R. Ueda, K. Shirahige, N. Miyata, *J. Med. Chem.* **2012**, *55*, 9562–9575.

[190] B. Peng, A.-G. Thorsell, T. Karlberg, H. Schüler, S. Q. Yao, *Angew. Chem. Int. Ed.* **2017**, *56*, 248–253.

[191] Y. Zhu, X. Li, X. Wang, X. Huang, T. Shen, Y. Zhang, X. Sun, M. Zou, S. Song, N. Jiao, *Org. Lett.* **2015**, *17*, 4702–4705.

[192] N. I. Bowers, D. R. Boyd, N. D. Sharma, P. A. Goodrich, M. R. Groocock, A. J. Blacker, P. Goode, H. Dalton, *J. Chem. Soc. Perkin 1* **1999**, 1453–1462.

[193] J. Barluenga, M. Tomás-Gamasa, C. Valdés, *Angew. Chem. Int. Ed.* **2012**, *51*, 5950–5952.

[194] J. W. Barlow, J. J. Walsh, *Eur. J. Med. Chem.* **2010**, *45*, 25–37.

[195] A. Kapat, A. König, F. Montermini, P. Renaud, *J. Am. Chem. Soc.* **2011**, *133*, 13890–13893.

[196] E. Nyfeler, P. Renaud, *Org. Lett.* **2008**, *10*, 985–988.

[197] N. P. R. Onuska, M. E. Schutzbach-Horton, J. L. R. Collazo, D. A. Nicewicz, *Synlett* **2019**, DOI 10.1055/s-0039-1690691.

[198] N. A. Romero, K. A. Margrey, N. E. Tay, D. A. Nicewicz, *Science* **2015**, *349*, 1326–1330.

[199] B. Das, P. THIRUPATHI, B. RAVIKANTH, R. KUMAR, A. SARMA, S. BASHA, *Chem. Pharm. Bull.* **2009**, *57*, 1139–1141.

[200] W. Chen, Z. Huang, N. E. S. Tay, B. Giglio, M. Wang, H. Wang, Z. Wu, D. A. Nicewicz, Z. Li, *Science* **2019**, *in press*.

[201] M. A. Windsor, D. J. Hermanson, P. J. Kingsley, S. Xu, B. C. Crews, W. Ho, C. M. Keenan, S. Banerjee, K. A. Sharkey, L. J. Marnett, *ACS Med. Chem. Lett.* **2012**, *3*, 759–763.

[202] Y. Chen, J. Sun, Z. Huang, H. Liao, S. Peng, J. Lehmann, Y. Zhang, *Bioorg. Med. Chem.* **2013**, *21*, 2462–2470.

[203] W. Lau, J. K. Kochi, *J. Am. Chem. Soc.* **1984**, *106*, 7100–7112.

[204] S. Racine, B. Hegedüs, R. Scopelliti, J. Waser, *Chem. – Eur. J.* **2016**, *22*, 11997–12001.

[205] F. de Nanteuil, J. Waser, *Angew. Chem. Int. Ed.* **2011**, *50*, 12075–12079.

[206] S. J. Meek, R. V. O'Brien, J. Llaveria, R. R. Schrock, A. H. Hoveyda, *Nature* **2011**, *471*, 461–466.

[207] T. Toma, J. Shimokawa, T. Fukuyama, *Org. Lett.* **2007**, *9*, 3195–3197.

[208] B. Zimmermann, W. I. Dzik, T. Himmler, L. J. Goossen, *J. Org. Chem.* **2011**, *76*, 8107–8112.

[209] T. Kawamoto, A. Sato, I. Ryu, *Org. Lett.* **2014**, *16*, 2111–2113.

[210] Z. Huang, Z. Chen, L. H. Lim, G. C. P. Quang, H. Hirao, J. (Steve) Zhou, *Angew. Chem. Int. Ed.* **2013**, *52*, 5807–5812.

[211] M. Jørgensen, S. Lee, X. Liu, J. P. Wolkowski, J. F. Hartwig, *J. Am. Chem. Soc.* **2002**, *124*, 12557–12565.

[212] M. Muehlebach, M. Boeger, F. Cederbaum, D. Cornes, A. A. Friedmann, J. Glock, T. Niderman, A. Stoller, T. Wagner, *Bioorg. Med. Chem.* **2009**, *17*, 4241–4256.

[213] N. Holmberg-Douglas, N. P. R. Onuska, D. A. Nicewicz, *Angew. Chem. Int. Ed.* **2020**, *59*, 7425–7429.

[214] Y.-C. Teo, F.-F. Yong, I. K. Ithnin, S.-H. T. Yio, Z. Lin, *Eur. J. Org. Chem.* **2013**, *2013*, 515–524.

[215] S. J. Barraza, S. E. Denmark, *J. Am. Chem. Soc.* **2018**, *140*, 6668–6684.

[216] B. Vinayak, M. Chandrasekharam, *Org. Lett.* **2017**, *19*, 3528–3531.

[217] I. Ghosh, J. Khamrai, A. Savateev, N. Shlapakov, M. Antonietti, B. König, *Science* **2019**, *365*, 360–366.

[218] J. Zhang, L. Shen, J. Wang, P. L. and Y. Hu, "Design, Synthesis and Biological Evaluation of Novel Non-peptide Boronic Acid Derivatives as Proteasome Inhibitors," **2014**.

[219] C. Schneider, E. Broda, V. Snieckus, *Org. Lett.* **2011**, *13*, 3588–3591.

[220] A. Polley, G. Bairy, P. Das, R. Jana, *Adv. Synth. Catal.* **2018**, *360*, 4161–4167.

[221] L. Bering, M. Vogt, F. M. Paulussen, A. P. Antonchick, *Org. Lett.* **2018**, *20*, 4077–4080.

[222] Y. Fu, Q.-S. Xu, C.-Z. Shi, Z. Du, C. Xiao, *Adv. Synth. Catal.* **2018**, *360*, 3502–3506.

[223] S. O'Sullivan, E. Doni, T. Tuttle, J. A. Murphy, *Angew. Chem. Int. Ed.* **2014**, *53*, 474–478.

[224] J. K. Laha, K. P. Jethava, N. Dayal, *J. Org. Chem.* **2014**, *79*, 8010–8019.

[225] E. Richmond, J. Moran, *J. Org. Chem.* **2015**, *80*, 6922–6929.

[226] M. Arisawa, Y. Terada, M. Nakagawa, A. Nishida, *Angew. Chem. Int. Ed.* **2002**, *41*, 4732–4734.

[227] J. Chan, K. D. Baucom, J. A. Murry, *J. Am. Chem. Soc.* **2007**, *129*, 14106–14107.

[228] J. H. Frederich, P. G. Harran, *J. Am. Chem. Soc.* **2013**, *135*, 3788–3791.

[229] D. M. M. M. Dissanayake, A. K. Vannucci, *Org. Lett.* **2019**, *21*, 457–460.

[230] S. Maiti, P. Mal, *Adv. Synth. Catal.* **2015**, *357*, 1416–1424.

[231] T. Biberger, S. Makai, Z. Lian, B. Morandi, *Angew. Chem. Int. Ed.* **2018**, *57*, 6940–6944.

[232] D. Hirose, M. Gazvoda, J. Košmrlj, T. Taniguchi, *Chem. Sci.* **2016**, *7*, 5148–5159.

[233] J. Huang, W. Xu, H. Xie, S. Li, *J. Org. Chem.* **2012**, *77*, 7506–7511.

[234] T. W. Liwosz, S. R. Chemler, *Chem. – Eur. J.* **2013**, *19*, 12771–12777.

[235] Z.-Y. Tang, Q.-S. Hu, *J. Am. Chem. Soc.* **2004**, *126*, 3058–3059.

[236] J. Xu, R. Tong, *Green Chem.* **2017**, *19*, 2952–2956.

[237] S. Roy, A. Eastman, G. W. Gribble, *Org. Biomol. Chem.* **2006**, *4*, 3228.

[238] O. Lozano, G. Blessley, T. Martinez del Campo, A. L. Thompson, G. T. Giuffredi, M. Bettati, M. Walker, R. Borman, V. Gouverneur, *Angew. Chem. Int. Ed.* **2011**, *50*, 8105–8109.

[239] Y. Shao, Z. Gan, E. Epifanovsky, A. T. B. Gilbert, M. Wormit, J. Kussmann, A. W. Lange, A. Behn, J. Deng, X. Feng, D. Ghosh, M. Goldey, P. R. Horn, L. D. Jacobson, I. Kaliman, R. Z. Khaliullin, T. Kuś, A. Landau, J. Liu, E. I. Proynov, Y. M. Rhee, R. M. Richard, M. A. Rohrdanz, R. P. Steele, E. J. Sundstrom, H. L. W. III, P. M. Zimmerman, D. Zuev, B. Albrecht, E. Alguire, B. Austin, G. J. O. Beran, Y. A. Bernard, E. Berquist, K. Brandhorst, K. B. Bravaya, S. T. Brown, D. Casanova, C.-M. Chang, Y. Chen, S. H. Chien, K. D. Closser, D. L. Crittenden, M. Diedenhofen, R. A. D. Jr, H. Do, A. D. Dutoi, R. G. Edgar, S. Fatehi, L. Fusti-Molnar, A. Ghysels, A. Golubeva-Zadorozhnaya, J. Gomes, M. W. D. Hanson-Heine, P. H. P. Harbach, A. W. Hauser, E. G. Hohenstein, Z. C. Holden, T.-C. Jagau, H. Ji, B. Kaduk, K. Khistyaev, J. Kim, J. Kim, R. A. King, P. Klunzinger, D. Kosenkov, T. Kowalczyk, C. M. Krauter, K. U. Lao, A. D. Laurent, K. V. Lawler, S. V. Levchenko, C. Y. Lin, F. Liu, E. Livshits, R. C. Lochan, A. Luenser, P. Manohar, S. F. Manzer, S.-P. Mao, N. Mardirossian, A. V. Marenich, S. A. Maurer, N. J. Mayhall, E. Neuscamman, C. M. Oana, R. Olivares-Amaya, D. P. O'Neill, J. A. Parkhill, T. M. Perrine, R. Peverati, A. Prociuk, D. R. Rehn, E. Rosta, N. J. Russ, S. M. Sharada, S.

Sharma, D. W. Small, A. Sodt, T. Stein, D. Stück, Y.-C. Su, A. J. W. Thom, T. Tsuchimochi, V. Vanovschi, L. Vogt, O. Vydrov, T. Wang, M. A. Watson, J. Wenzel, A. White, C. F. Williams, J. Yang, S. Yeganeh, S. R. Yost, Z.-Q. You, I. Y. Zhang, X. Zhang, Y. Zhao, B. R. Brooks, G. K. L. Chan, D. M. Chipman, C. J. Cramer, W. A. G. III, M. S. Gordon, W. J. Hehre, A. Klamt, H. F. S. III, M. W. Schmidt, C. D. Sherrill, D. G. Truhlar, A. Warshel, X. Xu, A. Aspuru-Guzik, R. Baer, A. T. Bell, N. A. Besley, J.-D. Chai, A. Dreuw, B. D. Dunietz, T. R. Furlani, S. R. Gwaltney, C.-P. Hsu, Y. Jung, J. Kong, D. S. Lambrecht, W. Liang, C. Ochsenfeld, V. A. Rassolov, L. V. Slipchenko, J. E. Subotnik, T. V. Voorhis, J. M. Herbert, A. I. Krylov, P. M. W. Gill, M. Head-Gordon, *Mol. Phys.* **2015**, *113*, 184–215.

[240] I. A. MacKenzie, L. Wang, N. P. R. Onuska, O. F. Williams, K. Begam, A. M. Moran, B. D. Dunietz, D. A. Nicewicz, *Nature* **2020**, *580*, 76–80.